Chemical biopsy via solid phase microextraction: strategies and applications for *in vivo* brain studies

by

Sofia Lendor

A thesis
presented to the University of Waterloo
in fulfillment of the
thesis requirement for the degree of
Doctor of Philosophy
in
Chemistry

Waterloo, Ontario, Canada, 2020

Examining Committee Membership

The following served on the examining committee for this thesis. The decision of the examining committee is by majority vote.

External Examiner	Prof. Robert Kennedy Professor and Department of Chemistry Chair Department of Chemistry, University of Michigan
Supervisor	Prof. Janusz Pawliszyn University Professor and Canada Research Chair Department of Chemistry, University of Waterloo
Internal Member	Prof. Wojciech Gabryelski Associate Professor Department of Chemistry, University of Guelph
Internal Member	Prof. Michael Palmer Associate Professor Department of Chemistry, University of Waterloo
Internal Member	Prof. Thilo Womelsdorf Associate Professor Psychology Department, Vanderbilt University
Internal-External Member	Prof. Mark Servos Professor and Canada Research Chair in Water Quality Protection Department of Biology, University of Waterloo

Author's declaration

This thesis consists of material which has been authored or co-authored by myself: see Statement of Contributions included in the thesis. This is the true copy of the thesis, including any required final revisions, as accepted by my examiners.

I understand that my thesis may be made electronically available to the public.

Statement of Contributions

Chapter 2 contains study carried out in collaboration with Attention Circuits Control Neuroscience Laboratory at Vanderbilt University. The SPME tools development and validation, as well as the instrumental analysis were carried out at the University of Waterloo, while the *in vivo* samplings were performed at York University (former location of the Attention Circuits Control Neuroscience Laboratory). Subchapters 2.2 and 2.4 have been published as an article entitled *Solid Phase Microextraction-Based Miniaturized Probe and Protocol for Extraction of Neurotransmitters from Brains in Vivo* (*Analytical Chemistry* **2019**, 91(7), 4896-4905), co-authored by Seyed-Alireza Hassani (equally contributing), Ezel Boyaci, Varoon Singh, Thilo Womelsdorf, and Janusz Pawliszyn. Subchapter 2.3 has been published as an article entitled *Multineuromodulator measurements across fronto-striatal network areas of the behaving macaque using solid-phase microextraction* (*Journal of Neurophysiology* **2019**, 122(4), 1649-1660), co-authored by Seyed-Alireza Hassani (equally contributing), Ezel Boyaci, Janusz Pawliszyn, and Thilo Womelsdorf. J. Pawliszyn and T. Womelsdorf initiated the collaboration, secured the funding, conceived the studies, and contributed to data interpretation. The initial optimization experiments and *in vivo* sampling were overseen by E. Boyaci. The extracting phase polymer synthesis was carried out by V. Singh. S.-A. Hassani and S. Lendor (the author of this thesis) were responsible for performing the *in vivo* experiments, data analysis, data interpretation and manuscripts writing. S.-A. Hassani carried out the animal subjects care and preparation, electrophysiology recordings, and statistical data analysis. The SPME probe development, *ex vivo* validation and instrumental analysis was carried out by the author of this thesis.

Chapter 3 (with the exception of the subchapter 3.3) has been published as an article entitled *Space-Resolved Tissue Analysis by Solid-Phase Microextraction Coupled to High-Resolution Mass Spectrometry via Desorption Electrospray Ionization* (*Analytical Chemistry* **2019**, 91(15), 10141-

10148), co-authored by Germán Augusto Gómez-Ríos, Ezel Boyaci, Harmen Vander Heide, under the supervision of Janusz Pawliszyn. H. Vander Heide was responsible for design and execution of the DESI spray interface, with the input from S. Lendor and G.A. Gómez-Ríos. Experiments planning and design, and experimental execution were carried out by the author of this thesis and overseen by G.A. Gómez-Ríos and E. Boyaci at the preliminary stage. Protocol development, data analysis and interpretation, as well as writing were performed entirely by the author of the thesis.

Chapter 4 contains yet unpublished results of a collaborative project between Prof. Janusz Pawliszyn Research Group at the University of Waterloo and Prof. Raag Airan Lab at the Stanford University, which is currently in progress. The *in vivo* sampling of rodent brain as well as all preparations related to the ultrasound-sensitive nanocarriers (synthesis, characterization, etc.) have been carried out in the facilities of the Radiology Department at Stanford University. J. Pawliszyn and R. Airan initiated the collaboration, secured the funding, conceived the studies, and contributed to data interpretation. Jeffrey B. Wang and Sofia Lendor coordinated the collaboration on the Stanford and Waterloo sides, respectively. Jeffrey B. Wang conducted the animal studies at the Stanford University with the assistance of Daivik B. Vyas. Mahaveer Prasad Purohit and Niloufar Hosseini-Nassab synthesized the ketamine-loaded nanoparticles and developed analytics for quantifying nanoparticle and drug loading properties. The SPME probe manufacturing and optimization, as well as development of protocols for the analysis and quantitation of ketamine and its metabolites via LC-MS/MS and DESI-MS/MS were carried out at the Department of Chemistry of the University of Waterloo by the author of this thesis. All data processing and writing of the related discussion presented herein have been completed by the author of this thesis.

Chapter 5 contains study carried out in collaboration with the Centrum for the Addiction and Mental Health (CAMH) in Toronto and has been published as an article entitled *Investigation of early death-induced changes in rat brain by solid phase microextraction via untargeted high resolution mass*

spectrometry: in vivo versus post mortem comparative study (*Chemical Neuroscience* **2020**, 11, 1827-1840), co-authored by Mariola Olkowicz (equally contributing), Ezel Boyaci, Miao Yu, Mustansir Diwan, Clement Hamani, Michael Palmer, Nathaly Reyes-Garcés, Germán Augusto Gómez-Ríos, and Janusz Pawliszyn. J. Pawliszyn and C. Hamani initiated the collaboration, secured the funding, conceived the studies, and contributed to data interpretation. The *in vivo* sampling was carried out in the facilities of the CAMH by M. Diwan, with the assistance of S. Lendor, E. Boyaci, N. Reyes-Garcés and G. A. Gómez-Ríos. C. Hamani performed the surgeries on the animal subjects. The post-processing experimental work and instrumental analysis was carried out by the author of this thesis with the assistance of E. Boyaci. The untargeted data processing was performed by the author of this thesis with the assistance of M. Olkowicz and M. Yu. Data interpretation and discussion was written by the author of this thesis and M. Olkowicz, with significant contribution from M. Palmer. The manuscript was written by the author of this thesis with the assistance of M. Olkowicz.

Abstract

Adequate and quantitative observation of neurochemical phenomena is instrumental in guiding efforts towards a better understanding of the mechanisms underlying brain functions. Although a plethora of highly focused mechanistic studies have been conducted to unravel or approximate the cause-result relationships of brain activities, the scattered pieces of fragmentary information often fail to consolidate into a holistic picture of brain's functional organization. Therefore, basic and applied brain research continues, powered by an explosive expansion of integrated initiatives and techniques continuously advancing the existing pool of knowledge. *In vivo* neurochemical monitoring in model organisms represents an invaluable strategy for capture of dynamic events or neural communication and the physiological state of the brain's chemical environment at homeostasis (or purposefully dysregulated). However, it also remains technically and experimentally challenging due to many restrictions regarding the choice of subjects, target analytes and the opportunity to reproduce or repeat the experiments in the future, as well as suitability and performance of existing *in vivo* techniques.

Solid phase microextraction (SPME) has inhabited the analytical chemistry landscape for several decades, however the progressing understanding of the microextraction phenomena applied to dynamic systems with minimal disturbance has only recently received recognition in the field of *in vivo* monitoring and granted the opportunity for SPME to grow beyond the proof-of-principle area. The chemical biopsy operation mode of this technique ensures that no tissue is removed or collected during the integrated sampling and analyte isolation step. The diffusion-based extraction of negligible amounts of an analyte from its unbound pool by the biocompatible probe spares the sampled system from drastic physiological re-adjustments to replenish its metabolites, and the binding to matrix components remains largely unchanged. These features, in principle, minimize disturbances to the studied system, making the *in vivo* results a close representation of its physiological state at the time of sampling. The work presented in this thesis capitalizes on these features and aims at critical stress-testing of SPME in several

studies involving diverse instrumental modes and scientific questions, with the *in vivo* neurochemical analysis of small molecules as the common theme.

One prerequisite for understanding neuronal communication and circuitry is the ability to dynamically measure concentrations of neurotransmitters in multiple brain regions simultaneously. This goal has been addressed by development of a miniaturized SPME-based probe, specialized for extraction of small hydrophilic molecules via synthesis and functionalization of the SPME extracting phase. The protocol for integrated *in vivo* sampling/sample preparation followed by LC-MS/MS analysis has been thoroughly characterized with respect to probe shape, desorption solvent, storage strategy, quantitative performance, and the balance between temporal resolution and sensitivity. The resulting tool and workflow were subsequently applied to the simultaneous electrophysiology-guided measurement of several neurotransmitters in three areas belonging to the fronto-striatal network in behaving macaques. The results indicated realistic prospect and capability of this approach to distinguish chemical fingerprints of different behavioral or pharmacologically induced brain activation states.

The linkage of molecular information with its spatial distribution in such complex system as the brain has been the aim of coupling SPME to desorption electrospray ionization mass spectrometry (DESI-MS) to yield a platform for unidimensional, spatially resolved analysis with quantitative capabilities. The work documents the development of a hardware interface for the coupling, and evaluation of the experimental protocol through quantitative reconstruction of the laminar and radial concentration gradients of xenobiotics introduced in multilayer gel arrangements and surrogate brain tissue models. Adequate quantitative results were achieved by proposing a novel strategy that combined signal correction via preloading of internal standard onto SPME probes and signal integration in scan-by-scan mode. The proposed approach allowed for fast and minimally-invasive probing and imaging of three-dimensional objects without the need for their slicing, allowing for *in vivo* applications with reduced number of required probe insertions, relative to SPME-LC-MS approach, in order to obtain information about analyte distribution with sub-millimeter resolution.

The culmination of the outlined strategies is subsequently illustrated by the development and *in vivo* application of a protocol for quantitative and spatially resolved analysis of a xenobiotic and its metabolites in rodent brain, tailored for characterization of local drug delivery via stimuli-responsive drug-loaded nanoparticles which release their cargo focally upon application of focused ultrasound. The presented data illustrate an SPME methodology capable of monitoring pharmacokinetics of ketamine and its metabolites in the infralimbic region of the medial prefrontal cortex *in vivo* after systemic administration of the drug. The space-resolved component of this study further explores the SPME-DESI-MS in terms of fundamental phenomena pertaining to the properties of the extractive substrate, interactions with microdroplet-based DESI mechanism and the resulting method performance. This work results in the first instance of unidimensional molecular imaging applied *in vivo* with subsequent LC-MS cross-validation.

Due to the high energy demand of brain and its vulnerability to metabolic stress, many neuronal properties expected to be valid in physiological conditions cannot be reliably inferred from *in vitro* experiments. The importance of *in vivo* studies is herein emphasized by investigation of changes in brain neurochemistry occurring immediately and shortly after death. The broad analyte coverage characteristic for SPME and untargeted analysis mode enabled by MS have been combined to determine death-induced changes affecting rat hippocampus in the first hour of postmortem interval (PMI). Significant changes in brain neurochemistry were found to occur as soon as 30 min after death, further progressing with increasing PMI, evidenced by relative changes in levels of metabolites and lipids. These included metabolic intermediates, signalling molecules, and inflammatory mediators. Additionally, thorough analysis of interindividual variability in response to death provided insights into how this aspect can obscure conclusions drawn from an untargeted study at single metabolite and pathway level.

Acknowledgements

I would like to thank the following individuals who enabled the completion of this PhD thesis.

The Supervisor
Professor Janusz Pawliszyn

The Advisory Committee Members
Professor Wojciech Gabryelski, Professor Michael Palmer, and Professor Thilo Womelsdorf

The External Committee Members
Professor Robert Kennedy and Professor Mark Servos

The Collaborators

Vanderbilt Team
Professor Thilo Womelsdorf and Ali Hassani

Stanford Team
Professor Raag Airan, Jeff Bond Wang, Daivik Vyas, Niloufar Hosseini-Nassab, and Mahaveer Prasad Purohit

CAMH Team
Professor Clement Hamani and Mustansir Diwan

UW Science Technical Services
Harmen Vander Heide, Hiruy Haile, Andrew Dube, Peter Kessel, and Krunomir Dvorski

UW Mass Spectrometry Facility
Dr. Richard Smith

Waterloo Advanced Technology Laboratory (WATLab)
Dr. Nina Heinig

The Industrial Partner – Waters Corporation
Dr. Mike Morris, John Vukovic

To whomever else gratitude is due – it was expressed in person.

Table of Contents

List of Figures

List of Tables

Chapter 1
Introduction

1.1 Brain-focused science: why study the most complex system in the Universe?

The significantly delayed emergence of fully autonomous androids originally expected to take place as early as in 1992 by science-fiction writer Philip K. Dick[1] is a result of the fact that human brain consists of over 120 billion neurons[2] (which are additionally outnumbered by glial cells) and more than 150 thousand kilometers of wiring in the form of myelinated neural fibers, creating several hundred trillion synaptic connections (a trillion synapses per cubic centimeter in the cerebral cortex alone).[3] Brain is the most complicated system in the universe[4] (known to humans), and also the most important and complex organ in a human body (according to the brain). Therefore, simulating human brain with the complexity of its neural circuitry is currently exponentially beyond the reach of existing technology and might remain so for the foreseeable future. So far, artificial neural networks have failed to do justice to the complexity required for brain-like functioning as well as encountered trouble overcoming issues posed by the incompleteness of the theory of thought.[5,6] Nevertheless, progress in understanding the brain through neuroscientific efforts continues to stimulate further developments in deep neural network technology, and vice versa.[7] Currently, neural networks do not present themselves as a good approximation of the self-aware, thought-generating mind formed as a result of a long evolutionary process[5]—however the pursuit of its recreation has undoubtably yielded technologies which revolutionized almost every aspect of modern life.[8]

What is then the point of studying brain using scientific methods? The first answer is: disorders. Improved understanding of brain's organization and functioning constitutes a logical step towards understanding the causes and mechanisms of disorders, which can in turn be addressed in an attempt to provide treatment.[9] In case of many brain disorders, especially those of neurodegenerative character, effective treatment strategies, conclusive etiologies or detailed mechanisms remain to be found.

Studying pathological brain states requires a comprehensive approach, as they are often associated not only with imbalances in neurotransmission systems, but also with connective patterns and neuronal synchronization[10,11]

Not necessarily all approaches in brain research aim at treating disorders; some have more of an exploratory role, aiming at answering questions pertaining to cognitive, affective and behavioral aspects, and ultimately the question of what makes us *us*.[12] It must also be noted that the basic research on brain structure, function, and circuit mapping does not cease. These aspects are indispensable pre-requisites to further exploration and interpretation of more complex inquiries such as linkage of specific neural activity patterns to behavior and cognition or the mechanisms of brain disorders.[9,13]

Finally, by generating complex questions (*de facto* about itself), human brain ultimately inspires development of more sophisticated and advanced technologies, aimed not only at recreating or simulating the brain, but also creating appropriate research tools required for studying it.

1.2 Current state of affairs in *in vivo* brain research

The second decade of 21st century marks an explosive expansion of integrated initiatives aiming at advancing brain research worldwide.[13,14] Of particular interest to this thesis is that the focal points of these initiatives include emphasis on micro- and nanotechnologies in service of measurements of brain activity and probing of the neurochemical environment. This involves not only improvement and advancement of the existing tools that are already a commonplace in neuroscience (for example, electrophysiological recordings), but also reaching far beyond what is currently considered possible, with ambitious objectives of overcoming fundamental limits in pursuit of new discoveries.[15] Finally, the intermediate category comprises existing techniques that may originate from fields other than neuroscience with the intention of expanding them beyond the existing proof-of-concept phase and

fine-tuning them to address biological questions pertaining to brain function. Contrary to those initial proof-of-principle studies, the next stage of investigation is intended to focus not on the technique itself, but on its contribution and suitability for answering fundamental questions about the nervous system.[13.15]

Enter analytical chemist. How does a scientist whose primary purpose is to pick things apart using intricate methods until they reveal their quality and/or quantity fit into the realm of big questions about the nature of thought and finding cures to diseases? Surprisingly (or perhaps not) neuroscience has adapted the science of measurement to a tremendous extent,[16,17] to which the *in vivo* measurements of neurochemicals in animal model are the best evidence. Moreover, analytical chemistry is a valuable source of techniques which were abandoned after the initial proof-of-concept but have a massive potential to be useful in other fields.

Further introduction and discussion will focus only on selected *in vivo* non-imaging techniques, as any attempt of doing justice to all existing *in vivo* methods in service of neuroscience would inevitably yield outrageous oversimplifications.

In vivo studies are perhaps more important in studying brain than they are with other organs. Due to the exceptionally high energy demand of brain, vulnerability to metabolic stress in the situation of energetic imbalance is inevitable. Since maintaining energy homeostasis in brain is a task of its own, functioning of neurons cannot be the same *in vivo* and *ex vivo*, when the energy reserves are shut down. Therefore, many neuronal properties expected to be valid in physiological conditions are not reliably transferable from *ex vivo* experiments.[18] *Ex vivo* investigations of even the most basic neuronal parameters using acute slice preparations might not be relevant for *in vivo* translation, as the effective electric field strength values required to give rise to action potentials and induce modulation of neuronal activity have been found to be much lower upon brain activity termination.[19] Considering that neural

communication is based on transient release of neurotransmitters from synaptic vesicles, and the extremely short half-life of some of these molecules in brain parenchyma, the timescale and dynamics of neurochemical events and their consequences requires an *in vivo* approach with high temporal resolution.[20] For pharmacological investigations or drug discovery studies it is of utmost importance to measure neurotransmitters and metabolites in awake and freely-moving animals both before and after administration of agents expected to affect the target neurotransmission systems.[21] As the correlation between the efficacy of a neurotherapeutic and its brain concentration is an important pharmacokinetic parameter, accurate measurements of unbound drugs *in vivo* are indispensable in drug development.[22] Finally, surrogate *ex vivo* systems and cell cultures often fail to represent the level of complexity and physiological functions existing in a living organism.[23]

In brain, again to a greater extent than in any other organ, maintaining the structure integrity and connectivity for various measurements is essential, due to its heterogeneity. Besides the obvious structural and functional levels of brain organization, neurochemical heterogeneity is also present within particular brain structures such as striatum and prefrontal cortex.[24,25] Moreover, even diffusion of chemicals in brain exhibits heterogeneity and anisotropy.[26]

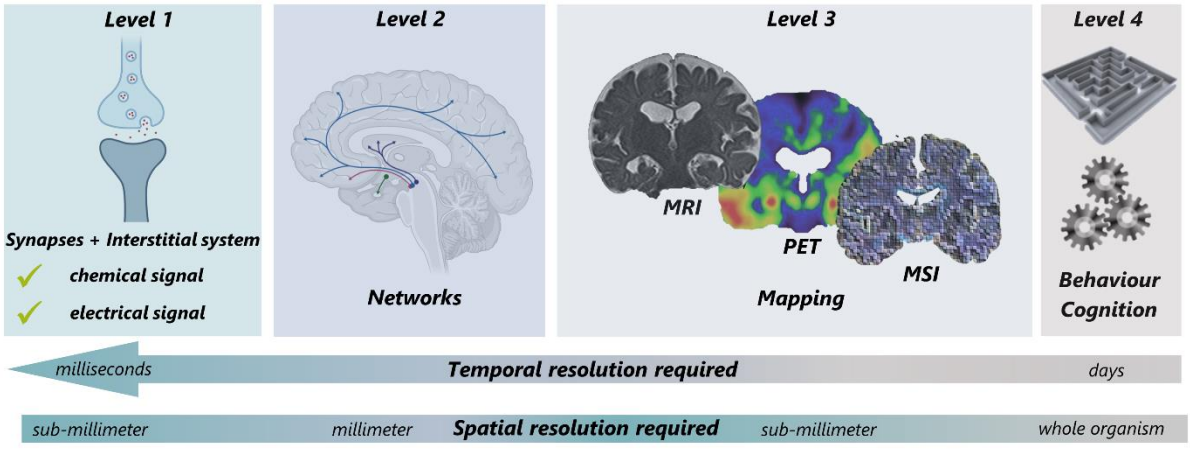

Figure 1.1: Simplified levels of brain organization illustrating the comprehensive nature of investigation methods required to cover the range of spatial and temporal resolution of measurements. MRI- magnetic resonance imaging, PET- positron emission tomography, MSI- mass spectrometry imaging.

Obviously, *in vivo* research is not free from limitations. *In vivo* methodologies often incur significant costs and are hindered by complexity, therefore are unsuitable for high-throughput pharmacokinetic studies at early stages of drug development.[22,27] Regarding the ethical aspect of *in vivo* studies, the 3R rule of replacement, reduction, and refinement puts in place guidelines regulating animal experimentation and welfare, however some invasive *in vivo* practices in animal research continue to face ethical concerns.[27] Nevertheless, *in vivo* experimentation on animal models remains invaluable as some mechanistic investigation and validation (e.g. lesion studies of behavior and cognition or knockout of genes for causality confirmation) can only employ animals.[28,29]

1.3 The need for (purposeful) innovation

Despite years of tireless brain research by scientists from many branches related to neuroscience constantly innovating their tools and theories, the overall picture of brain functioning and its disarray in disease state remains incomplete. While lack of effort can definitely be ruled out as the cause, brain complexity outlined previously is only partially responsible. The scattered state of the knowledge and lack of appropriate research tools can be pointed as specific areas in the need for improvement.[15] To be fair, *research tools not good enough* will perhaps remain an issue for eternity, as new tools lead to new discoveries, which bring more questions requiring even more advanced tools.

In the meantime, thorough review of the *future directions* sections of published studies, a list of ideal properties can be outlined for a technique characterized by high usefulness in brain research. Considering spatiotemporal characteristics of neurochemical events, the innovation direction should allow for simultaneous measurements of multiple modalities (*i.e.* molecular, electric, and imaging) in multiple brain regions in awake, behaving animals, with the possibility of local, non-disruptive delivery of pharmacological agents. All these goals additionally align with considerations for animal well-being in *in vivo* approach. Specific types of experiments would then require further features, for example,

capability to conduct high-throughput *in vivo* analysis for drug development studies or capability to monitor a broad range of molecular species simultaneously with physiological parameters for disease markers studies.

What might look suspicious in the above list is that all the components already exist and are being employed in neuroscientific research. However, what still makes the claimed innovation of the outlined approach valid is their integration and simultaneous employment. One might also wonder what the purpose of new developments is, since there exist outstanding techniques (*i.e.* microdialysis) which fit most of these requirements and are being used in neuroscience in conjunction with other tools. Firstly, every innovative methodology recognizes its limitations – no technique is a panacea, and enhancement of a single tool is a process that never truly ends. Secondly, innovation means range and variety to choose from to satisfy one's goals and specific scientific questions. Additionally, competitiveness between existing approaches and techniques (provided a healthy competition) also drives innovation by inspiring unusual solutions. Finally, scientists have their areas of expertise, preferences, and technical capacity (e.g. access to mass spectrometers or animal facilities). All this leads to the conclusion that the ultimate innovation perhaps lies in multidisciplinary approach as the most productive research model. Complex studies require the collaboration of many specialists, each bringing their unique expertise and skill set. The needed components include theories and hypotheses linked to properly designed experiments, development and application of experimental tools with consideration for their engineering and performance for a given purpose, animal models, instrumental platforms, data treatment and sharing, as well as validation via critical feedback loop between parties involved at each stage of the process. Valid and successful tools would be then given its own life by subjecting them to circulation and making them available for others.

On the note of innovation, it is easy to take mass spectrometry (MS) for granted. This technology has become so commonplace in analytical chemistry that it is by some seen as a routine detector,

inarguably with many operation modes and capabilities, but a detector nevertheless. For instance, mass spectrometers were used as the only "detector" type sufficient for the completion of this entire thesis. Throughout many published studies only a short instrumentation section is allotted to acknowledge that a single piece of instrumentation was used to detect hundreds or thousands of molecular species within seconds or minutes. In truth, mass spectrometry-based approaches constitute some of the most robust analytical methodologies with the most versatile qualitative and/or quantitative information available to obtain from complex biological samples.[30] Therefore, the continuous, unrelenting advancement in mass spectrometry will undoubtedly benefit any field that adapted this technology, including *in vivo* neurochemical analysis.

MS imaging deserves a special mention here. The unique features of this MS methodology enabling linkage of molecular information with spatial distribution within the sample[31] have contributed to its adaptation and expansion in neuroscience.[32] With versatility of several ionization mechanisms available for MS imaging, such as matrix-assisted laser desorption/ionization (MALDI), secondary ion mass spectrometry (SIMS), and desorption electrospray ionization (DESI), MS imaging has been successful in mapping small molecules (metabolites, neurotransmitters, and lipids) as well as peptides and macromolecules (nucleotides, glycopeptides, and peptides).[33,34] Even though this approach currently lacks real *in vivo* capabilities (this aspect has been further elaborated on in Chapter 4), the spatially-resolved analysis is a strength that plays to the issue of heterogeneity of brain tissue.

1.4 Solid phase microextraction: a condensed overview

Microextraction constitutes a branch of analytical techniques characterized by employment of extraction phase in amount that is significantly smaller than the sample volume and therefore generally does not allow for exhaustive extraction.[35] Solid phase microextraction (SPME) is an equilibrium-based technique which utilizes small volume of extracting phase dispersed on a solid support to isolate and

enrich analytes from a sample via diffusion-based partitioning mechanism by exposing the extracting phase to the sample for a well-defined period of time.[36] SPME further translates this concept into a family of sub-techniques with the common denominator of solid extraction phase being immobilized in a form factor enabling direct contact of the extracting phase with the sample. What is common for all existing formats and operation modes of SPME is integration of the analytical process into just several simple components, as the sampling, analyte isolation and preconcentration constitute a single step. Moreover, all SPME modes are characterized by environmental sustainability,[37] by minimizing the use of solvents required for analyte extraction and desorption (solvent desorption mode and LC applications), eliminating the use of solvents altogether (thermal desorption mode and GC applications[38]) or being in the grey area of solvent consumption, where only as much as several tens of microliters of solvent are used per sample analysis (direct-to-MS approaches[39]).

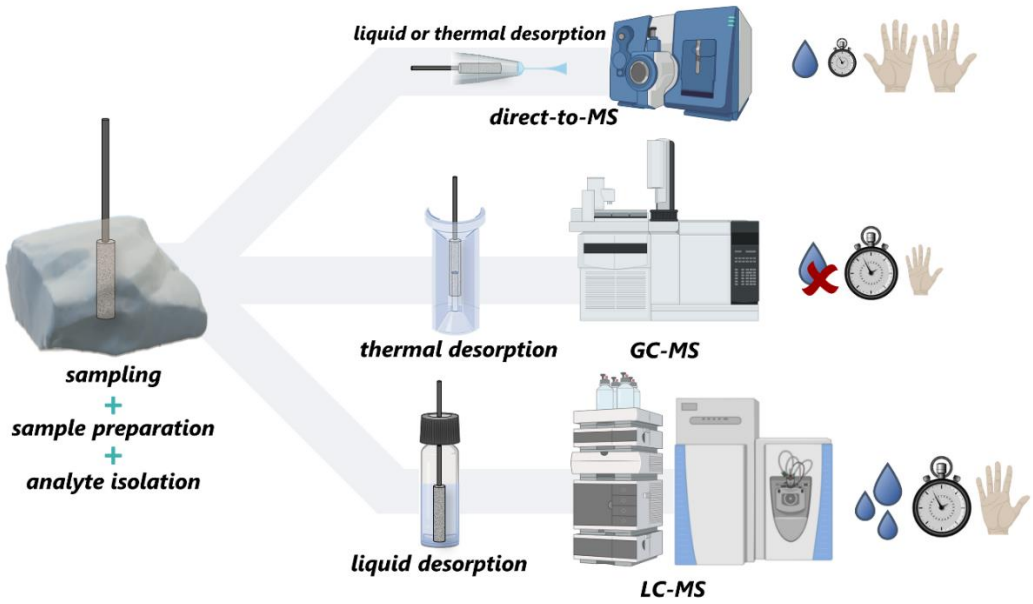

Figure 1.2: Available modes of coupling SPME to analytical instrumentation. The integrated sampling step combining sample preparation and analyte isolation can be followed by direct coupling to MS bypassing the separation step or undergo thermal or liquid desorption with subsequent GC or LC separation, respectively. Each strategy is characterized by certain solvent consumption, analysis time, and labour intensity schematically depicted in the figure.

Applications of SPME have populated multiple research areas, such as clinical analysis,[40] metabolomic and lipidomic research,[41] environmental monitoring[42,43] with prominent applications in water analysis,[44] food and agricultural products analysis,[45,46] and forensic toxicology[47] to name a few. Commercialization of SPME provided a *level-up* from purely academic use to routine laboratory practice[48] (in areas such as forensic analysis of volatile organic compounds in autopsy materials or environmental analysis of air pollutants), with many more methodologies meeting the appropriate requirements to keep up with regulated methods[49] or showing a promise of becoming so, yet lacking the inter-laboratory validation component.[50,51] The breadth of applications employing SPME has its source in the technique's simplicity and high level of tunability, whether regarding to the device format,[52] extracting phase chemistry and properties,[53,54] or coupling to various instrumental modes.[55]

The non-exhaustive and diffusion-based principle of SPME makes it relatively heavy on fundamental and theoretical aspects, whose understanding is crucial for its proper implementation and quantitation. In the simplest example, an SPME experiment consists of extracting phase exposure to the sample (here often referred to as *sampling*) and subsequent desorption. Desorption can be performed on-line, integrating this process with instrumental analysis (gas chromatography (GC) and direct-to-MS applications) or off-line, which permits the simultaneous desorption of multiple devices followed by high-throughput unsupervised instrumental analysis (liquid chromatography (LC) applications).

Sampling is time-dependent: analyte extraction commences as soon as the extracting phase comes into contact with the sample and the affinity-driven, diffusion rate-controlled mass transfer occurs until partitioning equilibrium is reached between the analytes and the extracting phase. The amount of analyte extracted as a function of extraction time (the so called extraction time profile) reflects the kinetics of SPME, which can be divided into *kinetic regime* and an *equilibrium regime*, describing the various rates of analyte adsorption over time. The initial linear portion of the kinetic regime reflects the fastest adsorption of the analyte, while the equilibrium regime reflects a period of only marginal further

analyte collection.[56] Under conditions fully characterized by the sample matrix and the extracting phase, the quantity of a given analyte extracted in equilibrium conditions (n_e) can be determined based on equations 1.1 and 1.2 for absorptive and adsorptive extracting phases, respectively.

$$n_e = C_s^0 \frac{K_{es} V_e V_s}{K_{es} V_e + V_s} \quad [1.1] \qquad n_e = C_s^0 \frac{K V_e V_s (C_{e\,max} - C_e^\infty)}{K V_e (C_{e\,max} - C_e^\infty) + V_s} \quad [1.2]$$

Where: C_s^0- concentration of analyte in the sample; K_{es}- distribution constant of analyte between the extracting phase and the sample matrix; V_e- volume of the extracting phase; V_s- volume of the sample; *K*- adsorption equilibrium constant of the analyte; $C_{e\,max}$- maximum concentration of the active sites in the extracting phase; C_e^∞- concentration of the analyte in the extracting phase at equilibrium.

The view that only equilibrium SPME can yield quantitative results is a common misconception. The quantity of an analyte extracted in pre-equilibrium conditions (*n*) is extraction time dependent and can be determined according to equation 1.3.[57]

$$n = n_e(1 - e^{-at}) \quad [1.3]$$

Where: *t*- extraction time; a- time constant (determined by the mass transfer coefficients, equilibrium constant as well as the physical dimensions of the extracting phase and the samplematrix; *a* is constant when the agitation conditions are also constant).

The main consequence of pre-equilibrium extraction is decreased amount extracted, which can translate to higher limits of detection (LOD) and quantitation (LOQ), as well as the fact that dynamic character of the time profile in pre-equilibrium may contribute to reduced precision, if the extraction time is not strictly consistent for all samples/replicates. These repercussions are however a reasonable trade off and can be relatively easily compensated via fine-tuning of other aspects of the method development, as in reality employing extraction times allowing for reaching equilibrium may be impractical.

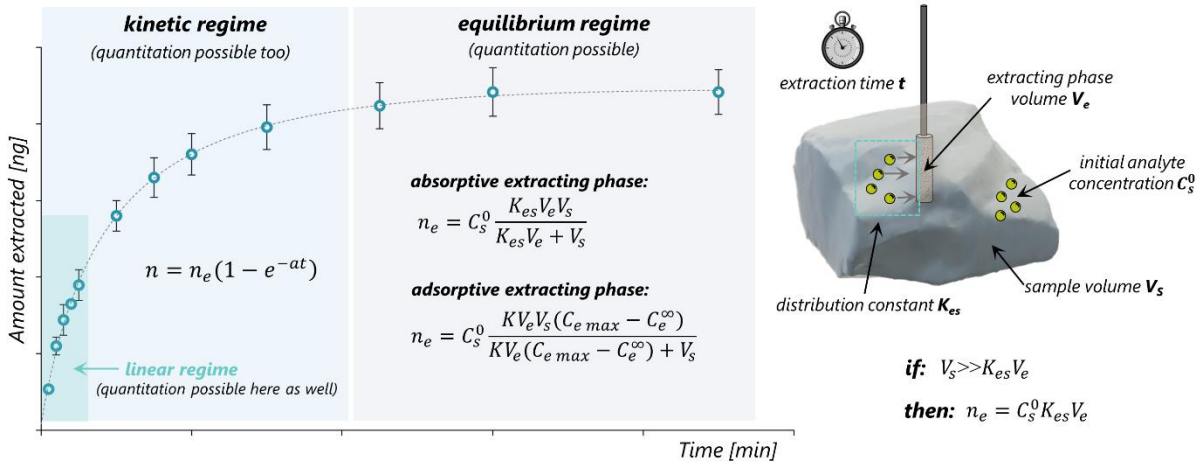

Figure 1.3: Kinetics of SPME illustrated by the extraction time profile with fundamental relations allowing for quantitation in all regimes of the kinetic curve.

While other fundamental aspects of SPME have been eloquently described elsewhere with great level of detail,[55] it is perhaps important to the practical aspect of SPME-specific method development that mass transport is affected by variables such as the binding matrix[58] and device geometry,[59] which in turn influence the extraction kinetics and equilibration time (t_e) according to equation 1.4. The equilibration time is assumed to be attained when 95% of the equilibrium amount of the analyte has been extracted ($t_{95\%}$).

$$t_e = t_{95\%} = \frac{3\delta_s K_{es} d}{D_s} \qquad [1.4]$$

Where: K_{es}- distribution constant of analyte between the extracting phase and the sample matrix; D_s- diffusion coefficient of the analyte in a given sample matrix; δ_s- volume of the boundary layer (an area surrounding the extracting phase where the flux of the analyte is controlled predominantly by diffusion); *d*- extraction phase thickness.

What the above translates to in practice is the influence of agitation conditions, coating thickness, and sample properties (*i.e.* tortuosity, presence of binding matrix, *etc.*) on SPME kinetics as well as analyte quantities extracted within a given pre-equilibrium time. Other relevant fundamental principles (especially related to diffusion within a tissue sample) will be discussed further on in this thesis in more specific and practically-oriented manner.

It is noteworthy that in practice the kinetic aspects of SPME are usually determined empirically and through calibration rather than from first principles.

1.4.1 Non-standard operation: *in vivo* tissue sampling

It is often stated that SPME integrates sampling and sample preparation, although this statement is only truly correct for *in situ* experiments, where a sample is never collected, and the sampling involves only collecting the isolated molecules on the SPME device. This would include *in vivo* SPME and its equivalent for technically non-living matter (e.g. air, water) sampled in field – *in situ* SPME.

Based on equations 1.1 and 1.2, whenever the extracting phase volume is so small relative to the sample volume that it can be neglected ($V_s >> K_{es}V_e$ and $V_s >> KV_e(C_{e\,max} - C_e^{\infty})$), the extracted quantity of analyte becomes independent on sample volume (equation 1.5).

$$n_e = C_s^0 K_{es} V_e \qquad [1.5]$$

The fact that amounts extracted by the SPME device are independent of the sample volume (when the requirement of negligible volume of extracting phase is fulfilled) and proportional to the initial concentration of the analyte in the sample constitutes the single most important feature that makes this technique suitable for quantitative *in vivo* measurements. This is fortunate for sampling of organs such as brain which, besides occupying a certain volume as a whole, is further divided into distinct functional and structural compartments of not always precisely known volumes. For external *in vitro* calibration of *in vivo* measurements, the threshold volume of a calibration sample at which the requirement of negligible ratio of extracting phase to the sample volume is fulfilled should be evaluated experimentally.[60]

Extraction via free form and balanced coverage

While the extent to which SPME can be considered minimally-invasive and the consequences of probe insertion into living tissue will be discussed in Chapter 5, the generally non-disruptive character of SPME implies that what is effectively being extracted is the free analyte fraction. This contrasts with techniques utilizing tissue collection and sample preparation via analyte isolation from tissue homogenate (for example solid-liquid extraction), which extract both free and bound fraction of the analyte. SPME can however provide information about both free and total analyte concentration in the sample, when calibration in surrogate tissue or non-binding matrix is performed, respectively.[61]

The consequence of extracting via the free form is that analytes with a low degree of binding to matrix components should have larger contribution to the pool of analytes extracted by SPME, and since hydrophilicity inversely corresponds to binding, hydrophilic compounds are often largely present in free form. However, hydrophilic compounds are often characterized by lower affinity towards the extracting phase (*i.e.* lower K_{es} values), which restricts their level of recovery, even if the extracting phase exhibits polar properties.[62] On the other hand, compounds with higher affinity towards the extracting phase (and higher K_{es} values) are likely to be hydrophobic, and therefore predominantly bound to matrix components. This balance between the compounds' availability and affinity prevents saturation of the extracting phase by unbound solutes present in high abundance in biological matrices, as well as allows for extraction of species covering a broad range of physicochemical properties important in untargeted studies.[41,63,64]

The truth is however, that the molecule's hydrophobicity is not the only factor that determines its level of binding. The extent of protein binding is typically determined with blood plasma, but such observations don't apply directly to brain tissue.[65] There, binding may occur both: nonspecifically to brain membrane lipids and proteins, as well as in much more specialized and controlled manner, through receptors or reuptake transporters localized on the cells building the central nervous system, diverse in their morphological, functional, and numerical characteristics.[66] The significant differences

between the free concentration in brain and in blood plasma are observed not only for the molecules that are actively transported through the blood brain barrier (BBB), but also for those that are transported passively or do not pass the BBB at all.[67] Moreover, nonspecific binding interactions with brain lipids and proteins are area-specific due to the regional differences in brain lipid composition.[66]

Biocompatibility

The prerequisite for a technique suitable for *in vivo* investigations is the biocompatibility of all materials building the sampling device, in case of the SPME probe the support, the extracting phase, and the binder. The biocompatibility is a feature ensuring appropriate host response in a given application,[68] in this case lack of adverse effects upon probe insertion into the tissue.[63] Thus, while the supporting metal or metal alloy wire and the polymeric extracting phase are biocompatible and suitable for sterilization, the binder choice is generally inspired by the materials used in biomedical devices, with the additional requirement for appropriate thermal stability and compatibility with organic solvents.[69,70] Due to the lack of continuous sampling and on-line coupling capabilities of SPME, the risks of severe biofouling effects common for biomedical devices[71] are eliminated, as the transient character of SPME sampling and probe insertion does not require long-term implantation.

From the sampling device and analytical performance point of view, the term matrix compatibility describes the properties preventing the probe fouling by interactions with the sample constituents. The most commonly used binder in biocompatible SPME devices suitable for direct immersion and liquid desorption applications – polyacrylonitrile – is characterized by hydrophilicity and creates a negatively charged synthetic membrane between the polymeric extracting phase and the biological environment.[72] These properties make the material inert to the sample matrix and prevent the attachment of macromolecules,[73] which could limit the diffusion of small molecules towards the extracting phase and contribute to decreased recoveries, as well as cause the occurrence of matrix effects along the line in instrumental analysis.[74] Eliminating adhesion of macromolecules and cells also prevents the organism

from triggering its defensive mechanisms,[75] which could in turn influence the physiological environment being sampled.

Given these properties and the principled suitability for *in vivo* analysis it seems that sampling of living organisms should be amongst the primary applications of SPME. In practice, what the technique seems to be built for remains an obscure non-standard operation mode attempted by few, and the routine use by non-experts continues to be a future prospect for this technique.

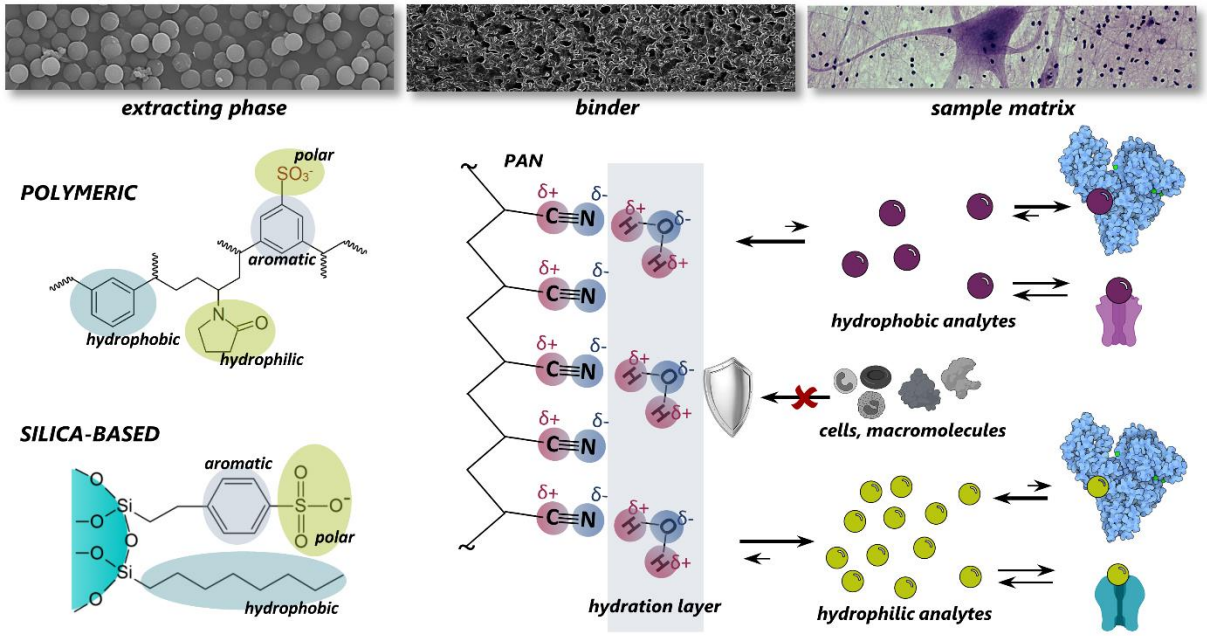

Figure 1.4: Selected properties of all components involved in *in vivo* sampling of brain tissue via SPME. **Left:** The polymeric or silica-based extracting phase (here: hydrophilic-lipophilic polymer- HLB, functionalized with benzenesulfonic acid (top) and octadecyl and benzenesulfonic acid functionalized silicate (bottom), respectively) provide balanced analyte coverage through multiple and various interactions with different classes of compounds. **Middle:** The polyacrylonitrile (PAN) binder introduces biocompatibility through formation of hydration layer with the aqueous environment of the sample, limiting the attachment of macromolecules and cells. **Right:** The availability of an analyte for SPME is a product of its physicochemical properties and the extent of its binding to proteins and receptors, as well as the coefficient of partitioning between the sample matrix and the extracting phase (generally lower for hydrophilic molecules and larger for hydrophobic compounds).

Measuring dynamic concentrations

A major challenge of *in vivo* brain analysis is the dynamic character of release and uptake of neurochemicals resulting in effectively establishing multiple equilibration profiles throughout the sampling event.[76] Perhaps a good mental visualization of this process is a loading bar that starts increasing when the extraction commences, however every time a release of neurochemicals takes place during the extraction- the progress restarts. This process is additionally obscured as the reset loading bar is now a different, alternate loading bar not identical to the initial one, due to the fact that when the neurochemical event occurred, the probe already extracted certain amount of the analyte.

Due to the fluctuating concentration of analyte in the sample, the statement for equation 4 can be modified to state that the amount of an analyte extracted via SPME is proportional to its average concentration in the sample over the sampling time.[35] This case is called the time-weighted average sampling (TWA) and it's been adapted from its previous employment in cases where the concentration of analytes varies over long periods of sampling time, such as in case of in situ water and air analysis, and the access to the extracting phase is spatially restricted.[77] The important consequence of the inevitable TWA model of sampling in live brain is that if the concentration of a neurochemical was to significantly decrease as a result of re-uptake or depletion, the extraction equilibrium may shift all the way towards desorption from the extracting phase into the tissue (this would be additionally dependent on the interaction type between the extraction phase and the analytes – this aspect will be discussed in Chapter 2). Thus, to prevent analyte leaching via reversed diffusion, it is recommended to employ short sampling times.[78] This would not only contribute to improvement of precision of TWA measurements, but also to enhancement of the temporal resolution of the sampling. Practically, the dynamic neurochemical events such as neurotransmitter release, degradation, and reuptake occur on a sub-second timescale, well below the typical SPME sampling times of several or several tens of minutes. Moreover, many neurochemicals and metabolites operate within distinct physiological concentration

range. Therefore, unless the extraction time is decreased to sub-second duration, these strategies are expected to play less of a role in *in vivo* brain sampling than in *in situ* environmental analysis.

Calibration of *in vivo* measurements

Several approaches have been proposed for calibration of *in vivo* measurements in pre-equilibrium conditions as well as successfully employed in real cases.[79] One such method is the kinetic calibration with internal standard (IS) preloaded in the extracting phase. This strategy assumes that desorption of the IS preloaded in the extracting phase in known quantity will occur in the sample, as well as that the kinetic profile of IS desorption will be symmetrical to the uptake of target analyte from the sample. Based on the knowledge of the amount of IS desorbed, the amount of analyte extracted can be calculated if the distribution constant of the analyte between the extracting phase (K_{es}) and the sample matrix and the extracting phase volume (V_e) are known.[36] Since the calibration occurs in the target system, this approach compensates for the fact that the agitation conditions (in *in vivo* system related to tissue perfusion rather than actual agitation) cannot be reproduced during external matrix-matched calibration, as well as for any diffusion difference effects related to temperature and presence of the binding matrix.[80,81] This strategy has been previously successfully employed for calibration of *in vivo* measurements in rodent blood,[82] fish muscle tissue,[83] and rodent brain.[84] The reliance of isotopically-labelled IS, high level of reproducibility of IS preloading, and the requirement of the desorbed amount being measurable and significantly larger than experimental error are practical limitations of this approach. However, a fundamental limitation can also be found when considering the suitability of method introducing exogenous molecules into the sample for *in vivo* brain analysis with a behavioral component or when monitoring the undisturbed neurochemical environment in its physiological conditions is of interest. In these cases, it is likely that the threshold or sub-threshold amounts of

desorbed IS (which is purposefully almost identical to the target molecules) could alter the sampled environment, biasing the obtained results.

The standard-free kinetic calibration approach was conceived as a remedy to the inconvenience or inability to match target analytes with appropriate internal standards with high similarity of physicochemical properties, as well as to insufficient IS desorption during a short sampling event.[85] This method only requires sampling of the target system at two different time points to calculate the concentration of analyte in the sample. Similarly, the knowledge of the K_{es} and V_e are required. Moreover, this method assumes the sampling rate to be constant throughout the entire extraction period,[36] which excludes its suitability for calibration of measurements in dynamic systems such as the brain. For these reasons, this approach has been only proven suitable for *in situ* sampling of water an air using absorptive extracting phases, rather than *in vivo* sampling of tissue with solid, adsorptive coatings.

The outlined calibration approaches rely on knowledge of constants determined via *in vitro* experiments,[83] in tissue homogenates, or complex flow-through systems in equilibrium conditions. This proves that for *in vivo* measurements the idea of a method which does not employ a system attempting to mimic the target conditions is highly elusive or impossible. In this case, the conventional external matrix-matched calibration strategy constitutes an adequate solution for *in vitro* calibration for *in vivo* measurements, characterized by its ability to accurately reflect the composition of matrix binding sites occurring in live tissue. The main limitation of this approach is however the lack of the ability to appropriately mimic the conditions of flow-mediated solute transport occurring in live brain. The suitability of tissue homogenates as a surrogate matrix for calibration of measurements in intact tissue have been confirmed for lung analysis.[60] The several advantages of this approach include practical simplicity and adjustability of the calibration range to multiple analytes existing at drastically different concentration levels. The calibration range modification and the matching of IS to analytes for suitable

correction can be done *post hoc* and directed by the knowledge obtained from *in vivo* experiments. Moreover, external calibration can be made independent of the variable instrumental response by simple conversion of the calibration relation to amount of analyte extracted as a function of concentration in the sample. This allows for building only one matrix-matched calibration curve for multiple *in vivo* measurements analyzed in batches, which is particularly useful for long term behavioral studies.

1.5 The tale of two *in vivo* sampling techniques

A staggering majority of SPME literature on the subject of *in vivo* sampling contains a comparison to microdialysis (MD) as a technique to match, outperform and triumph over. Similarly, throughout this thesis, making several comparisons could not be avoided. The purpose of this sub-section is to prove that this is due to the similarity of these two techniques and a natural drive of the younger of the two to look up to the more senior, gain approval and respect, and be allowed to sit at the same table (the table here is *in vivo* neurochemical analysis in truly exploratory studies, beyond the proof-of-principle applications). It only makes sense to compare tools that are akin to one another and based on related principles (similarly to the only valid comparison of two Formula 1 drivers being their evaluation of driving in equal machinery).

Based on the provided overview, one might realize that SPME is characterized by simplicity, versatility and capability of providing good figures of analytical merit. However, the application to *in vivo* brain analysis is a more complex case: throughout the method development process the experimental parameters cannot always be chosen arbitrarily or freely to provide competitive figures of merit, as is the domain of proof-of-concept studies. The parameter choices in *in vivo* analysis are predominantly guided by practicality and the very clearly defined goals of the studies. Perhaps the best example to illustrate this is the choice of extraction time: while longer exposure times are favorable for

attaining better sensitivity via SPME, the realistic timeframe of *in vivo* experiment often limits the extraction to only several minutes and requires a rapid sampling. Examples of such cases include monitoring of neurochemistry during transient states in studies with behavioral component, monitoring of drug pharmacokinetics (especially with local release of the drug and its fast clearance), or intraoperative sampling in clinical analysis.

To conclude the dispute on differences between SPME and MD and the areas of their superiority: temporal resolution, on-line coupling capabilities, and proficiency at extracting highly hydrophilic molecules are the domains of MD,[86,87,88] while high affinity towards hydrophobic molecules, low experimental complexity, and versatility of coupling to various instrumental modes are the strengths of SPME.[70] Otherwise, multiple aspects and limitations remain shared, such as fairly complex calibration strategies, challenge of measurements in dynamically changing systems, the potential for disruption of the studied system by requiring probe insertion, *etc.* The progressing amenability for miniaturization[89,90] and quantitative capabilities,[91] remain common for both techniques as well.

Another shared feature is the fact that both techniques show unquestionable promise (SPME) or approval (MD) for *in vivo* brain studies, despite being invasive and inevitably causing an insult to the neural tissue upon probe insertion. This is however a fair price to pay for the ability to employ mass spectrometry, with which both techniques are compatible. The innovation and possibilities brought by MS deem MS-compatible techniques a valuable resource for monitoring the chemistry of brain microenvironments.

Both techniques recover analytes in proportion to their free concentration, which is used in pharmacokinetic studies of neurotherapeutics as the measure of molecules' activity in central nervous system.[22] The multi-analyte extraction ability and coupling to LC-MS determines suitability of MD and SPME for investigation of metabolic changes during neuron activation, as well as the sequence of the

metabolic events, which have been of interest to neuroscience for decades.[92] Importantly for the emphasized heterogeneous nature of brain, the above information can be obtained in area-specific way, with good and constantly improving spatial resolution. Moreover, due to the MD and SPME probe size ranges, the sampled compartment includes predominantly the extracellular space, with some contributions from the vascular system and neural cells ruptured upon probe insertion. The interstitial system constitutes a very important compartment of the brain microenvironment associated with several brain disorders and instrumental for local delivery of neurotherapeutics, and is often overlooked in studies focusing on phenomena related to neural cells.[93]

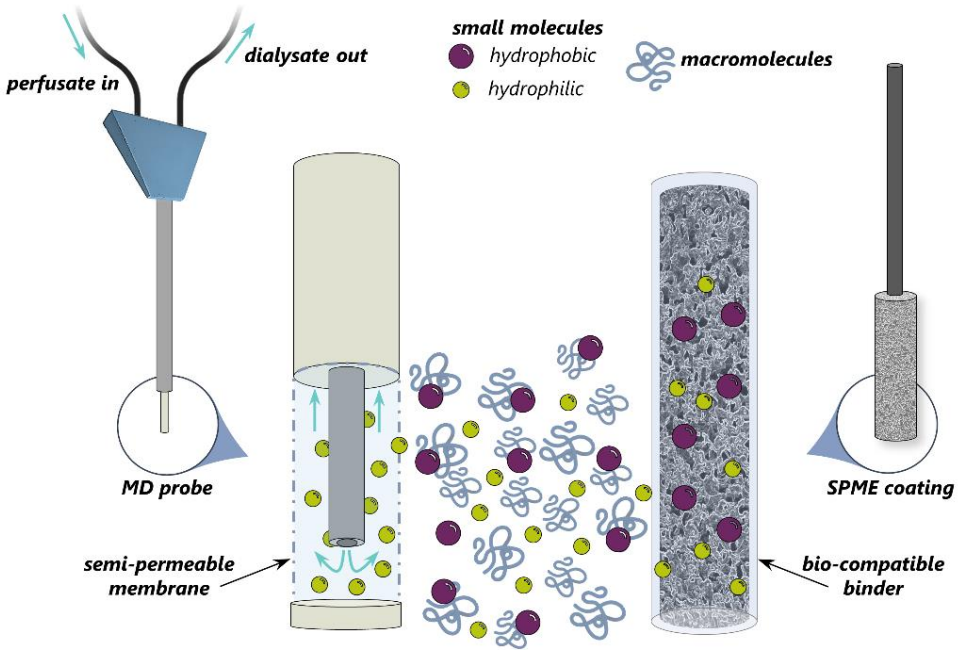

Figure 1.5: Similarities between the principles of *in vivo* MD and SPME and differences between the classes of molecules extracted. Both techniques are diffusion-based and extract via the free fraction of analytes available in the sample. MD extracts small hydrophilic molecules and peptides with high efficiency, while SPME demonstrates higher affinity towards hydrophobic molecules than hydrophobic species.

1.6 Research objectives

The increasing complexity of scientific questions being asked to determine the mechanisms of brain function and malfunction brings the challenge of reliable and versatile monitoring of neurochemical environments to analytical chemistry. The constant drive to improve and refine the existing tools and develop new solutions must satisfy the requirements of neurochemical measurements at various levels of the brain's functional and structural organization, from synaptic events, through neuronal signaling and circuitry interactions to the resulting cognitive and behavioral effects. Approaches relying on the use of one technique may no longer suffice, as any appropriate package of information should ideally contain data about action potentials, molecular identities and concentrations, as well as their linkage to distribution within cortical layers, neural circuits and the whole brain. This thesis explores the use of *in vivo* solid phase microextraction coupled to various MS-based instrumental and data acquisition modes as a chemical biopsy tool for brain studies. The developed *in vivo* sampling approaches have been stress-tested in several model situations or real-life applications involving measurement or monitoring of both endogenous and xenobiotic molecules in order to identify the technique's place in interdisciplinary neuroscience research and the barriers to its broad adaptation beyond the proof-of-principle studies.

The introduction was meant to provide general insight into motivation behind brain studies and the challenges associated with it from the interdisciplinary standpoint, as well as outline the theoretical principles of solid phase microextraction. Details pertaining to the analytical aspects and techniques employed for neurochemical and pharmacokinetic monitoring are discussed in the introductions to respective chapters.

Fulfilling the identified need for a multidisciplinary approach, **Chapter 2** follows the development and validation of a new SPME probe and methodology dedicated for quantitative analysis of neurotransmitters *in vivo* in nonhuman primates. The first phase involved thorough optimization of the

extracting phase and the probe shape, ultimately fine-tuned to yield an in-house synthesized and functionalized SPME coating immobilized on a recessed support. In the second phase, the protocol has been applied for MRI- and electrophysiology-guided measurement of absolute concentrations of several neurotransmitters in three brain areas simultaneously while nonhuman primates were engaged in goal-directed behavior. The study was further extended to investigate the possible area-specific detectability of other neurochemicals and metabolites in an untargeted metabolomic profiling. The presented approach is evaluated in terms of its applicability as a low-barrier-to-entry tool for measuring multiple neurochemicals in non-human primate brains.

Chapter 3 documents the development of a direct-to-MS coupling of SPME capable of performing spatially resolved measurements utilizing the mechanism of desorption electrospray ionization (DESI). This work follows all necessary steps for establishment of a new derivative technique (created from the pre-existing components of SPME and DESI), including development of a hardware interface for the coupling, designing and testing of the protocols and methods for the analysis and signal processing, and linking the existing fundamental physicochemical phenomena of molecules diffussing in tissue samples to the realistic expectation for the technique's performance. Finally, the system was evaluated through the quantitative reconstruction of the laminar and radial concentration gradients of exogenous small molecules (drugs and pharmaceuticals) introduced in multilayer gel arrangements and surrogate brain tissue models.

Chapter 4 addresses the common need to monitor pharmacological agents, their concentration gradients and distribution margins in brain via rapid measurements in *in vivo* conditions, without the need of animal sacrifice per each sample and tissue slicing, which effectively limit the throughput of pharmacokinetic investigations. This work represents a culmination of several strategies developed in Chapters 2 and 3 and applies the quantitative and spatially resolved capabilities of *in vivo* SPME to characterization of systemic and local release of ketamine in brain via LC-MS/MS and DESI-MS/MS.

This chapter presents an in-depth investigation of parameters deciding the *in vivo* and real-life applicability of the SPME-DESI-MS approach, with regard to the internal standard incorporation into the SPME probe, stability of the spatial imprint during storage, as well as attaining appropriate quantitative performance by balancing the extraction time and extracting phase thickness.

The revolutionary capabilities of mass spectrometry enabled broadening of the focus from primarily neurotransmission and neuromodulation-related effects on brain function and its deterioration to now include the system's metabolic status. Metabolites monitored alongside the neuroactive molecules constitute an end product of gene and protein expression, as well as cellular environment, hence their large contribution to brain's functional status and importance of their role in pathophysiological states. **Chapter 5** explores the broad analyte coverage provided by SPME in the context of untargeted metabolomic profiling of the hippocampal response to the occurrence of death. Purely death-induced changes affecting endogenous molecules in rat hippocampus in the first hour of post mortem interval are investigated, leveraging the unique possibility of sampling the same brain area of each animal both *in vivo* and *post mortem* via SPME.

Each chapter concludes with a description of immediate or future steps to be undertaken to address the identified limitations or expand the presented scope of work to further validate the developed tools. Several dead-end strategies and optimizations bringing no clear improvement are included, highlighting the importance of failure and its informativeness in guiding the subsequent potentially successful steps. Detailed experimental workflows and improvement ideas are provided with the hope that the outlined strategies will go beyond merely showing promise *on paper* and will find application in near future in truly exploratory efforts aiming at better understanding of brain function.

Chapter 2

In vivo monitoring of endogenous compounds and neurochemical environments via solid phase microextraction

2.1 Preamble

This chapter contains sections that have already been published as 2 articles- in *Analytical Chemistry* and *Journal of Neurophysiology*. Subchapters 2.2 and 2.4 include the article entitled *Solid Phase Microextraction-Based Miniaturized Probe and Protocol for Extraction of Neurotransmitters from Brains in Vivo* by Sofia Lendor, Seyed-Alireza Hassani, Ezel Boyaci, Varoon Singh, Thilo Womelsdorf, and Janusz Pawliszyn, *Analytical Chemistry* 2019, 91(7), 4896-4905. Subchapter 2.3 includes the article entitled *Multineuromodulator measurements across fronto-striatal network areas of the behaving macaque using solid-phase microextraction* by Seyed-Alireza Hassani, Sofia Lendor, Ezel Boyaci, Janusz Pawliszyn, and Thilo Womelsdorf *Journal of Neurophysiology* 2019, 122(4), 1649-1660. The contents of the articles are herein being reprinted with permission of the American Chemical Society and American Physiological Society, in compliance with both publishers and the University of Waterloo policies.

2.2 Solid phase microextraction-based miniaturized probe and protocol for extraction of neurotransmitters from brains *in vivo*

2.2.1 Introduction

Efficient neural communication has been proposed to be dependent on the transient balancing of multiple neurochemicals at and outside neural synapses.[94,95] Small aberrations of the balance between interacting neurochemicals disrupt neural communication and distort cognitive functioning as is characteristic in the brains of patients with neuropsychiatric diseases.[96,97] Despite the importance of understanding the neurochemical profile underlying efficient neuronal communication, effectual measurement of multiple neurochemicals in the awake brain remains a challenge. Neurotransmitters act within a limited dynamic range, where concentrations that are too large or too small are

detrimental.[98,99] This highlights the need for techniques sensitive within this range and capable of simultaneous measurements in several brain regions in order to identify alterations in the neurochemical milieu of dysfunctional brain tissue characteristic of neuropsychiatric disorders.[100,101]

In vivo monitoring is widely regarded as an invaluable step towards a better understanding of brain functions; however, it remains challenging in practice due to numerous restrictions associated with the choice of techniques, the availability of subjects, the analytes under study, as well as the prospects of reproduction or repetition of such experiments. Current state-of-the-art in *in vivo* analysis of neurotransmitters in brains includes employment of various neuroimaging techniques, such as magnetic resonance imaging (MRI) or positron emission tomography (PET), which however do not allow for direct quantitation of neurotransmitters.[102,103] The most prominent examples of non-imaging techniques include push-pull perfusion, microdialysis (MD), voltammetry, and sensors. The push-pull technique, often considered a precursor of MD, has been almost completely replaced by the latter due to the suspected substantial damage to brain tissue caused by perfusion at high flow rates,[104] and the need for anesthesia during the procedure, which limits its application in behavioral studies.[105] This state however seems to be changing in favour of push-pull technology again, as novel miniaturized probes start emerging, combining high spatial and temporal resolution of measurements while enabling continuous direct-to-MS coupling during *in vivo* sampling.[106] MD is currently the most widespread *in vivo* brain sampling technique owing to its suitability for extraction of low molecular mass neurotransmitters from the brain's extracellular space, suitability for behavioural studies[107] and continuous sampling capabilities.[24] It operates with a semipermeable membrane that allows for the continuous collection of the available extracellular neuromodulators through passive diffusion and can even be used to locally release pharmacological agents.[20,24,108–110] Despite the feasibility of coupling MD to a variety of separation techniques and detectors,[24,109] the presence of salts and buffers in the dialysate may be problematic for MS detection, however ion suppression in the ESI source can be avoided by

introduction of an additional desalting step[111] or diverting the early-eluting salts to waste. Implantation of the MD probe is suspected to cause damage to nerve tissue, temporarily giving rise to artifacts and altered neurotransmitter concentrations, thus requiring stabilization; however, the consensus on severity of these phenomena remains largely unresolved.[112] Recent developments have aided in overcoming some of the limitations inherent in MD, improving the technique's sensitivity[113,114,115] as well as its spatial[116] and temporal[117,118] resolution to the range of sub-millimeter and a single minute, respectively. Electrochemical methods (i.e. fast-scan cyclic voltammetry and related techniques) are characterized by excellent spatial and temporal resolution of measurements (micrometer and sub-second ranges, respectively), low invasiveness, and high chemical sensitivity. However, such methods are prone to interferences caused by changes in extracellular pH, and are practically limited to simultaneous measurement of only a narrow range of compounds (significantly differing by their structures).[119] Microelectrode biosensors employ biological components such as enzymes or antibodies to bind with analytes allowing even better spatially and temporally resolved measurements of neuroactive compounds *in vivo* (micrometer and millisecond ranges, respectively),[120] however, their relatively recent introduction restricts their wide applicability due to limited sensor availability. Additionally, biosensors can only monitor one compound at a time.[121] The most recent advancements in microelectrodes and biosensors manufacturing[122] enabled real-time monitoring of choline, dopamine, ascorbic acid, and oxygen in brains of freely moving rats.[120,123–127] It is also noteworthy that new direct-to-MS-compatible technologies such as probe electrospray ionization are being adapted for *in vivo* brain sampling in rodents.[128]

Solid phase microextraction (SPME) is a recent candidate for an *in vivo* technique capable of surmounting some of the described challenges as well as complementing existing approaches. SPME, similar to MD and unlike electrochemical methods and sensors, is broad in its ability to detect neurochemicals, although it does not have continuous sampling capabilities. The unique versatility of

SPME may not only allow it to complement the mentioned techniques well, but also to fill in roles that traditional methods cannot execute.[55] Due to the balanced coverage of extracted compounds, SPME can provide information regarding multiple compounds from functionally and structurally different groups,[129] as well as short-lived species,[130] whose roles in brain function modulation might not have been explored to date. The platform presents itself as a powerful exploratory tool with great potential for *in vivo* applications, as negligible depletion of the sample combined with high enrichment of the analytes enables *in vivo* sampling without causing disturbance to the system under study.[131] Examples of applications of *in vivo* SPME in animals include untargeted investigation of metabolic profile in rat blood,[132] a targeted pharmacokinetic study of anticonvulsant drug in the same matrix,[82] metabolic profiling and pharmaceuticals monitoring in pig lung and liver,[133] extraction of polyunsaturated fatty acids from fish,[134] untargeted lipid profiling in fish,[130] lipidomic analysis in zebrafish and *Daphnia magna* by SPME-nanoESI-MS,[135] and monitoring of 4 neurotransmitters in rat brain which was later further extended to metabolomic profiling of a broader range of compounds, including hydrophobic species.[136] Nevertheless, SPME of very polar compounds with high specificity and recovery, especially when present in sample at low concentrations still remains to be improved.

Regardless of the employed technique, quantitative analysis of non-derivatized neurotransmitters represents a challenge, as their ions fall within the range of the most highly populated region of abundance vs. m/z distribution of ions, giving rise to interferences that result in increased noise and decreased signal-to-noise (S/N) ratios.[137] Additionally, they are prone to poor ionization, yielding non-specific fragments (loss of water or ammonia)[138] or in-source fragmentation. Such occurrences in turn limit the selection of specific fragments as quantifiers, cause interferences, and issues with quantitative data interpretation of closely related compounds due to the transformation of analytes or co-extracted interferents into precursors or metabolites of compounds of interest.[139,140] Data interpretation becomes

even more complicated, as amino acid neurotransmitters in addition to being signalling molecules, also have a variety of functions associated with metabolic regulation in brain.[141]

In this study, we present optimization steps undertaken to develop an SPME-based brain probe tailored for improved extraction of neurotransmitters, with the end application of neurochemical profiling of non-human primate brain *in vivo*. The final miniaturized SPME probe utilized an in-house synthesized extraction phase coated on a 3 mm recessed tip with a total diameter of less than 200 µm. We provide recommendations for the sampling time selection and a sample storage strategy based on experimental assessments. The developed protocol was validated by quantitation of neurotransmitters and additional related neurochemicals extracted from brain surrogate matrix. The developed probe is expected to supplement existing *in vivo* sampling toolbox, as it allows for simpler, reliable, minimally invasive, and generally matrix-effect-free measurements of polar endogenous neurochemicals.

2.2.2 Experimental

Materials, supplies, and chemicals

The LC-MS-grade solvents methanol (MeOH), acetonitrile (ACN), isopropanol (IPA) and water, as well as the acetylcholinesterase inhibitor phenylmethylsulfonyl fluoride (PMSF) were purchased from Fisher Scientifc. MS-grade formic acid and acetic acid, polyacrylonitrile (PAN), N,N-dimethylformamide (DMF), the standards of the neurotransmitters γ-aminobutyric acid (GABA), glutamic acid (Glu), acetylcholine (Ach), histamine (Hist), serotonin (5-HT), dopamine (DA), taurine (Taur), and choline (Cho), and the deuterated analogues γ-aminobutyric acid-D6, glutamic acid-D5, acetylcholine-D9, histamine-D4, serotonin-D4, and taurine-D4 were purchased from Millipore-Sigma (Oakville, ON, Canada). The components needed to prepare the 1M phosphate buffered saline solution (PBS; pH 7.4) and artificial cerebrospinal fluid (aCSF, pH 7.4), namely sodium chloride, potassium chloride, potassium dihydrogen phosphate, disodium hydrogen phosphate, sodium dihydrogen phosphate, sodium bicarbonate, magnesium chloride, calcium chloride and D-glucose, were also

purchased from Millipore-Sigma. Epinephrine (Epi), norepinephrine (NE) and their deuterated analogues epinephrine-D5 and norepinephrine-D5 were obtained from Cerilliant Corporation (Round Rock, TX, USA). Standards of dopamine-D4, choline-D9, phenylalanine-D8, and tryptophan-D5 were purchased from Cambridge Isotope Laboratories (Tewksbury, MA, USA). Individual stock standard solutions were prepared in methanol or water with 0.1% formic acid at a concentration of 1 mg/mL and stored at −80 °C for a maximum period of one month, after which they were discarded, and new standards were prepared. Quality control samples as well as samples used to build the instrumental calibration curve were prepared in desorption solvent in the range of 0.1-200 ng/mL and 20 ng/mL, respectively, by serial dilution of the stock standard mixture of all analytes at 1 µg/mL. The concentration of the internal standards was kept constant at 20 ng/mL in all samples.

Fresh lamb brains used to prepare the surrogate brain matrix were obtained locally from a food market. The tissue was homogenized within several hours on the same day as the brains were harvested and frozen at -80°C immediately after homogenization. An appropriate portion of brain homogenate was then thawed on the day of each experiment.

The polymeric particles used as SPME extracting phases were kindly provided by Waters Corporation (Oasis HLB- hydrophilic-lipophilic balance, MCX- strong cation exchange, MAX- strong anion exchange, WCX- weak cation exchange and WAX- weak anion exchange) and Millipore-Sigma (DSC-MCAX and LC-SCX, both with strong cation exchange properties). The reagents used for synthesis of hydrophilic-lipophilic balance polymer particles functionalized with strong cation exchange groups, namely 1,2-dichloroethane, ethanol, acetic anhydride, concentrated sulphuric acid, concentrated hydrochloric acid, azobisisobutyronitrile, divinylbenzene, and N-vinylpyrrolidone, were purchased from Millipore-Sigma. The stainless steel wire (grade AISI 304, 150 µm diameter) used for manufacturing of SPME probes was purchased from Unimed S.A. (Lausanne, Switzerland). The

stainless steel tubing used for *in vivo* brain sampling as guiding cannulas (270 µm O.D.; 200±5 µm I.D.) was obtained from Vita Needle (Needham, MA, USA).

LC-MS/MS conditions

All experiments were carried out using an Ultimate 3000RS HPLC system coupled to a TSQ Quantiva triple quadrupole mass spectrometer (Thermo Fisher Scientific, San Jose, California, USA). MS/MS analysis was performed in positive ionization mode under selected reaction monitoring (SRM) conditions (details in **Table 2.1**). Data acquisition and processing was performed using Xcalibur 4.0 and Trace Finder 3.3 software (Thermo Fisher Scientific, San Jose, California, USA). The employed chromatographic conditions consisted of a modified method previously reported by Cudjoe et al.[142] A Kinetex® PFP LC column, 100 x 2.1 mm, 1.7 µm particle size (Phenomenex, Torrance, CA, USA) held at 30°C was used for chromatographic separation of the target neurotransmitters. Mobile phase A consisted of water/MeOH/ACN 90:5:5 (v/v/v) with 0.1 % formic acid, and mobile phase B was ACN/water 90:10 (v/v) with 0.1% of formic acid. The following chromatographic gradient at a flow rate of 400 µL/min was applied (%B): 0-1 min 100%; 1-4 min convex gradient function (5) to 0%; 4-5.5 min held at 0%; 5.5-5.6 min linear gradient function 100%; re-equilibration at 100% until 6.5 min. The injection volume was 10 µL. All analyses were carried out in positive ionization mode with capillary voltage set at 2 kV, with the remaining electrospray source conditions set to the following values: vaporizer temperature 358 °C, ion transfer tube temperature 342 °C, sheath gas pressure 45, auxiliary gas pressure 13, and sweep gas pressure 1 (arbitrary units). The instrumental stability was monitored throughout the duration of the LC-MS/MS acquisition by analysis of an instrumental QC sample consisting of all target analytes and their internal standards spiked into a neat desorption solvent at 20 ng/mL.

Table 2.1: Selected properties of target neurotransmitters and their corresponding internal standards: hydrophilicity (expressed as logP), dissociation constants, retention times, and monitored SRM transitions.

Compound	logP*	pKa*	Physiol. charge	Rt [min]	Precursor ion [m/z]	Fragment ion (Quan) [m/z]	Confirming fragment ion (Qual) [m/z]	Collision energy Quan/Qual [V]	RF Lens Quan/Qual [V]
GABA	-2.9	4.53	0	3.40	104	87	69	11/15	30
Hist	-0.7	14.46	1	5.21	112	95	68	14/22	30
Ach	-4.2	-7b	1	3.73	146	87	43	14/26	35
Glu	-3.7	2.23	-1	2.99	148	84	56	15/26	30
DA	-0.9	8.93	1	3.46	154	91	137	23/10	30
NE	-1.2	9.58	1	3.36	152/170	77	107	30/20	50/30
Epi	-1.4	8.59	1	3.44	166	135	107	14/20	59
5-HT	0.5	9.31	1	3.55	177	160	115	10/28	30
Cho	-3.6	-3.2	1	3.53	104	60	58	16/28	44
Taur	-2.2	9.34	0	0.61	126	65	64	37/52	45
PheAla-D8	-1.4^{+}	9.45^{+}	0^{+}	3.19	174	128	-	13	32
Trp-D5	-1.1^{+}	9.40^{+}	0^{+}	3.27	210	193	-	10	34
GABA-D6		n/r		3.40	110	93	-	10	30
Hist-D4		n/r		5.21	116	99	-	15	30
Ach-D9		n/r		3.73	155	87	-	15	30
Glu-D5		n/r		2.99	153	88	-	17	33
DA-D4		n/r		3.46	158	141	-	11	30
NE-D6		n/r		3.36	176	111	-	21	30
Epi-D6		n/r		3.44	190	172	-	11	33
5-HT-D4		n/r		3.55	181	164	-	10	30
Cho-D9		n/r		3.53	113	69	-	18	48
Taur-D4		n/r		0.61	130	112	-	12	44

*values from DrugBank (version 5.1.1); n/r- not relevant; $^{+}$- values for the non-labelled compound

Analytical procedure for optimization experiments

The following general procedure was applied during all optimization experiments, and successively modified according to our findings, leading to more optimal conditions. Further details concerning spiked concentrations, as well as volumes and composition of the desorption solvent can be found in the Results section and in the figures' captions. *Preconditioning*: SPME probes were left to soak in 1 mL of 50:50 MeOH/water (*v/v*) overnight, then submitted to vortexing at 1500 rpm for 30 min in 1 mL of fresh solvent mixture. *Extraction*: Optimization experiments to select the most appropriate coating

chemistry as well as the most suitable desorption solvent were carried out in 500 µL of PBS solution spiked with the target neurotransmitters, and extractions were performed for 15 min in static mode. Extraction time profile experiments as well as quantitation and validation experiments were carried out in 500 µL of a brain surrogate matrix. *Wash*: Following extraction, fibers were wiped with a lint-free tissue, immersed into 300 µL of MS-grade water for 3 s, then wiped again. *Desorption*: Fibers were desorbed for 1 h with agitation at 1500 rpm. All experiments carried out prior to desorption solvent selection utilized a mixture of water/ACN 3:2 (v/v) with 0.1% formic acid and IS at 20 ng/mL.

Samples were injected into the LC-MS system for neurotransmitter analysis within a few hours of desorption. The amounts of nanograms extracted were determined based on instrumental calibration curves consisting of all target analytes spiked into a neat desorption solvent in the range of 0.1-200 ng/mL, with internal standards at a constant level of 20 ng/mL. The ratios of peak areas of the analytes and the peak areas of their corresponding IS were used as analytical response.

Quantitation of neurotransmitters in brain homogenate surrogate tissue

Quantitation of targeted neurotransmitters was performed based on the signals of the analytes in the surrogate matrix calibration curve. For glutamate, GABA, choline, taurine, phenylalanine, and tryptophan, quantitation was based on the signals of their deuterated isotopologues. A surrogate matrix consisting of agar gel (2% agar in PBS solution, *w/v*) mixed with lamb brain homogenate in the ratio 1:1 (*v/w)* was spiked with a mixture containing all analytes ranging between 5-3000 µg/mL for isotopically labelled compounds, and 10-2000 ng/mL for remaining compounds. Prior to mixing the agar gel containing analytes with the brain homogenate, the homogenized tissue was incubated with 1 mM PMSF for 1 h at 37°C to prevent enzymatic activity of acetylcholinesterase, which would lead to loss of acetylcholine. The matrix was left to set for approx. 30 min, and extractions were then carried out from 0.5 mL of the matrix for 20 min using the optimized SPME probes. The obtained weighted linear regression equation fitted to the analytical response in the function of concentration was applied

to quantify the analytes in the QC samples at 3 concentration levels. Limits of quantitation (LOQ) were determined as the lowest concentration of analyte producing a signal to noise ratio ≥ 5, with a relative standard deviation (RSD) of 4 replicate measurements below 20%, and accuracy within 20% of the relative error.[143] The method's precision was expressed as percent RSD of 3 replicate measurements at each QC concentration level. Accuracy was calculated as the relative percent error of concentrations of analytes in the QC samples determined experimentally with the use of calibration curves versus theoretical (spiked) concentrations. The absolute matrix effect was investigated by analysis of blank samples spiked with analytes post-extraction in comparison to obtained signals of each analyte in the neat desorption solvent at three concentration levels (where signal is designated as the ratio of the peak area of the analyte and the peak area of its internal standard).[144]

2.2.3 Fabrication and characterization of the miniaturized recessed SPME probes

The fabrication procedure involved modification of the supporting stainless steel wire to create a recession on the tip and subsequent immobilization of the extracting phase on the modified wire (**Figure 2.2**). The composition of the slurry containing the extracting phase suspended in a binder was optimized in order to enable deposition of polymeric micrometer-size particles on a thin support, as effective and uniform deposition becomes increasingly difficult as the ratio of the supporting wire diameter to particle size is decreased. This observation was made during the coating optimization step, where particles of different sizes from different vendors were available (5 μm for Waters HLB, 20 μm for remaining types of Waters Oasis particles, and 30-60 μm for Supelco DSC-MCAX particles). The biggest particles were ground into a fine powder in order to enable their deposition onto the wire. However, grinding could potentially lead to loss of benzenesulfonic acid functional groups due to the substantial heat produced during the process, resulting in decreased extracting capabilities (results of energy dispersive X-ray spectroscopy measurements carried out to test this hypothesis are discussed in below). Therefore, in-house synthesis of functionalized polymer particles (HLB with strong cation exchange groups: HLB-

SCX) was proposed as a method for customization of the SPME probe design while maintaining good extracting capabilities.

Synthesis of hydrophilic-lipophilic balance (HLB) polymer particles

HLB particles were synthesized by precipitation polymerization. In a three-necked round bottom flask equipped with a mechanical stirrer and inlet for nitrogen gas purging, 150 mL ACN and 50 mL toluene were mixed and purged with nitrogen for 30 min. Monomer (N-vinylpyrrolidone; 1 mL) and crosslinker (divinylbenzene; 4 mL) were added to the resulting solution in the ratio of 2.5% with respect to the polymerization solvent, with 50 mg azobisisobutyronitrile (AIBN) as initiator. Free radical polymerization was induced thermally at 70 ^{o}C and carried out for 24 h with stirring at 100 rpm. After 24 h, a reaction mixture was collected by centrifugation at 10000 rpm for 15 min. HLB particles obtained as such were then washed with 100 mL of ethanol and dried under vacuum at 80 ^{o}C for 24 h.

Functionalization of HLB particles with strong cation exchange groups (sulfonation)

The 1.3 μm HLB particles were dispersed in 1,2-dichloroethane by sonication for 2 min and left to soak for 4 h. In the meantime, the functionalizing reagent acetyl sulphate was synthesized by reacting acetic anhydride (10 mL) with concentrated sulphuric acid (3 mL) in 1,2-dichloroethane (10 mL). Due to the reaction of acetyl sulphate formation being exothermic, the reaction flask was kept below -20°C in a cooling bath consisting of ethanol and liquid nitrogen, which was added as needed with continuous stirring. The reaction mixture was stirred until the solution turned pale yellow. Once the reagent reached room temperature, the HLB particle suspension was added and functionalized for a pre-determined period of time (1 h, 3 h or 12 h), after which the reaction was terminated by adding deionized water. The functionalized particles were then filtered and washed with water until a neutral pH was confirmed. After additional washing with ethanol to remove any organic impurities, the sulfonated particles were dried in a vacuum oven overnight at 60°C.

Characterization of HLB-SCX particles

The synthesized particles were characterized by field emission scanning electron microscopy (FE-SEM Zeiss UltraPlus; Carl Zeiss Meditec AG, Jena, Germany), specific surface area analysis (Autosorb iQ-MP, Quantachrome, Boyton Beach, FL, USA), and Fourier Transform Infrared Spectroscopy (Bruker Optics Inc., Tensor 27, Germany) for determinations of size and shape, surface area, and chemical composition of the particles, respectively. FT-IR spectrum was recorded from 400-4000 cm^{-1} on an ATR cell (Pike Technologies, Madison,WI, USA) in powder form (**Figure 2.1**). The samples were coated with a gold layer prior to FE-SEM analysis, and images were captured with the secondary electron detector at 4-10 kV (1 nm resolution at 15 kV).

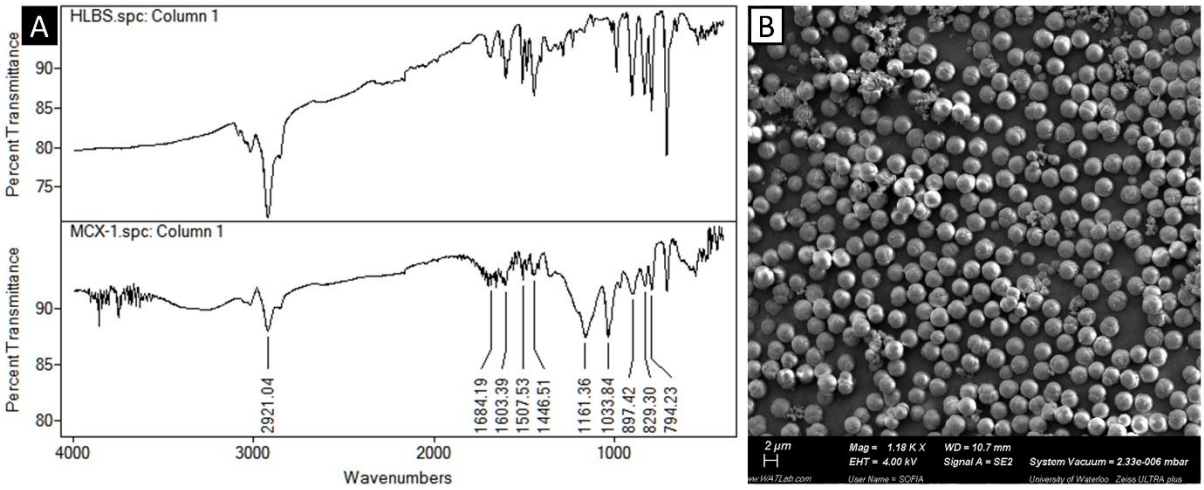

Figure 2.1: (**A**) FTIR spectra of HLB (top) and HLB-SCX (bottom) particles. Peaks at 1684.36 cm-1 confirms presence of -C=O groups in the HLB backbone and peaks at 1449.28, 1520.45, 1626.78 cm-1 evidence the presence of divinylbenzene ring in the final product. In the HLB-SCX spectrum, a peak at 1161.36 cm-1 indicates the presence of -SO3H groups, which confirms successful sulfonation of HLB particles. (**B**) FE-SEM images of HLB particles. The particles are uniform, spherical and monodisperse in nature. Particle diameter was found to be predominantly 1.3 µm

Coating suspension preparation

The SPME coating was deposited on the miniaturized probes according to the modified procedure developed in our laboratory and reported previously.[145] The binder substance acting as a biocompatible glue was prepared by dissolving 2.5 g of polyacrylonitrile (PAN) in 36.5 mL of N,N-dimethylformamide (DMF) in elevated temperature (90°C) for 1 h with stirring every 15 min. After reaching room temperature, the glue was mixed with the particles to obtain a 5% (w/w) suspension. After overnight stirring at 900 rpm, more particles were added to reach a final content of 15% (w/w) particles in glue. For the commercially available particles tested in this work, the content was kept at 10%, while ground particles were mixed at 15%.

Preparing the recessed supporting wire and depositing the coating on a recession

A stainless steel wire with an initial diameter of 150 μm was used as support for the probes. A silicon GC septum was pierced with the wire, with 4 mm of the wire protruding through it. The assembly was placed in a vial with concentrated hydrochloric acid, allowing only the unprotected wire tip to be immersed, while the septum with the remaining length of the wire floated on the surface of the acid (**Figure 2.2**). The vial was exposed to ultrasound in a water bath for total of 70 min, after which the wire was removed from the septum and washed with water. The entire length of the wire, both etched and un-etched segments, was subsequently sonicated in water for 10 min and in MeOH for another 10 min so as to remove any acid residues and facilitate faster drying, respectively. The procedure resulted in obtaining the support wire with the tip (4 mm long segment) decreased to 100 μm in diameter.

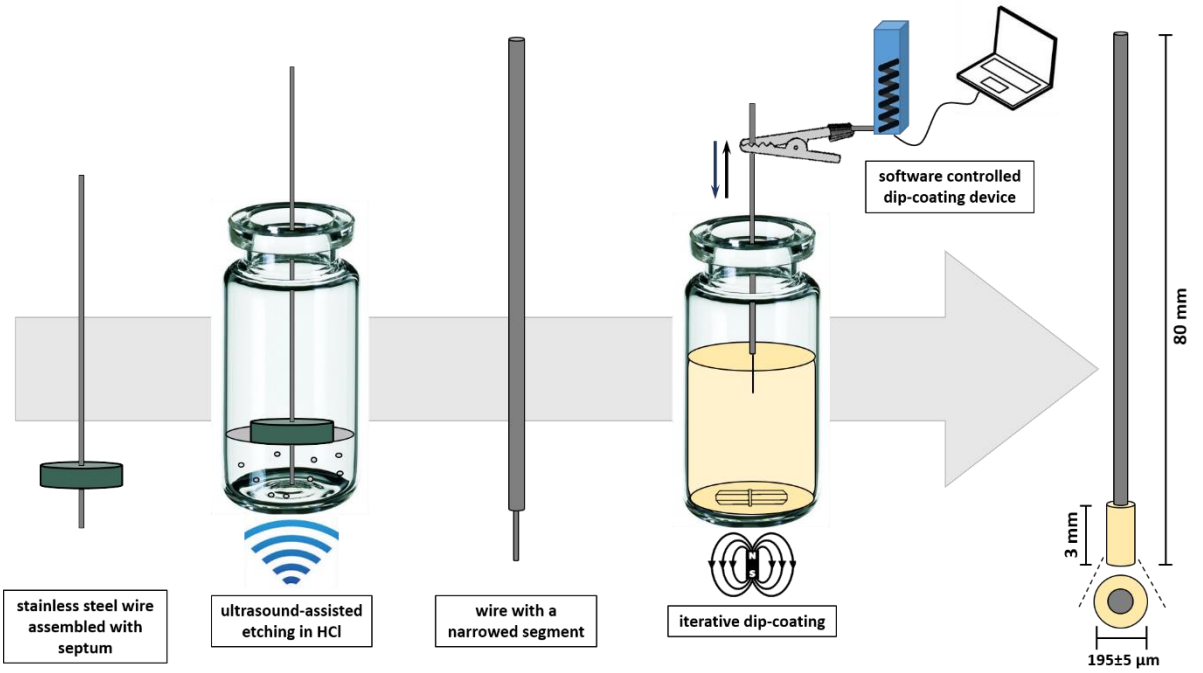

Figure 2.2: Schematic depiction of the recessed wire preparation and deposition of SPME coating.

The coating was deposited on the support by repeated dipping of the 4 mm recessed tip of the wire in a vial containing the extracting phase suspension at a speed of 3 mm/s, until the desired coating thickness was reached (total diameter of the coated tip was in the range of 195±5 µm - **Figure 2.3**). After the deposition of each layer, the coating was cured in an oven for 1 min at 125°C, while the coating suspension was stirred at 900 rpm so as to retain homogeneity and prevent phase separation. Different types of tested particles required different numbers of layers to reach the same coating thickness. Given that the dipping process causes the tip of the wire to accumulate more material, thus yielding a thicker coating in that region, the top 1 mm of the probe tip was cut off to ensure evenness throughout the length of probe, resulting in a final probe with 3 mm of coated length. After the manufacturing procedure was concluded, SPME probes were soaked in a mixture of MeOH/ACN/IPA 50:25:25 (v/v/v) under vortex conditions at 1500 rpm for 60 min to remove any residues that were incurred during the manufacturing process, such as uncured glue, monomers, and loose polymer particles.

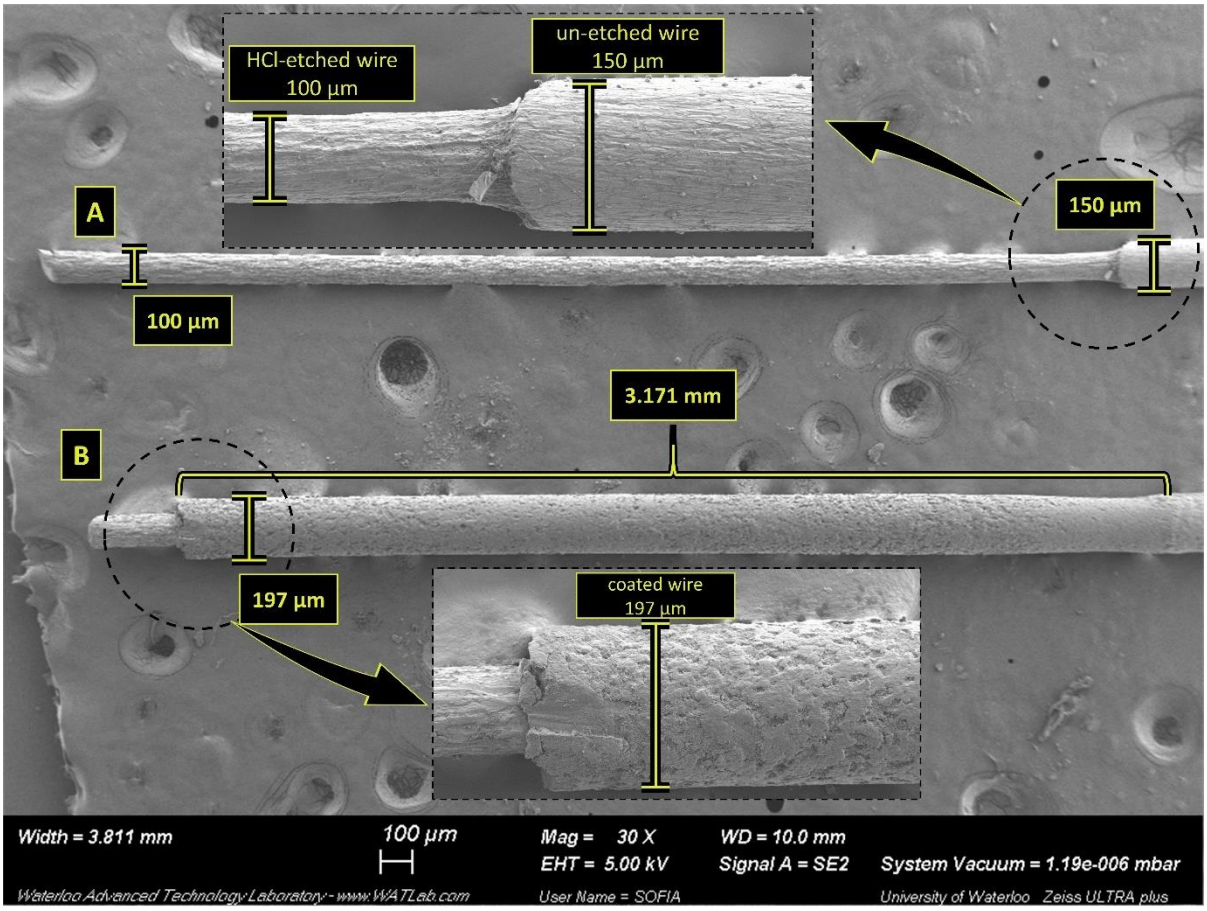

Figure 2.3: SEM image of the SPME probe at different stages of manufacturing. **A**: acid-etched wire with recession to accommodate the coating; **B**: wire coated with synthesized HLB-SCX-3h extracting phase.

Employment of small particles with low size dispersion (in-house synthesized HLB-SCX; **Figure 2.4** A1 and A2) translates to better coverage on a miniaturized probe (small wire diameter), smoother coating (less tissue attachment), decreased carryover and better extraction kinetics, as the particles are not buried in the binder completely, as is the case of the extracting phase that has been ground down (**Figure 2.4** B1 and B2).

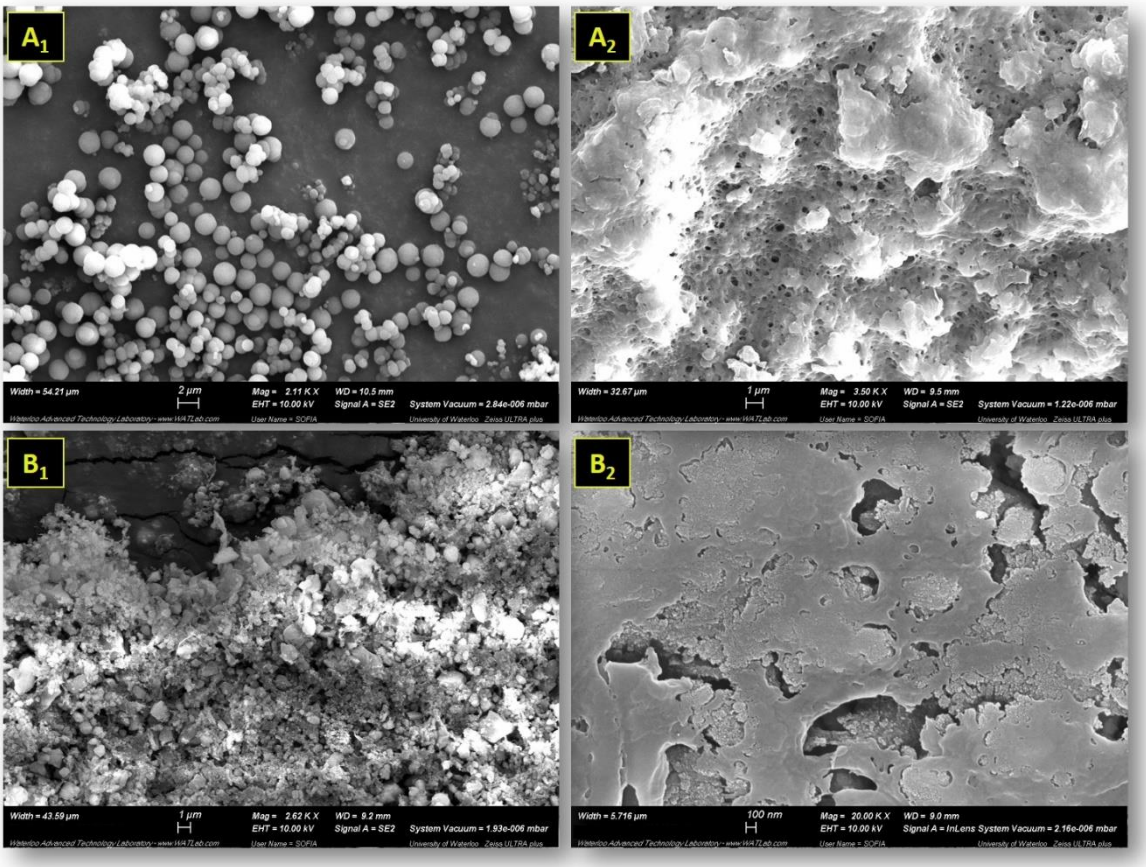

Figure 2.4: SEM images of the in-house synthesized coating (HLB-SCX; top) and commercially available ground particles (Supelco DSC-MCAX; bottom). **A1** represents uniform, minimally dispersed and small particle sizes of the synthesized and functionalized polymer. **A2** shows the uniform, highly porous structure created once particles are mixed with the binder and coated on the wire. **B1** shows the morphology of the ground particles with highly irregular shapes and sharp edges that could potentially cause tissue attachment. **B2** shows how ground particles are almost completely buried in the PAN binder when coated on fiber, thus decreasing the exposure of functional particles to the sample while also increasing the time required for extraction equilibrium to be reached due to the lack of porosity.

It is worth mentioning that the PAN binder doesn't only act as a glue, but it could also be considered as a membrane-like medium between the two environments of different pH (the sample or desorption solvent and the extracting phase). Therefore, future direction could involve leveraging this fact by pH modifications to the coating surface or to the external phase (e.g. desorption solution acidity) that could further promote extraction/desorption of solutes.

In order to determine how the yield of sulfonic acid groups in the structure of polymers used as SPME coatings might affect both extraction and desorption, these groups were semi-quantitatively assayed by SEM coupled to an energy dispersive X-ray spectroscopy (EDX)- **Figure 2.5**. FE-SEM Zeiss UltraPlus scanning electron microscope (Carl Zeiss Meditec AG, Jena, Germany) equipped with an Apollo XL EDX system (AMETEK, Mahwah, NJ, USA) was used, operated by Team software. Due to the semi-quantitative character of these measurements, they should be considered as results of tentative and supplementary character.

It was hypothesized that some amount of sulfonic groups from the Supelco DSC-MCAX particles was lost during the grinding process, due to the significant amount of heat generated by friction in the ball mill grinder chamber. The comparison of relative percentage of sulfur and oxygen present in the whole and ground particles shows that the differences are not statistically relevant (**Table 2.2**).

Table 2.2: Results of SEM-EDX analysis of tested particles with respect to the sulfur and oxygen content.

Sample	Atomic % (%Error)	
	Oxygen (O)	Sulfur (S)
Waters HLB	10.28 (9.93)	1.06 (7.64)
Supelco DSC-MCAX	36.93 (7.76)	0.20 (19.32)
Supelco DSC-MCAX ground	28.70 (8.19)	0.18 (18.29)
HLB-SCX 1.5h	3.44 (11.26)	0.25 (16.72)
HLB-SCX 3h	5.79 (11.11)	0.68 (7.24)
HLB-SCX 12 h	7.05 (10.18)	2.01 (4.21)

The second hypothesis was related to the increasing amount of functionalized sites obtained with increasing duration of the functionalization reaction, in the case of the in-house synthesized HLB-SCX particles. The findings confirmed the correlation between the amounts of neurotransmitters extracted (**Figure 2.6**) and the relative amounts of sulfur and oxygen in the extracting phase (**Table 2.2**). The highest content of sulfur in the polymer subjected to functionalization reaction for 12 h (higher than in the Waters MCX particles) supports the observation of significant carry over in the extract obtained

from the second desorption of the same probe occurring when the HLB-SCX-12h coating was used, as a result of the analytes being very strongly retained by the interactions with predominating sulfonic groups.

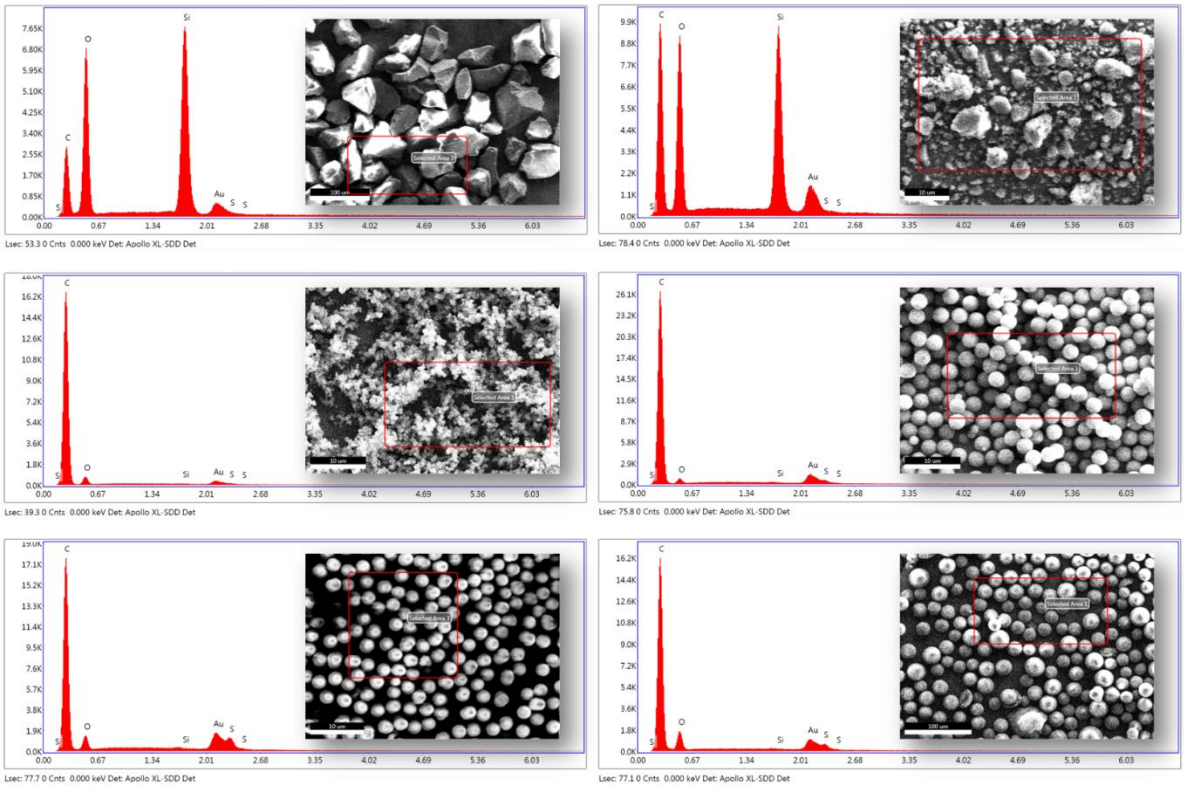

Figure 2.5: SEM-EDX analysis of the particles tested as SPME coatings within the strong cation exchange group. The following elements were locked: carbon, sulfur and oxygen (sulfonic groups), silicon (core of the Supelco particles), and gold (all samples were gold-coated prior to the SEM-EDX analysis). For consistency, these elements were measured in all the samples.

2.2.4 Results and Discussion

Evaluation and selection of SPME coating for small polar molecules

SPME coating selection criteria included the number and amounts of neurotransmitters extracted within a 15 min extraction period in static mode, as well as the reproducibility of extracted amounts. Optimization experiments to select the most suitable coating chemistry and desorption solvent were carried out in PBS solution at pH 7.4 without any further pH adjustments, since matrix modifications

would not be possible during *in vivo* sampling, where alteration of physiological pH is both undesirable and technically difficult. **Figure 2.6** (Phase I) shows amounts of neurotransmitters extracted by each tested type of coating, normalized to the best-extracting coating for each analyte, expressed as percent. The in-house synthesis of extracting phase was carried out as means to adjust the physicochemical properties of the coating to the characteristics of the analytes of interest.[146] HLB-SCX was selected based on its superior performance in terms of number of neurotransmitters extracted with the highest efficiency, as well as the improved reproducibility of the extracted amounts. These favourable properties of the coating are owed to the combination of the selectiveness of sulfonic acid for interaction with polar compounds, and a high specific surface area enabled by the small size of particles. Waters MCX yielded the second best performance; however, the relatively large size of the particles introduced substantial technical difficulties with respect to coating deposition during probe manufacturing, as the particle diameter was only a few times smaller than the supporting wire's diameter. The third coating selected for the second phase of testing was the commercially available Supelco DSC-MCAX. The particles were ground down due to their initial large size and high size dispersion; however, the grinding process was later shown to compromise the quality of the coating (**Figure 2.4**). The suitability of strong cation exchange-functionalized SPME coatings for extraction of neurotransmitters has been already demonstrated by Cudjoe et al.[142] However, due to the used thin-film blade format and no considerations for *in vivo* analysis and miniaturization, particle size was not of importance to that study.

Although the developed probes were not intended as reusable devices (new, sterile probes are required for *in vivo* brain sampling), carry-over after the first desorption was investigated as a means to assess whether analytes were lost due to their retention on the coating. Several coatings, including the in-house synthesized HLB-SCX, presented significant carry-over as observed after the first desorption. The synthesis protocol was therefore modified accordingly with respect to the time of functionalization with strong cation exchange groups. The reaction was carried out for 1.5 h and 3 h,

instead of 12 h as previously done. We hypothesize that the polyacrylonitrile (PAN) binder acts as a membrane separating two environments (the sample and the extracting phase) characterized by different pH, similarly to the case of three-phase liquid membrane microextraction.[147,148] Thus, modifying the extracting phase by introducing appropriate amount of acidic groups behind the PAN membrane creates environment to which the neutral fraction of polar analytes migrates to then become charged upon encountering lower pH. This in turn results in more efficient extraction of basic neurotransmitters. More fundamental insight into the mechanism of extraction through the layer of biocompatible PAN membrane could be leveraged to further improve recoveries of polar analytes, while immobilization of buffering moieties would further improve reproducibility of measurements by providing an environment with controlled and stable pH.

The newly synthesized coatings were submitted to a second phase of testing, narrowed down to the best performing SCX coatings (**Figure 2.6**). As expected, the choice of coating for extraction of multiple analytes of interest represents a compromise between the extracting capabilities and the technical aspects dictated by the application. Although the commercially available MCX material showed the best overall performance in terms of extraction efficiency, its use for the miniaturized brain probe was hindered due to the large size of particles, which made it difficult to attain a uniform coating on the wire. This in turn translated into decreased reproducibility of replicate extractions. Previous results, supported by SEM analysis, showed that grinding of particles does not provide an ideal solution to the abovementioned particle size issue, as such a procedure can modify the properties of the coating in an oftentimes undesirable manner.

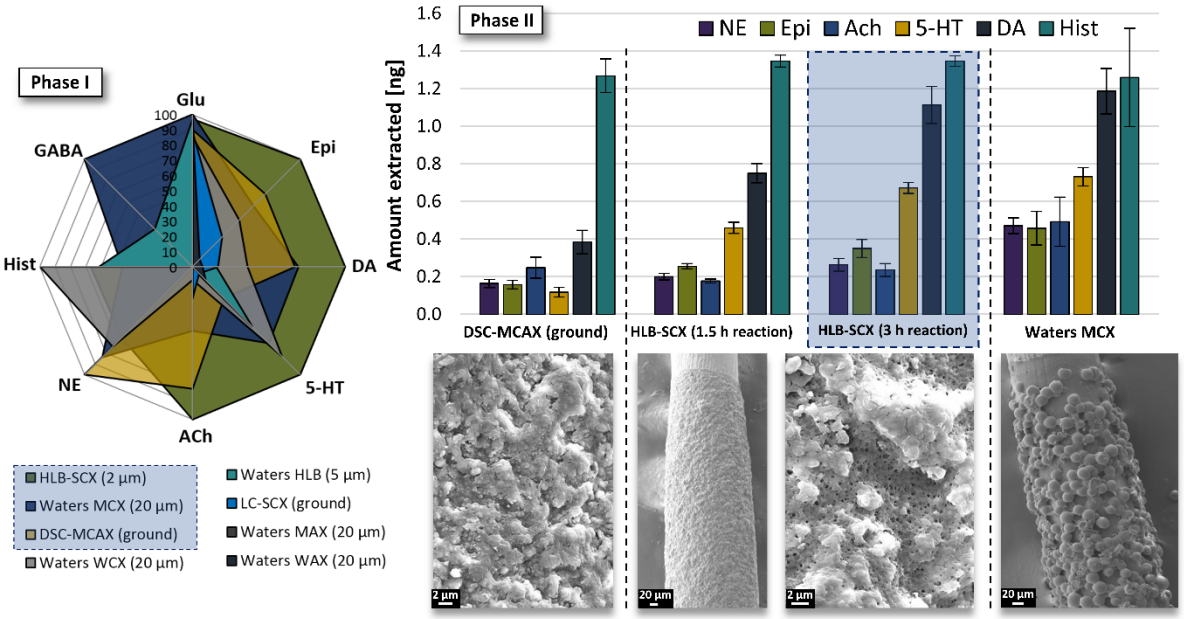

Figure 2.6: Extracting phase evaluation. **Phase I**: comparison of amounts extracted by each coating. Extractions from 500 µL of PBS spiked with neurotransmitters at 100 ng/mL; Desorption into 30 µL of solvent. 100% refers to the amount extracted by the best-extracting coating, used for normalization of the remaining results within the group of each analyte. The coatings were then ranked according to the total area of summarized amounts of all neurotransmitters extracted. **Phase II**: within the group of SCX coatings. Extractions from 500 µL of PBS spiked with analytes at 200 ng/mL for 15 min; probes were desorbed into 60 µL of solvent. Top figures: amounts of neurotransmitters extracted by each type of tested coating (amounts for histamine were divided by 2 for better visual representation of all compounds); Bottom figures: SEM images of coatings deposited on fibers; as seen, superior porosity and coverage was attained in the case of the in-house synthesized polymer.

Grinding of the DSC-MCAX particles into a fine powder enabled creating a smooth coating surface. However, it also resulted in burying the extraction phase under thick protection layer of the binder, leading to reduced kinetics and insufficient porosity, parameters that are required for high capacity of the extraction phase. Between the two types of synthesized coatings, longer functionalization yielded better performance for all neurotransmitters. Additionally, the carry-over relative to the previous iteration of this polymer (functionalized for 12 h) was significantly reduced or eliminated. The reason for the observed effect is likely the increased yield of sulfonic groups, which dcreases pH of the coating surface, thus increasing its extracting capabilities (results of EDX spectroscopy measurements supporting this claim have been presented in **Figure 2.5**). However, this also results in analytes being strongly retained on the coating, which translates to an increased carry-over. Given the above

considerations, we chose the HLB-SCX-3h extraction phase in view of its superior performance together with the ease of deposition on wire (due to small particle size), and possibility of further customization according to any possible future needs or modifications to the sampling method.

Selection of desorption solvent

It was anticipated that due to the types of interactions taking place between the ion exchange groups and the analytes, addition of formic acid at the relatively high level of 1% would facilitate more efficient desorption as the released analytes are trapped in the desorption solvent in their ionized form which prevents them from penetrating through the protection layer on the coating surface and being back-extracted.[149] Acidity of the desorption solvent would serve to additionally protect analytes (especially catecholamines) from auto-oxidation, therefore increasing their stability during the period of time between desorption and analysis.[150] Further, a desorption solvent containing a combination of solvents of various levels of polarity would improve the coverage of analytes being desorbed. The latter feature is highly desirable when extending the study to include untargeted analysis, as evidenced by the *in vivo* application of this work, discussed in sub-chapter 2.4. In consideration of the abovementioned factors and given its highest yield for the quantities of neurotransmitters desorbed (**Figure 2.7**), an acidified mixture of water, ACN, and MeOH was selected as desorption solvent.

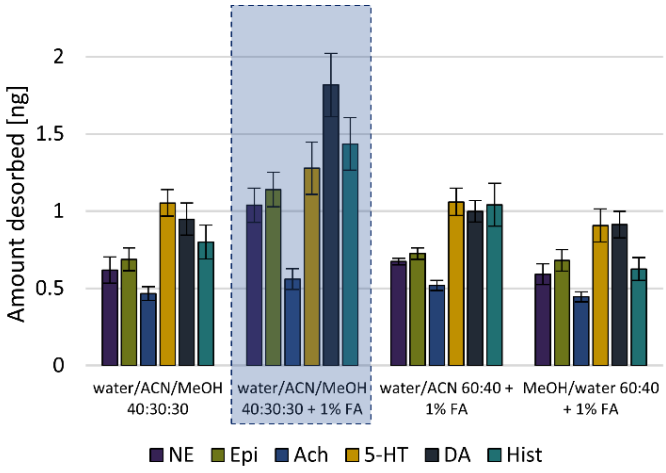

Figure 2.7: Comparison of amounts of neurotransmitters desorbed into 4 tested solvent mixtures. Extractions from 500 µL of PBS spiked with neurotransmitters at 300 ng/mL for 15 min, using the HLB-SCX-3h coating. Probes were desorbed into 50 µL of solvent.

Considerations for the *in vivo* sampling procedure

The SPME probe shape. One of the most important considerations for development of a suitable *in vivo* sampling protocol concerns the overall shape and dimensions of the miniaturized probe, capable of accommodating enough extracting phase to ensure sufficiently good recoveries, while at the same time minimizing damage to sampled tissue by reducing its size. The recessed SPME fiber design has been proven advantageous for *in vivo* sampling of fish tissue by Poole et al. due to its robustness and the protection of the extracting phase against damage during insertion into tissue through fish scales.[134] The currently presented work introduces a new type of recessed SPME probe modified to suit the purpose of *in vivo* brain sampling, an application which presents a completely different set of challenges than fish sampling. Besides the brain tissue being much softer than fish scales, the brain sampling is assisted by a software-controlled precise driving system, which is equipped with a needle that pre-pierces the brain dura mater to enable probe introduction. Therefore, the developed probe did not require a sharp point for insertion, while the recessed aspect of the design was utilized to enable deposition of larger volumes of extracting phase on the wire without significantly increasing the overall probe diameter. Additionally, the probes used in this study did not include a non-coated tip, as the additional length of the non-extracting part of the probe would cause unnecessary damage to the brain areas of interest and reduce reproducibility of measurements in the same location. This design maintained the guiding/sheathing cannula for *in vivo* sampling, since the coating must be protected from contact with tissue until the very moment the probe reaches the brain area of interest to prevent unwanted extraction. Otherwise, identified and quantified compounds could not be associated with any specific target area. Moreover, the diameter of the probe should match the internal diameter (ID) of the cannula as closely as possible to avoid inflowing of extracellular fluid (ECF) into the gap and contaminating the probe. The final probe consisted of a flexible stainless steel wire of adjustable length (preferentially 40-50 mm for in-lab experiments, and longer for *in vivo* sampling) with a 3 mm long

coated recessed tip. The wire diameter was 100 µm and 150 µm at the recession site and non-coated segment, respectively. The maximum diameter of the probe (at the coated tip) was 200 µm, with a coating thickness of approx. 50 µm (**Figure 2.3**).

Extraction and sampling time. The extraction time profile was evaluated by isolation of target neurotransmitters from surrogate brain matrix. For GABA and glutamate, equilibrium was reached after 20 and 30 min, while the remaining compounds reached equilibrium between 30 and 45 min, with the exception of epinephrine (**Figure 2.8**). *In vivo* extraction time is mainly dictated by experimental limitations. In general, equilibrium extractions are desirable in SPME applications as they enable relatively simple calibration, as well as decreased irreproducibility arising from inaccuracies pertaining to extraction time. Extraction at equilibrium also affords the maximum possible extraction efficiency by a given fiber in particular conditions. This is may be especially beneficial for improvement of limits of detection in *in vivo* sampling, where the intrinsically static conditions impose longer equilibration times.

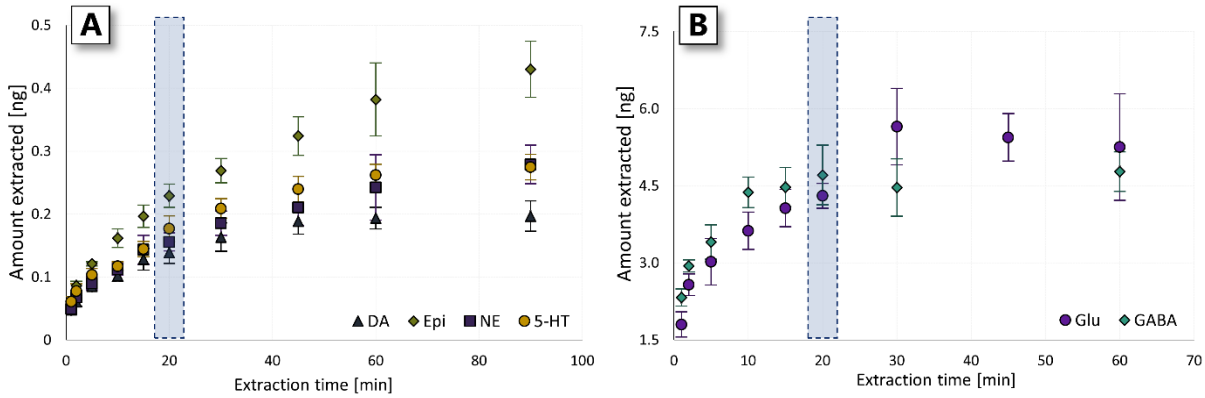

Figure 2.8: Extraction time profiles of target neurotransmitters. Extractions from surrogate brain tissue spiked with 480 ng/mL DA, Epi, NE and 5-HT (**A**) and extracting endogenous pool of Glu and GABA (**B**). Probes were desorbed into 40 µL of solvent.

Ultimately, 20 min was chosen as the final extraction time for the *in vivo* procedure. Despite not reaching extraction equilibrium within that time for all targeted compounds, 20 min represents a

compromise between reasonably and sufficiently long sampling, providing sufficient recoveries and good reproducibility of measurements, while maintaining temporal resolution suitable for *in vivo* pharmacokinetic or behavioral studies (although on the higher end of the acceptability range). The software-controlled probe introduction/withdrawal to and form brain combined with precise and accurate extraction time control eliminates introduction of any irreproducibility stemming from non-equilibrium extraction conditions.

Time and strategy of storage. *In vivo* sampling does not always permit immediate instrumental analysis, as the animal facility and analytical laboratory may at times be located at different sites, in some cases even different cities or countries. In such instances, it is essential that the utilized protocol includes a storage and transport strategy capable of ensuring minimal changes to the sample and preserving its representativeness for the studied system at the time of sampling. Some of the compounds of interest in this study (e.g., catecholamines) are known to be prone to oxidation or light-induced degradation.[151,152,153] Therefore, a storage stability test was designed and carried out to assess whether the transport and storage strategies elaborated for the developed *in vivo* application would yield reliable results without incurring significant analyte loss. The expected storage strategy entailed placement of SPME probes in glass vials on dry ice immediately following extraction and wash steps, for a period of 2 hours to simulate transportation conditions. Next, samples were moved to a -80°C freezer for several days, and subsequently desorbed and analyzed. The above described conditions were simulated in the laboratory with four test groups representing all combinations of the following storage strategies: samples preserved on probes or in solution; desorption solvent containing anti-oxidant mixture or unmodified. Storage tests were carried out for a total of 22 and 11 days for the in-solution and on-probe storage, respectively. The anti-oxidant mixture contained L-cysteine, ascorbic acid, and acetic acid at final concentrations in desorption solvent of 100 ng/mL, 100 ng/mL and 1 mM, respectively. This experiment aimed at answering the following questions: Does any analyte loss occur during storage?

Is retention of analytes better during in-solution or on-fiber storage? Does the addition of an anti-oxidant mixture prevent the analyte loss?

We found that the analytes were not significantly affected by storage in the desorption solution, as the difference in amounts extracted over the tested time period (expressed as RSD of all measurements) ranged between 6 and 14%. Addition of antioxidants did not significantly influence the stability (RSD ranging from 5% to 16%), most likely because the high concentration of formic acid in the unmodified desorption solvent already introduces antioxidative properties.[150] The observed trend for lower amounts attained after analysis of samples desorbed into the solvent containing additional antioxidants can be attributed to the higher salt content of this solution, resulting in suppressed electrospray ionization of target neurotransmitters. Interestingly, the stability of the neurotransmitters stored on the SPME probe was worse for every analyte as compared to the in-solution storage. In the case of histamine, the extracted amount significantly decreased between the third and eleventh day of storage on the SPME probe. Detailed data for each compound has been included in **Figure 2.9**. Moreover, for several compounds (including acetylcholine and catecholamines) on-fiber storage followed by desorption into the solvent containing antioxidants resulted in progressively increasing amounts recovered over time. The reason and mechanism behind compromised stability of neurotransmitters on the SPME probe require further investigation into the interactions taking place between the ion exchange extracting phase, polar analytes, and salts present in the solvent during the storage period as well as upon desorption.

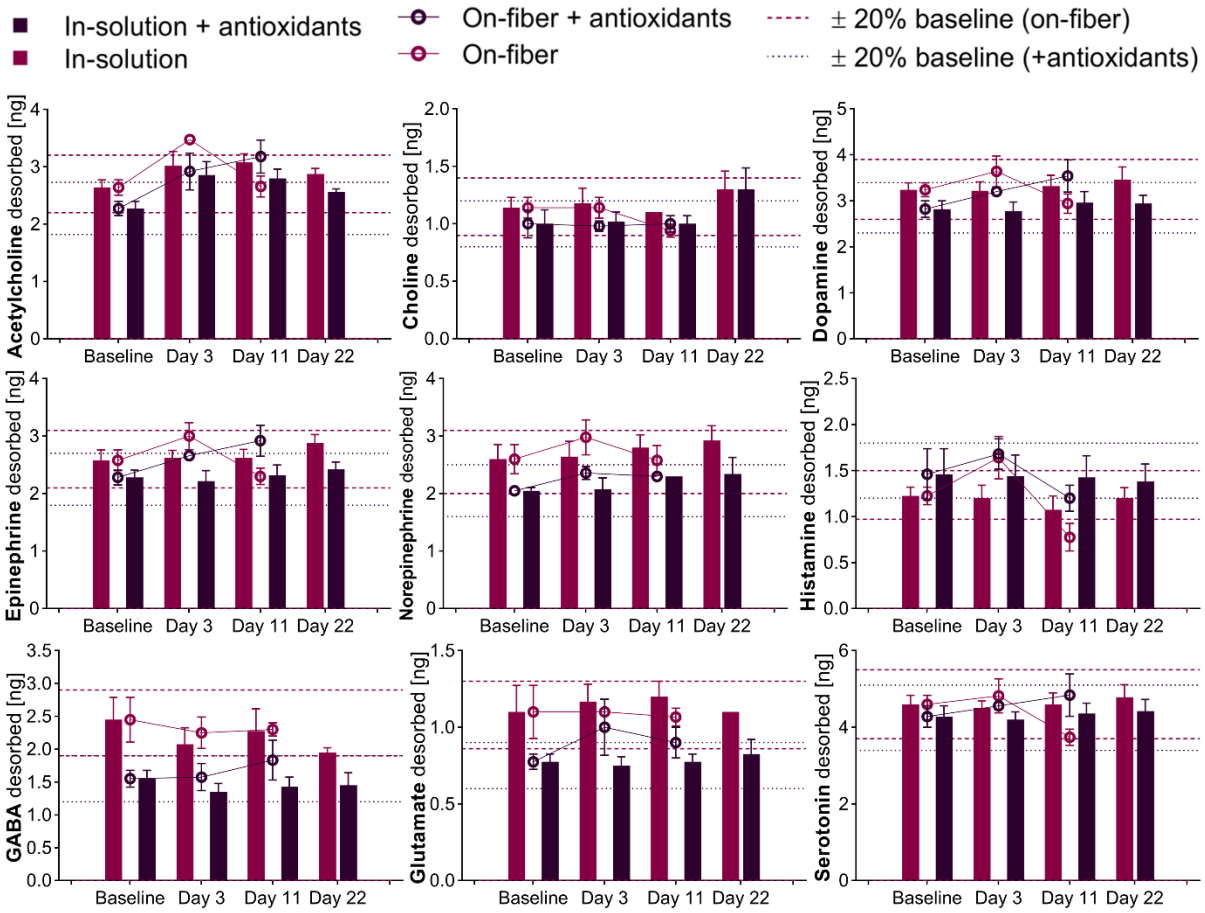

Figure 2.9: Changes in recovered amounts of neurotransmitters throughout the entire period of stability study (up to 11 days and 22 days for on-fiber and in-solution storage, respectively). Extractions were performed over 20 min in static mode from 1 mL of aCSF spiked with analytes at 500 ng/mL and subsequently desorbed into 50 µL of desorption solution – unmodified or containing antioxidants.

The experimental design described above was later deemed flawed in regard to the used model sample type – artificial cerebrospinal fluid was not a matrix of interest for this study, raising questions about relevance of obtained results for brain tissue analysis. Due to differences in chemical environments of these matrices, it is very likely that significantly different species are coextracted that could in turn influence the stability of the analytes during storage. Therefore, an improved stability test was carried out employing the surrogate brain matrix as sample and exploring additional strategies of storage. Besides the immediate desorption and storage in desorption solution in -80°C freezer (considered as baseline), the following strategies were investigated: immediate desorption followed by

purging of the desorption solution and the storage vial with nitrogen gas to provide inert atmosphere, storage in -80°C freezer; snap-freezing of the fiber by dipping in liquid nitrogen for 10 s immediately after extraction followed by on-fiber storage in -80°C freezer; on-fiber storage in room temperature. Additionally, an extended list of neurochemicals was subjected to this test.

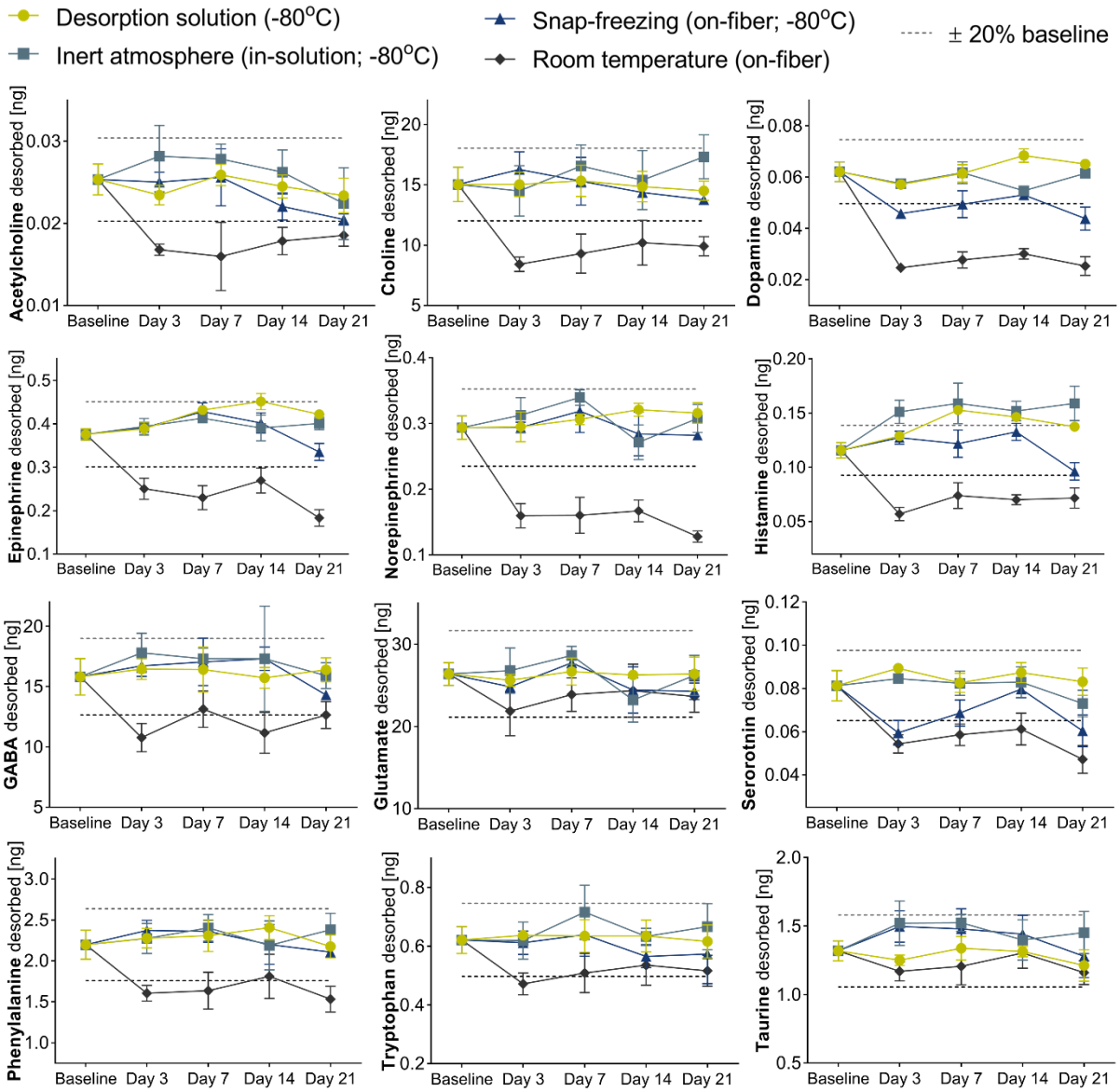

Figure 2.10: Second iteration of the neurotransmitters stability study - changes in recovered amounts of neurotransmitters throughout 21 days. Extractions were performed over 20 min in static mode from 0.5 g of surrogate brain homogenate matrix spiked with analytes at 250 ng/g (except glutamate, GABA, phenylalanine, tryptophan, and taurine, for which the endogenous fraction was extracted) and subsequently desorbed into 50 µL of desorption solution.

As previously, generally good stability was observed for samples stored in solution. Additional purging of the desorption solution and the storage vials with nitrogen to introduce inert atmosphere did not improve stability. The majority of tested neurochemicals (expect for dopamine and serotonin) can also be stored frozen on-fiber up to 7 days without significant analyte loss, while some remain stable in these conditions throughout the entire investigated storage period of 21 days. For all analytes belonging to the neuromodulatory group (catecholamines, serotonin, histamine, and acetylcholine) and choline the initial period of 3 days in room temperature storage resulted in approx. 50% drop of recovered amounts with no further decrease until the end of the stability test. For the remaining compounds the initial recovery drop was on the 20% border, while glutamate and taurine remained stable on fiber in room temperature even during prolonged storage time up to 3 weeks.

Given the attained results, it is thus recommended that *in vivo* sampling applications employ the in-solution method for storage with desorption into dark vials with solvent containing some form of antioxidant (with formic acid being recommended for this application), and instrumental analysis is carried out as soon as it is permissible for best results. When practicality calls for on-fiber storage for shipment/transportation it is recommended to desorb the fibers immediately after transport and further storage in-solution if necessary. If immediate analysis is not possible it is recommended that samples be stored in a freezer; however, increasing changes are expected to progress over time.

Quantitation of neurotransmitters in brain surrogate matrix

A performance evaluation of the developed probes and protocol, involving extraction and quantitation of target neurotransmitters in brain tissue *in vitro* in laboratory conditions, was herein carried out as a means to assess the efficacy prior *in vivo* nonhuman primate brain sampling. For this purpose, we developed a brain surrogate matrix consisting of brain homogenate and agar gel to be used in lieu of live tissue. This matrix serves as a good approximation of the chemical composition and physical consistency of brain matter, while also enabling easy spiking with analytes. A homogeneous

analyte distribution is important when performing external matrix-matched calibration, a feat which proves difficult to achieve when spiking intact brain tissue due to the fact that brain tissue is heterogeneous in nature.

Preliminary tests unveiled that acetylcholine standard undergoes significant enzymatic degradation by acetylcholinesterase following its introduction into brain homogenate. This degradation occurs even after freezing tissue at -80° for several months.[154] Therefore, an enzymatic activity inhibition step was introduced into the procedure of calibration points preparation. Addition of 1 mM PMSF to brain homogenate followed by incubation at 37°C for 1 h prior to mixing with the analyte-containing agar gel successfully eliminated the degradation of acetylcholine, thus enabling extraction of this analyte.

To further strengthen the reliability of the method in conditions resembling real sampling scenarios, several more compounds, for which the method was not optimized, were quantified. The selected compounds are endogenously present in brain homogenate, and represent a group of neurochemically relevant compounds which either participate in neurotransmission (taurine), are precursors for the synthesis of several neurotransmitters (phenylalanine, tryptophan, choline), or are products of their metabolism (choline).[155] Due to the high endogenous concentration of these compounds (as well as glutamate and GABA) in the brain homogenate, quantitation of these compounds was based on the signals of their corresponding deuterated isotopologues. This approach is valid even if the compounds of interest are present in the blank matrix.[156,157,158]

Use of surrogate brain matrix has been proven as a suitable solution for external calibration of *in vivo* measurements with two different IS correction strategies, meeting the acceptance criteria for precision and accuracy. The first strategy employed addition of IS in the desorption solution, while the second utilized the signals of deuterated isotopologues of analytes corrected with the endogenously present compounds (**Figure 2.11** and **Figure 2.12**). Given the excellent linearities and very low RSDs

of replicate measurements achieved via correction with endogenously present and stable compounds, this strategy is worth exploring for *in vivo* measurements, provided identification of suitable endogenous IS in practice.

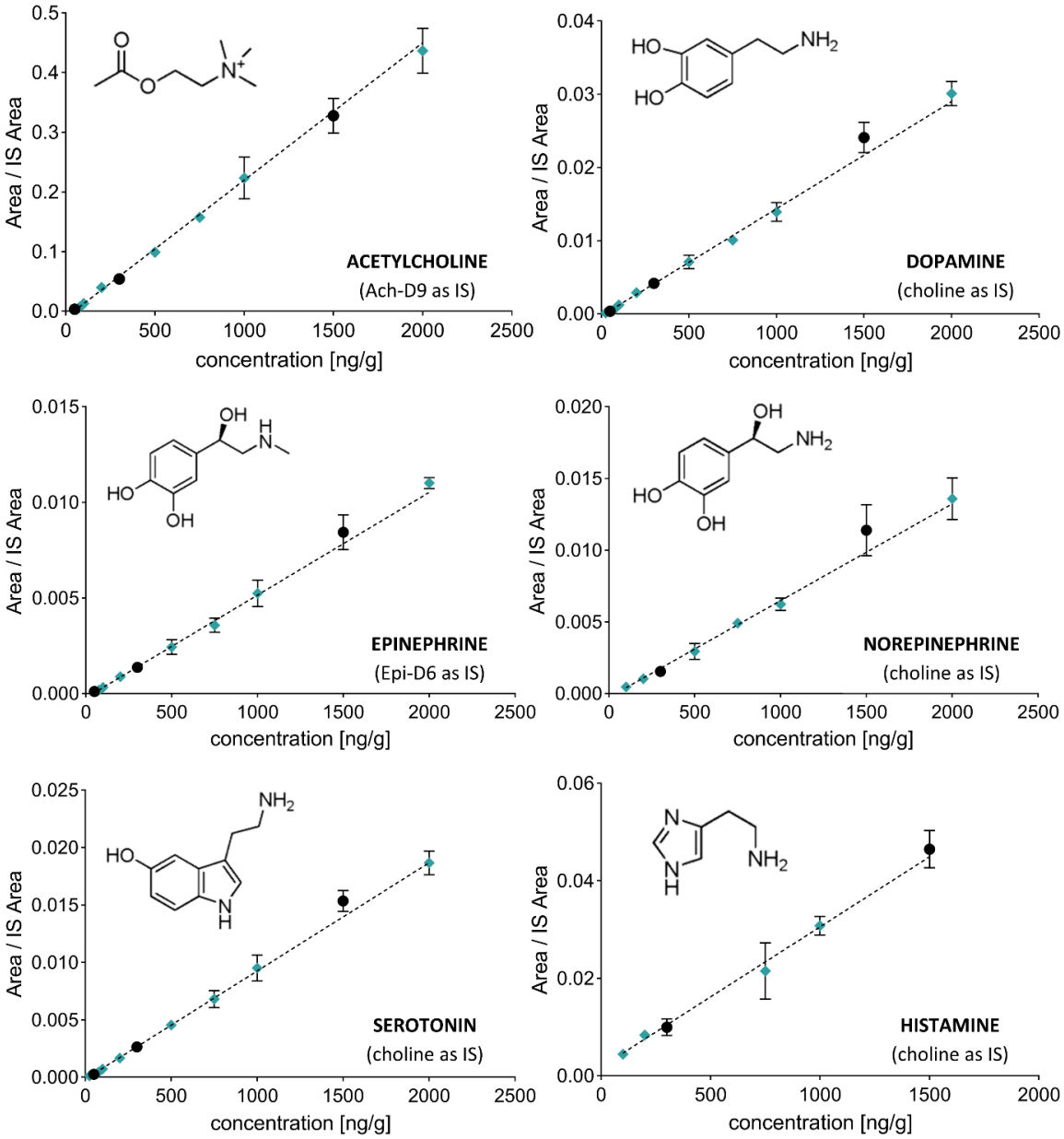

Figure 2.11: Quantitation of targeted neurotransmitters with different strategies of IS correction. Acetylcholine, dopamine, epinephrine, norepinephrine, serotonin, and histamine were calibrated with the endogenously present choline. The black circles represent the validation points. Error bars represent standard deviations of four replicate measurements.

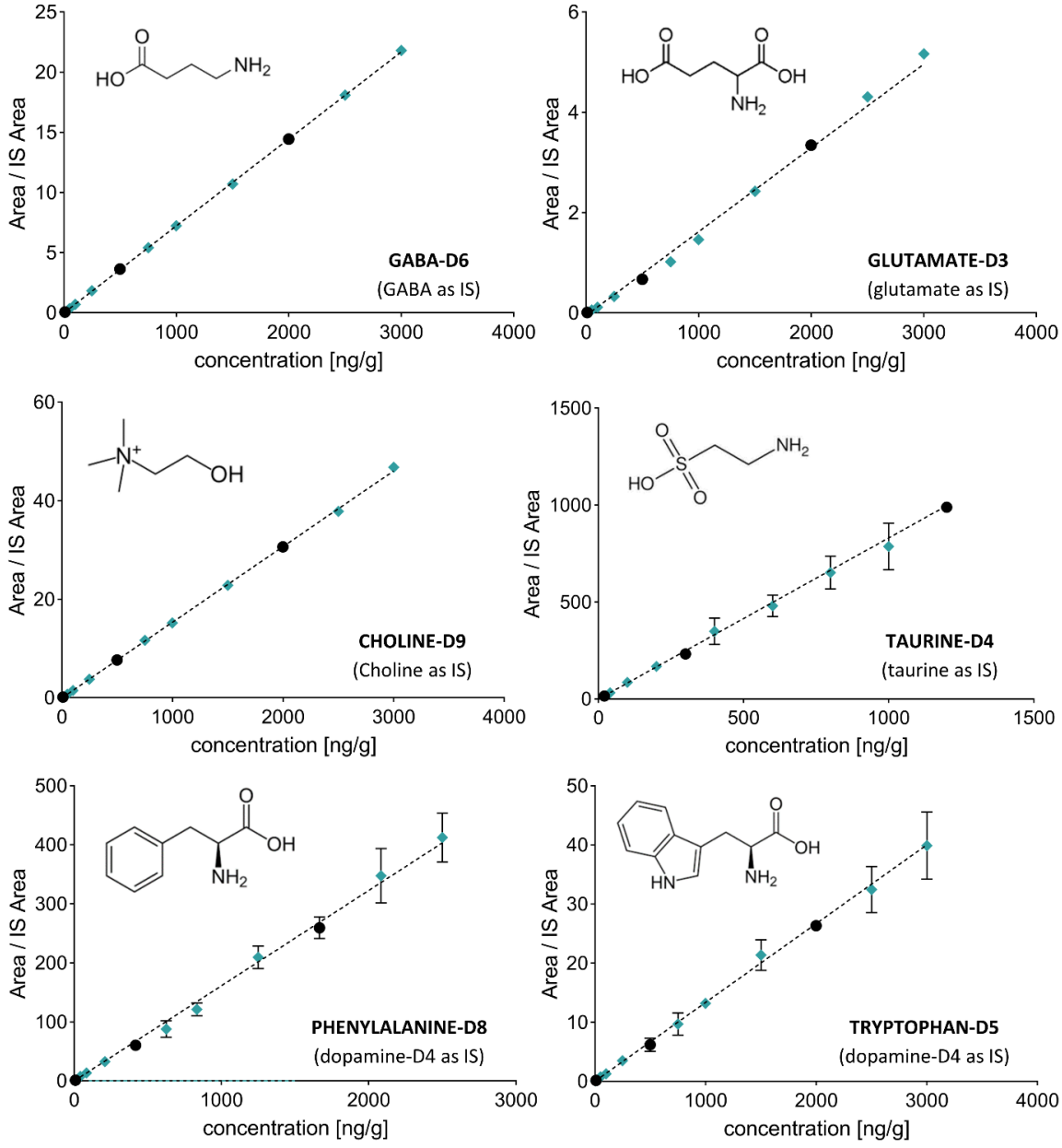

Figure 2.12: Quantitation of targeted and additional neurochemicals with different strategies of IS correction. Glutamate, GABA, choline, taurine, phenylalanine, and tryptophan (present in brain at endogenously high concentrations for which a "blank" matrix does not exist) were quantified based on their deuterated isotopologues used as analytes and the endogenous compounds as IS. In the case of the amino acids phenylalanine and tryptophan, an IS added to the desorption solution (dopamine-D4, given its close retention time to these compounds) was used for correction. The black circles represent the validation points. Error bars represent standard deviations of four replicate measurements.

Table 2.3: Parameters of calibration curves used for quantitation of neurotransmitters and neurochemically relevant compounds in surrogate brain matrix.

Compound	Slope $[\frac{1}{ng/mL}]$	Intercept	R^2	Weight
Ach	2.3e-4	-0.0104	0.983	$1/x^2$
5-HT	9.4e-6	-0.0002	0.992	1/x
Hist	2.9e-5	0.0019	0.972	1/x
NE	6.8e-6	-0.0003	0.985	1/x
Epi	5.4e-6	-0.0002	0.985	$1/x^2$
DA	1.5e-5	-0.0003	0.993	1/x
Compound	Slope $[\frac{1}{\mu g/mL}]$	Intercept	R^2	Weight
GABA	7.2e-3	-0.0052	0.999	1/x
Glu	1.5e-3	-0.0048	0.995	1/x
Cho	1.5e-2	-0.0047	0.999	1/x
Taur	8.3e-1	0.3258	0.979	$1/x^2$
PheAla	1.6e-1	0.0875	0.987	1/x
Trp	1.4e-2	0.0225	0.988	1/x

Table 2.4: Absolute matrix effect and figures of merit for quantitation of neurotransmitters and neurochemically relevant compounds in surrogate brain matrix using the miniaturized SPME probe.

Compound	LOQ [ng/mL]	Accuracy: % Error (n=3)			Precision: %RSD (n=3)			Absolute matrix effect [%]		
		50 ng/mL	300 ng/mL	1500 ng/mL	50 ng/mL	300 ng/mL	1500 ng/mL	1(5*) ng/mL	50 ng/mL	200 ng/mL
Ach	50	20	7	2	7	12	9	87	99	100
5-HT	25	12	1	10	7	2	6	111	104	101
Hist	100	-	6	6	-	17	17	123	120	118
NE	100	-	11	15	-	9	16	96*	97	105
Epi	50	20	2	7	4	5	14	94	102	101
DA	25	15	1	11	7	7	9	102	105	101
Compound	LOQ [ng/mL]	Accuracy: % Error (n=3)			Precision: %RSD (n=3)			Absolute matrix effect [%]		
		10(20*) µg/mL	500 µg/mL	2000 µg/mL	10(20*) µg/mL	500 µg/mL	2000 µg/mL	1(5*) ng/mL	50 ng/mL	200 ng/mL
GABA	5	1	1	0	4	2	1	95*	97	104
Glu	10	7	9	12	5	1	1	125	90	90
Cho	5	2	0	0	5	3	1	107	91	88
Taur	20	4*	12	1	4*	12	2	101*	100	108
PheAla	4	5	9	3	8	7	7	107*	93	99
Trp	5	3	12	7	6	18	1	156*	100	99

Limits of quantitation of the method certainly represent an area which leaves room for improvement, as several compounds would not be quantified at their physiological levels in brain ECF, as reported in the literature (e.g., glutamate, taurine, and GABA in rat hippocampal ECF at 0.43 µg/mL, 2.6 µg/mL, and 0.08 µg/mL, respectively[159]). However, LOQs for the other analytes were shown to be suitable or significantly lower than needed for detection and quantitation reported elsewhere: acetylcholine at 2870 ng/g of whole rat brain,[160] choline at 125-156 µg/mL in 4 different locations of human brain,[161] dopamine at 2520 ng/g of whole rat brain,[162] epinephrine at 99-297 ng/g and norepinephrine at 161-1367 ng/g in several different rat brain locations,[163] serotonin at 1604 ng/g in rat hypothalamus tissue,[164] and histamine at 292 ng/g in rat hypothalamus tissue.[165] When assessing the applicability of a method, it is important to take into consideration that different analytical techniques and sample preparation methods yield different values of concentrations.[166] A differentiation must also be made between brain areas and compartments within these areas: the concentration of glutamate can fluctuate by several orders of magnitude when considering compartments such as brain ECF, synaptic cleft, and synaptic vesicles, or measurements in brain homogenate.[167]

The absolute matrix effect was evaluated with the criteria of acceptance assumed at ≤20% at the lowest level and ≤15% at the remaining concentration levels. The response of the analytes in regard to which the matrix was blank, was corrected with their corresponding deuterated IS. The response of analytes endogenously present in the matrix was corrected with deuterated isotopologues eluting at the most approximate time (except for taurine, which eluted in the dead volume and was thus arbitrarily matched with NE-D6). Histamine was affected by interfering matrix components throughout the entire concentration range, while GABA and tryptophan were affected at the lowest concentration levels (**Table 2.4**). The complex matrix had no significant influence on the remaining compounds at all tested concentration levels.

Attained results indicate that the used IS correction strategy sufficiently eliminates matrix effects in most cases (with exception of tryptophan and glutamate at the lowest concentration level). However, histamine quantitation may require a different IS correction strategy or no correction at all, as the matrix effect was absent at the middle and high concentration levels when no correction was applied.

2.3 Multineuromodulator measurements across fronto-striatal network areas of the behaving macaque

2.3.1 Introduction

Neurotransmitters and neuromodulators constitute a group of compounds that have undoubtedly one of the biggest contributions to observable processes occurring in the brain. These endogenous neuroactive chemicals directly influence neuronal communication by electrically altering the membrane properties of neurons by acting on ionotropic receptors, which are directly coupled to ion channels that may open or close upon binding of their respective neurotransmitter.[23,168] Another mode of action is binding to the metabotropic receptors which initiate the signal transfer into the cell leading to the activation of second messengers (cyclic nucleotides, diacylglycerol, calcium or inositol triphosphate) as well as to the phosphorylation of proteins.[168] This in turn changes the internal processes of neurons by activating or deactivating proteins and genes. Neurotransmitters acting in this way are often managed by brain nuclei (dense clusters of neurons with similar neurochemical properties) located in subcortical areas. They can influence neuronal communication in a subtler and slower manner due to the lack of direct electrical influence,[168] however a timescale in the range of several seconds is not uncommon.[23] Understanding of the role of these chemicals in cognition and behavior relies on the ability to dynamically measure their concentrations in local brain regions.

Extracellular concentrations of neuromodulators influence firing regimes, input-output relationships, and neural interactions in local circuits and long-range brain networks[95,169] and are dysregulated in virtually all psychiatric disorders.[170,171] Accumulating evidence suggests that these fundamental roles of neuromodulators for circuit functioning are unlikely realized by single neuromodulators operating in isolation. Rather, neuromodulatory systems are heavily inter-twined[170,172,173] and operate simultaneously on individual cells and circuits.[95,174–176] In each circuit, local mechanisms exert control over the release of neuromodulators from terminals of brainstem-originating projection neurons. This local control proceeds through activation of presynaptic glutamatergic receptors.[177–182] These insights suggest that an understanding of the contribution of neuromodulators to circuit functioning requires simultaneous measurement of multiple neuromodulators in conjunction with ongoing glutamatergic neurotransmitter concentrations and action. Consistently with this conclusion, single neuromodulator theories often fail to account for all observable symptoms in psychiatric diseases.[183–185] Despite the accumulating evidence for the interdependence of neuromodulator actions, few methods exist for their simultaneous measurement *in vivo* and across multiple brain areas.

Most of these existing neurochemical sensing methods allowing multineuromodulator sampling have a barrier to entry by requiring specialized equipment and trained experts preventing data collection by scientists who are otherwise interested in the role of endogenous and exogenous neuroactive chemicals in cognition and psychiatric disorders. Here, we set out to address some of these limitations with a novel protocol for measuring multiple neuromodulators *in vivo* in discrete 20-min intervals using solid phase microextraction (SPME) probes and protocol optimized in the previous subchapter.[36,77] SPME provides an alternate method for neurochemical data collection, compatible with instrumental analysis tools such as LC-MS. This method has been shown to extract in neural tissue dynamic changes in dopamine and serotonin levels with comparable precision to MD.[186,187] Additionally, due to the

similarity of SPME probes to commonly used microelectrodes in electrophysiological recordings, relatively minor adjustments can allow for the adaptation of conventional microelectrode driving systems for SPME use. This, combined with post-collection analysis through standard chemistry facilities, makes SPME an attractive and easy-to-use tool for electrophysiology laboratories. SPME has the potential to be a powerful new tool to complement the mentioned methods well suited for neurochemical profiling that spans both multiple neuromodulators as well as multiple brain regions simultaneously. Such data allow for global observation of slow neuromodulator dynamics that could better inform our hypotheses and help relate global neuromodulator levels to electrophysiology and behavior. Thus, the ability of SPME to report major neuromodulators as well as glutamate and GABA were tested in two behaving rhesus macaques. Probes were repeatedly and simultaneously inserted into two cortical regions and the striatum to observe interareal differences between extracellular neuromodulator concentrations. We found that extracellular concentrations of glutamate, dopamine, acetylcholine, and choline could be reliably distinguished and differed systematically between brain regions.

2.3.2 Experimental

Animals

Data were collected from two 8-year-old male rhesus macaques (*Macaca mulatta*) weighing 8–12 kg. All animal care and experimental protocols were approved by the York University Animal Care Committee and were in accordance with the Canadian Council on Animal Care guidelines. Details regarding the experimental setup, recording procedures, and reconstruction of recording sites have been described previously.[188] Briefly, animals were implanted with a 20 mm x 28 mm recording chamber over the frontal region of the right hemisphere guided by stereotaxic coordinates[189] and magnetic resonance images (MRI). The animals were seated in a custom-made primate chair and head stabilized with their eyes 65 cm away from a 21’ LCD monitor refreshed at 85 Hz. Eye traces were collected by

a video-based eye-tracking system (Eyelink 1000 Osgoode, Ontario, Canada, 500-Hz sampling rate). The animals were engaged in an overtrained attention task in which they would use saccadic eye movements to acquire juice reward (**Figure 2.13**). The specifics of the task are described elsewhere.[190] Both animals showed stable performance and acquired similar reward volumes on all recording days. In both tasks, stimulus presentation and reward delivery was controlled through MonkeyLogic (https://www.brown.edu/Research/monkeylogic/).

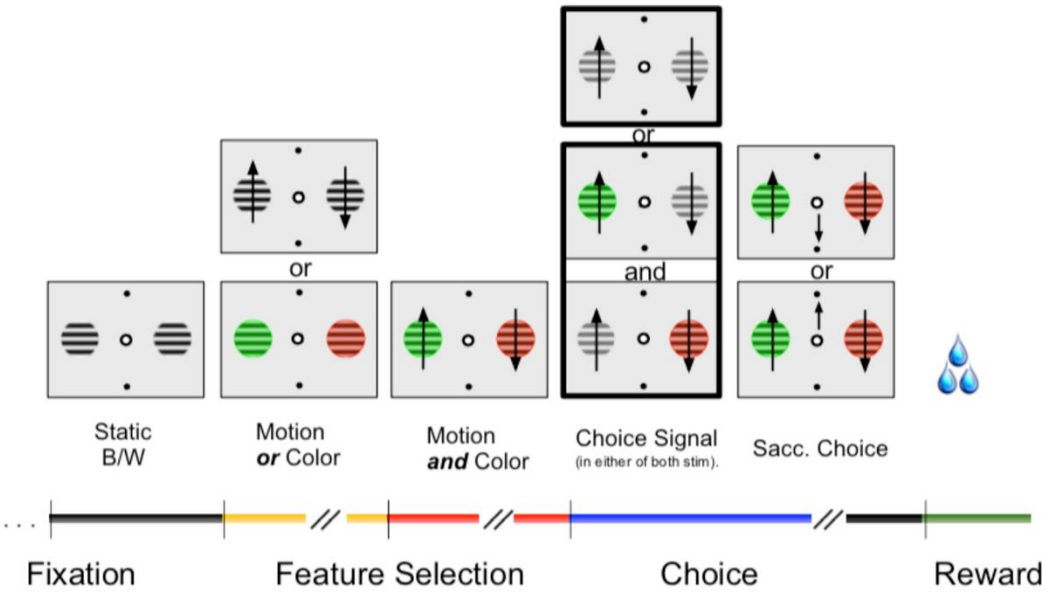

Figure 2.13: Behavioral task that the monkeys were engaged in. Briefly, the monkey was expected to fixate a central fixation point until criterion when two graded stimuli appeared. The graded stimuli acquired color and motion of the graded stripes, featured in either order. The two stimuli then either simultaneously dimmed (go-signal) or dimmed one at a time in either order. The monkey, through trial and error, identified the rewarded stimulus via its color feature which was the sole identifying feature informative of reward. The monkey was then expected to wait until the dimming of the selected stimulus and respond in the same direction as the motion of the graded stripes on the chosen stimulus. If the monkey correctly accomplished this, it would receive deterministic reward in the form of liquid juice. Monkey As was engaged in a variation of this task with reduced complexity in order to match monkey Ke in performance and reward acquisition over the sampling period. Figure reproduced from Hassani et al.[190]

MRI guided electrophysiological mapping of target brain areas

The anatomical coordinates of the brain regions of interest were first identified through 3T MR images (**Figure 2.14**). The MR images were then verified with extracellular electrophysiological

recordings of the target areas, which provided the gray and white matter boundaries for the cortical sites and the dorsalmost aspect of the head of the caudate nucleus (CD). Tungsten microelectrodes were 200 µm thick with an impedance of 1–2 MΩ. All electrodes, SPME probes, and their accompanying guiding cannulas were driven down into the brain and later out by using software-controlled precision microdrives (Neuronitek, Ontario, Canada). Electrodes were connected to a multichannel acquisition processor (Neuralynx Digital Lynx System, Bozeman, MT) which was used for data amplification, filtering and acquisition of spiking activity. Spiking activity was obtained by applying a 600- to 8,000-Hz bandpass filter, with further amplification and digitization at a 32-kHz sampling rate. For every recording day, electrodes were lowered until the first detection of spiking activity (indicative of gray matter) at the depth suggested by the MR images.

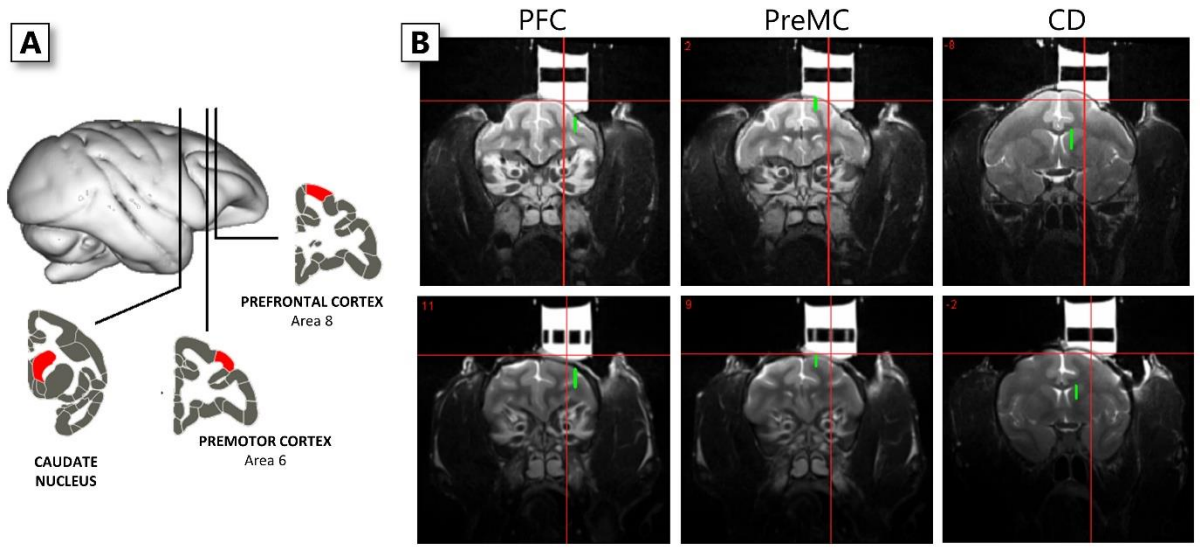

Figure 2.14: SPME sampling events in the right hemisphere of two Rhesus Macaques. **A)** Target brain regions are highlighted in red and include two cortical regions: prefrontal cortex (PFC) area 8 and premotor cortex (PreMC) area 6 as well as a subcortical region: the head of the caudate (CD). **B)** MR images with the target brain regions marked in green; Top row – monkey As, bottom row – monkey Ke.

SPME sampling and postprocessing procedures

The SPME probes manufacturing, LC-MS/MS analysis, and quantitation of neuromodulators were performed according to the procedures delineated in subchapter 2.2. For the *in vivo* sampling, two

additional features were added to the final probe and procedure. The probes were sterilized in steam at 121°C for 15 min, after the cleaning and conditioning steps. Then, they were assembled with sheathing cannulas to prevent unwanted extraction on the way to the target brain areas. The cannulas underwent the same cleaning and sterilization procedure as the probes and the lengths of both components of the SPME assembly were adjusted to 60–70 and 70–80 mm for the probes and cannulas, respectively. When choosing the size of the cannulas, it was critical that their ID matched the probe diameter as closely as possible in order to avoid ECF entering the gap between the internal walls of the cannula and the SPME coating, causing contamination of the probe. Moreover, the cannulas should have thin walls to keep the overall probe assembly size as small as possible to attain low invasiveness of the sampling. The cannulas assembled with the developed probe had 200 µm ID and 270 µm OD, meeting the above requirements.

All three SPME assemblies were simultaneously driven to 200 µm above the point of first spiking detection. SPME assemblies were located ~1 mm away from the electrode penetration location. Then, only the SPME probes were inserted 3 mm into the areas of interest. On average, macaque cortical thickness is only 2 mm while the head of the CD at the point of sampling was well over 3 mm. A pre-equilibrium extraction time of 20 min was selected to satisfy the practical requirement of the *in vivo* sampling, as discussed in subsection 2.2.4. After the 20-min extraction event, all SPME probes were driven back 3 mm into the guiding cannulas and all SPME assemblies were withdrawn from the brain (**Figure 2.15**). The microdrives were then removed from the chamber to enable unclamping of the SPME probes, a brief wash, and then storage in glass vials surrounded by dry ice until being placed in a -80°C freezer. The desorption of the probes, LC-MS/MS analysis and quantitation using external surrogate matrix-matched calibration protocol were conducted according to the workflow described in subchapter 2.2. For *in vivo* measurements, the IS was included in the desorption solution at 20 ppb and each analyte was corrected with its corresponding deuterated isotopologue.

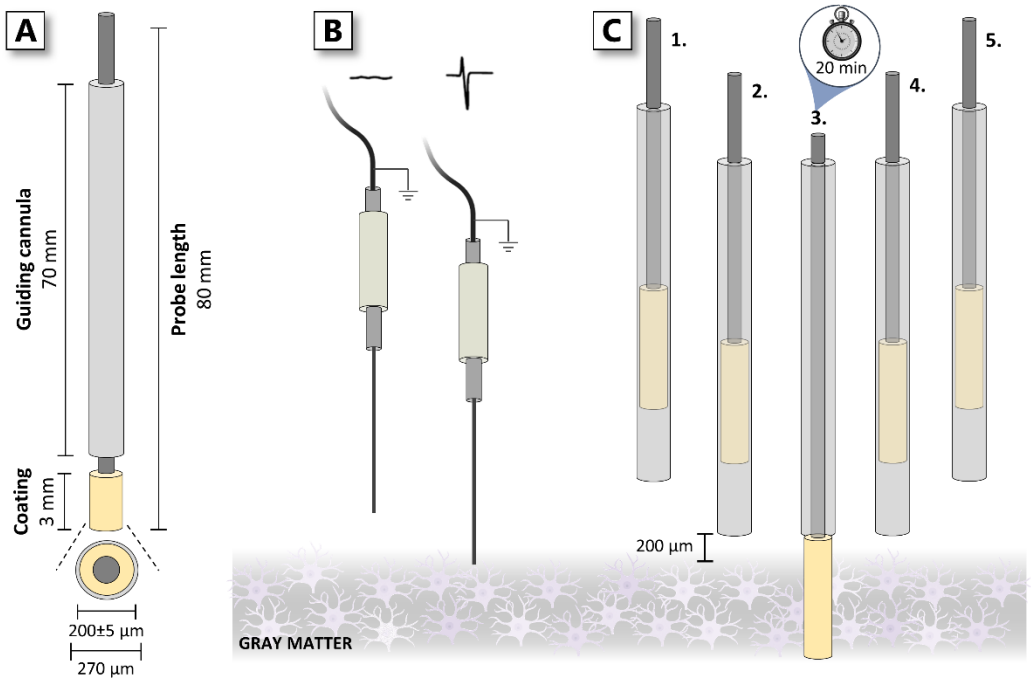

Figure 2.15: *In vivo* SPME sampling protocol in macaque brain. **A**: dimensions of the SPME probe and the accompanying cannula. The SPME coating made up the terminal 3 mm of the entire probe and was placed in a cannula with an internal diameter of 200 µm and an external diameter of 270 µm. **B**: tungsten microelectrodes were lowered into the brain guided by 3 T MR images to map the depth at which detectable spiking was observed matching expectations from the MR images. **C**: 1. Initial position with 3 mm buffer from the opening of the cannula and the start of the coating; 2. SPME probes and their accompanying cannulas in all brain areas are simultaneously lowered to 200 µm above the point of first observable firing in the target brain region; 3. the SPME probes are lowered to expose the 3 mm coating; 4. After 20 min of extraction, the SPME probes are retracted 3 mm back into the cannula; 5. The probes and their accompanying cannulas are removed from the brain. All elements of each assembly (microelectrode, SPME probe and cannula) were driven at 30 µm/s.

One entire sampling event (one extraction in three different brain areas together with assembling the SPME probes and cannulas, driving into and out of brain, washing, and preparing for storage) was performed within 50 min, except for the first sampling event in each sampling day. The first sampling event, with the area identification using electrophysiology recording, was performed within 75 min. The removal of the SPME probe from the gray matter and the positioning of a new SPME probe in the same location limits the temporal continuity of sampling. We believe that further optimizing of the probe switching procedure with, e.g., preloaded SPME probes will allow replacing them within 2–10 min. Alternatively, SPME probes could be used in spatially separate but adjacent guiding tubes

(separation of ~300 µm), which would allow to switch sampling from one to other probe without temporal delays.

2.3.3 Results and Discussion

Results

During all measurements, animals were engaged in a cognitively demanding task with stable behavioral performance to minimize state-dependent fluctuations of basal extracellular concentrations of neuromodulators. Three brain regions were selected to provide a sample of extracellular neuromodulatory concentrations. Two cortical regions, prefrontal cortex (PFC) area 8 and premotor cortex (PreMC) area 6, as well as one striatal region- the head of the caudate nucleus (CD) were selected (**Figure 2.14**). In three daily sessions, we sampled three times per session simultaneously from all three areas. Monkey As had an additional 3 days of recording with one sample collected on each day. Overall, we collected and analyzed 12 probes in monkey As and 9 probes in monkey Ke. We were specifically interested in major neuromodulators and neurotransmitters but successfully measured other compounds such as amino acids (e.g., glutamine, taurine, phenylalanine, etc.) that we do not discuss here. To allow comparison of the SPME extraction results to those typically reported in MD studies, we calculated the relative change in measured concentrations across the three successive sampling events per session pooled across monkeys to enhance the statistical power of the analysis (**Figure 2.16**). Relative to the end of the first sampling event, the second and third sampling events started after 40 min and 100 min, respectively. We expected that the variability of measurements (indexed as standard error of the median) is comparable to repeatedly measured MD of an identical, active brain state. We found that measured concentrations did not change significantly across sampling events for any compound area combination (Wilcoxon rank-sum test; **Figure 2.16**). We found that four target neurotransmitters and neuromodulators were reliably detected in each animal: glutamate, dopamine, acetylcholine, and choline. Serotonin was also detected on several probes but always near the LOD and therefore was

excluded from analyses here. Glutamate concentrations were several orders of magnitude higher than all other observed compounds of interest in all areas and both animals. Relative to glutamate, choline concentrations were >15 times lower, dopamine concentrations were >700 lower and acetylcholine concentrations were >8,300 times lower (**Figure 2.17**).

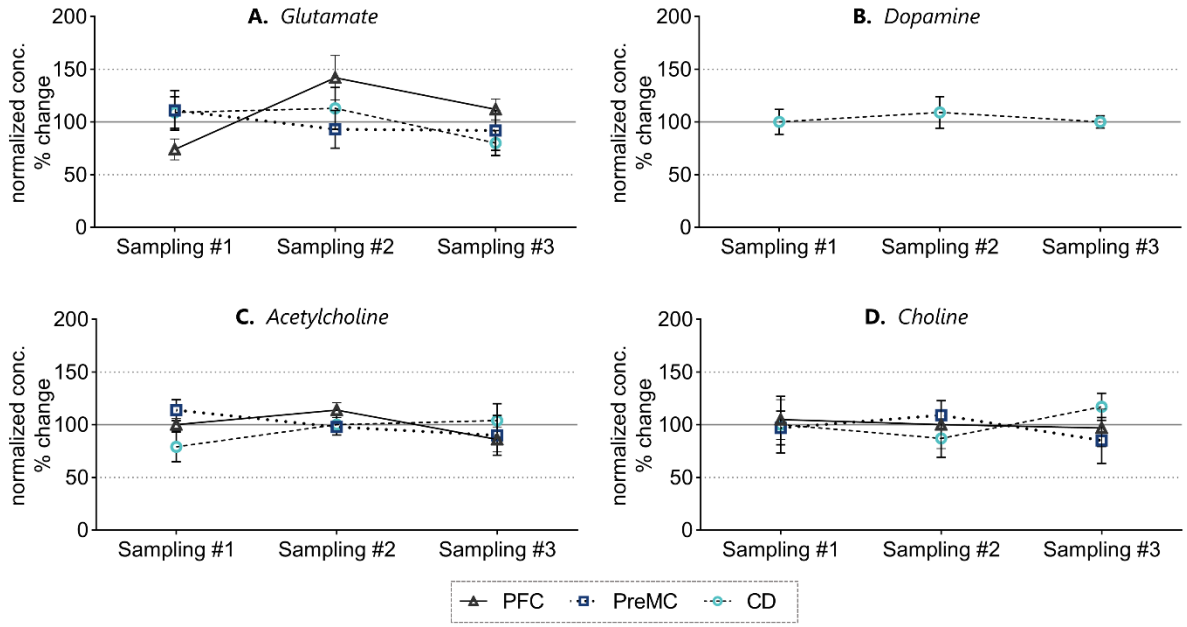

Figure 2.16: Relative changes of amounts of neuromodulators extracted *in vivo* by SPME throughout the sampling session in each sampled brain region. The median concentration of glutamate (**A**), dopamine (**B**), acetylcholine (**C**), and choline (**D**) with standard error of the median plotted for each sampling time and location. Data was normalized for each subject separately and for the respective neurochemical and area combinations. Sampling events were 20 min in length and the time between the end of one sampling event to the start of the next sampling event was 40 min (SD 2 min), making the second sampling event 40 min and the third 100 min from the initial measurement. No significant change was observed for any neuromodulator in any brain region (Wilcoxon rank-sum test). Note that a single prefrontal choline data point was excluded in this analysis for being >4 standard deviations from the median (data point is present in **Figure 2.17**).

Glutamate concentrations (across areas), measured as median ± standard error, ranged from 159,147 (±19,395) to 233,659 ng/mL (±33,917) in monkey As, and from 135,523 (±22,945) to 184,333 ng/mL (±33,516) in monkey Ke. In both monkeys, glutamate concentrations were highest in the head of the CD, which was significantly different from glutamate concentrations in the PreMC in monkey As (Kruskal-Wallis test with Tukey's HSD correction, P=0.048) but not in monkey Ke [Kruskal-Wallis

test with Tukey's HSD correction, P=0.847, not significant (ns)]. Glutamate concentrations between the CD and PFC, as well as the PFC and PreMC were not significantly different for either animal. Comparisons between monkeys showed no significant differences between the glutamate concentrations in any of the measured areas (**Figure 2.17**). In addition to glutamate, dopamine could be reliably detected in both monkeys in the CD at concentrations of 232 ng/mL (±47) in monkey As, and 226 ng/mL (±31) in monkey Ke. These concentrations were similar between monkeys (Wilcoxon rank-sum test P=1, ns). Dopamine was not found above detection limits in frontal cortex.

Acetylcholine measurements in the three brain areas ranged from (across areas) 25 (±2) to 36 ng/mL (±5) in monkey As and from 29 (±2) to 36 ng/mL (±4) in monkey Ke. In monkey As, extracellular acetylcholine concentrations between the CD and PreMC were significantly different (Kruskal-Wallis test with Tukey's HSD correction, P=0.008). Cortical areas were not significantly different from one another (Kruskal-Wallis test with Tukey's HSD correction, P=0.476, ns) nor was there a significant difference between the CD and PFC (Kruskal-Wallis test with Tukey's HSD correction, P=0.145, ns). In monkey Ke, only one cortical region had concentrations of acetylcholine above quantitation limits, which approached significant difference to the concentrations measured in the CD (Wilcoxon rank-sum test, P=0.08). Measurements of extracted acetylcholine in the PreMC of monkey Ke were consistently below detection limits (**Figure 2.17**). We also measured choline, which is a main product of the enzymatic breakdown of the highly regulated acetylcholine and which is a main indicator of attentional modulation of cholinergic activity in frontal cortex.[191] Choline concentrations ranged across areas from 2,914 (±590) to 5,078 ng/mL (±675) in monkey As and from 3,408 (±3,705) to 5,533 ng/mL (±860) in monkey Ke. Choline concentrations between the CD and PreMC were significantly different in monkey As (Kruskal-Wallis test with Tukey's HSD correction, P=0.030), but not in monkey Ke (Kruskal-Wallis test with Tukey's HSD correction, P=0.729, ns). All other area comparisons were not significant for both monkeys. Comparisons of choline concentrations between monkeys were not

significant in any of the measured areas. Overall, serotonin concentrations were not observed as reliably as the other reported neurochemicals and therefore were excluded from the main analyses. However, in monkey As, serotonin was observed near the LOQ in the prefrontal cortex as well as the CD in a subset of probes. Within the nine probes placed in both areas, serotonin was detected in 22% of samples (2/9 probes) in the prefrontal cortex and 33% of samples (3/9 probes) in the CD. Serotonin observations ranged from 149 to 232 ng/mL with a median of 171 ng/mL (±18.5 ng/mL; standard error of the median) with a LOQ of 100 ng/mL. The proximity of the measurements to the LOQ suggest that the other probes likely collected concentrations of serotonin below the detection threshold. No serotonin observations were made in monkey Ke.

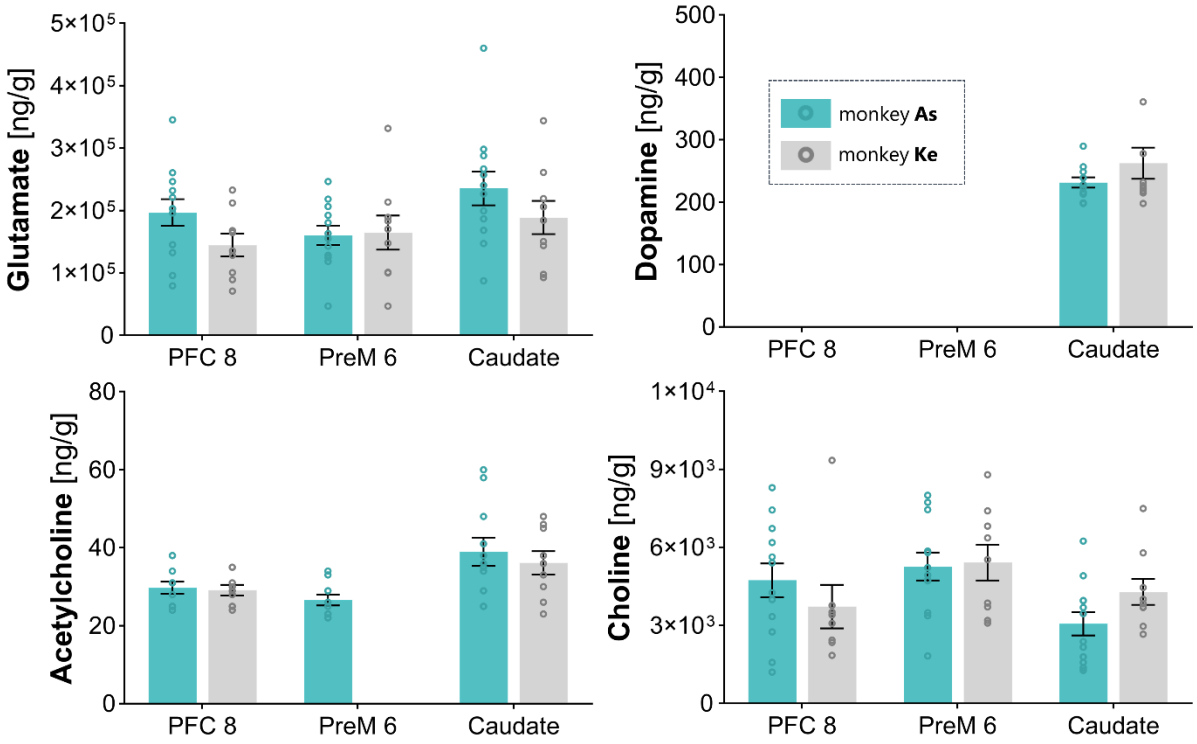

Figure 2.17: Quantitation of neuromodulators in the macaque brain. Median and standard error of the median of n=12 probes for monkey As and n=9 probes for monkey Ke with no data excluded. Four neuromodulators were reliably measured: glutamate, dopamine, acetylcholine, and choline. All brain regions had high concentrations of glutamate and relatively much lower concentrations of acetylcholine and choline extracted (with the exception of monkey Ke PreM6 lacking detectable acetylcholine). The only tested region to yield measurable dopamine was the caudate.

Discussion

We demonstrated reliable measurements of glutamate, dopamine, acetylcholine, and choline simultaneously within cortical and subcortical regions of awake and behaving macaques using solid phase microextraction probes. Glutamate concentrations were several orders of magnitude higher than dopamine, acetylcholine, and choline across brain regions. Extracellular concentrations of choline, dopamine, and acetylcholine were detected at >15, >700, and >8,300 times lower than glutamate, respectively. Dopamine was readily detected in the CD but not observed at detectable concentrations in the cortical regions measured. Acetylcholine concentrations showed a statistical trend of being different between the CD and measured cortical areas and with high consistency between monkeys. Choline concentrations, a product of acetylcholine degradation as well as a precursor for its synthesis, were negatively correlated with acetylcholine ($R=-0.355$; $P=0.01$). Together, these findings provide new and rare insights about the neurochemical circuit profiles during an active brain state in three areas of the primate fronto-striatal network. The high consistency of measured concentrations within animals, between brain areas, and between monkeys suggests that SPME probes could provide a versatile neuro-technique for understanding how variations of the neurochemical milieu relate to local and long-range circuit operations and ultimately cognitive functioning.

Extracellular concentrations of glutamate, dopamine, acetylcholine, and choline

Our results revealed particularly high levels of glutamate within all measured brain regions (PFC, PreMC, and CD) relative to other neuromodulators. This finding is consistent with its ubiquitous role as major excitatory neurotransmitter. This holds true even in the CD, which consists exclusively of GABAergic neurons but receives glutamatergic inputs from the cortex.[25] Tonic concentrations of glutamate within the striatum have been previously reported to be comparable to that of the hippocampus, prefrontal cortex, and other cortical areas due to glutamatergic inputs, extrasynaptic release and glial release.[166,192,193] In contrast, classical neuromodulators such as dopamine and

acetylcholine are released in extracellular space through volume transmission where they are highly regulated and may bind to receptors on multiple neurons.[101,194–196] This regulation may help explain the relatively low observed concentrations of dopamine and acetylcholine and may be a large source of extracellular choline through the enzymatic breakdown of acetylcholine.

Extracellular dopamine was measured well above the detection threshold in the striatum. In combination with glutamatergic and cholinergic concentrations, our results show promise in the application of SPME to further our understanding of the relationship between glutamatergic inputs to the striatum and the neuromodulatory acetylcholine and dopamine signals impinging on striatal circuits. Such circuits are strongly involved in hypo- and hyperkinetic diseases.[171,184] Although the presence of dopamine in the PFC is well documented[197–199] it was not detected in either of the cortical regions and failed to exceed the LOQ of the method. The difference between the detection of dopamine in the CD versus PFC and PreMC cortex may be due to differences in available dopamine, release concentrations, and dynamics.[200] A possible explanation for the lack of detectable cortical dopamine could be the documented susceptibility of catecholamines to oxidation, however the results of the stability test described in the previous subchapter suggest that no significant loss of dopamine should be observed within the timeframe and the conditions employed in our protocol.

Few previous studies have documented acetylcholine concentrations *in vivo* in nonhuman primates due to its rapid breakdown by acetylcholinesterase (AChE) and the challenges of neurochemical testing in primates.[195,201,202] Acetylcholine plays a major role in organizing local circuits, deployment of attention, locomotion, and reward through different receptors present in cortical and subcortical regions.[173,203,204] It has been difficult to discern which acetylcholine concentration corresponds to efficient endogenous circuit operations. Our finding of measurements in all sampling locations except for PreMC in monkey Ke is therefore a promising starting point for future studies comparing acetylcholine concentrations, in conjunction with other neuromodulators, during different cognitive

states. The fast turnaround of acetylcholine due to AChE, however, likely leads to an underestimation of acetylcholine concentrations by SPME. Although AChE does not undergo adsorption onto the SPME probe, preventing any enzymatic degradation of already adsorbed pool of acetylcholine, the dynamic equilibration process and TWA character of the measurement in such instance may lead to a continuous transfer of acetylcholine out of the extracting phase, following the concentration gradient of the rapidly depleted acetylcholine into the extracellular space as discussed in the Introduction.

Among other sources, choline is created as a byproduct of acetylcholine degradation by AChE. Choline is also a precursor for the synthesis of acetylcholine. Given this relationship, a negative correlation between choline concentrations and acetylcholine is expected which we indeed observed in our data set. Despite the difference in the measured concentrations of choline and acetylcholine, other studies with similar differences have demonstrated the relationship of acetylcholine and choline to behavior within the cortex.[191] Future studies may focus on quantifying this relationship across a wider range of brain states.

Many factors may contribute to variation in measured concentrations of neuromodulators including behavioral state, the specific brain region measured, and individual differences among others. Importantly, different methods may yield different estimates of absolute extracellular concentrations. For example, comparable measurements of extracellular glutamate via MD or voltammetry as opposed to electrophysiological estimates can differ by orders of magnitude and may be attributed to differences in probe size or to sensitivity to different sources of glutamate.[166]

Reliable measurement of individual differences of state-specific neuromodulatory tone

Our results suggest that SPME probes provide reliable measurements in consecutive sampling events within an experimental session and between sessions on consecutive days. These results were obtained while we controlled brain states across measurement events by engaging animals in a cognitive task. This experimental control could have contributed to the comparable extracellular levels of

neuromodulators from sample to sample within and between days from similar brain locations (**Figure 2.16**).[95,205–207] The reproducibility of multiple measurements at the same anatomical location within and between days suggests that the SPME penetrations did not significantly disturb tissue.[186] This conclusion contrasts with reported experience from MD measurements, where the initial placement of the probe or guiding cannula causes transient measurement instabilities that can require up to several hours of settling time before reliable, steady-state neuromodulator concentrations are measurable.[166,199,208–210] These waiting periods must be taken into account when designing MD experiments for *in vivo* tracking of neuromodulators during behavioral tasks in awake and restrained animals. Furthermore, the reliability of observations for the reported neurochemicals with SPME is high. We present 100% reliability in reporting glutamate and choline concentrations in all brain regions and subjects. Acetylcholine concentrations were reported with 100% reliability in one animal and 92% (11/12 probes) in the other within the prefrontal cortex, 0% reliability (below detection threshold) in one animal and 83% (10/12 probes) in the other within the PreMC and 100% reliability in one animal and 92% (11/12 probes) in the other within the CD. Dopamine concentrations were reported with 100% reliability in both animals in the CD and were not observed above detection thresholds in the cortex.

Qualities and characteristic of SPME in the context of *in vivo* measurements in behaving nonhuman primates

Our results demonstrate several inherent advantages of using SPME to measure neurochemical profiles in brain circuits,[211] as illustrated in **Table 2.5**. Practically, the arbitrary length of the supporting wire and where the SPME coating is deposited allows for robust placement within the brain. The narrow diameter of the SPME probe that is within the range common to electrodes for electrophysiological recordings allows for repeated, simultaneous sampling at multiple sites without observable changes to detected extracellular neuromodulator levels using 20-min sampling times.

Table 2.5: A comparison of selected methods capable of measuring single or multiple neurochemicals *in vivo*.

Technique / Criterion	PET imaging	Electrochemistry	Microdialysis	SPME
Temporal resolution	Minutes	Highest (millisecond range)	<1-30 minutes; dependent on analytical method sensitivity, target, etc.	<5-30 minutes; dependent on analytical method sensitivity, coating thickness, target, etc.
Spatial resolution	Voxel	High; probe size and surface area may vary (relevant for enzyme-based methods)	Diffusion-based; probe size may vary (0.5-4 mm)	Diffusion-based; probe size may vary (3-4 mm); sub mm via DESI-MS
Sensitivity	Indirect measurement via competitive radiolabelled species	High	Depending on post-hoc methods (*i.e.* MS)	Depending on post-hoc methods (*i.e.* MS)
Neuroactive targets	A few at most	A few at most	Many	Many
Non-neuroactive targets	No	No	Yes, greater efficacy for hydrophilic compounds	Yes, greater efficacy for hydrophobic compounds
***In vivo* feasibility**	Difficult in awake, behaving animal models; movement highly restricted	Good (low reliability in NHPs)	Good, often requires chronic implant of cannula for repeated measurements	Very good; robust placement of multiple simultaneous probes and repeatable acute measurements
Cost	High	Low; requires special equipment	Moderate to high (if coupled to LC-MS); requires special equipment and chemistry core	Moderate to high (if coupled to LC-MS); easy to port to an acute micro-electrode setup; requires chemistry core

PET – positron emission tomography; NHP – non-human primate

Spatial resolution. In principle, the spatial resolution of the SPME measurements can reflect laminar concentration gradients across areas as small as several hundreds of micrometers. In our protocol we coated 3 mm in length with 50 μm of extracting phase thickness and desorbed the entire extraction phase segment into an organic solvent mixture for subsequent LC-MS/MS analysis. However, with the use of other techniques, such as desorption electrospray ionization (DESI), which represents a direct-to-MS approach,[212] much smaller areas of the SPME probe may be sequentially analyzed at a time allowing for laminar or near-laminar resolution. The characteristics and limitations of this strategy are outlined in the subsequent Chapters. Direct coupling of SPME probes to MS provides the advantage of rapid analysis and in principle allows the simultaneous measurement of separated compartments of a cortical column with a single probe. The absolute spatial resolution of

SPME is difficult to estimate as the technique operates through diffusion and dynamic equilibration similar to MD. As a consequence, the sampled volume will depend on sampling time, the compound's diffusion coefficient, as well as the target tissue and its properties affecting the rate of diffusion such as tortuosity.[101]

Temporal resolution. Several factors determine the appropriate extraction time using SPME. Depending on the goals of an experimenter, resolutions of several minutes may be achieved if the detection/quantitation limit is exceeded within the first few minutes of extraction. As sampling continues, the extracting phase will eventually reach an equilibrium with the external environment. In principle, sampling times beyond reaching the equilibrium will not result in increase of the amounts extracted by SPME.[36] However, in the brain there is no single stable equilibrium point and thus, even with long sampling times, there will be some variation in amounts extracted beyond the equilibrium. As outlined in the Introduction, extraction times operating within the pre-equilibrium regime of the extraction time profile, can by all means still be employed for quantitation. In practice, the fastest possible extraction time will be determined by the relation between the method's LOD and the free concentration of the analytes in the sample. This in turn is determined by the combination of factors pertaining to the physicochemical characteristics of the extracting phase, the affinity of the analytes towards that extracting phase, properties of the sample matrix and in practice also level of pre-concentration during liquid desorption and sensitivity of the employed instrumentation. All these factors also practically dictate the thickness of the extracting phase, as thinner coatings could in principle increase temporal resolution but would extract lower amounts of the analyte overall, requiring higher sensitivity to detect. With higher sensitivity, less time is required for the thin coating to extract sufficient amounts to exceed limits of detection and quantitation. This then means that the compound for which the sensitivity is the lowest, limits the temporal resolution because it will be the slowest to reach detectable concentration (assuming similar kinetic profile of the target analytes). Measurements

in the dynamic range require consistency of extraction times as differences in time will lead to variations of extraction yields in a range that can be estimated from the SPME extraction time profiles. Given the dynamic nature of brain networks and the lack of a stable equilibrium point, we expect consistency in brain states to be one of the biggest factors in reducing replicated variability. Moreover, SPME measurements are inherently an average of the temporal dynamics of the target tissue milieu. This means that due to the bidirectional exchange of neuromodulators from the extracellular space and the extracting phase, longer periods of stable concentration gradients will be more strongly reflected in the extracted measurements.

Utility and ease of use. Employment of SPME probes allows for multiple simultaneous measurements that can be reliably repeated within the same measurement sessions at the same locations with no evidence of damage induced disruption of the neurochemical environment. The additional critical advantage of SPME for the outlined here purpose is its ease of use and accessibility. Due to their similar size to recording microelectrodes used for electrophysiology, little adjustment is required for conducting SPME measurements using existing acute microelectrode positioning systems. Measurements in deeper structures should use an accompanying guide tube (**Figure 2.15**) as traveling through nontarget tissue will result in unwanted chemical collection. Beyond the sampling, a chemistry core is required to analyze the samples via LC-MS/MS, allowing for relatively easy quantitation of extracellular compounds of interest, as outlined in the previous subchapter.

Detection methods. SPME is ultimately a sampling method, much like MD, that provides data for analytical tools such as chromatography and/or MS. In fact, once the analytes have been desorbed from the probe into a solvent, data provided by SPME and MD are treated very much the same. Thus, the advancement in detection limits and reliability of post hoc analytical methods utilized by MD also benefit SPME, and vice versa.

Extension of SPME measurements beyond classical neuromodulators. A unique advantage of SPME over alternative methods of *in vivo* detection of compounds within the brain is its potential affinity for hydrophobic compounds. Although MD is capable of collecting metabolomics data similarly to SPME,[24,213,214] the artificial cerebrospinal fluid that is commonly traversing the semipermeable membrane better facilitates the collection of hydrophilic molecules. This means that molecules that cross the semipermeable membrane and are therefore collected and quantified via LC-MS are much more likely to be hydrophilic. SPME, in contrast, provides balanced analyte coverage, which means that in principle certain extracting phases have similar affinity for both hydrophilic or hydrophobic compounds.[73] Data collected here includes other neurochemicals of interest such as amino acids (e.g., glutamine, taurine, phenylalanine, etc.) as well as lipids and fatty acids, discussed in the subsequent subchapter. In practice, the detection of very polar molecules such as monoamines and catecholamines requires coating chemistry that facilitates hydrophilic compound extraction. Comparatively, many lipids play important roles in intracellular signaling and have been suggested to provide biomarkers for psychiatric disorders,[215,216] therefore making SPME a potentially versatile and comprehensive tool for brain neurochemistry studies.

Implications for understanding and treating psychiatric disease states

Most psychiatric disorders are accompanied by neuromodulatory dysregulation.[171] However, this fact is seldom studied in a multimodulatory manner with single or few nuclei or neurochemicals being observed at a time. This is an increasingly evident problem because models attributing symptoms of a disorder to a single neuromodulator often fall short in explaining many symptoms.[183,185] For example, in Parkinson's disease, outside of the well-characterized dopaminergic deficits, there is evidence for deficits in noradrenergic, cholinergic, and serotonergic systems as well.[173,184] Many cognitive deficits observed within Parkinson's disease are linked to such nondopaminergic deficits. Such findings emphasize the need to simultaneously observe multiple neuromodulatory systems. Thus the

simultaneous measurement of multiple neuromodulators in multiple brain regions within healthy and clinical populations may allow for a better understanding of the underlying causes of symptoms and progression of psychiatric disorders.[170,171,217] A better understanding of psychiatric disorders through multimodulator methods may also lead to more accurate understanding of the action of pharmacological agents. Previously, many studies aimed at identifying the locus of action of a pharmacological agent have used local injection methods such as iontophoresis or microinjections.[218,219] Although highly informative about the role of neuromodulators in modulating the activity of individual cells and circuits, this approach does not allow physiologically realistic exploration of a systemically administered pharmacological agent. Pharmacological agents are often administered in some systemic fashion and, even with highly specific receptor affinities, may interact with multiple neuromodulatory systems through the actions of heteroreceptors.[170–172] Multimodulator measurements, as described here, may allow for a better understanding of pharmacological agents, as well as providing novel insights into the development of more effective drugs or combinations of drugs to better treat the clinical population.

2.4 Untargeted neurochemical profiling of macaque brain by SPME-LC-HRMS

2.4.1 Introduction

In vivo studies employing SPME are usually done by means of untargeted metabolomic profiling or an expansion of a clearly defined targeted component into supplementary untargeted profiling. A brief look into the literature confirms this.[55,84,133,134,220] The outlined strategy arises from the *in vivo* aspect of the sampling and this study is no exception. With the great effort of sampling living organisms, many of which are sacrificed following the end of sampling (rodents, in particular), the value of obtained samples is proportional to the effort (of both animal and analyst) of acquisition. MS-based untargeted analysis is a way of matching the diversity of molecular species extracted by SPME with their detectability (this statement is not exclusive to SPME and can be extended to any non-specific sample preparation or extraction method characterized by broad coverage and multi-analyte capabilities). Sample analysis coupled with *post hoc* data interpretation can be convenient to 'immortalize' the samples, with the archived data set enabling revision upon change in the study direction, newly emerged hypotheses or new available data processing tools.

These capabilities often come at the cost of feasibility of metabolite quantitation and inambiguous identification.[221,222] Continuous improvements in the performance of separation and MS instrumentation methodologies, as well as strategies and platforms available for untargeted data processing work towards mitigating these challenges.[221,223] Various acquisition modes exist to maximize the coverage of detected metabolites, with the usual choice of trade-off between the analysis time, level of data convolution, and metabolome coverage (for example: full scan MS followed by MS/MS focused on only selected metabolites as a strategy resulting in lower throughput but also lower data complexity than data independent acquisition (DIA) approach, which produces highly convoluted spectra with lower MS/MS quality, but enhanced metabolome coverage and higher throughput).[224] The increasing advancement and complexity of MS acquisition modes, with the goals of streamlining the

analytical process and increasing throughput by answering several analytical questions within one acquisition cycle, inevitably lead to a swell in the size of the generated datasets. Therefore, data management and reduction of redundancy to extract meaningful information is of high importance and has become a branch of bioinformatics on itself.[225,226]

It appears appropriate to introduce the term *feature* here, as for convenience this term will prevail in any discussion concerning untargeted data analysis. A feature is an output of the first step of a typical metabolomic data processing workflow, involving peak detection and association with the mass spectral data. Resulting from these operations and the character of the employed analytical method, feature is a two-dimensional data point containing chromatographic and mass spectral response – retention time and mass-to-charge ratio (m/z), respectively.[225] Since a single metabolite can form several different adducts in electrospray ionization (ESI),[227] and a single retention time may contain spectral signal from several co-eluting metabolites, a particular peak can be assigned with m/z corresponding to the molecular ions, in-source fragments, various adducts, ions with different charges or isotopes.[225,226] This leads to the number of detected features being an overwhelmingly larger number than the number of actual detected metabolites.[228] Due to this ambiguity, the term feature was coined to refer to the output data at the pre-identification stage of data processing.

Although the broad analyte coverage of SPME has been previously demonstrated in numerous reports,[55] this study has been extended into an untargeted metabolite profiling in order to investigate if this protocol, specifically fine-tuned for highly hydrophilic molecules, is capable of providing additional semi-quantitative information about molecules with drastically differing properties, found in nonhuman primate brain.

2.4.2 Experimental

The same SPME extracts collected *in vivo* in three brain areas of two macaques according to the procedure described in subchapter 2.3 were analyzed by LC-MS, employing Vanquish Flex LC system coupled to a high resolution instrument Exactive with Orbitrap mass analyzer (Thermo Scientific, San Jose, CA, USA). Details regarding the method and acquisition parameters were listed in **Table 2.6**. Xcalibur (version 3.0.63) and Thermo Exactive Tune (version 1.1) software was used for data acquisition. The instrument was calibrated using the Pierce™ LTQ Velos ESI Ion Calibration Solutions for positive and negative ionization modes (Thermo Scientific, San Jose, CA, USA) and additional real-time calibration was performed throughout all runs using LockMass function. Instrumental performance was monitored using standard quality control sample, as well as pooled QC sample prepared by mixing 5 µm of each extract. Raw data files were converted into mzXML format required for further data processing using MSconvert toolkit (ProteoWizard 3.0).[229] Optimization of peak-picking related settings was carried out by applying the IPO package[230] to pooled QC samples. The subsequent operations on data (peak extraction, filling, grouping, and alignment) were performed using XCMS package[231] integrated in an in-house developed R-script.[232,130] The list of detected features then underwent filtering in order to discard artefacts originating from blank samples (characterized by signal-to-noise ratio < 5) and peaks with significant variance (>30% RSD). Univariate statistical analysis was carried out using MetaboAnalyst[233] (version 4.0). Tentative annotation of detected compounds was performed using reference databases: METLIN,[234] and LIPID MAPS.[235]

Table 2.6: LC-MS acquisition parameters and method details used for analysis of metabolomic profile of macaque brain sampled *in vivo* by SPME probes.

Thermo Exactive Mass Spectrometer (heated electrospray ionization source)	
Spray voltage [kV]	4.0 (-2.9)
Sheath gas [a.u.]	35 (30)
Auxiliary gas [a.u.]	5
Sweep gas [a.u.]	0
Capillary temperature [°C]	280
Heater temperature [°C]	300
Mass range [m/z]	84-1000 (80-1000)
Acquisition mode	Full Scan
Max. inject time [ms]	100
AGC target	Balanced: 1e6
Resolution	High: 50,000 @ 2Hz
Lock Mass	m/z 391.28429 (positive); m/z 255.23295 (negative)
High Performance Liquid Chromatography (Thermo Vanquish Flex)	
Column	Supelco Discovery HS F5, 3 µm, 100 x 2.1 mm with 3 µm, 20 x 2.1 mm guard column
Mobile phase A	H_2O + 0.1% FA (H_2O + 1mM AA)
Mobile phase B	ACN + 0.1% FA (ACN + 1mM AA)
Flow rate [µL/min]	300
Column temperature [°C]	25
Samples temperature [°C]	5
Injection volume [µL]	5
Gradient [%B]	0 min-0%; 3 min-0%; 25 min-90%; 34 min-90%; 35 min-0%; 40 min-0%

Negative ionization mode parameters in brackets; FA- formic acid; AA- acetic acid

2.4.3 Results and discussion

Although untargeted metabolomic analysis is predominantly done to differentiate groups expected to possess divergent treatment- or state-dependent metabolic profile, here (due to the basal character of all measurements) it was applied to the only meaningful variable – the sampled brain regions. Out of the statistically significant features differentiating the neurochemical environment of the three brain regions (**Figure 2.18**), only those which yielded unique tentative identification based on accurate mass (with Δ5 ppm and Δ10 ppm tolerance for positive and negative ionization mode, respectively) were considered for further analysis and discussion.

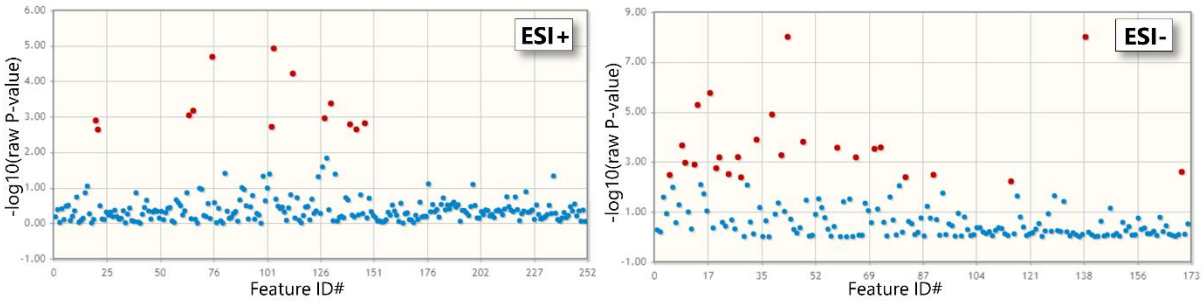

Figure 2.18: Univariate analysis using non-parametric ANOVA (Kruskal-Wallis test) with a false discovery rate adjusted *p*-value cutoff of 0.05. Red dots represent the statistically significant features which discriminate the three compared brain regions. 13 and 25 discriminating features were found in positive and negative ionization mode, respectively.

Throughout the untargeted analysis, additional important neurochemicals were detected, which were not the focus of initial method development and *in vivo* protocol. Several metabolites belong to the tryptophan-related pathways (**Figure 2.19**), with 5-hydroxyindoleacetic acid (5-HIAA) being the final product of serotonin metabolism, after biosynthesis of serotonin from tryptophan. Kynurenine and N-formylkynurenine both belong to another, parallel branch of tryptophan biotransformation.[236] The kynurenine pathway is important for regulating serotonin availability, as in the presence of several pro-inflammatory cytokines the activation of indoleamine 2,3-dioxygenase converts tryptophan into N-formylkynurenine, a precursor of kynurenine, which after several subsequent metabolic conversions results in the production of nicotinamide adenine dinucleotide (NAD^+), which is protective against inflammation-induced neurotoxicity.[237,238] Tryptophan itself (**Figure 2.20**), being the precursor for biosynthesis of both serotonin and kynurenine, was found to be equally abundant in all sampled brain regions, while its metabolites were consistently more abundant in premotor cortex than in the prefrontal cortex and the caudate.

Another pathway with several members represented in the detected pool of metabolites is related to dopamine biosynthesis[239] from phenylalanine through tyrosine (both phenylalanine and tyrosine were found to be more abundant in PreMC, **Figure 2.19**), as well as its biotransformation to 3,4-

dihydroxyphenylacetic acid (DOPAC; equally abundant in all sampled brain regions, **Figure 2.20**) and homovanillic acid (HVA; only found in the caudate). The presence of HVA limited to CD somewhat corresponds to the fact that dopamine was also only detected in this region as well as the fact that the nigrostriatal dopamine pathway, projecting into the caudate and putamen, is estimated to traffic 80% of the dopamine pool in brain.[240]

Taurine was found with significantly lower abundance in CD than in the cortical regions (**Figure 2.19**). This amino acid, besides serving the role of an inhibitory neurotransmitter in brain, fulfills other roles, such as stabilization of cell membranes, regulation of calcium ions transport, and neuroprotection.[241,242] Although taurine release has been postulated to negatively correlate to the concentration of dopamine,[243] it must be emphasized that one of the intrinsic limitations of the untargeted metabolomic profiling approach is its relatively-quantitative character, meaning that the abundances cannot be compared between metabolites, as they do not represent absolute concentration but merely an instrumental response.

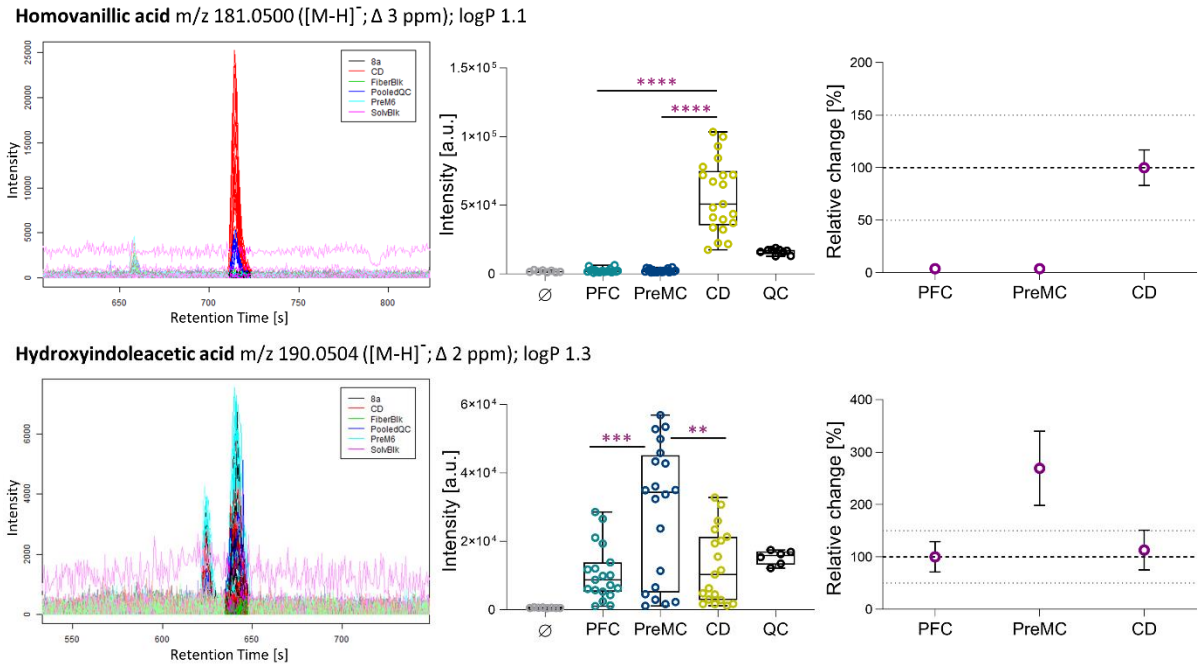

Taurine m/z 126.0220 ([M+H]⁺; Δ 0 ppm); logP -2.2

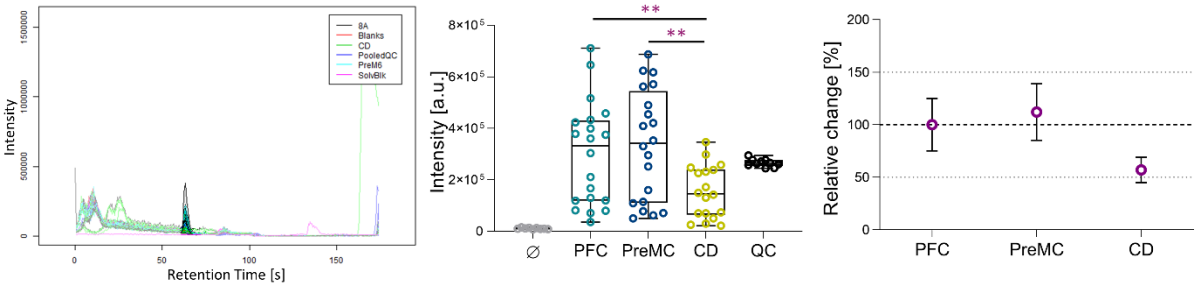

Phenylalanine m/z 166.0864 ([M+H]⁺; Δ 0 ppm); logP -1.4

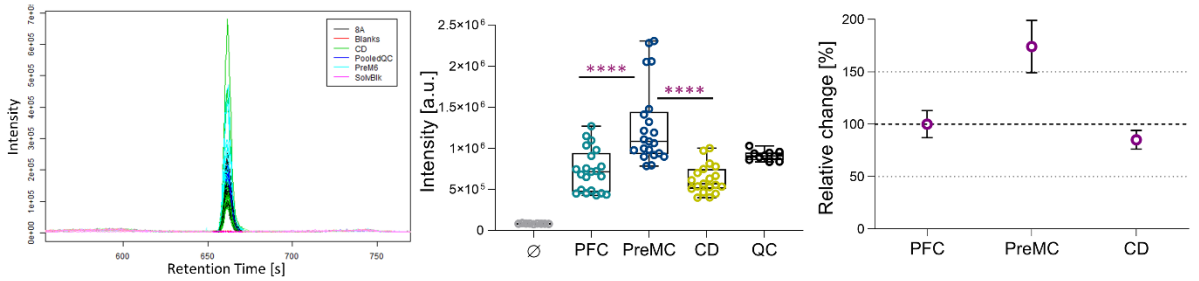

Tyrosine m/z 182.0813 ([M+H]⁺; Δ 0 ppm); logP -2.4

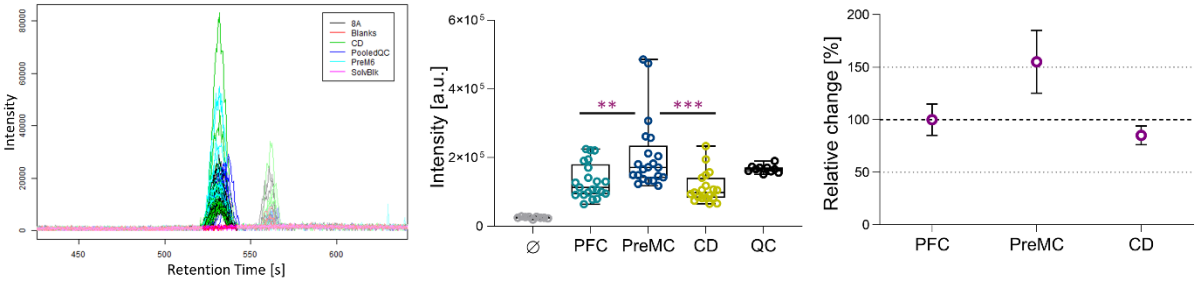

Kynurenine m/z 209.0922 ([M+H]⁺; Δ 0 ppm); logP -1.9

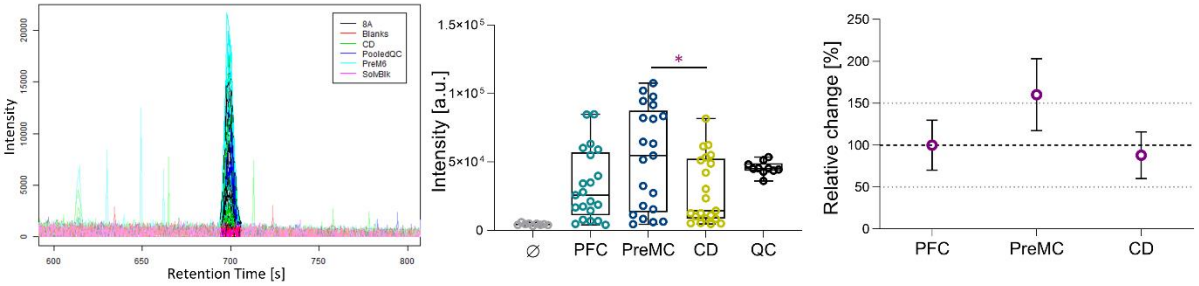

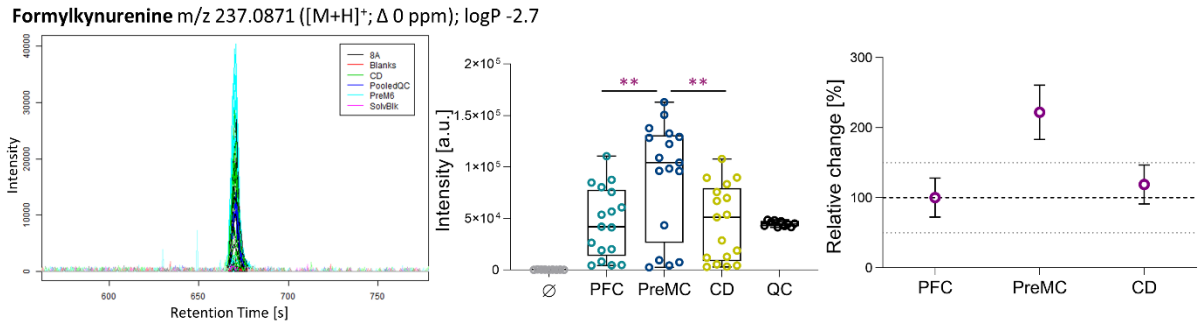

Figure 2.19: Neurochemicals with statistically significantly different abundance between any two brain regions. **Left panel** – extracted ion chromatogram; **Middle panel** – boxplots showing mean and range of all collected samples as well as difference across brain areas by means of unpaired, two-tailed *t*-test (* $p<0.05$; ** $p<0.01$; *** $p<0.001$ **** $p<0.0001$); **Right panel** - relative change of compound's abundance across brain areas normalized to the signal intensity in PFC (except for homovanillic acid where data was normalized to the signal intensity in CD), each point represents mean and standard error of mean.

The detection of multiple metabolites down the line of synthesis/biotransformation pathways of several neurochemicals emphasizes the importance of metabolite monitoring in order to obtain comprehensive information about the area-specific roles of neuromodulators. The presence and concentration of their metabolites may serve as supporting information in the instances where a neurochemical possesses several possible functions. The data interpretation should then focus on investigation of trends correlated between a neurochemical and its metabolites, rather than trends occurring for single neurochemical (this point was further elaborated on in discussion to Chapter 5). However, proper interpretation often requires comparison of the absolute brain concentrations and the semi-quantitative untargeted approach may aid inclusion of important metabolites into quantitative targeted protocols.

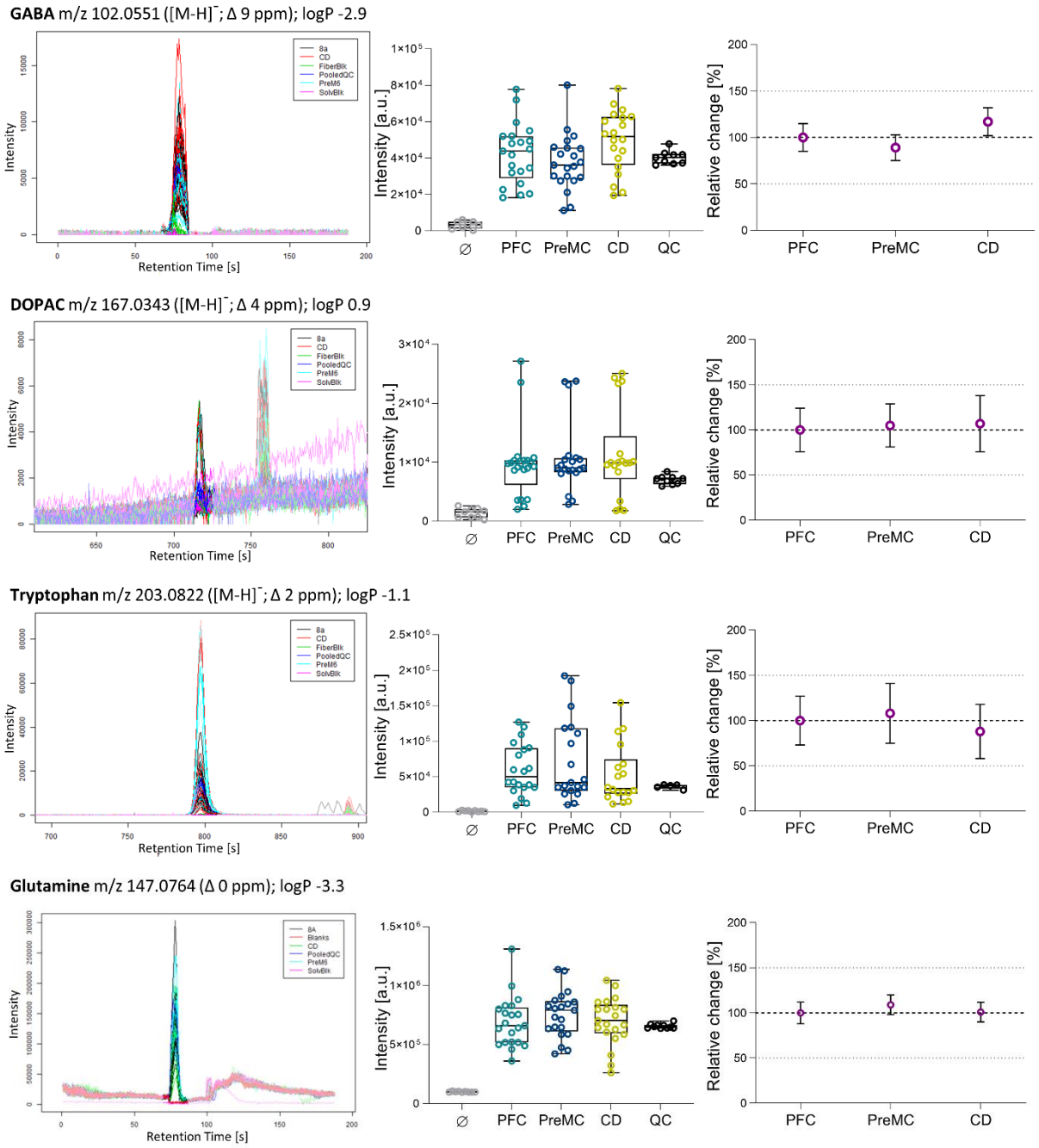

Figure 2.20: Neurochemicals with no significant abundance differences between any two brain regions. **Left panel** – extracted ion chromatogram; **Middle panel** – boxplots showing mean and range of all collected samples; **Right panel** - relative change of compound's abundance across brain areas normalized to the signal intensity in PFC, each point represents mean and standard error of mean.

In the context of brain neurochemistry, it is equally important to monitor metabolites which exhibit differences between the tested conditions (behavioral, pathophysiological, time-course of a treatment,

or as in this example – in different brain areas), as those which do not.[244] However, the latter remains a manual task to date, as metabolomic studies are predominantly focused on comparing healthy vs. pathophysiologically changed specimens, with the goal of discovering biomarkers of the change.[30,245] Additionally, the immense reliability of the list of non-altered metabolites on unambiguous feature identification contributes to the challenge of this approach.

Amongst the compounds exhibiting no relative change in abundance across all sampled brain regions, glutamine and GABA were found, with relatively low variability of measured signal (**Figure 2.20**). Both these compounds, together with the glutamate quantified in the targeted portion of this study, belong to the common pathway where glutamine serves as a precursor of glutamate and GABA *de novo* synthesis in neurons.[246] Glutamine is also a product of glutamate degradation, which takes place in astrocytes after considerable amount of glutamate is shuttled there after its release.[247]

Several fatty acids and lipids (specifically, phosphatidylethanolamines (PE) belonging to the glycerophospholipid subclass) were found with varying abundances across the sampled brain regions (**Figure 2.20**). The extent of this variability, generally larger than for the discussed above neurochemicals and their metabolites, points out that the area-specific diversity of lipids in brain reflects the plethora of distinct compounds belonging to a single subclass and their multiple functions.[248] These include formation of the lipid bilayer, being precursors for second messengers, and constituting an energetic reserve.[245] Unlike neurotransmitters, which are bound to operating within certain concentration ranges for proper brain function, and due to their structural function, the expected or acceptable concentration variability for lipids is largely unknown. Yet, alterations of specific lipid species and their distributions have been investigated as linked to several major neurodegenerative brain disorders, such as Alzheimer's and ALS.[249,248] Due to the lack of systematic and fundamental studies so far, the availability of brain phospholipids for isolation by *in vivo* SPME and the possibility of their quantitation remains unexplored, while the feasibility to quantify endocannabinoids[250] and

oxylipins[251] has already been demonstrated. This gap in systematic studies contributes to the fact that conclusions about the lipids found in brain via SPME are somewhat vague and speculative. With the future studies aimed at closing this gap, the prospects of measuring changes in eicosanoids and glycerophospholipids alongside neurotransmitters are especially meaningful given the role of the first in neuroinflammation[252] and neuroprotection[253] and the latter being postulated to modulate neurotransmitters' receptors in ways directly affecting neurotransmission.[254]

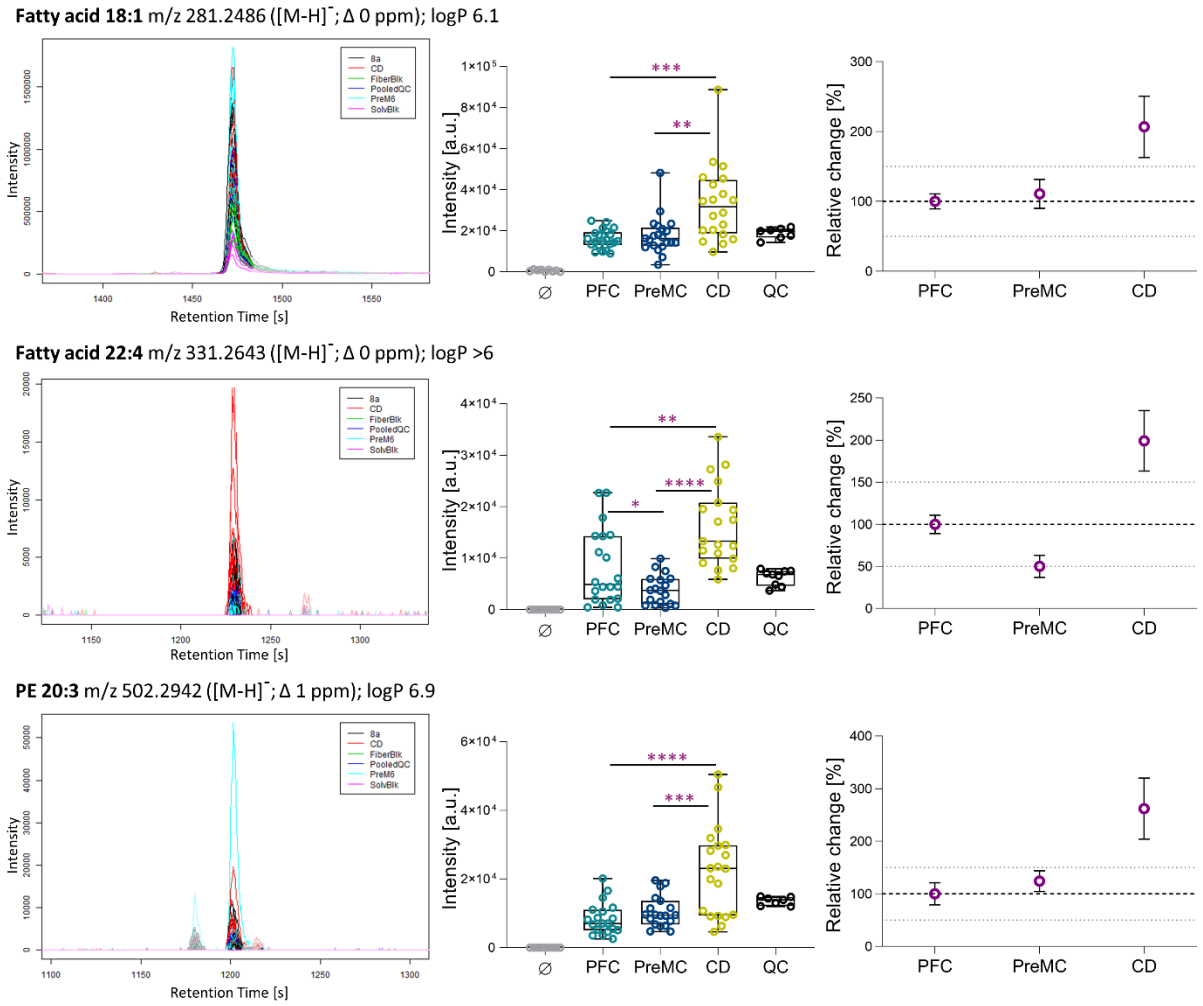

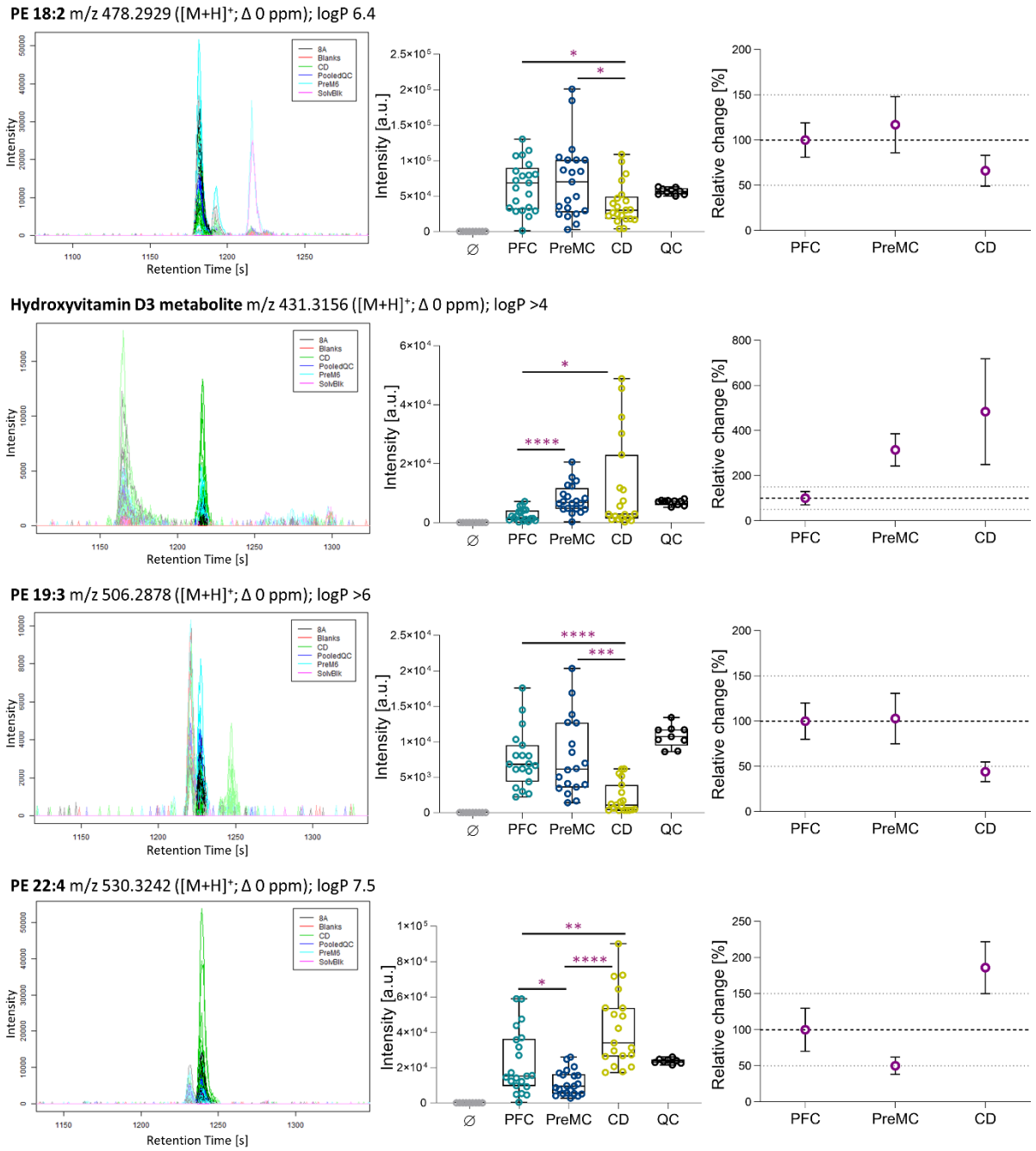

Figure 2.21: Hydrophobic compounds with statistically significantly different abundance between any two brain regions. **Left panel** – extracted ion chromatogram; **Middle panel** – boxplots showing mean and range of all collected samples as well as difference across brain areas by means of unpaired, two-tailed *t*-test (* $p<0.05$; ** $p<0.01$; *** $p<0.001$ **** $p<0.0001$); **Right panel** - relative change of compound's abundance across brain areas normalized to the signal intensity in PFC, each point represents mean and standard error of mean.

Despite of the focus of the SPME probe and protocol on the hydrophilic neurotransmitters, the untargeted metabolomic profiling of the brain extracts unraveled substantial physicochemical diversity of compounds extracted by the developed probe. Spanning from highly polar and hydrophilic small molecules such as GABA and glutamine (additionally to the discussed before and quantified neurotransmitters), through moderately hydrophobic fatty acids, up to glycerophospholipids, the covered logP range falls between -3 and 7. Due to the baseline character of all samples (steady behavioral state was ensured throughout the *in vivo* sampling) our investigation focused more on evaluating the range of compounds that can be detected by the SPME probe rather than systematic comparison of local neurochemistry in cerebral cortex and striatum. Up to date only a few studies incorporated MS-based metabolomic profiling of primate brain,[255,256] however, such analysis was never before performed on samples acquired *in vivo*. This attempt at profiling broad range of metabolites in primate brain *in vivo* opens up new prospects such as correlating levels of neurotransmitters with other, more hydrophobic metabolites or lipophilic drugs, but also helps to identify the limitations of sacrificing the informativeness level of measurements (quantitation and metabolite identification) for broad analyte coverage.

2.5 Chapter conclusions

Neurotransmitters often act within a limited dynamic range where concentrations that are too large or too small are detrimental. This highlights the need for techniques that can measure local levels of different neurochemicals that may be used for comparisons between clinical and healthy populations, specifically in brain regions that may be implicated in behavioral symptoms. These comparisons could allow for the guidance of therapeutic efforts to correct for such imbalances and relieve symptoms. It is also desirable to measure multiple compounds simultaneously in several brain regions implicated in neuropsychiatric disorders, as neurotransmitters exhibit area-specificity in their action, meaning that

the inputs and outputs for local circuits can differentially regulate local neuromodulator release which would then be targets for sampling.

This study proposes and evaluates a novel experimental protocol for extraction and analysis of underivatized neurotransmitters that addresses several current challenges in *in vivo* measurements of neurotransmitters in brain tissue as well as identifies the limitations yet to overcome. We show how the unique features of SPME can be leveraged for *in vivo* neurochemical profiling with non-disruptive and broad detection of multiple neurochemicals using minimally invasive probes, combined with quantitative analysis. Conditions mimicking real life scenarios were applied in order to select the most appropriate solutions with respect to sample storage, sampling time, and probe characteristics. The developed SPME probe has been proven to be a versatile tool with adjustable characteristics enabling application in a variety of scenarios, allowing for further broadening of the method's applicability to analysis of other classes of neurochemicals or for improvements to its identified shortcomings, such as recoveries and/or stability for selected neurochemicals. Continuous development of MS technology will likely facilitate improvement in detection and even further miniaturization of the probes.

A high level of applicability of the developed strategy for *in vivo* brain studies is demonstrated, as special attention was placed on considerations characteristic of this challenging type of sampling. We applied the developed protocol to simultaneous measurements of multiple modulators in three brain regions in behaving nonhuman primates. Reliable measurements of the area-specific basal concentrations of several neurochemicals and metabolites were achieved, as well as semi-quantitative untargeted analysis of macaque brain neurochemistry was explored. Our results suggest that SPME both supplements current methods of neuromodulator detection and allows for novel measurements previously not possible in nonhuman primates for the investigation and dissection of neuromodulatory systems, their role in physiological brain processes, and their modulation by pharmacological agents.

2.5.1 Future directions and areas of improvement for neurochemical sensing via SPME

The next immediate step for the continued testing of SPME's utility as a neurochemical sampling method is to evaluate its ability to report behavioral state-dependent changes in extracellular neuromodulator concentrations. Similar testing as described here is being conducted at the moment with varying stable behavioral states, including passive state of drowsiness/sleepiness as well as pro-cognitive states with active engagement into a feature-based reversal learning task with attention demands and varying uncertainty levels. We predict that the various brain regions tested will display different changes in neuromodulator concentrations as a function of behavioral state.

Further validation of the technique for non-disruptive *in vivo* neurochemical sensing will combine the above state-dependent measurements with pharmacological challenge throughout the multi-site neurotransmitter monitoring in order to investigate potential area-specific pro-cognitive states induced by systemic or local drug administration. These studies will combine simultaneous neurochemical sampling of endogenous neurotransmitters and administered drugs via SPME, electrophysiological recording of local field potentials, behavioral task, and drug administration to yield comprehensive basis for further investigation of cognitive flexibility aspects.

Several improvements to the protocol could make SPME more informative. Enhancing the method's LOQs for the target analytes that were not successfully measured *in vivo*, such as for serotonin and norepinephrine is of utmost priority. Efforts could also be directed at improvement of extracting phase synthesis, functionalization protocols, and coating chemistry investigation for increased extracting capabilities of SPME probes. Post-desorption derivatization strategies are being pursued to decrease the MS background and interferences for target analytes and further decrease the LOD and LOQ values. The most promising strategy, previously applied to MD extracts with impressive results, involves

derivatization by reagent increasing the compounds' hydrophobicity, resulting in better MS signal-to-noise, such as benzoyl chloride,[113,114] or dansyl chloride.[115] The benzoyl chloride direction is currently being pursued in order to enhance the method's performance for the experiments involving state-dependent measurements. One of the main challenges to overcome for the derivatization protocol is to balance the acidic conditions required for efficient desorption with the basic conditions required for derivatization.

An increase in sampling throughput and limiting the risk of analyte loss during the post-sampling period could be achieved by faster coupling of sampling to desorption. This would involve a more streamlined process of fiber placement and retraction involving a static cannula maintained through several sampling events. This mechanism would also allow for a faster replacement of SPME probes resulting in a shorter delay between consecutive measurements.

The failure to distinguish the GABA signal from an interference extracted only from *in vivo* samples occurring at the same retention time, using a triple quadrupole mass analyzer (but distinguishable using a longer chromatographic gradient and a high resolution orbitrap mass analyzer) points out that fine-tuning of the instrumental analysis method is required, with the knowledge and insights gained from the analysis of real *in vivo* samples. Since GABA has been previously reported to be successfully extracted and quantified in rat brains using non-custom SPME probes,[136] our failure to do so is perhaps a result of severe device customization, including in-house extracting phase synthesis. Further material characterization is required to avoid similar mistakes.

Since amino acid neurotransmitters fulfill both the signaling and metabolic regulation functions in brain, distinguishing between those two pools poses a substantial challenge and correlating measured concentration solely with behavioral observations may not be accurate.[141] This interpretation is especially ambiguous when employing techniques which extract compounds predominantly from the

extracellular compartment, such as MD or SPME. Further miniaturization of the devices or spatially-resolved sampling could be investigated as potential strategies to mitigate this issue, although both approaches have their own technical and performance-related limitations.

Finally, neuropeptides were conveniently omitted, even in the context of untargeted profiling of neurochemical environment. Neuropeptides constitute the largest subclass of neuromodulators with indubitable importance for regulation of proper brain function. Like neurotransmitters, they are synthesized in neurons and subsequently released into the interstitial space and are in some cases able to exert specific effects via neuronal receptors.[168] Since they consist of 3 to around 100 amino acid residues (and are therefore not considered macromolecules) and are present in free form in the brain, they have been available for and extensively researched by MD-based studies, despite the challenge of existing at very low concentration levels in brain tissue and stability concerns.[257,111] Despite their suitability for SPME due to the molecular mass range and physicochemical properties, as well as documented promise in overcoming the issue of low concentrations by employment of SPME in conjunction with a direct-to-MS approach involving MALDI,[258] peptides have not been a frequent target for SPME-based investigations. However, as first steps in extracting phase properties optimization for LC-MS analysis of peptides isolated from biological tissues by SPME are currently underway, the future perspective of adding peptides into the target list for *in vivo* neurochemical investigations seems highly probable.

Chapter 3

Space-resolved brain tissue analysis by solid phase microextraction coupled to mass spectrometry via desorption electrospray ionization (SPME-DESI-MS)

3.1 Preamble

Section 3.2 of this chapter has already been published as an article entitled *Space-Resolved Tissue Analysis by Solid-Phase Microextraction Coupled to High-Resolution Mass Spectrometry via Desorption Electrospray Ionization* by Sofia Lendor, Germán Augusto Gómez-Ríos, Ezel Boyaci, Harmen Vander Heide, and Janusz Pawliszyn, *Analytical Chemistry* **2019**, 91(15), 10141-10148. The content of the article is herein being reprinted with permission of the American Chemical Society and in compliance with the publisher and the University of Waterloo policies.

3.2 Development of interface and strategy for quantitative analysis via SPME-DESI-MS

3.2.1 Introduction

New analytical strategies are constantly being developed to keep up with the demand for fast approaches that can provide maximal chemical information, while also being reliable, quantitative, and simple enough to be used by non-experts in real-life settings. This demand has been reflected in the unprecedented expansion of ambient or direct-to-MS techniques featuring modified versions of pre-existing ionization/sample introduction methods, yielding tens of derivative methods (each of which having its own acronym).[259–262] To date, several ambient and vacuum mass spectrometry technologies have been developed to assess the spatial distribution of chemicals on 2D-surfaces in complex matrices, including desorption electrospray ionization (DESI),[263] matrix assisted laser desorption ionization (MALDI),[264] laser ablation electrospray ionization (LAESI),[265] nanospray-desorption electrospray ionization (nano-DESI),[266] and liquid extraction surface analysis (LESA).[267] Fundamentally, these technologies use a liquid or laser to perform micro-extractions from a given surface, which is followed

by the ionization of the analytes and subsequent MS analysis. Although technologies such as MALDI[268] and nano-DESI[269] are capable of astonishing spatial resolution, they are intrinsically limited to analyses of samples that can be placed on a flat surface, for example, tissue slides, bacterial cultures,[270] or tissue smears.[271] However, researchers have recently begun to explore the potential of combining DESI imaging with 3D reconstructions of tissue sections or depth-profiling using computational approaches.[272,273] Undoubtedly, DESI presents itself as one of the most versatile and simple approaches to MS imaging, though its substantial number of optimizable parameters has led some to question this claim. Due to the vast body of literature related to DESI, it would be futile to attempt to summarize its myriad applications. Nonetheless, several unique variations of DESI should be mentioned, including configurations that removed the constraint of close proximity to the sampling object[274] or control of the setup geometry;[275] those that introduce coupling to UV photodissociation,[276] postphotoionization,[277] field asymmetric waveform ion mobility[278] or shear force microscopy;[279] and, finally, those that focus on reaction monitoring rather than tissue imaging.[280] To date, substrate-based DESI has been relatively unexplored, with only a few variations—namely, paper,[281] medical swabs,[282] and nanofiber mat[283]—having been developed. However, with only one exception,[284] most of these substrates serve as neutral sample carriers without any significant interactions with the analytes.

Conceptually, solid phase microextraction (SPME) comprises a group of geometrically diverse solventless microextraction technologies that integrate sampling, sample preparation, and molar fraction enrichment into a single step.[55] Versatility of this technology allows for its use for *in vivo* analyses[211,134] or direct coupling to mass spectrometry.[285,286] Space-resolved SPME (SR-SPME) was used to study the heterogeneous spatial distribution of environmental pharmaceuticals in onions[287] and in fish *in vivo.*[288] Sampling was performed using segmented SPME fibers and sequential desorption into solvent (after cutting off the previously desorbed segments) and analysis via LC-MS. In essence, this strategy combined spatially resolved sampling with an analytical technique that lacked this feature.

While the simplicity of this approach was diminished by the need to precisely cut the segments, this work nevertheless highlighted the advantages of acquiring a reduced number of spatially resolved samples as opposed to repeated sampling, especially in case of living organisms. Additionally, due to their small size and since SPME probes do not remove any tissue, they allow revisiting the same site with minimum damage, which distinguishes this method from depth-profiling by ablation as in the case of LAESI and other techniques.[289]

On the opposite side of the spectrum are studies that have combined techniques with spatially resolved capabilities (DESI) with SPME fibers or thin-film blades to sample homogenous matrices like urine,[290,291] office media headspace,[292] and waste water.[293] DESI has also been applied in a non-space-resolved fashion to medical swabs coated with SPME extracting phases.[294] The recent combination of *in situ* solid phase extraction (SPE) and spatially-resolved analysis is a step towards recognizing the advantages of preconcentration and selective extraction for MS imaging.[295]

In this study, we combine two techniques with spatial distribution analysis capability, SPME and DESI, and couple them to high resolution mass spectrometry (**Figure 3.1**). At this initial stage we selected to use SPME fibers, as they allow for the unidimensional probing of the laminar distributions of molecules without requiring the slicing of the sample or the SMPE fibers. The workflow developed in this pilot study was used to reconstruct the concentration gradients of a set of xenobiotics in a multilayer gel system, followed by increasingly more complex models based on brain homogenate surrogate tissue and, finally, real rat brains *ex vivo*. Quantitative analysis was enabled by the development of appropriate internal standard (IS) correction and signal processing strategies. Although the technology presented herein cannot provide the same degree of spatial resolution as regular DESI or MALDI, due to the diffusion-based extraction mechanism, it can be considered suitable for non-invasive *in vivo* tissue probing. Moreover, and perhaps most significantly, this technology could

realistically be used to monitor the local release radius of xenobiotics in the brain[296] and the associated patterns of evoked physiological responses based on monitoring of endogenous molecules.

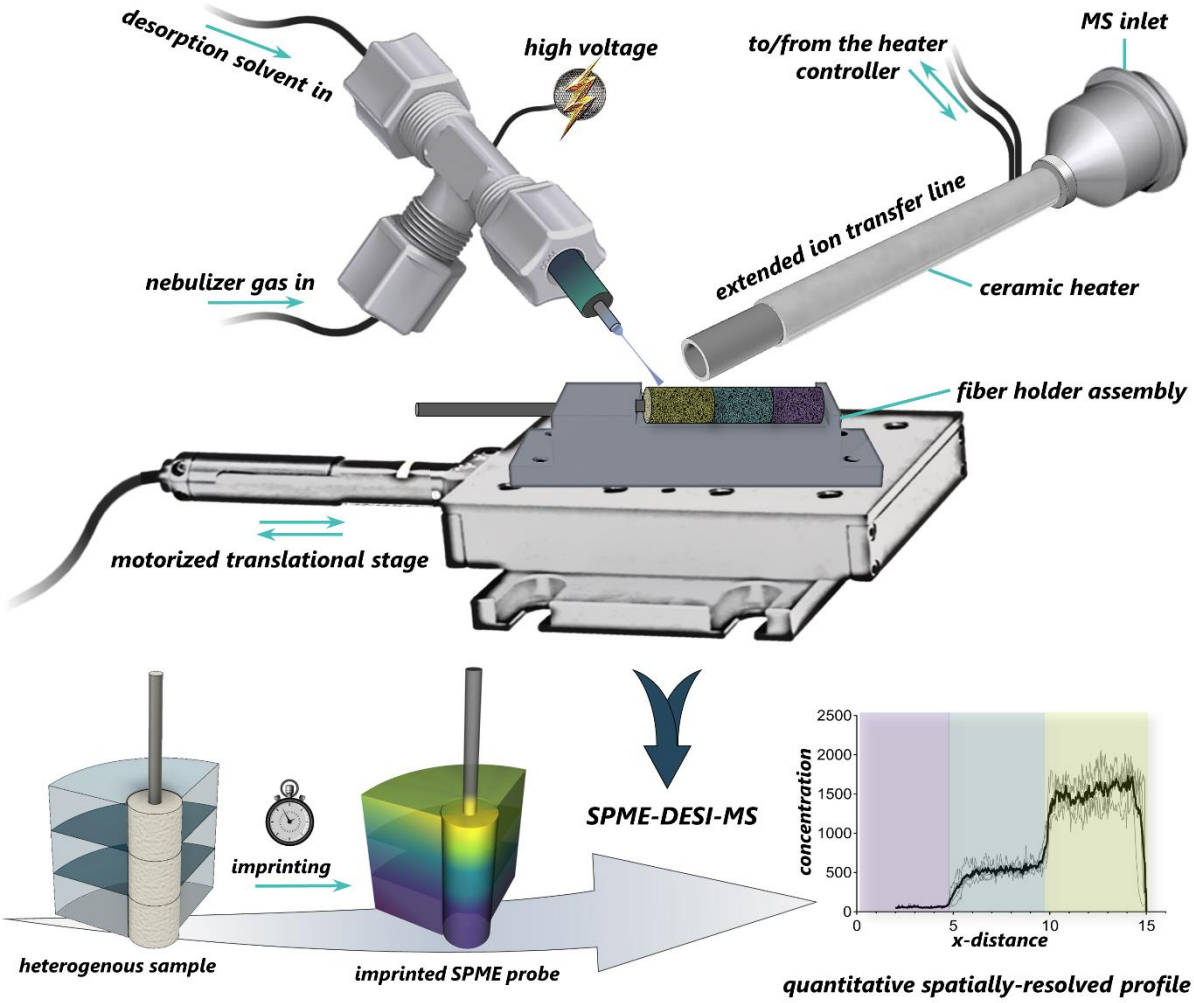

Figure 3.1: Principle of the SPME-DESI-MS coupling employing SPME fibers for unidimensional space-resolved profiling of heterogeneous tissue samples.

3.2.2 Experimental

SPME-DESI-MS interface and setup

This study was conducted using an in-house-built DESI setup that was coupled to a quadrupole time of flight mass spectrometer (Xevo G2-S QTof, Waters Corporation, Manchester, UK) (**Figure 3.2**). The DESI source consisted of a sprayer and a software-controlled unidimensional motorized

translational stage (Thorlabs, Newton, NJ, USA) that had been equipped with an SPME probe holder and a motion controller, which was operated by the APT software. The sprayer was mounted on a combined XYZ and rotational stage (Thorlabs, Newton, NJ, USA) to ensure that the spray plume position could be freely adjusted relative to the sample and MS inlet during the optimization step. The DESI source and the MS were operated under the conditions listed in **Table 3.1**.

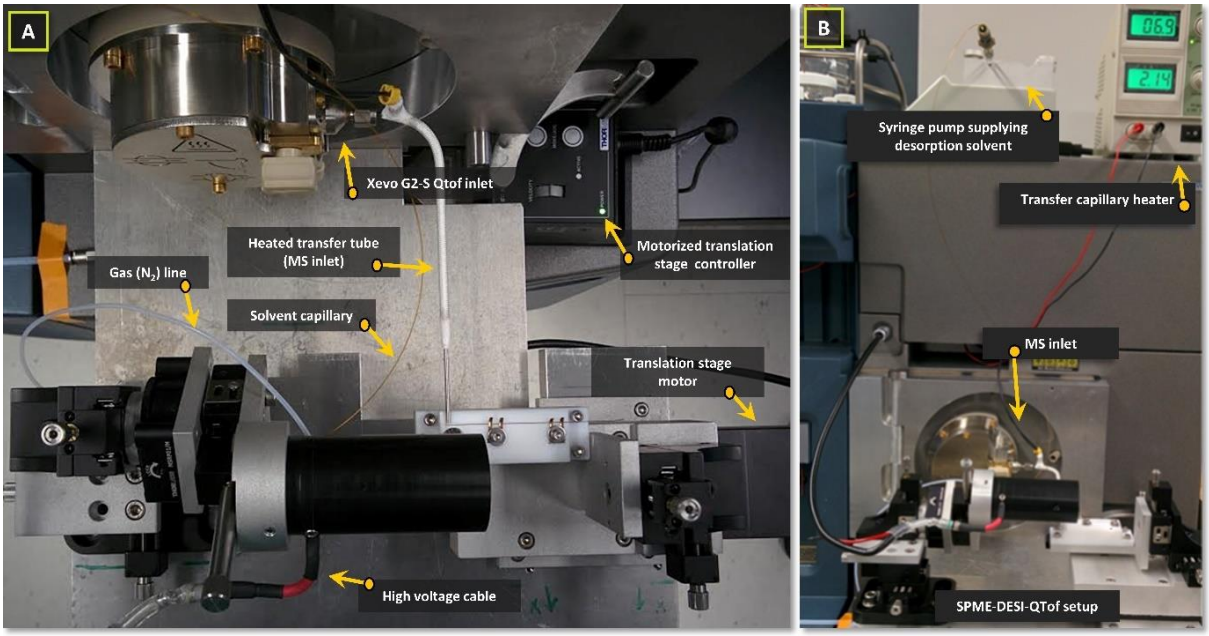

Figure 3.2: In-house-built SPME-DESI interface designed for the Xevo G2-S mass spectrometer. A) view of the SPME-DESI source from above with all main elements labelled; B) view of the SPME-DESI source mounted on the MS showing the solvent supply system and external transfer tube heater.

The steps undertaken to improve the signal's stability and intensity, and to maximize the spatial resolution included optimization of the desorption solvent flow rate, positioning of and distance between the sprayer tip and the SPME probe, and the distance between the SPME probe and the MS inlet. The parameters were tested with changes in the Leu-enkephalin (LeuEnk) signal being observed and acquired in real time.

Table 3.1: Experimental conditions used for SPME-DESI-MS/MS.

Xevo G2-S QTof MS	Spray voltage	3 kV
	Cone voltage	40 V
	Source offset	80 V
	Heated capillary temperature	250 ˚C
	Source block temperature	100 ˚C
	Acquisition mode	Sensitivity; MS/MS (Tof MRM)
	Scan time	250 ms
	Mass range	70-400 m/z
	Mass resolution	22000
	Acquisition time	5 min
	LockMass acquisition	LeuEnk (fragment m/z 120.0813); scan time 300 ms; interval 5 s; 3 scans to average
	Mass calibration	0.5 mM sodium formate in MS/MS mode between 70-400 m/z (weekly); real-time correction with LockMass (LeuEnk included in desorption solvent)
DESI source	Nebulizing gas pressure	100 psi
	Solvent flow rate	3 µL min-1
	Spray solvent	methanol/water (95:5, v/v) + 0.1% FA + 5 ppm LeuEnk
	Tip-to-surface height	2 mm
	Distance inlet-sample	2 mm
	Angle tip-sample	45 °
	Angle inlet	10 °
	Distance tip-inlet	4.5 mm
	Fiber scanning speed	50 µm/s
SPME fibers	Extracting phase	Hydrophilic-lipophilic balance (HLB)
	Coating length	4 mm or 15 mm
	Coating thickness	27.5 µm ± 2.5 µm
	Max. probe diameter	255 µm ± 5 µm

A custom holder was designed allowing the SPME probes to be reproducibly positioned, exchanged and stabilized during desorption and analysis by restricting their freedom of movement, especially movement created by vibrations from the DESI sprayer gas blow (**Figure 3.3**). The holder assembly is removable and can be customized to accommodate the length and size of the SPME probe being used. The holder assembly guaranteed that the probe would remain stable and secure during desorption and analysis. This was achieved by encapsulating the non-coated portion of the SPME probe inside of a two-piece polytetrafluoroethylene (PTFE) block that was held together with two screws. To provide further stability, the probe was inserted into a tight-fitting sleeve, which fits into a groove that had been carved inside of the PTFE block. Both of these measures (along with the stopper located at the front end of the holder assembly) successfully restricted the probe's freedom of movement during the analysis (against vibrations produced by gas blow). Moreover, the holder assembly was equipped with

a lower-level segment located below the level on which the coated probe was placed in order to support the heated transfer capillary. Seating the transfer capillary on this flat, smooth surface during the movement of the whole holder assembly proved an effective remedy to initially observed baseline signal instability. This combination of solutions ensured that fiber placement was reproducible, and, as there was only one possible and correct way to place the probe in front of the MS interface, it also ensured minimal sensitivity to inter-operator variability. The SPME probes were fixed in position by simply inserting their non-coated side (back-loading) into the tight-fitting sleeve. The holder assembly then positioned the coating orthogonally in front of the MS transfer capillary.

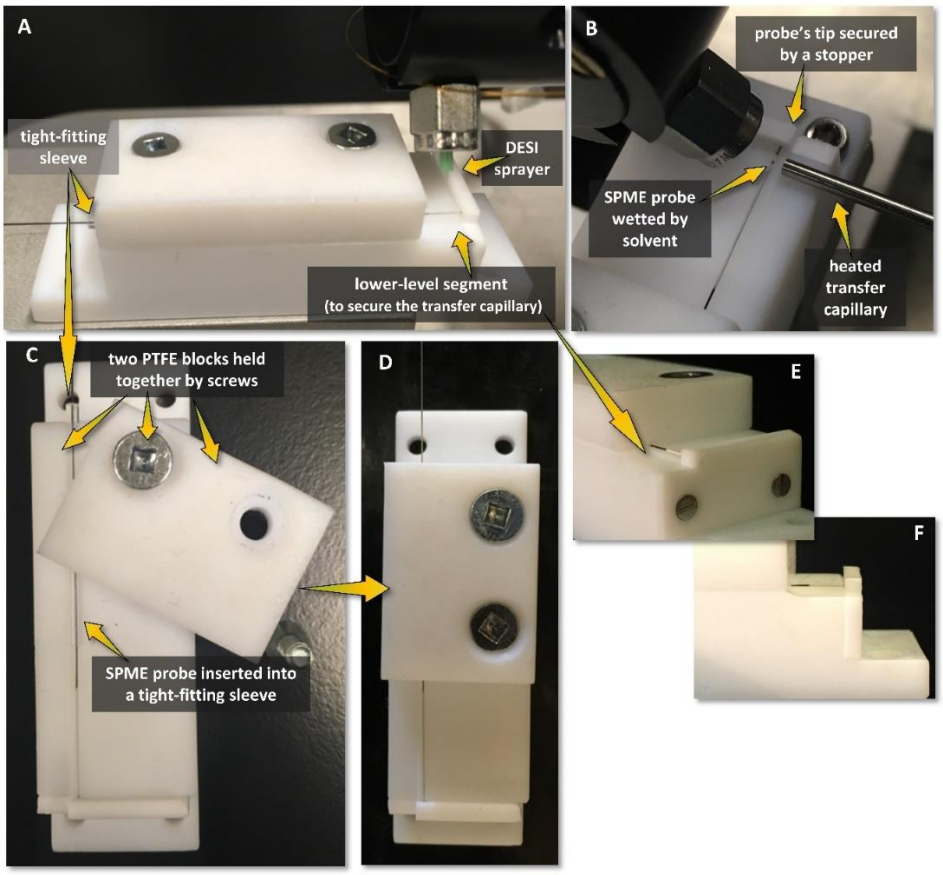

Figure 3.3: SPME probe holder assembly. A) holder capable of accommodating 4 mm coated probes; B) 15 mm coated probe being analyzed. This image shows the alignment of the spray plume with the SPME probe and the heated transfer capillary; C) partially disassembled holder assembly ready for probe replacement; D) SPME probe secured in position inside of the holder assembly; E) and F) detailed view of the lower-level segment, which was carved into a PTFE block in order to seat the extended MS inlet (heated transfer tube) in an appropriate position for ion transfer.

Table 3.2: Summary of drugs and pharmaceuticals targeted in this study, including their corresponding internal standards. Table shows hydrophilicity, expressed as logP, as well as dissociation constants, and monitored Tof-MRM transitions.

Compound	logP*	pKa**	Precursor ion [m/z]	Fragment ion [m/z]	Collision energy [eV]
Benzoylecgonine	1.71	9.54	290	168.1025	18
Citalopram	3.58	9.78	325	109.0448	27
Clenbuterol	2.94	9.63	277	203.0159	15
Cocaine	1.97	8.85	304	182.1189	18
Cocaethylene	2.53	8.77	318	196.1372	20
Fluoxetine	4.09	9.8	310	148.1126	8
Propranolol	3.03	9.67	260	116.1084	17
Benzoylecgonine-D3	n/r		293	171.1126	18
Citalopram-D6	n/r		331	109.0448	25
Clenbuterol-D9	n/r		286	204.0223	17
Cocaine-D3	n/r		307	185.1394	19
Cocaethylene-D3	n/r		321	85.0839	27
Fluoxetine-D6	n/r		316	154.1513	8
Propranolol-D7	n/r		267	116.1062	17

*values from ALOPPS 2.1; ** basic pKa; values from DrugBank (version 5.1.1); n/r- not relevant

Data acquisition, signal processing, and quantitation

Data acquisition and processing were performed using MassLynx version 4.1. As the acquisition commences, the translational stage (which houses the holder and the probe) begins to move at a speed of 50 µm/s, while the sprayer continuously supplies desorption solvent. The signal of the analytes desorbed from the fiber is registered as soon the wetted coating spot is aligned with the sprayer and the MS inlet **(Figure 3.3-B)**. After the readout from the specified length of fiber is obtained, the acquisition stops, the fiber is replaced, and the system becomes available to perform the next acquisition.

The ratio of the analyte signal intensity to its corresponding IS signal intensity, which was calculated scan by scan, was used as the analytical response (**Figure 3.4**). Quantitation was performed by averaging and plotting the ratios of all scans collected from a given calibrator sample against the concentration of the calibrator. When an "unknown" sample was acquired, the obtained calibration curve equation was applied to each scan acquired across the probe. This enabled the concentration to

be plotted as a function of fiber length (representative for unidimensional distance or depth in the sample) that reflects the analyte concentration distributions in the studied system.

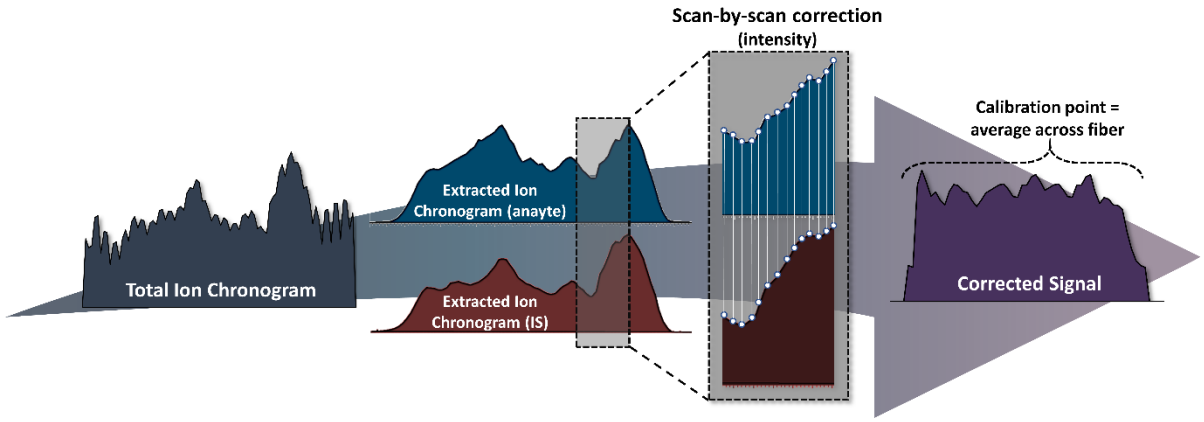

Figure 3.4: Signal processing strategy employed for spatially-resolved SPME-DESI-MS. Ion chronograms of the analyte and its corresponding IS are extracted from the total ion chronogram. The intensity vs. the scan list is exported, and ratios of analyte and IS signal intensity are calculated for each scan. The resulting response is plotted against time, or more specifically, distance, on the scanned fiber.

Sample preparation

The general SPME workflow described below was followed throughout the experiments. SPME probes were preconditioned in MeOH/H_2O 1:1 for 1 h prior to the extraction. Following preconditioning, internal standards were pre-loaded onto the probes by extracting the deuterated compounds from 600 µL of water spiked at 250 ng/mL. For convenience, all probes used in the experiments were pre-loaded overnight (≈ 15 h), dried, and subsequently stored in the freezer at -80°C until use. The samples were spiked with the appropriate amounts of analytes, while ensuring that the total amount of organic solvent never exceeded 1% (v/v) of the matrix's total volume. SPME probes were inserted directly into the sample and extraction was carried out for 8 min in static mode. The probes were quickly withdrawn, wiped with a lint-free tissue to remove any loosely attached matrix, and rinsed by vortexing in ultrapure water for 3 s. The probes were then analysed as quickly as possible via DESI-MS to avoid any analyte diffusion within the SPME coating. Although freezing is

hypothesized to slow down the diffusion process across the coating, evaluation of the effect of storage stability was outside of the scope of this study and was characterized at a later time (see Chapter 4).

Three matrices were used in this study: agar gel, brain surrogate tissue, and real rat brain, representing progressively more complex and more difficult to control systems. The agar gel was prepared by dissolving agar (BioShop, Burlington, ON, Canada) in PBS buffer (2%, w/v) at elevated temperature. After cooling the gel to ≈50°C it was spiked with analytes, vortexed, sonicated to remove any air bubbles, and left to set at room temperature. Three batches of gel were prepared with final analyte concentrations of 0, 500, and 1000 ng/mL. These layers were arranged in three different configurations (**Table 3.5**) and sampled by a 15 mm coated SPME probe to pierce the entire gel stack. The brain surrogate tissue was prepared by mixing the agar gel with lamb brain homogenate at a 1:1 ratio (v/w). 2 mL of the surrogate tissue was injected into a 3D-printed polycarbonate box with dimensions of 10 mm x 10 mm x 20 mm (*Brain in the box*). The model was subsequently spiked with the mixture of analytes by injecting 5 µL of stock solution into one of the corners. After 1 h of diffusion/equilibration time, the model was sampled using one long (15 mm coated) probe and three short (4 mm coated) probes, which were positioned perpendicularly to the long probe (**Figure 3.14**). In the second iteration of this model 5 mL of surrogate tissue was introduced into a Petri dish (400 mm diameter, 4 mm depth) and injected with 5 µL of stock solution into the center. This model (*Brain on a dish*) was subsequently sampled with total of 4 or 9 fibers using the same approach as in the box model (**Figure 3.15**). Finally, real rat brains were used to test the developed procedure. Prior to euthanization, the male Fisher rats (≈220 g) were intramuscularly injected with fluoxetine at 10 mg/kg (all procedures were approved by the University of Toronto Animal Care Committee and the Animal Care Committee of the Centre for Addiction and Mental Health). Following euthanization, the rats' brain hemispheres were separated and stored in a freezer at -80 °C until analysis. Before extraction, the frozen brain halves were embedded in the agar gel blocks in order to stabilize the tissue and to allow the probes to be positioned in the

intended brain area more easily (**Figure 3.18**). Two long fibers were inserted into each brain along the sagittal and coronal planes, piercing through the hippocampus.

SPME probes manufacturing and selection of the most appropriate coating thickness

The SPME probes used in this study were manufactured utilizing a dip-coating technique reported elsewhere.[145] A supporting nitinol wire (SE508 alloy, 198 µm diameter, Confluent Medical, Fremont, CA, USA) was coated with hydrophilic-lipophilic balance (HLB) polymer particles to create a biocompatible extraction phase with a total thickness of 27.5 ± 2.5 µm and a length of 4 mm or 15 mm. The monodisperse Oasis HLB particles (5 µm diameter) were kindly provided by Waters Corporation. The HLB particle suspension was prepared using a ratio of 10% particles in PAN-DMF binder (7% PAN in DMF, *w/v*). In accordance with the fundamentals of dip-coating, the thickness of the deposited layer is proportional to the speed at which the supporting material was withdrawn from the suspension.[297] In this study, the ratio of particles to the binder and the suspension's viscosity (which also influence the coating thickness) were kept constant. Thus, the coating's thickness was varied by simply changing the withdrawal speed and the number of deposited layers.

The use of thin and uniform SPME coatings has been critical to achieving fast compound extraction, as well as rapid and efficient desorption/ionization by DESI. The latter is particularly important for enhancing sensitivity, which may be inherently diminished as a result of SPME-DESI coupling (for example, in some cases less than one percent of analyte amount is extracted, several percent of that fraction is then desorbed as the sample traverses the DESI source, and no more than a small fraction of the desorbed analyte is then effectively moved into the gas phase, ionized, and introduced into the MS[298]).

In order to select a coating thickness that would ensure fast and efficient desorption upon contact with the solvent deposited by DESI sprayer and good signal reproducibility, three sets of probes were

compared based on the extraction of a model compound: fluoxetine. The IS (fluoxetine-D6) was preloaded onto the SPME probes by performing extractions from 1 mL of water spiked at 500 ng/mL for 30 min in static mode. The extraction of fluoxetine was carried out for 8 min in static mode from PBS spiked at 1 µg/mL. The extraction time of 8 min was selected to ensure that sufficient amounts of analytes were extracted, while keeping the diffusion path length below 1 mm[299] (see the Discussion section for in-depth explanation). After a quick rinse with H_2O, the probes were analysed via DESI-MS. The compared sets of probes differed in terms of number of layers of HLB coating, withdrawal speed from the particle suspension during the coating preparation, and total coating thickness.

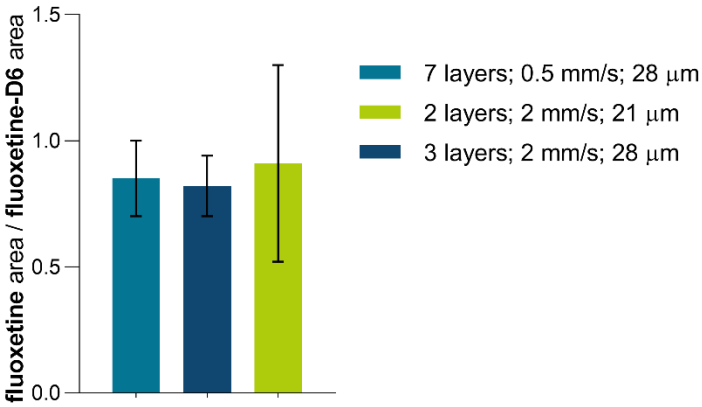

Figure 3.5: Comparison of response and response reproducibility corresponding to the extraction of fluoxetine from PBS using three sets of SPME probes with different coating thicknesses and manufacturing methods (*n*=5).

As **Figure 3.5** shows, the most reproducible measurements were obtained by the probes that had been manufactured using 3 layers of coating applied at a withdrawal speed of 2 mm/s for a final thickness of 28 µm. Although it is desirable to use as few layers as possible because it decreases manufacturing time and labour, the probes featuring only 2 layers of coating yielded results that were less reproducible.

SPME-nanoESI-MS setup and procedure

The spatially resolved information obtained from the analysis of the SPME probes via DESI-MS was compared to the information obtained from analyses using nanoESI-MS. The in house built SPME-

nanoESI-MS interface, which has been described elsewhere[300,286] was modified to fit the front end of the QTof instrument used in this study. The nanospray emitters (GlassTip coated: 1.0 mm OD, 0.78 mm ID, 4 µm tip ID) were obtained from New Objective Inc. (Woburn, MA, USA). The optimal ionization voltage was determined by testing voltages ranging between 800 and 2100 V (step size = 100 V) while spraying the desorption solution spiked with analytes. Ultimately, 1200 V was found to provide the highest and most stable signal for most of the target analytes. With the exception of the concentration and time of IS preloading used in the extractions for nanoESI-MS analysis (30 min extraction from 600 µL of water spiked with IS mixture at 5 ppb), all extractions from the gel layers were carried out identically for both nanoESI-MS and DESI-MS analysis. Immediately following each extraction, the probes were wiped, rinsed with water, and placed in glass capillaries (1 mm ID) filled with 10 µL of desorption solvent containing 500 ppb LeuEnk. Desorption was then carried out for 20 min with agitation at 1500 rpm, and the extracts were subsequently transferred to nanoESI emitters using a micro-syringe and analyzed.

Table 3.3: Xevo G2-S QTof acquisition parameters used for nanoESI-MS analysis.

Parameter	Value
Spray voltage	1.2 kV
Cone voltage	40 V
Source offset	80 V
Heated capillary temperature	250 ˚C
Source block temperature	100 ˚C
Acquisition mode	Sensitivity; MS/MS (Tof MRM)
Scan time	200 ms
Mass range	70-400 m/z
Mass resolution	22000
Acquisition time	1 min
LockMass acquisition	LeuEnk (fragment m/z 120.0813); scan time 200 ms; interval 5 s; 3 scans to average

3.2.3 Results and discussion

Quantitation considerations: Signal stabilization and correction

Given the spatially resolved nature of both components of the SPME-DESI coupling, each virtual "segment" on a single fiber contains information about the varying concentration of a given analyte across the sample. Contrary to the conventional approach of desorbing the entire SPME fiber at once, which produces an average concentration value, wetting each portion of the coated fiber by DESI spray will return qualitative and quantitative information regarding gradients existing in the sample. However, this configuration proved to be particularly susceptible to the negative effects of signal instabilities from physical sources (e.g. positioning of the fiber or the spray plume). This is a particular hindrance for reliable quantitation, as any signal increase or decrease stemming from signal instability could be falsely attributed to a change in the local analyte concentrations in the sample. With regards to hardware, the custom holder assembly significantly contributed to stabilizing the instrumental signal; this ran counter to our initial belief that placing the probe on a flat surface and securing the wire at two points would be sufficient for this purpose (beta version of the fiber holder visible in **Figure 3.2**). The signal reproducibility was further improved using an IS correction strategy. During the preliminary experiments, the SPME fibers were preloaded with IS and scanned in both directions (starting from the tip of the fiber first and then going back) in order to confirm that the high amounts of pre-loaded internal standard enabled strong signals to be recorded from a single fiber multiple times (**Figure 3.6**). This incomplete desorption of analyte extracted onto the fiber is an effect of very short interaction times between the desorption spray plume and the SPME coating, additionally occurring on a spot size as small as several hundreds of micrometres. The ion chronograms acquired in both directions were symmetrical, which suggests that the source of signal instability lies in the local imperfections of the fiber's surface (**Figure 3.7**). The presented SPME-DESI format uses fibers with a relatively thin

coating. As a consequence, any coating damage or features such as local variabilities in intra-fiber coating thickness, would be reflected in the obtained MS signal.

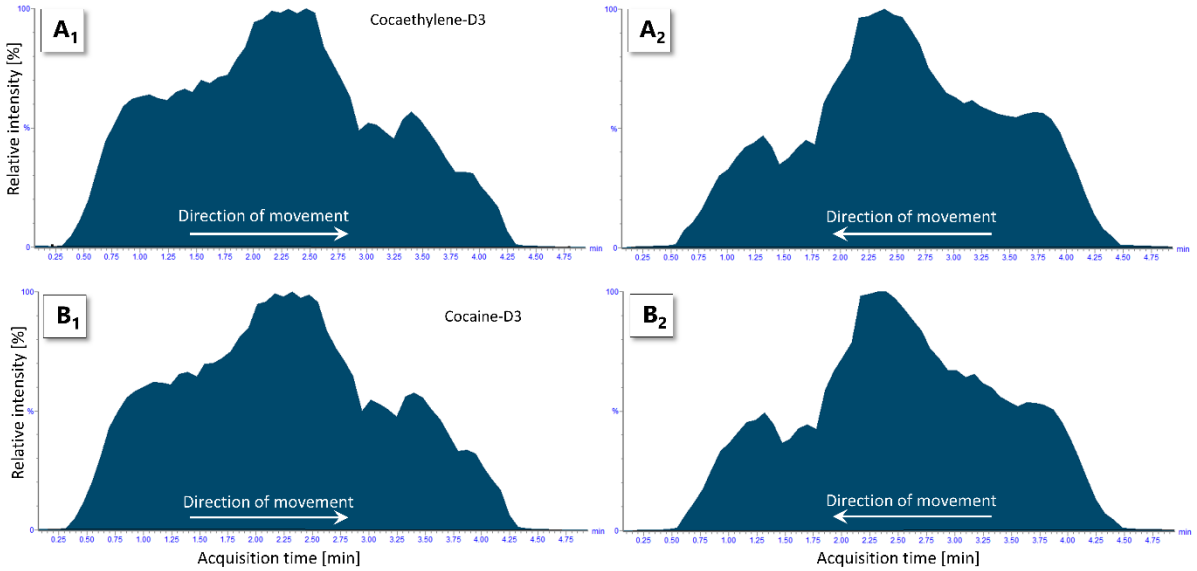

Figure 3.6: Ion chronograms obtained by scanning SPME fibers preloaded with IS in both directions. The high amounts of preloaded deuterated analyte analogues enabled multiple strong signals to be recorded, unveiling a symmetrical signal-fluctuation profile (the entire fiber was uniformly preloaded with compounds; therefore, in absence of signal instability sources, the profiles were expected to be stable). An additional factor that could potentially contribute to this observation is microscale bending of the probe mounted on the holder.

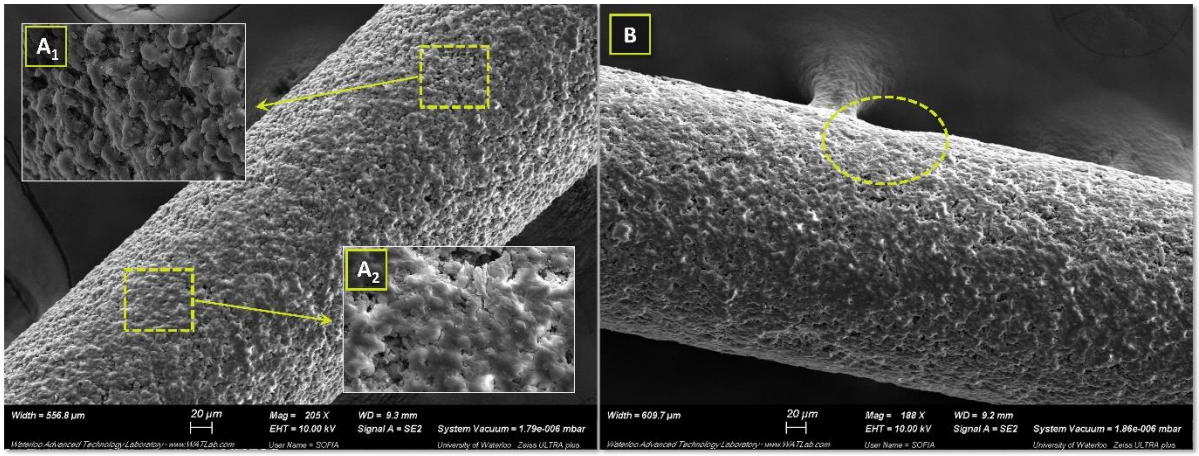

Figure 3.7: FE-SEM images of the HLB-coated SPME fibers used in this study, emphasizing areas with surface imperfections as the source of signal fluctuations (acquired on an FE-SEM Zeiss UltraPlus instrument; Carl Zeiss Meditec AG, Jena, Germany). The samples were coated with a gold layer prior to FE-SEM analysis, and images were captured with the secondary electron detector at 10 kV. A1 and A2 represent areas on the coating surface with more exposed particles or biocompatible binder, respectively. B shows an area with coating indentation. Since these effects impact the different sides of the SPME probes differently, uniform IS pre-loading ensures signal correction independently on fiber rotation.

This posed a problem, as it raised the possibility that these artefacts might be associated with the actual analyte concentrations in the sample. Although this issue does not affect cases where the spatial distribution of analytes is not of interest and the whole fiber is desorbed into the solvent, the use of SPME-DESI nevertheless requires special attention to fiber quality and coating distribution uniformity. Other possible sources of variation may include physical bending of the fiber in the holder (unnoticeable by the naked eye) due to the two-point securing system, and differences in effectiveness of coating surface wetting due to fiber's movement. To mitigate these strict requirements regarding probe quality and positioning, on-fiber IS preloading was employed.

Compound	Ion chronogram signal area [a.u.]				%RSD
	Rep. 1	Rep. 2	Rep. 3	Average	
Fluoxetine	4538	1335	5844	3906	59
Fluoxetine-D6 (IS)	1115	364	1306	928	54
Fluoxetine/IS	4.1	3.7	4.4	4.4	10

Table 3.4: Improvement in measurement reproducibility achieved by preloading IS onto the fiber, investigated via fluoxetine extraction from agar gel (IS was preloaded for 30 min from 1 mL of water spiked with fluoxetine-D6 at 500 ng/mL; 8 min extraction from 1 mL of 2% agar with fluoxetine at 1 µg/mL).

While this approach proved effective for correcting response in terms of signal areas (**Table 3.4**), this kind of response is not necessarily of interest for the proposed type of spatially resolved analysis, as the signal profile would need to be "sliced" into area portions corresponding to MS scan time or DESI spatial resolution, which is simply not practical. Therefore, the signal correction strategy depicted in **Figure 3.4** was employed, using signal intensity as the response, and scan-by-scan correction with IS. All outlined strategies enabled quantitation and provided good correction of any fiber- or spray-related signal fluctuations, as these random events affect both the analyte and the IS correspondingly.

Spatial resolution: The art of compromise

The spatial resolution of DESI-MS is the product of multiple variables, related to the characteristics and operation parameters of the sprayer hardware; the nature of the sample and its surface; and the mass

spectrometer's inlet geometry and acquisition parameters.[301,302] The effects of solvent composition and substrate wettability[303] will be even more pronounced in case of SPME-DESI-MS due to the substrate being coated with extracting phase. The solvent/coating interaction must facilitate sufficient wetting to desorb the analytes; however, extensive wetting decreases spatial resolution due to solvent spillage across the fiber, which promotes analyte diffusion within the larger spot area.

If we define spatial resolution as the spot size, sensitivity is one of the most significant limiting factors of spatial resolution levels in SPME-DESI-MS. SPME's non-exhaustive characteristics, combined with desorption from a small portion of the probe (determined by the spot size), leads to effective detection of a very small fraction of the analyte pool present in the sample. Traditionally, SPME efficiency can be improved by increasing the coating thickness and extraction time. However, this is not a viable solution in spatially resolved analysis: thicker coatings require more time to ensure effective wetting and desorption, while increased extraction times lead to the potential loss of defined spatial information, as the analyte molecules residing further from the probed area will start diffusing towards the coating in response to the transient local displacement of the molecules from the sample matrix into the coating (**Figure 3.8**).[304] Likewise, longer exposure times may lead to diffusion of the target analytes within the coating.

Another variable that affects spatial resolution is the linear speed at which the SPME fiber moves between the DESI sprayer and the MS inlet. However, this variable cannot always be optimized in a wide range of values due to its correlation with the wettability considerations. Here, 50 μm/s was chosen, despite the faster fiber scanning rate resulting in smaller spot size. This decision was largely made because the insufficient coating surface wetting that occurred at higher scanning rates caused decreased analyte signal intensity and stability.

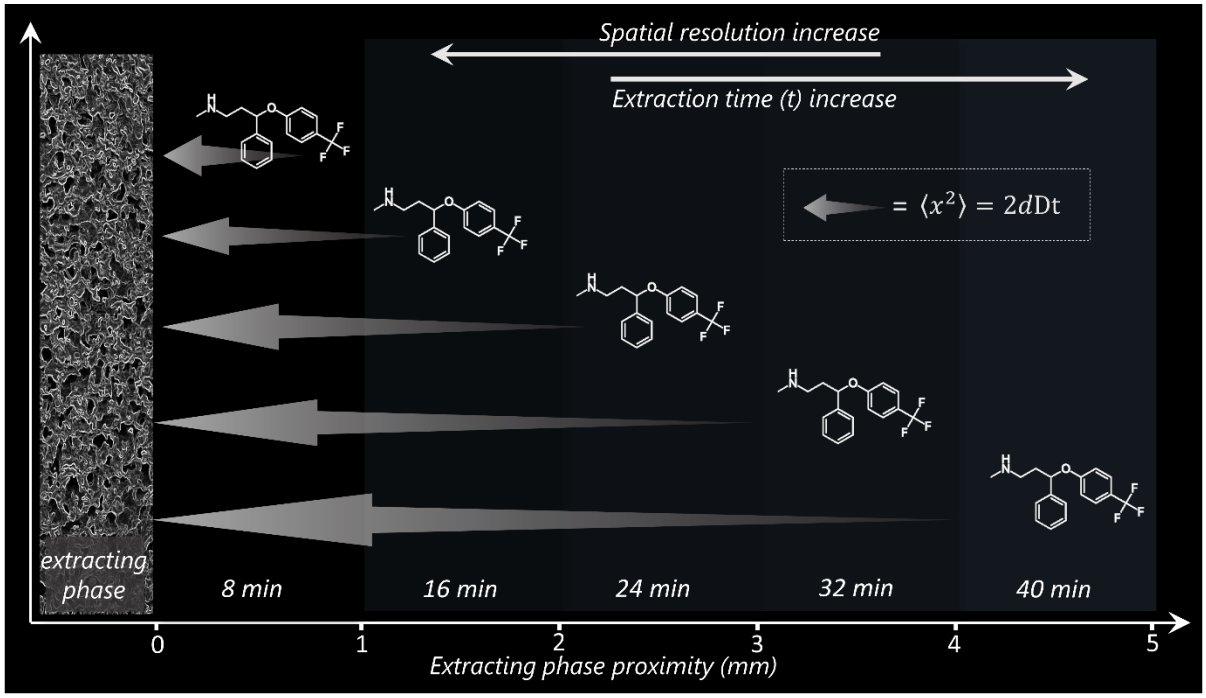

Figure 3.8: The relationship between the spatial resolution of SPME measurements and extraction time in gel matrix. The negative trend, wherein spatial resolution decreases as exposure time increases, is driven by the migration of analyte molecules from the bulk matrix towards the SPME coating as the local pool of analyte nearest to a coating becomes depleted due to extraction.

Upon examining the observable wetted spot on the SPME coating, it was determined that the estimated spatial resolution, defined as the physical spot size, was approximately 500 µm. Even though this level of spatial resolution cannot realistically compete with those reported in various DESI-MS imaging studies,[305,306] it represents an appropriate balance for the level of spatial detail achievable by SPME, given its diffusion-based principle. Based on Fick's law, the mean-square displacement $<x^2>$ during normal diffusion is proportional to the molecule's diffusion coefficient (D) and time (t).[307]

$$\langle x^2 \rangle = 2d\mathrm{Dt} \qquad (3.1)$$

Assuming the diffusion coefficient of a small drug molecule in a free medium (water) is in the order of $5.8 \cdot 10^{-6}$ cm^2/s [308] and decreases by 5% in 2% agar gel,[307] an 8 min extraction time will result in a displacement value of approximately 720 µm. In this study, an extraction time of 8 min was selected as a reasonable middle-ground, as it allowed sufficient amounts of analytes to be extracted, while

limiting the length of the diffusion path of the analytes in the sample to less than 1 mm. This can be interpreted as the spatial resolution of SPME probe in gel matrix. In extractions from tissue, increased tortuosity and analyte binding to matrix constituents results in limited dispersion of analytes and lower diffusion coefficient values, which are inversely proportional to local matrix viscosity.[26] *D* can therefore assume values constituting 8-42% or 14-24% of those measured in agar gel (depending on solute size) in the caudate and neocortex regions, respectively. Moreover, in the presence of binding matrix the mass transfer is related to effective diffusion D_{eff} which accounts for the fact that analytes bound to tissue or the SPME coating exhibit limited or no diffusion. The effective diffusion coefficient D_{eff} given by equation 3.2 describes the analyte adsorption or desorption in the coating,[309] which can be extended analogously to the analyte's behaviour in the tissue in the presence of binding matrix.

$$D_{eff} = \frac{\mathrm{D}}{1+\mathrm{k}} \tag{3.2}$$

$$k = \frac{K}{V_s/V_f} \tag{3.3}$$

Where: *D* is absolute diffusion coefficient, *k* is the partition constant of the extracting phase, *K* is partition coefficient of analyte between intercellular fluid and the investigated tissue, where V_s is volume of the binding matrix and V_f is volume of the intracellular fluid

The analytes` adsorption onto the binding matrix present in the tissue limits or eliminates their diffusion, analogously as in the case of their adsorption onto the SPME coating during storage or DESI-MS analysis. The binding properties of the analyte in a tissue with unknown concentration of the binding matrix have been described by numerical modeling and experimental approach elsewhere.[310] The discussion above indicates that the spatial resolution will be different for different compounds and will depend on their affinity to the matrix and the SPME coating, defined by K_{eff}.

Thus, SPME probes can be expected to provide higher spatial resolution for measurements in real brain tissue, especially for heavily bound compounds, indicating that the resolution is related to affinity of a given molecule to the investigated matrix and the SPME coating. Although trying to attain a spot

size significantly under 500 μm in order to improve spatial resolution while working with gel matrix would be a futile attempt to contravene the physics of diffusion, it could still be beneficial by allowing more scans per SPME spatial resolution unit to be obtained, thus improving ion statistics. However, when shorter extraction times are sufficient for attaining or improving LOQ values (e.g. by means of improved instrumental sensitivity or extracting phase with higher affinity for the target analytes), efforts to decrease the spot size would be justified and desirable to be in sync with improved spatial resolution of SPME sampling.

Model 1: Laminar distribution of analytes in gel

The gel model aimed to demonstrate that SPME-DESI-MS could be used to reliably produce quantitative reconstructions of laminar concentration gradients. This highly controlled environment of compartments, with their defined volumes, borders, and drastically different analyte concentrations, was merely an approximation of the environment in a real brain. Indeed, in a real brain, the layers are constantly in dynamic contact with one another, allowing compounds to be diffused and transported by various mechanisms, whereas the layers in the gel model were assembled only for the short extraction period. **Figure 3.9** shows the obtained laminar profiles for selected compounds overlaid onto the expected profiles corresponding to the arrangement of the layers in the gel stacks (profiles of remaining analytes are presented on **Figure 3.10**). Three replicate measurements were taken for each stack configuration, and the average quantitative profiles reflected the actual system accurately.

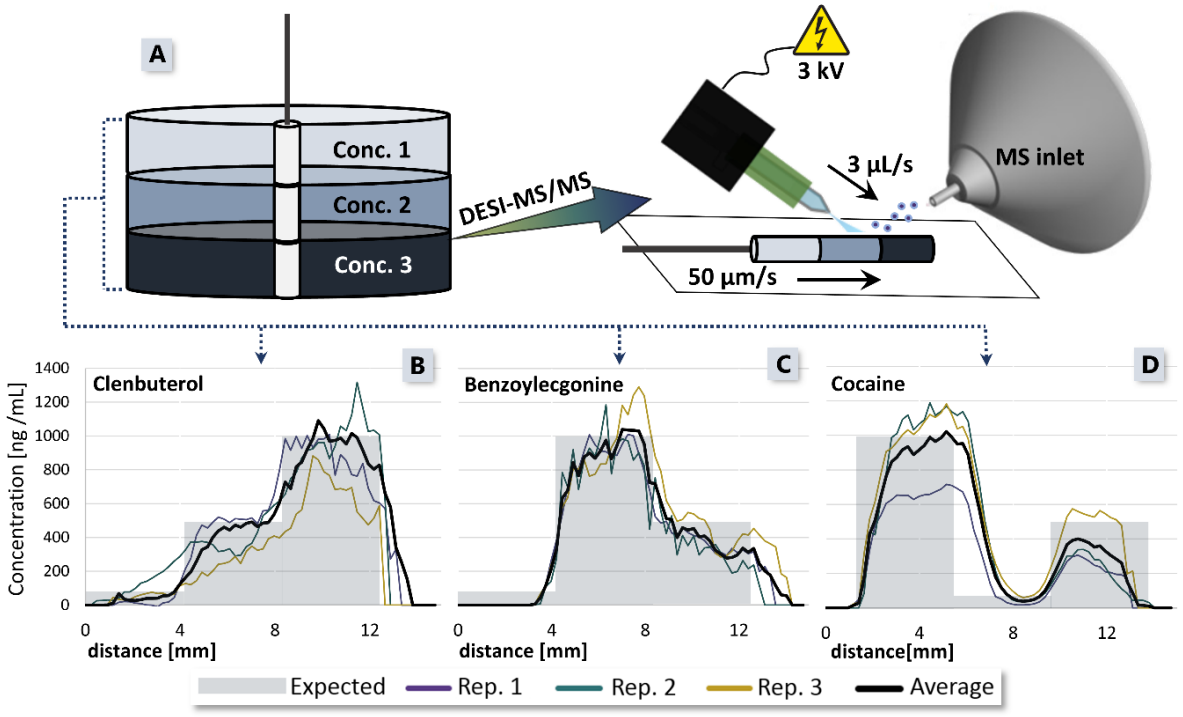

Figure 3.9: Space-resolved laminar concentration gradient investigation in gel model by SPME-DESI-MS. A) General experimental setup; B) gel stack configuration (Config. 1) with increasing analyte concentrations in a top-down direction; C) gel stack configuration (Config. 2) with the highest concentration layer in the middle; D) gel stack configuration (Config. 3) with a blank layer sandwiched between 1000 and 500 ng/mL layers.

It can be noted that the thickness of the analyte-free layer is underestimated when it is surrounded by layers enriched with analytes (**Figure 3.9-D and Figure 3.10-C**). The mechanism responsible for this behavior is likely the diffusion of analytes into the middle layer. Even though the extraction time was relatively short, and the gel layers were assembled right before fiber deployment, it is highly likely that concentration-gradient-driven diffusion between layers occurred. Moreover, this effect is more pronounced when the blank layer receives analyte influx from both sides. This hypothesis was later confirmed by performing similar experiments with the layers separated by a physical barrier (see Chapter 4).

Layer	Config. 1	Config. 2	Config. 3
Bottom	⦸	⦸	1000 ng/mL
Middle	500 ng/mL	1000 ng/mL	⦸
Top	1000 ng/mL	500 ng/mL	500 ng/mL

Table 3.5: The order of layers in each configuration of the gel stack used in the experiments depicted in **Figure 3.9** and **Figure 3.10**.

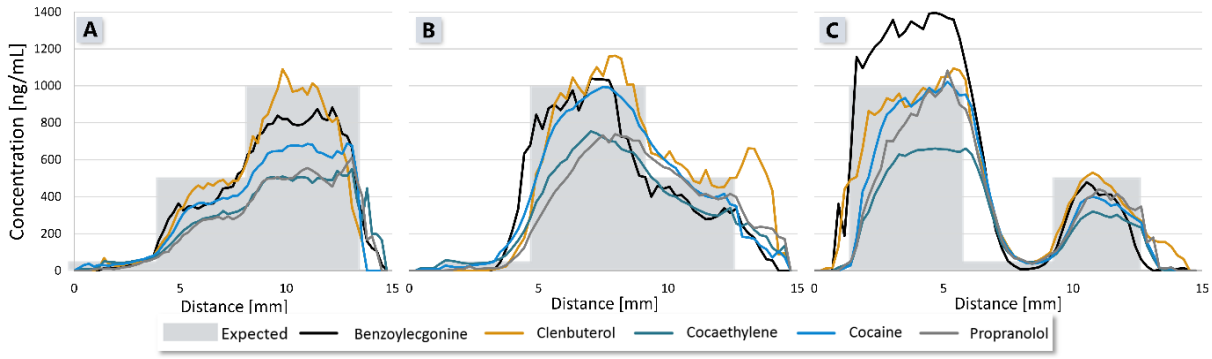

Figure 3.10: Gel layer profiles acquired via SPME-DESI-MS for all tested compounds. Each profile represents the average of 3 collected fibers for every gel stack configuration. A), B), and C) correspond to gel stack configurations included in **Table 3.5**: Config. 1, Config. 2, and Config. 3, respectively.

The quantitative performance of the SPME-DESI-MS setup was evaluated by constructing calibration curves, which were summarized in **Table 3.6**. Limits of quantitation (LOQ) for each matrix were defined as the lowest concentration of an analyte producing a signal-to-noise ratio ≥ 5, with a relative standard deviation (RSD) of 4 replicate measurements below 20%, and an accuracy within 20% of the relative error.[311]

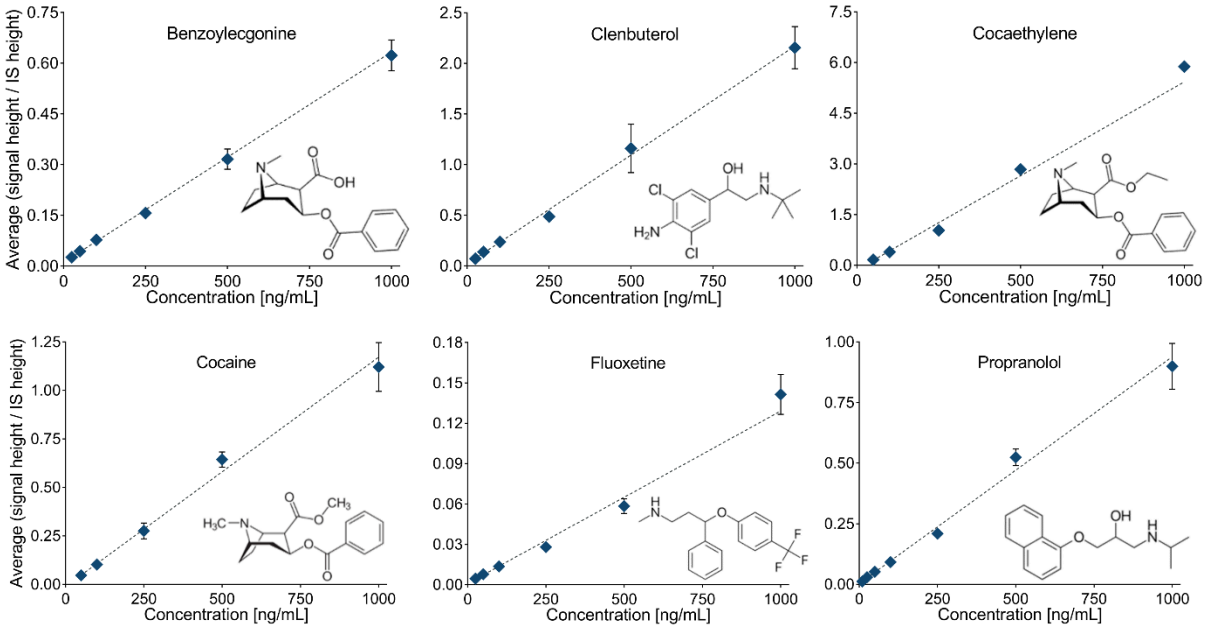

Figure 3.11: Calibration curves for the quantitation of target analytes in agar gel matrix via SPME-DESI-MS with 4 mm long fibers. The slope, intercept, and R2 for each calibration function can be found in **Table 3.6**.

Space-resolved analysis vs. 'space-weighted average'

The ability of SPME-DESI-MS to maximize the amount of information obtained within one sampling was demonstrated repeating the gel layer model experiments followed by desorption and analysis of the SPME fibers via nanoESI-MS. We hypothesized that the obtained analyte concentrations would reflect an average of the entire sampled area (in this case, 500 ng/mL).

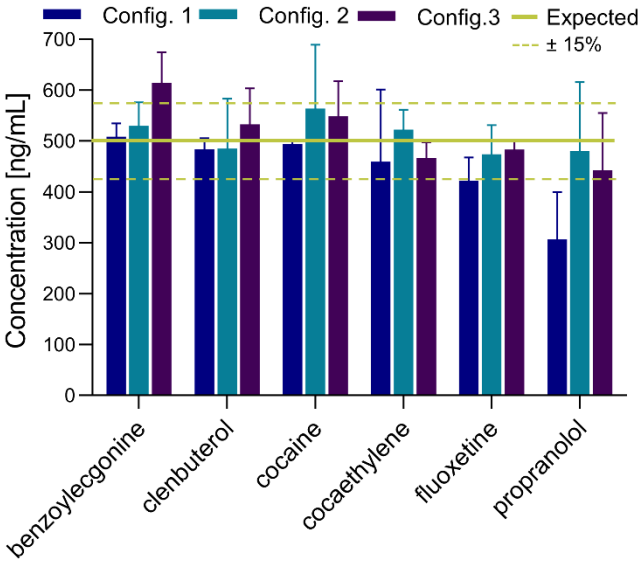

Figure 3.12: Space-weighted average measurements in gel stacks analogous to B, C, and D in **Figure 3.9** via SPME-nanoESI-MS. The detailed order of gel layers in each stack configuration can be found in **Table 3.5**.

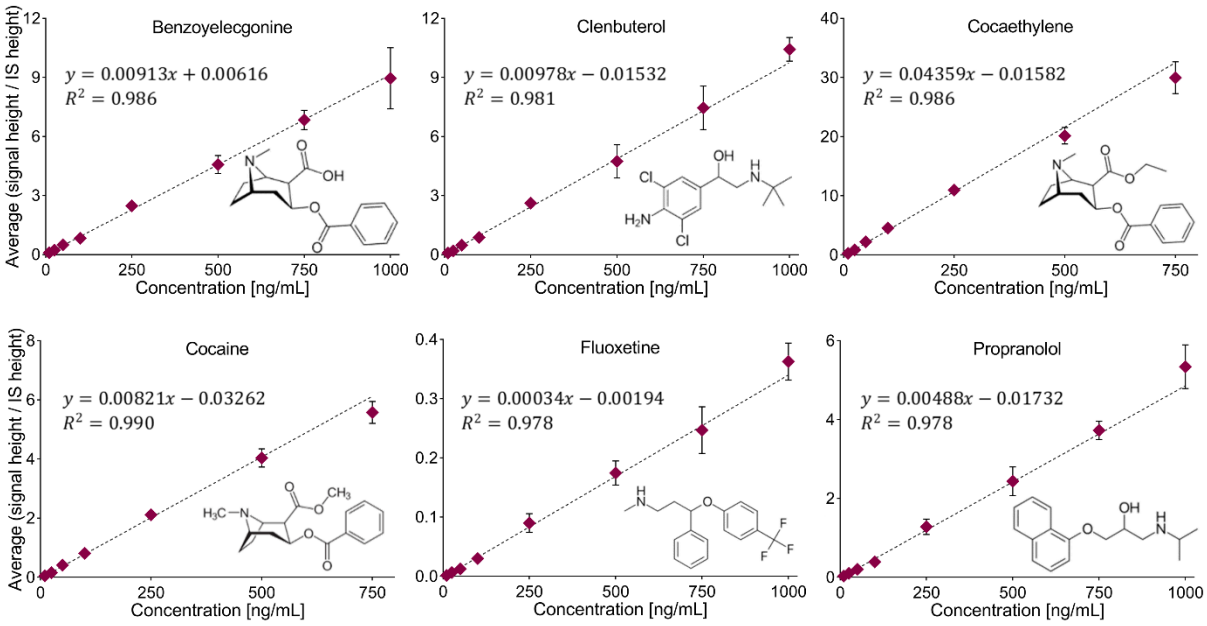

Figure 3.13: Calibration curves for the quantitation of target analytes in agar gel matrix via SPME-nanoESI-MS with 4 mm long fibers. Weighing factor ox $1/x^2$ was applied to all the calibration curves.

In general, good agreement between the experimental results and our expectations was achieved (**Figure 3.12**), thus confirming that SPME provides space weighted average concentrations when conventional, non-spatially resolved instrumental methods are used. Even though the concentration gradients in the solid or semi-solid sample are imprinted on the SPME fiber (in static extraction mode

and with resolution determined by the analyte's diffusion coefficient), the information is lost upon desorption into the solvent. For spot sampling, decreasing the coating's length results in increased spatial resolution, but this entails the necessity of multiple fibers to be deployed to a larger area in order to ensure an appropriate level of detail.[287] Therefore, SPME-DESI-MS offers a simpler and faster alternative for sampling of heterogenous systems.

Model 2: Concentration gradient in surrogate brain tissue.

The surrogate brain tissue approximated the composition and consistency of a real brain; however, the heterogeneity of a real brain was not accounted for in order to simplify the introduction and diffusion of analytes. This matrix has previously been shown to be suitable for external matrix-matched measurement calibrations in brain tissue via SPME.[136,211] We expected the diffusion processes to be better approximated than in brain homogenate due to the tortuosity of the surrogate matrix, which more closely resembled that of actual brain tissue.

***Brain in the box* model.** Based on the experimental design depicted in **Figure 3.14**, it was anticipated that the spatially-resolved analysis of several fibers orthogonally placed in the sample would result in a quasi-2D reconstruction, since the short fibers were offset from the long fiber. Alternatively, if the short fibers were overlapped with the long fiber, they could be utilized as confirmatory spot samples. Following the injection and distribution of the analytes, a gradient was created within the sample with the maximum at the injection site. The tip of the long fiber deployment site overlaps with the concentration maximum, with the gradient significantly decreasing within the distance of second short fiber placement and remaining analyte-free in the distance of 8.5 mm from the box wall (6 mm from the injection site). Placing the short fibers farther away from the injection site than the long fiber caused the measured analyte concentration to be lower at the maximum for each short fiber than at the corresponding area for the long fiber. The gradient pattern was also conserved in the z direction, decreasing with distance from the injection site.

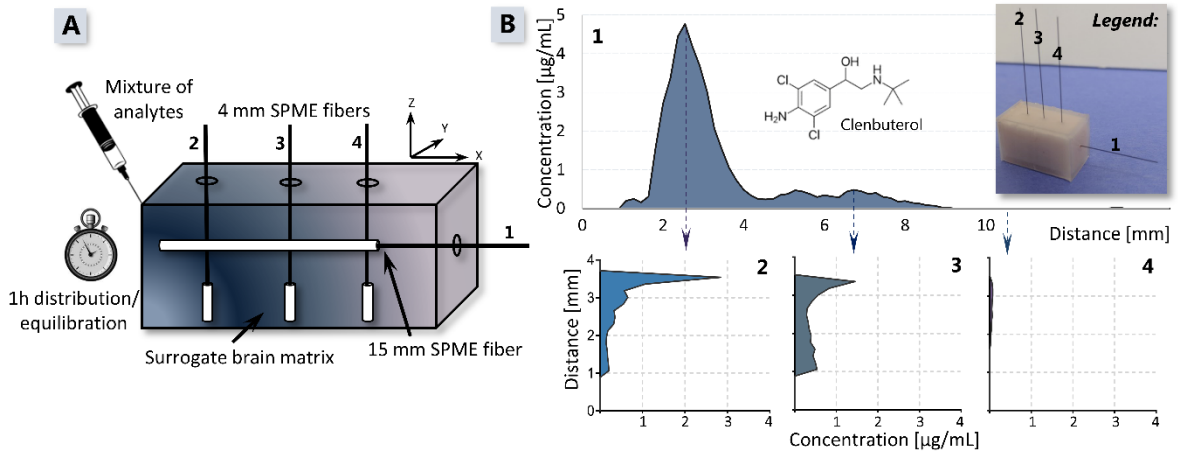

Figure 3.14: The *Brain in the box* model. **A**) schematic of the experimental design for investigating analyte distribution in a surrogate brain matrix placed in a box and spiked with a mixture of drugs and pharmaceuticals in one of the corners; **B**) results of a quantitative, quasi-2D reconstruction of clenbuterol distribution in the model.

The key advantage of employing SPME probes in this configuration is that they can easily be inserted into the tissue from any practically available angle due to their minimal space requirements, customizability, and flexibility. In a real-life scenario, such as intra-operative sampling, this feature would not only make the described approach compatible with robotic systems such as robotic surface analysis (RoSA)[312] or the DaVinci surgical system,[313] but it would also offer the additional advantages of spatially-resolved analysis and analyte preconcentration. Although this approach offers more direct and faster tissue analysis than intra-operative DESI of tissue sections,[314] it is still more of a depth-profiling technique than an imaging technology.

***Brain on a dish* model.** The second model employing surrogate brain tissue simulated the radial diffusion of the analytes, following introduction of the compounds at the center of the matrix surface. Similar to the previous model, good representation of the expected concentration profile was obtained, as shown in **Figure 3.15**. Two variations of this model involved deploying the tip, or center, of the long fiber at the injection site, while leaving the positions of the short fibers unchanged.

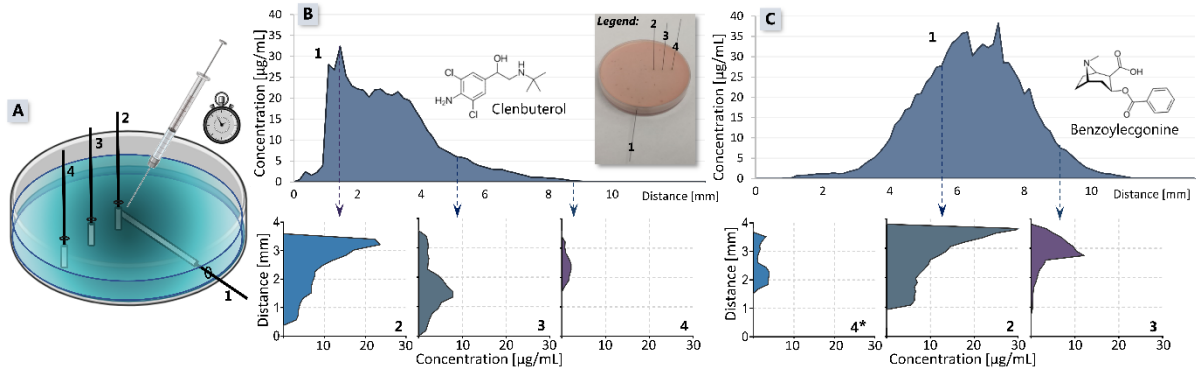

Figure 3.15: The *Brain on a dish* model: **A**) experimental setup for investigating the distribution of analytes in a surrogate brain matrix placed in a Petri dish and spiked in the center; **B**) reconstruction of clenbuterol distribution using the long SPME probe with its tip placed in the dish center; **C**) reconstruction of benzoylecgonine distribution with the long SPME probe's tip placed in the center of the dish. Fiber 4* was placed in the dish area that was not covered by the long fiber 1. Figures on top and bottom represent data acquired with the long and short fibers, respectively. In both variants of the model the injection site was the center of the dish.

As expected, it was observed that the concentration gradient decreases with increasing distance from the injection site and with increasing depth of fiber penetration into the matrix. Likewise, this approach allows estimating the 3D distribution of the target analyte when multiple fibers are deployed to probe larger area (**Figure 3.16**). This strategy could be useful to obtain information about the *in vivo* concentrations of brain pathophysiology biomarkers (e.g. 2-hydroxyglutarate[315]) in close vicinity to the tissue affected by the disease.[271]

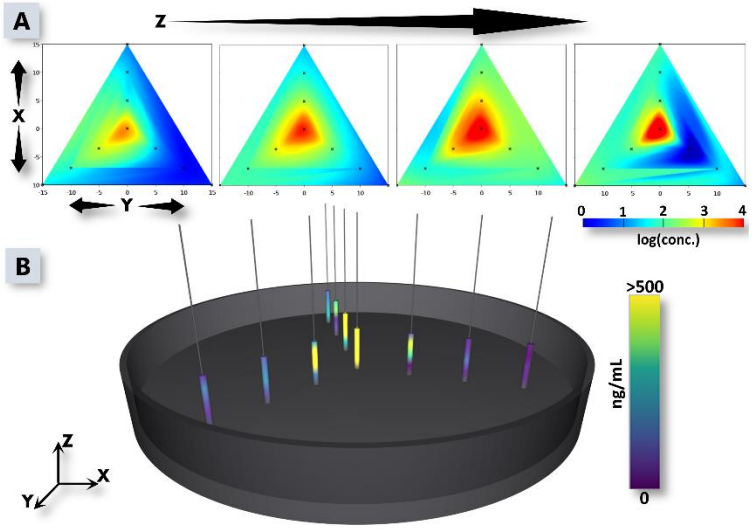

Figure 3.16: Estimated 3D distribution of cocaine in the *Brain on a dish* model. **A**) Contour plots representing depth-profiling of concentration gradient in the sample at each unit of SPME spatial resolution (from left to right: top of the fibers to their bottom, with 720 µm step size); **B**) Visualization of 3D molecular map of cocaine in the dish created with 'ili software.[316]

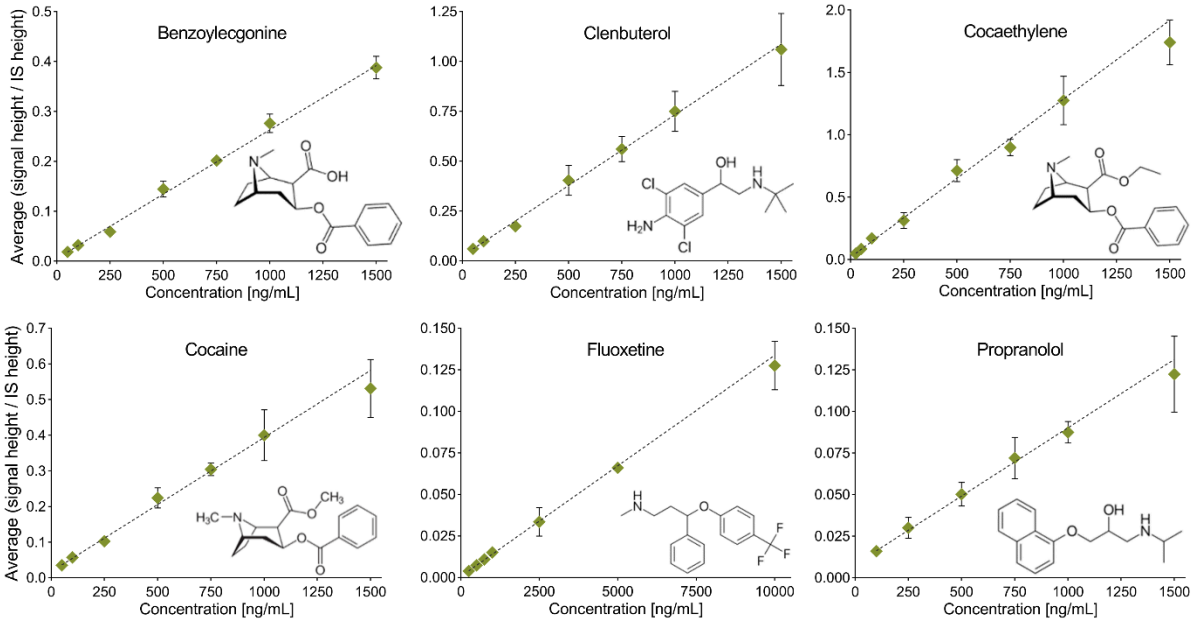

Figure 3.17: Calibration curves for the quantitation of target analytes in brain surrogate matrix via SPME-DESI-MS with 4 mm long fibers. The slope, intercept, and R2 for each calibration function can be found in **Table 3.6**.

Table 3.6: Figures of merit for the quantitation of drugs and pharmaceuticals in gel and surrogate brain matrices via SPME-DESI-MS.

Analyte	Gel matrix					Surrogate brain matrix				
	slope	intercept	R^2	weighing	LOQ [ng/mL]	slope	intercept	R^2	weighing	LOQ [ng/mL]
benzoylecgonine	0.0006	0.0113	0.979	$1/x^2$	25	0.0003	0.0069	0.984	$1/x^2$	50
clenbuterol	0.0022	0.0201	0.965	$1/x^2$	25	0.0007	0.0187	0.967	$1/x^2$	50
cocaine	0.0012	-0.0111	0.981	1/x	50	0.0004	0.0142	0.973	$1/x^2$	50
cocaethylene	0.0056	-0.1282	0.997	$1/x^2$	50	0.0013	0.0224	0.979	$1/x^2$	25
propranolol	0.0009	0.0033	0.980	$1/x^2$	10	0.0001	0.0077	0.977	$1/x^2$	100
fluoxetine	0.0001	0.0009	0.975	1/x	25	0.0001	0.0007	0.950	$1/x^2$	250

Model 3: Spatial distribution of fluoxetine in rat brain

The model drug chosen for this study, fluoxetine has been proven effective in treating clinical depression and altering multiple physiological processes in the hippocampus.[317] Numerous studies have found evidence to suggest that fluoxetine positively influences hippocampal synaptic plasticity and long-term potentiation,[318] enhances neurogenesis,[319] has neuroprotective effects,[320] including anti-inflammatory properties,[321] and prevents oxidative stress.[320] For spatially-resolved analysis of rat

brains, the probes were inserted along the plane containing hippocampus. This decision was made for two reasons: first, fluoxetine has a notable impact on the hippocampus region; and second, convenience of *ex vivo* targeting of this region in brain halves. **Figure 3.18** shows selected quantitative fluoxetine profiles in rat brains. It is noticeable how the profiles for given fiber introductions drastically differ between animals in terms of fluoxetine concentration in the hippocampus and the distribution of the drug in adjacent areas. This is most likely due to a combination of factors. Inter-animal variability causes identical doses of an administered drug to result in different concentrations in the hippocampus of each animal.

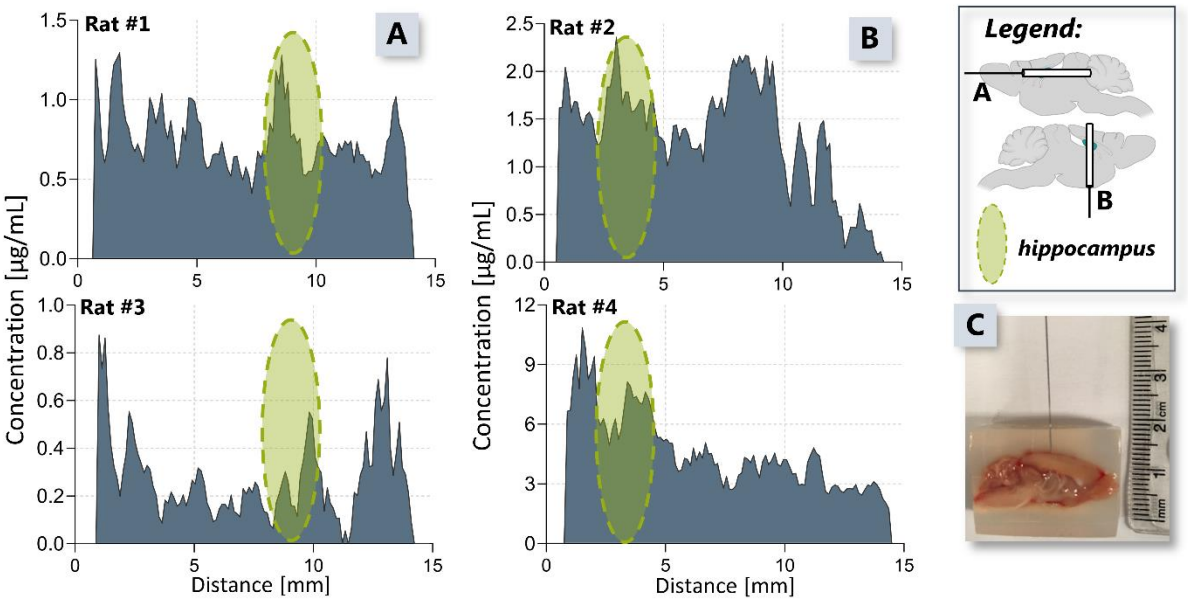

Figure 3.18: Space-resolved quantitative profiles of fluoxetine in brains of 4 rats measured ex vivo (after in vivo 10 mg/kg drug administration). **A**) profiles acquired from long fibers inserted along the sagittal plane; **B**) profiles acquired from fibers inserted along the coronal plane; **C**) experimental setup with rat brain half embedded in agar gel block and the probe piercing through the hippocampus. The areas of the SPME fibers that were extracting from hippocampus were marked with green circles.

Moreover, despite attempts to aid the targeting of the hippocampus by embedding the brain samples in gel blocks, manual fiber insertion *ex vivo* remains prone to poor positioning precision (positioning was based on the stereotaxic coordinates for rat brains[322]). *In vivo* sampling allows for better

reproducibility in terms of fiber deployment due to the brain's defined position (i.e. enclosed in the skull) and the cannulation of the animal based on stereotaxic coordinates. Moreover, while precise, software-controlled systems guided by electrophysiological recording can be used to accurately introduce probes into small brain structures,[323] these methods can only be used in living brains.

The brain's inherent heterogeneity can undoubtedly hinder interpretation of the obtained fluoxetine profiles across the sample due to the area-specificity of matrix effects, which affect the obtained signal and concentrations.[324] Cerebrospinal fluid and white and grey brain matter can significantly differ in their lipid[325] and metabolite compositions, cation concentrations,[324] and metabolism,[326] thus creating different local environments that interact with the analytes and the extraction phase. Moreover, the diffusion coefficients of solutes can vary depending on the sampled brain area or compartment,[307] the brain's pathophysiology, and the subject's age,[26] thus affecting the spatial resolution of measurements. These effects are not taken into account during external matrix-matched calibration, however the standard on fiber approach employed for signal correction in this study can compensate for these effects, as they affect the extraction of target analytes and desorption of the IS in the same way.

The *ex vivo* quantitation of fluoxetine across rat brains in this study did not provide any evidence that its positive effects on hippocampal physiology correlate to its accumulation in that particular brain area. The strategy for improvement of this model involves implementation of *in vivo* sampling to bypass the need of storage and freeze-thaw cycle of the brains, which could cause fluoxetine's redistribution. To further test the developed protocol's performance in real samples, perhaps a better model can be proposed, that enables the verification of target analyte distributions predicted and confirmed by previous studies that have used different methods. Such models include the accumulation of cocaine in striatum or the persistent presence of methamphetamine in white matter,[327] as well as the accumulation of methamphetamine in dopamine-rich regions.[328] We also foresee our approach as being suitable for

examining the spatial resolution of local drug uncaging in the brain and the radius of the resultant neuromodulation effects.[329]

3.2.4 Conclusions

The presented experimental results enable a better understanding of SPME-DESI-MS's capabilities and limitations for reconstructing the laminar- and radial-concentration gradients existing in a given sample. Unlike other SPME technologies coupled directly to MS via microfluidic open interface (MOI) coated blade spray (CBS) or nano-ESI, which yield the average concentration across the sample, SPME-DESI provides insight into the spatial distribution of the analytes. The final protocol was applied to three model situations, showing good agreement with the expected spatial profiles of the analytes in the sample. Furthermore, the proposed protocol indicated its future prospect as a tool for analyzing real unknown samples such as rat brains, provided further validation in a suitable animal model. The results also indicated this technology's potential for use in *in vivo* analyses of compounds that are relevant to brain studies, such as drugs and pharmaceuticals, with future expansion of this scope of analysis to include the untargeted profiling of endogenous compounds and metabolites. The exploratory capabilities of the SPME-DESI-MS protocol were further strengthened by its good quantitative performance, which was enabled by stabilizing and correcting the obtained ion signal on both the hardware and signal processing levels via scan-by-scan correction with internal standards. We postulated that the developed IS correction strategy could mitigate the issues with proper interpretation of spatial profiles of drugs in brain arising from the tissue's inherent heterogeneity and the area-specificity of matrix effects. This technology possesses numerous features that would make it appealing to specialists from other fields, such as medical doctors or neuroscientists. With the anticipated future addition of accurate, software-controlled robotic systems for SPME fiber deployment and with further improvements, we expect that the presented SPME-DESI-MS setup will deliver insights into hypothesized area-specificity of action and accumulation of various compounds in living brain.

Furthermore, we foresee SPME-DESI-MS for space-resolved applications as a complementary technique to existing ambient MS technologies already used in the clinical setting such as REIMS,[330] SpiderMass,[331] and MassSpec Pen.[332]

3.2.5 Considerations for *in vivo* sampling via SPME-DESI-MS

As highlighted in the laminar gel model, the concentration of analytes in the analyte-free layer was in some cases overestimated, leading to underestimation of the thickness of that particular layer. While this effect was predominantly attributed to the lack of physical barrier between the gel layers causing diffusion of the analytes to the blank layer, another possible contributor is related to the technical aspect of the sampling. In cases where high concentration layer precedes the analyte-free layer on the path of the probe insertion, the probe segment which will be placed in the blank layer during the extraction event may become contaminated by the analytes. In an instance of high affinity of a particular analyte to the extracting phase (high K_{ef} value), quantifiable amounts can be extracted within the very brief period of probe insertion.[62] The high K_{ef} value would then prevent the analyte to be desorbed into the blank layer of the sample, especially if short extraction time is employed.

One proposed solution is to accompany the SPME probe with a guiding tube that would sheathe the extracting phase on the way to the target area and prevent premature extraction (**Figure 3.19**). This approach is similar to the strategy outlined in Chapter 2 employing guiding cannula with an internal diameter closely matching the probe diameter to eliminate analyte pick-up during the probe deployment in the sub-cortical region. The modification of that workflow for spatially resolved analysis would have to include placement of the guide-probe assembly in the target area and subsequent withdrawal of the guide tube to expose the extracting phase to the tissue. Following the extraction completion, the guide tube would then be re-inserted onto the SPME probe to sheathe the extracting phase during the withdrawal from the tissue.

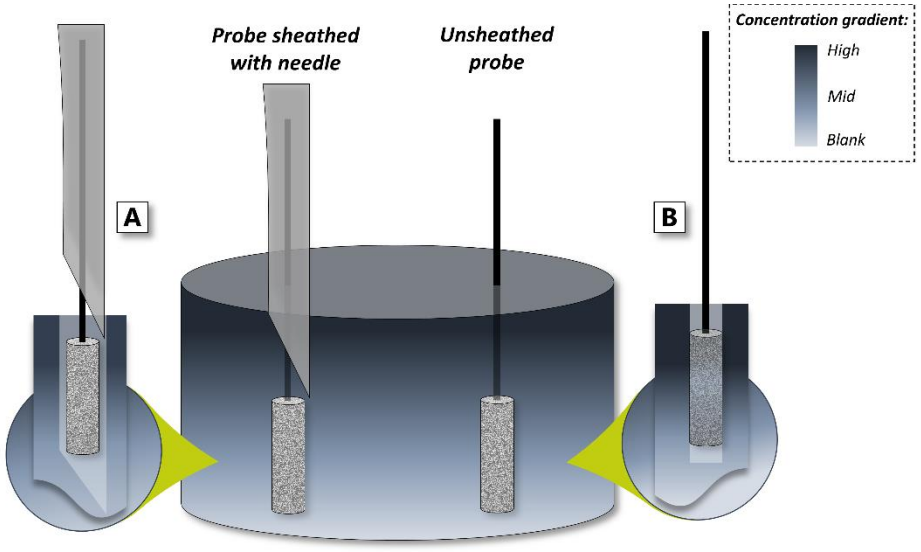

Figure 3.19: Possible imprint distortions occurring in space resolved sampling with SPME. **A)** SPME probe accompanied with the guide tube, sheathed on the way to the target location, with the guide tube being a potential source for distortion of the spatial distribution of the analytes in the tissue sample. **B)** The unsheathed probe placed in analyte-free region becomes contaminated with the analytes during the insertion into the target location.

However, there exists a possibility that the guide tube insertion and withdrawal to expose the SPME coating would disturb the spatial distribution of the analytes. Moreover, this approach would rely on employment of guide tubes with the possibly smallest wall thickness, as upon the guide tube withdrawal the pierced tissue would have to seal around the exposed probe, which could contribute to analyte distribution distortions. The relationship between the insertion speed and imprint distortion as well as the extent of the described effects (i.e. if their severity exceeds the spatial resolution of the technique) should be the subject of future investigations.

Another proposed solution takes advantage of the fact that only a portion of the entire SPME coating undergoes desorption via DESI, therefore in principle half-coated probe would remain suitable for the intended spatially resolved analysis. This probe would be sheathed with a modified guide tube resembling an elevator by having an opening on the bottom, matching the width and length of the coated portion of the probe (**Figure 3.20**). The sampling would involve insertion of the assembly into the tissue in its inactive form- with the non-coated side of the probe facing outward. The extraction would

commence upon probe rotation by 180° exposing the coated part of the probe to the sample. After extraction the rotation would revert the assembly to its inactive form for withdrawal from the tissue.

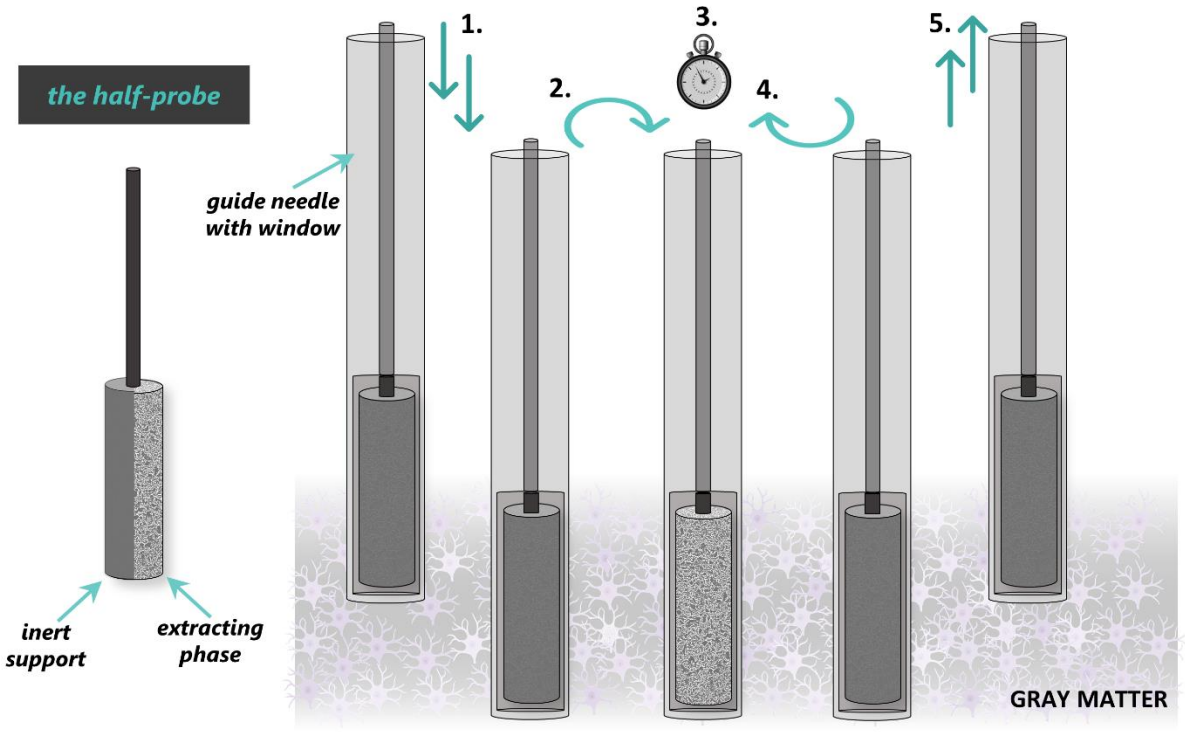

Figure 3.20: Proposed strategy of spatially resolved in vivo tissue sampling with SPME, eliminating the imprint distortion and contamination. 1. The half-probe accompanied by modified guide tube with opening at the bottom is driven into the target brain area in inactive form with no coating exposure to the tissue; 2. The probe is rotated by 180° to 3. expose the coating to the tissue and commence the extraction; 4. After extraction the probe is rotated by 180° again and reverted to the inactive form; 5. The SPME assembly is withdrawn from the brain tissue.

This strategy may impose a technical challenge, as all sampling steps require precise software controlled operation by microdrives. Additionally, the robustness and reproducibility of the half-coated probe manufacturing would have to be ensured. This approach, however, represents a viable direction for future employment in in vivo spatially resolved analysis by SPME-DESI-MS.

3.3 Pursuing performance-enhancing strategies for SPME-DESI-MS

3.3.1 Introduction

The inherent consequence of short interaction time between the desorption solvent spray and the extracting phase, as well as the superficial character of desorption off of the SPME coating by DESI, is the fact that relatively small amounts of analyte are effectively being desorbed, ionized and transferred to the MS. The need for enhancing desorption efficiency from the solid substrate during the transient interaction has been therefore identified as one of the most important requirements to be addressed in order to enable attainment of LOQ values sufficient for real *in vivo* applications of this technique. Desorption efficiency in this context can be tuned by manipulation of the extracting phase thickness or spray solvent properties. The effect of varying the coating thickness on the LOQ values and quantitative capabilities as well as the effects of solvent composition on the signal intensity are discussed in Chapter 4. It is important to note that in SPME-DESI-MS the properties of each solvent have to be weighed equally from the perspective of the extracting phase interaction and microdroplet dynamics (the desorption aspect) as well as feasibility to obtain a stable electrospray and ion current (the ionization aspect),[303] which in combination determine the signal's stability and quantitative accuracy.

Since desorption, ionization, and MS acquisition occur simultaneously and in real time, delaying the desorption relative to the acquisition constitutes a way of gaining additional time for analyte dissolution and enhancement of desorption efficiency.[333] While this delay can be achieved by decreasing the speed at which the sample is moved between the sprayer and the MS inlet, this approach significantly extends the analysis time. The alternative involves employment of two sources of desorption solvent: one to pre-wet the coating surface and initiate the desorption and the other to perform the standard DESI function. The study described herein aims at assessment of the feasibility of this approach and evaluation of the potential gains in terms of signal enhancement, which would in turn translate to improvement of LOQ values.

3.3.2 Experimental

Two sources of the desorption solvent were employed: the Waters sprayer assembly[302] as the primary sprayer with DESI function, and an in-house built sprayer without a high voltage supply (the wetting sprayer). For the purpose of aiding the hardware setup development with the two sprayers, the preliminary tests were performed using the developed for this purpose coated stubs assembly (**Figure 3.21**) as it enables a more visible and convenient tracking of the wetted areas on the coated surface rather than on a narrow SPME probe.

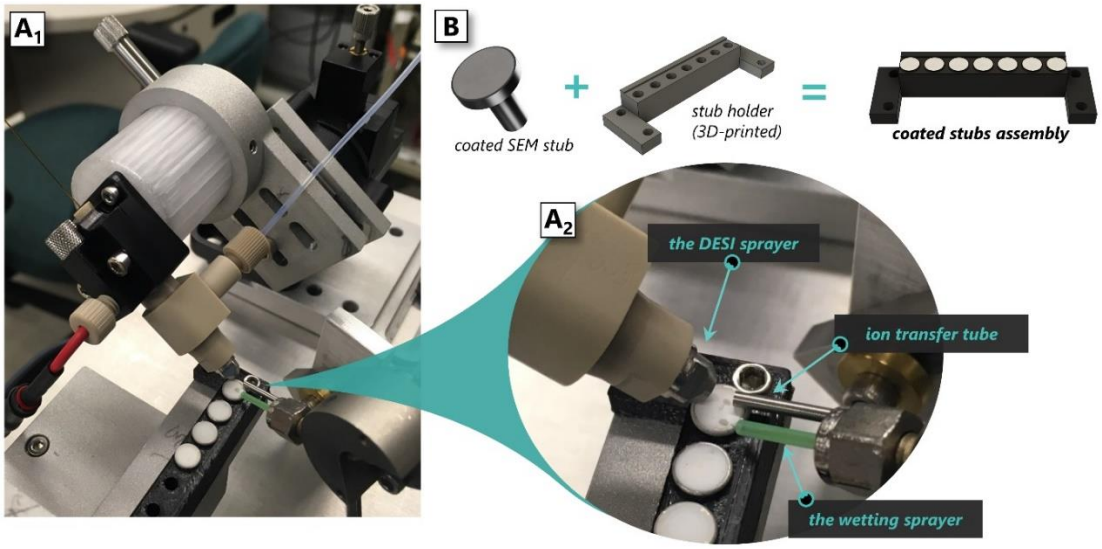

Figure 3.21: Experimental setup for SPME-DESI-MS with two sprayers and the coated stubs assembly for preliminary testing. **A1)** Initial positioning of the two sprayers relative to each other and to the MS inlet. **A2)** Detailed view of the sprayers' positions with the desorption spot and pre-wetted area. **B)** Coated stub assembly for rapid testing of different configurations consisting of SEM stubs coated with the extracting phase and 3D-printed holder.

Following establishment of the optimal position of the two sprayers relative to each other, the sample surface, and the MS inlet, further evaluations employed the setup with SPME probe assembly described in subchapter 3.2 and the experimental conditions summarized in **Table 3.7**. Ketamine and its two metabolites were selected as the target analytes due to their relevance to *in vivo* analysis in brain (elaborated on in Chapter 4), as well as their hydrophobicity range. The analytes were uniformly deposited onto the coated stub or extracted from a homogenous solution as only the signal improvement

was evaluated in this study. The influence of pre-wetting on the spatial resolution and possible imprint distortions would be further evaluated in heterogeneous systems in an instance if the pre-wetting strategy was deemed successful.

Table 3.7: SPME details and DESI-MS interface settings and parameters used for the delayed desorption trials.

SPME	Extracting phase	Hydrophilic-lipophilic balance (HLB)		
	Coating length	13 mm		
	Coating thickness	27.5 µm ± 2.5 µm		
	Max. probe diameter	255 µm ± 5 µm		
	IS pre-loading	1h static extraction from 600 µL of water spiked at 250 ppb		
	Analytes extraction	30 min static extraction from 600 µL of PBS spiked at 250 ppb		
DESI	Nebulizing gas pressure	100 psi		
	Solvent flow rate	3 µL/min DESI spray; 5 µL/min wetting spray		
	Spray solvent	methanol/water (95:5, v/v) + 0.1% FA + 5 ppm LeuEnk		
	Wetting solvent	methanol/water (95:5, v/v)		
	Tip-to-surface height	2 mm DESI spray; 2 mm wetting spray		
	Distance inlet-sample	2 mm		
	Tip-sample angle	50° DESI spray; 90° wetting spray		
	Inlet angle	5°		
	Fiber scanning speed	50 µm/s		
MS (Xevo G2-S QTof)	Spray voltage	3 kV		
	Cone voltage	40 V		
	Source offset	80 V		
	Heated capillary temperature	250 ˚C		
	Source block temperature	100 ˚C		
	Acquisition mode	Sensitivity; MS/MS (Tof MRM)		
	Scan time	250 ms		
	Mass range	70-400 m/z		
	Acquisition time	4 min		
	LockMass acquisition	LeuEnk (fragment m/z 120.0813); scan time 300 ms; interval 5 s		
	Monitored transitions	Ketamine	238 → 125.017	(logP 3.1)
		Norketamine	224 → 207.060	(LogP 2.2)
		Hydroxynorketamine	240 → 195.058	(LogP 1.1)
		Ketamine-D4 (IS)	242 → 224.116	IS for Ket
		Norketamine-D4 (IS)	228 → 211.084	IS for NKet and HNKet

Two configurations of the delayed DESI were employed, with the pre-wetting solvent source in spray mode (**Figure 3.22**-B) or infusion mode (**Figure 3.22-C**) creating a liquid junction between the SPME coating surface and the pre-wetting solvent. The standard DESI approach with one sprayer was used as a baseline (**Figure 3.22-A**).

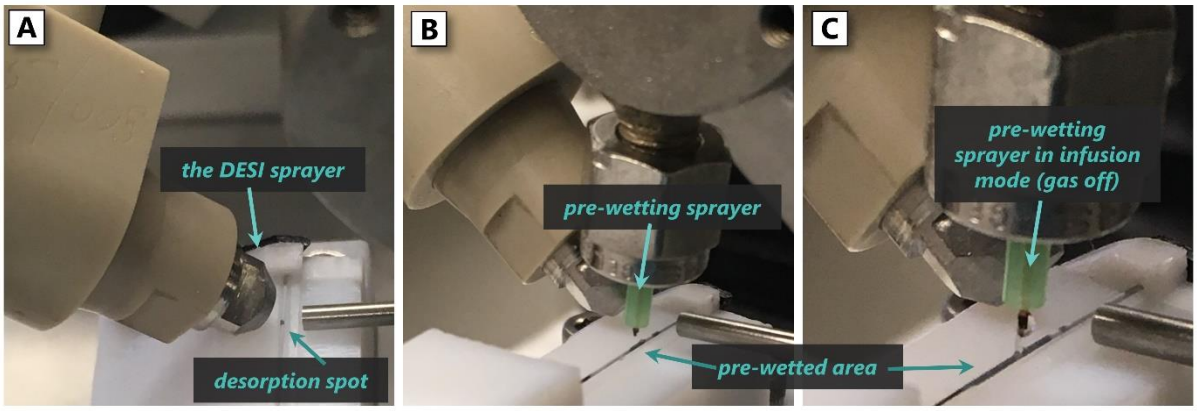

Figure 3.22: Experimental configurations employed for the investigation of SPME-DESI-MS with delayed desorption. **A)** The conventional setup with one sprayer and one desorption spot (considered as baseline in this comparison). **B)** The setup for delayed desorption employing second, pre-wetting sprayer positioned at 90° relative to the sample surface. **C)** The setup for delayed desorption utilizing the same configuration as shown in B, except the nebulizing gas input to the pre-wetting spray has been shut off to create a liquid junction between the supplied pre-wetting solvent and the surface of the extracting phase.

3.3.3 Results and discussion

Coarse setup testing with coated stubs

In porous media such as the SPME coating, the desorption process is slow; therefore, a clear separation between the solely desorption function of the pre-wetting solvent and solely ionization function of the primary DESI sprayer can not be made, as the primary DESI sprayer possesses both desorption and ionization properties. Therefore, the function of the pre-wetting solvent was to pre-desorb the analytes within the delay time required for the sample to arrive at the sampling area between the DESI sprayer and the MS inlet, where further desorption and ionization take place. For this reason, the investigation reported here was limited to the use of the same desorption solvent in both sprayers. The unknown contribution of each of the sprayers to the resulting desorption efficiency, as well as analyte-dependent effects of different solvent systems on desorption and ionization[334] would make an accurate deconvolution of the two sprayers' effects difficult in practice.

Including the second solvent source into the SPME-DESI-MS setup drastically increased the complexity of hardware-related optimizations and freedom of positioning tuning within the interface. The high importance of optimal geometry, distances, and relative positions of all DESI setup components,[335] including the second solvent source in the form of a sprayer, decreases the system's practicality and user-friendliness. An interesting alternative was reported as a pre-wetting solvent source in the form of a quill,[333] accessing the sample surface, logically, from the least crowded direction analogous to the primary sprayer position. The spatial constraints of the in-house developed DESI-MS setup used here only allowed to position the pre-wetting sprayer in an angle of 45° approaching the sample from the MS side, or the angle of 90° perpendicular to the sample surface (**Figure 3.23**).

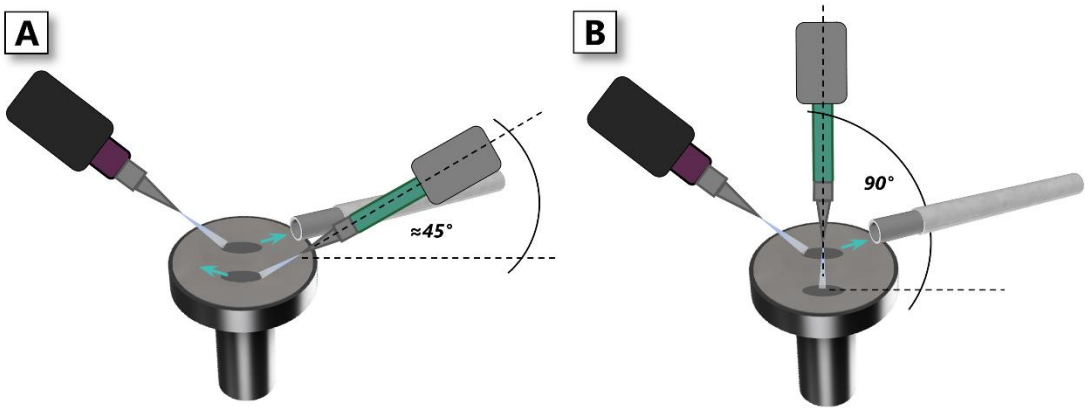

Figure 3.23: Positioning of the wetting sprayer relative to the DESI sprayer and the MS inlet. **A)** The configuration that is favorable in terms of practicality of the setup (the two sprayers do not constitute a spatial hindrance for each other), however the pre-desorbed analytes are being transported away from the DESI spray spot and the MS inlet; the tip-sample angle for the wetting sprayer is too low. **B)** Configuration with the tip-sample angle for the wetting sprayer increased to 90°, expected to pre-desorb the analytes without relocating them.

With the angled positioning of the pre-wetting solvent source working in the spray mode, the pre-desorbed pool of the analytes was displaced prematurely and in the direction opposite to the MS inlet. In the configuration perpendicular to the sample surface the signal improvement was not observed, regardless of the employed speed of the sample movement between the DESI sprayer and the MS inlet (**Figure 3.24**). Nevertheless, this configuration was selected for further investigation.

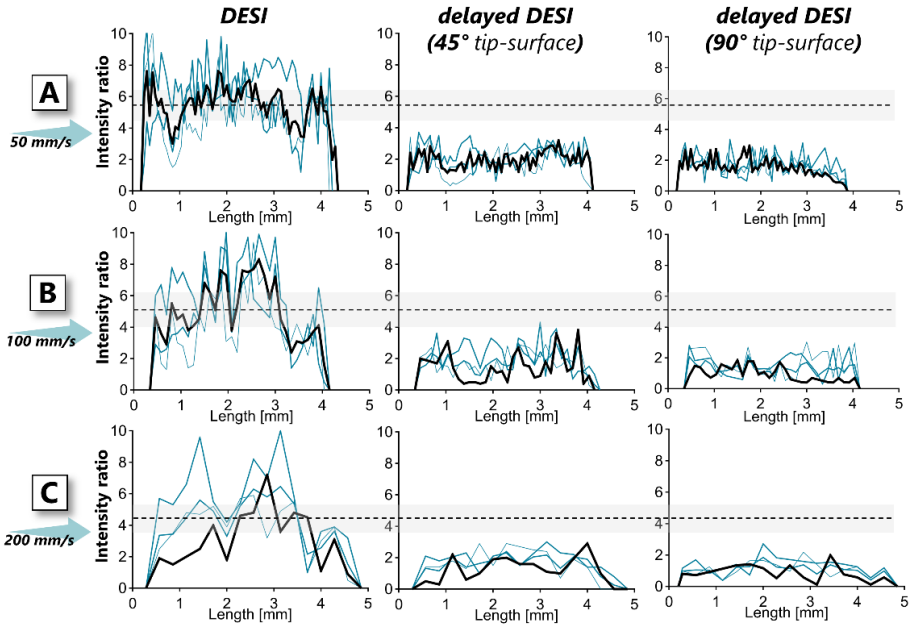

Figure 3.24: Corrected ion chronograms of **ketamine** desorbed off the coated stubs in three sprayer configurations. A. B, and C represent speed of sample assembly movement between the DESI sprayer and the MS inlet (50, 100, and 200 mm/s, respectively). The black traces represent the average profile of 3 replicate measurements, while each thin trace represents a single replicate. The dashed line represents average value of corrected signal across the profile obtained for the unmodified DESI configuration.

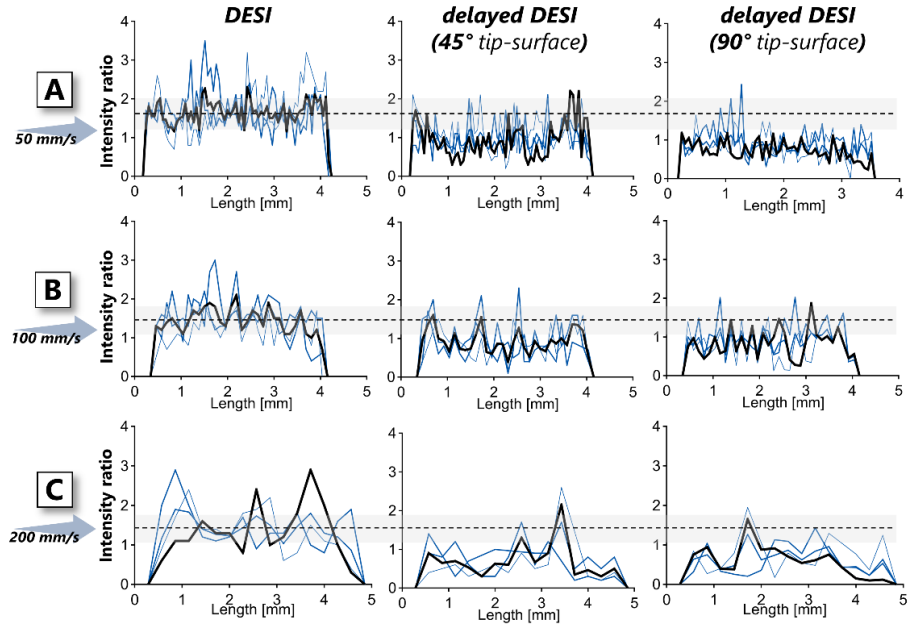

Figure 3.25: Corrected ion chronograms of **norketamine** desorbed off the coated stubs in three sprayer configurations. A. B, and C represent speed of sample assembly movement between the DESI sprayer and the S inlet (50, 100, and 200 mm/s, respectively). The black traces represent the average profile of 3 replicate measurements, while each thin trace represents a single replicate. The dashed line represents average value of corrected signal across the profile obtained for the unmodified DESI configuration.

Fine-tuning of delayed DESI for SPME probes

The displacement of pre-desorbed analytes was further confirmed by employing the SPME device in the probe form factor. By acquiring the imprint of analytes from a single probe containing both pre-wetted and dry areas, it could be observed that pre-wetting in fact results in significant signal decrease (**Figure 3.26**).

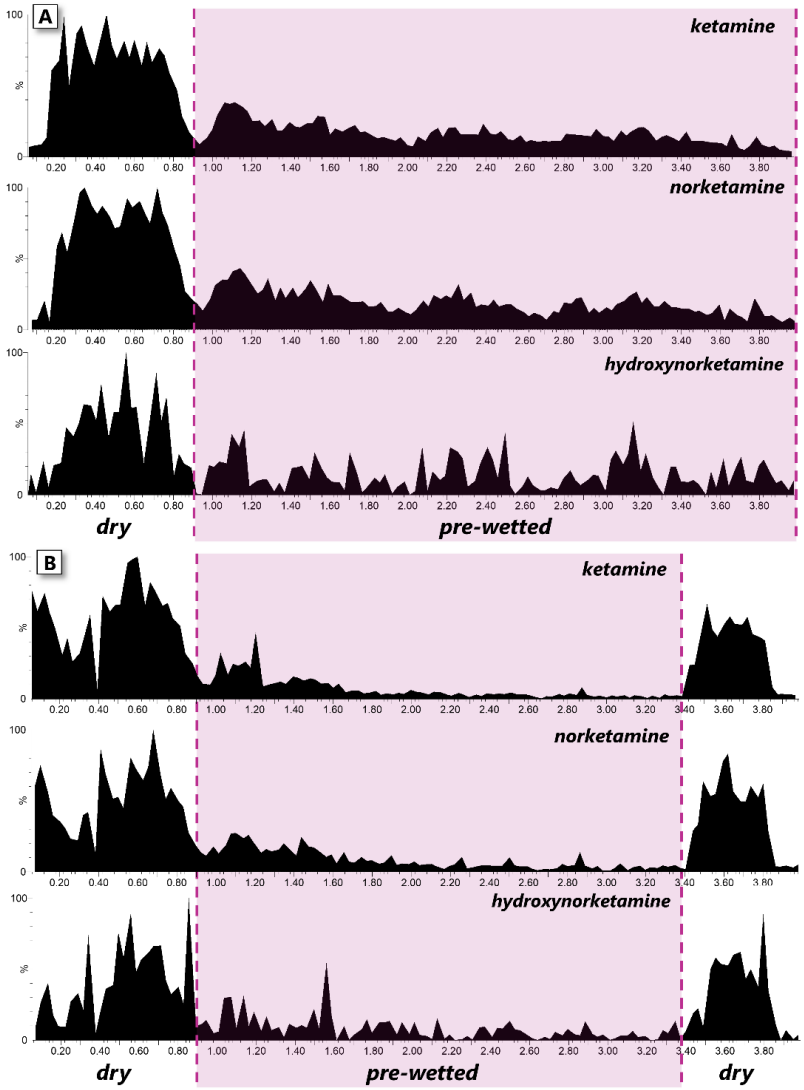

Figure 3.26: Ion chronograms (uncorrected) for the target analytes subjected to analysis by delayed DESI-MS demonstrating the raw signal decrease when pre-wetting in the spray mode is employed. **A**) The front segment of the probe which was not subjected to pre-wetting results in higher signal for all target analytes. This phenomenon is further evidenced in **B**, where additionally the back end of the probe was kept dry before the DESI sprayer's arrival.

The suspected cause of analyte loss in this configuration was the fact that the pre-wetting solvent source was employed in the spray mode. Despite the low power of the secondary sprayer and its direction perpendicular to the sample surface these conditions turned out to be too aggressive to avoid loss of analytes. To mitigate these effects, the pre-wetting solvent was applied in an infusion mode, with the secondary solvent source creating a liquid junction on the surface of the SPME coating. However, this approach yielded the corrected signal and the signal-to-noise values analogous to those obtained by delayed DESI with a secondary sprayer, indicating that the analyte displacement occurs in the liquid junction mode as well.

In summary, both investigated pre-wetting strategies resulted in the same average corrected signal values as the unmodified DESI protocol for all tested analytes (**Figure 3.27**). This suggests that all pre-desorption efforts affected the analyte and IS pre-loaded onto the extracting phase in the same way. However, since the main goal of the enhancements was to obtain lower LOQ values, ultimately the S/N values would constitute the factor deciding about the effectiveness of the delayed DESI approach. The substantial decrease in S/N values observed for both pre-wetting strategies (**Table 3.8**) confirms that the analyte displacement effect is in fact caused by the close proximity of the primary DESI sprayer to the pre-wetted spot on the extracting phase. Despite the plume of nebulized solvent being focused on the sampled spot on the SPME probe, the high nebulizing gas pressure prompts its expansion to adjacent areas.[333] Increasing the distance between the two sprayers to avoid this effect was not a feasible option, as the pre-wetted spot dried out by the time it arrived at the sampling area between the DESI sprayer and the MS inlet. Additionally, secondary source of desorption solvent introduces dilution, further contributing to decreased S/N values.

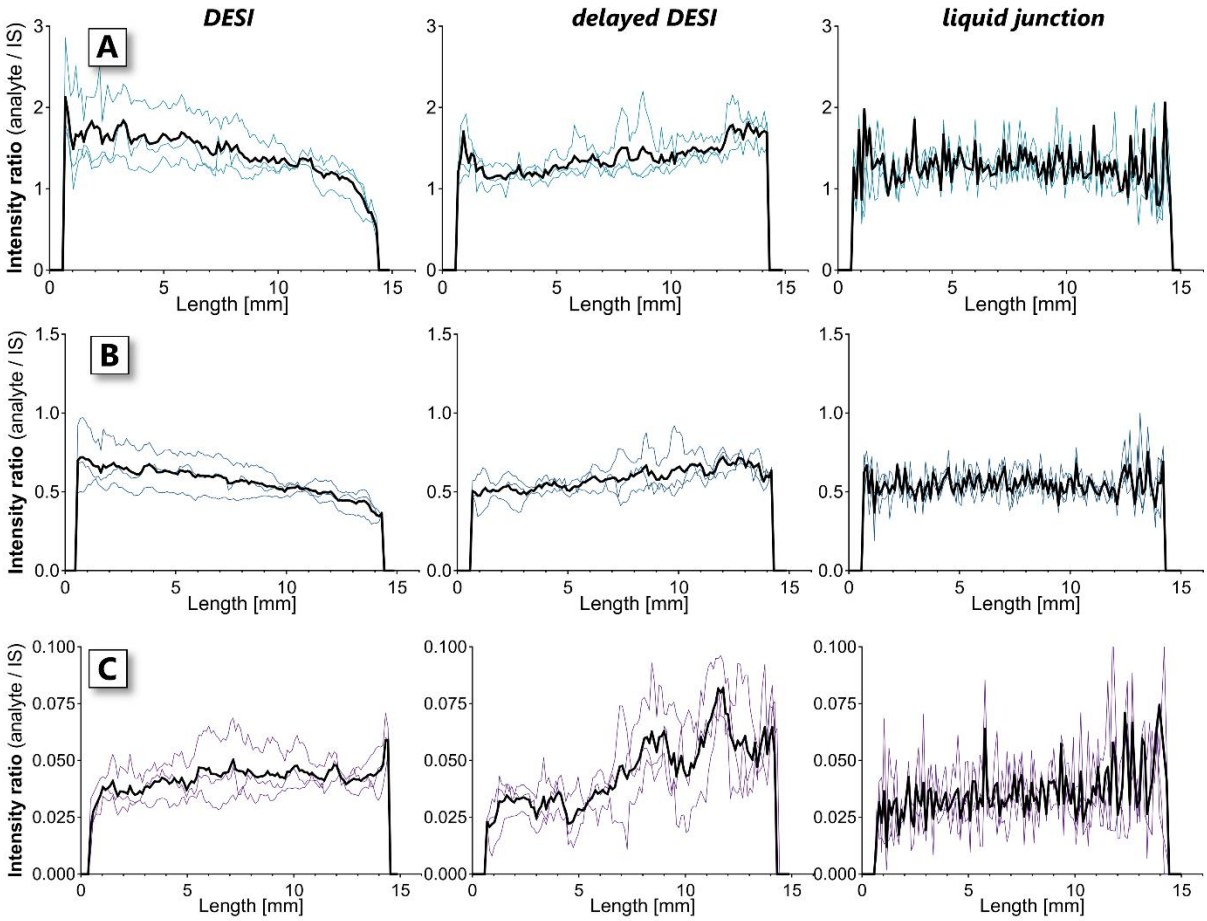

Figure 3.27: Corrected ion chronograms obtained for ketamine, norketamine and hydroxynorketamine (A, B, and C, respectively) via SPME-DESI-MS in all three compared configurations. The black traces represent the average profile of 3 replicate measurements, while each thin trace represents a single replicate.

Table 3.8: Summary comparison of average corrected signal and average signal-to-noise ratio values obtained for the target analytes via SPME-DESI-MS in all three compared configurations.

Setup	Ketamine		Norketamine		Hydroxynorketamine	
	Intensity ratio (%RSD)	S/N	Intensity ratio (%RSD)	S/N	Intensity ratio (%RSD)	S/N
DESI	1.44 (19)	1126	0.57 (15)	154	0.04 (19)	32
delayed DESI	1.39 (13)	51	0.59 (11)	48	0.05 (35)	10
liquid junction	1.28 (17)	47	0.55 (12)	52	0.04 (38)	8

3.3.4 Summary

The introduction of a secondary desorption solvent source to enhance desorption efficiency has been proven to be a technically demanding modification, ultimately bringing no gain and leading to S/N values deterioration due to analyte displacement and dilution. While further improvements of the hardware setup could be attempted, the pre-wetting strategy itself has been proven to only bring marginal gains elsewhere.[333] Future efforts of improving the sensitivity of analysis via SPME-DESI-MS should focus on fine-tuning of the SPME-related aspects (e.g. coating thickness, extracting phase properties, desorption solvent) rather than hardware modifications to maintain the technique's approachability and practicality.

Chapter 4

Quantitative and spatially-resolved *in vivo* characterization of drug release in brain

4.1 Preamble

This chapter contains yet unpublished results of a collaborative project between Prof. Janusz Pawliszyn Research Group at the University of Waterloo and Prof. Raag Airan Lab at the Stanford University which is currently in progress. The *in vivo* sampling of rodent brain as well as all preparations related to the ultrasound-sensitive nanocarriers (synthesis, characterization, etc.) have been carried out in the facilities of the Radiology Department at Stanford University. The SPME probe manufacturing and optimization, as well as development of protocols for the analysis and quantitation of ketamine and its metabolites via LC-MS/MS and DESI-MS/MS were carried out at the Department of Chemistry of the University of Waterloo by the author of this thesis. All data processing and writing of the related discussion presented herein have been completed by the author of this thesis. All co-authors have approved of the use of the data in this thesis.

4.2 *In vivo* approach for quantitation of ketamine and its metabolites in rat brain via SPME-LC-MS/MS

4.2.1 Introduction

Localized drug delivery via nanocarriers with subsequent stimuli-triggered release is currently a heavily researched and rapidly developing field presenting itself as what might ultimately become the future of drug delivery in clinical practice and neuroscience. Minimizing the side effects of systemic drug delivery and improving the clinical efficacy via bypassing the degradation pathways of the first-pass effect and upon transport through the cell membranes[336] is highly desirable in clinical practice[337] (particularly cancer treatment), where the development of several stimuli-responsive nanocarriers have

progressed to clinical trials.[336] In neuroscience, the high spatial and temporal resolution of release along with the non-invasiveness of ultrasonic drug uncaging makes it a well suited exploratory tool for investigating the effects of locally constrained modulation of brain activity.[338,329] These *avant-garde* methods of local drug delivery *via* biodegradable nanoparticles[339] require equally sophisticated techniques for accessing the localized chemical information associated with the drug delivery, including effective concentration of the drug and its metabolites, pharmacokinetic profile and area of release, to name a few aspects. With the existing emphasis on safety of localized drug delivery, the techniques for local measurements have to keep up with this requirement and offer minimal invasiveness and no local system disruption.[337] With the main advantage of local drug release being the possibility of noninvasive access to brain structures which are otherwise hard to access by injection or infusion methods, the hindered entry is also an inherent consequence that extends to any attempts to locally measure the resulting concentrations.

In this context, solid phase microextraction (SPME) emerges as technique continuously proving and recently rapidly expanding capability of monitoring and quantitation of chemicals in brain in vivo.[211,250,323,340,341] Operating on a *chemical biopsy* basis with no tissue collection or removal,[342] it offers diverse fit-for-purpose modes for *in vivo* analysis, ranging from the conventional desorption followed by liquid chromatography separation (SPME-LC), direct-to-MS coupling via nano-electrospray ionization (SPME-nanoESI)[135], and recently explored unidimensional spatially-resolved quantitation via desorption electrospray ionization (SPME-DESI).[343]

In recent years ketamine has attracted significant attention due to the acute and long-lasting antidepressant effect produced by low (subanesthetic) doses of this drug via an unclear mechanism.[344] Even though these effects have been researched for the past two decades, the efforts to understand the underlying mechanisms of its action and the neural circuits involved in the anti-depressive properties have been intensified recently, due to the approval of S-isomer of racemic ketamine (esketamine)

antidepressant by the U.S. Food and Drug Administration (FDA).[345] Notably, subanesthetic doses of ketamine are capable of exerting alleviation of the depressive symptoms in patients resistant to other forms of treatment.[344] The classical definition of ketamine as a non-competitive antagonist of the N-methyl-D-aspartate (NMDA) receptor largely mediates the hypnotic effects, but does not suffice to explain the rapid and sustained antidepressant properties.[346] Other interactions of ketamine involve opioid, muscarinic and monoamine receptors,[347] as well as enhancement of brain-derived neurotropic factor, and stimulation of synaptogenesis.[346,348] Ketamine has also been associated with influencing the affective response to chronic pain[349] and has been widely used in chronic pain management.[350,351] The psychedelic effects of ketamine on the CNS have resulted in its classification as a drug of abuse and brought concerns about risks associated with its upcoming routine use in treatment of major depressive disorder (MDD).[347]

The aim of this study was a comprehensive characterization of ultrasound-assisted drug delivery to rat infralimbic cortex via a ketamine-loaded phase-change nanoemulsion investigated by SPME-LC-MS/MS and SPME-DESI-MS/MS. This includes quantitative pharmacokinetics of ketamine and its metabolites (subchapter 4.2) in the area extending to the ultrasonic release zone with 3 mm spatial resolution using a single SPME probe, as well as mapping of the release area by spatially resolved SPME-DESI down to sub-millimeter resolution (subchapter 4.3). Localized administration into the medial prefrontal cortex in this study is anticipated to enable understanding which other structurally or functionally connected regions participate in ketamine response. The prerequisite for these advanced investigations was establishment of a SPME methodology capable of monitoring pharmacokinetics of ketamine and its metabolites in brain *in vivo* after systemic administration of the drug. This report focuses on the *in vivo* protocol development, while the studies involving ultrasonic drug uncaging are currently underway.

4.2.2 Experimental

Experimental model and subject details

All experiments described in this work involving vertebrate animals were approved under the Stanford Administrative Panel on Laboratory Animal Care (APLAC), protocol 32874, conforming to institutional and national guidelines and regulations. In this work, healthy wild-type male Long-Evans rats (Charles River Laboratories, Wilmington, MA) were used. Subjects were not previously used for any other procedures. Rats were housed in cages with 2 inhabitants, with a day-night cycle enforced from 7 AM-7 PM. Animal husbandry was provided by veterinarians and technicians at the Stanford Veterinary Services Center (VSC). Food and water were freely available.

Ultrasound Setup

Ultrasound was delivered with a 650 kHz centered single element transducer (Sonic Concepts, Bothell, WA, USA). Input to the transducer was provided with a function generator (Siglent, Solon, OH, USA) connected to an RF amplifier (Electronics & Innovation, LTD., Rochester, NY, USA). The sonication parameters were summarized in **Table 4.1**.

Table 4.1: Sonication parameters used in SPME experiments.

Sonication Parameter	Value
Frequency	650 kHz
Pulse Repetition Frequency (PRF)	0.5-2 Hz
Burst Length	50 ms
Peak Negative Pressure (*in situ*)	1.8 MPa
Duration of Sonication	240 s

SPME probes and assembly

SPME fibers were manufactured in house using the dip-coating procedure described in Chapter 2. The Oasis HLB (hydrophilic-lipophilic balance) polymeric particles (5 μm, monodisperse) used as SPME extracting phase in this study were kindly provided by Waters Corporation. The wire (304

stainless steel; 0.004" diameter) and tubing (304 stainless steel; 0.008" OD, 0.002" Wall Thickness) used for manufacturing of SPME probes for LC-MS/MS analysis was purchased from Component Supply (Sparta, TN, USA) and McMaster-Carr (Robbinsville, NJ, USA), respectively.

The probes intended for solvent desorption and LC-MS/MS analysis had 3 mm coating and followed the design reported previously with modified support wire narrowed at the tip,[211] to yield total probe diameter of 200 µm and coating thickness of ≈50 µm. The difference in this case was an improved manufacturing procedure which substituted acid etching (to obtain the desired shape and diameter) with assembling the shape using a wire inserted into a tubing and subsequently coated with the extracting phase (**Figure 4.1**). This method has proven to be more reproducible with the added advantage of eliminating the use of concentrated hydrochloric acid for the support wire etching.

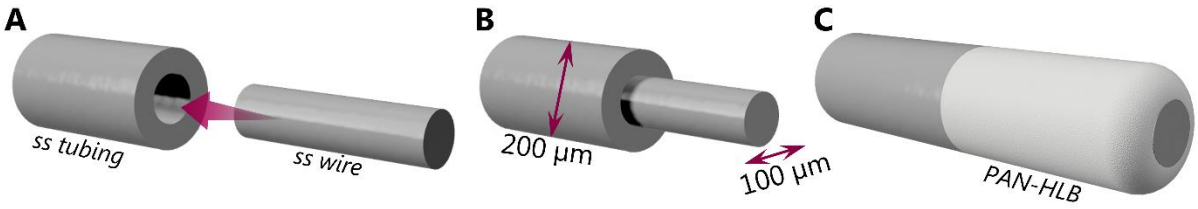

Figure 4.1: Schematic of SPME brain probe preparation by assembling. A- 100 µm wire is inserted into a 100 µm I.D. 200 µm O.D tubing; it is bent before insertion in order to secure it in place inside of the tubing; B- assembled supporting wire before coating; C- probe coated with PAN-HLB extracting phase. The thickness of the coating is approx. 50 µm and overall probe diameter does not exceed 200 µm.

A miniaturized custom probe holder was designed (**Figure 4.2**) to facilitate the probe positioning in the brain and enable rapid insertion and withdrawal during repeated sampling.

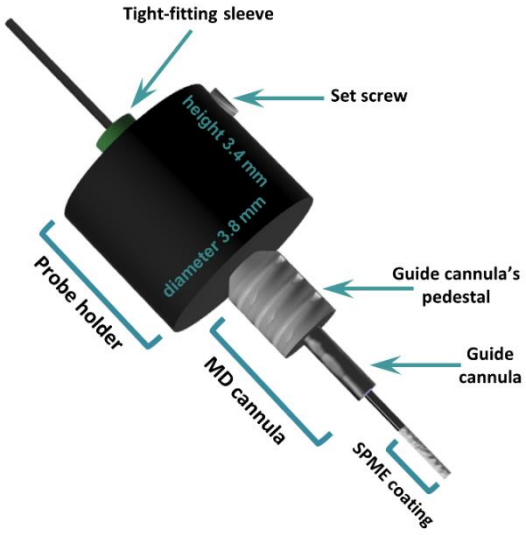

Figure 4.2: The SPME probe assembly for *in vivo* rat brain sampling used in this study. **The probe holder:** The tight-fitting sleeve centers the probe in the assembly. The set screw secures the probe in position suitable to the desired depth of penetration into the tissue, corresponding to the target sampled brain area. **The MD cannula**: The pedestal of the C315GS-2 cannula (P1 Technologies, Roanoke, VA) embedded in the dental cement sealing the skull fits the probe holder shape, securing the probe assembly in brain during the sampling. The guide cannula bridges the brain tissue with the external environment and is positioned directly above the target sampled area.

In vivo SPME session

Prior to each session, the work bench was sprayed down with 70% v/v ethanol and wiped down to avoid the contamination with ketamine from the environment. Long-Evans rats (350-450 g) were anaesthetized with 4% isoflurane in 100% oxygen and maintained at 2-3%. The rat was then prepared by shaving the head and establishing tail vein access with a 26G cannula. The animal was then loaded into a stereotaxic instrument (Stoelting, Wood Dale, IL) and the surgical field was sterilized with povidone-iodine swabs. A rostrocaudal incision, extending from the occipital-cervical junction to the interocular line, was made using surgical scissors, followed by a transverse incision along the interaural line. The subsequent flap was excised, exposing the dorsal surface of the skull. The fascia and periosteum were cleaned with lactated Ringer's solution and hydrogen peroxide. Two burr holes were drilled over the cannulation site (**Table 4.2**) and posteriorly for an anchoring screw, with the former being drilled at a 45-degree angle anteriorly. An anchoring screw was placed in the second burr hole, and the cannula (P1 Technologies, Roanoke, VA; cut to 7 mm long) was inserted in the first at a 45-degree angle until the bottom edge is flush with the skull. The setup was finally secured with dental cement.

Table 4.2: Stereotactic coordinates of relevant sites for SPME experiments.

Site	Caudal from Bregma (mm)	Lateral of Midline (mm)	Depth from Bregma (mm)
Cannula	-2.5	0.5	0
Sonication Site	2.5	0.5	-5

SPME probes were loaded into a plastic holder designed to interface with the P1 cannulae. Each probe was washed in deionized water and wiped gently off with a Kimwipe before being inserted sequentially through the cannula into the brain for four minutes. After the four-minute exposure period elapsed, each probe was removed, and the next probe was inserted. After exposure, the probe was immediately washed with deionized water and wiped again with a Kimwipe before being stored in a glass vial at -80°C for up to one week. Probes were then shipped on dry ice to the chemistry core facility for desorption, LC-MS/MS analysis and quantification, with the analyst being blinded to the probes' identities.

For experiments with systemic ketamine, free ketamine (Vedco Inc., St. Joseph, MO) was injected intravenously after two four-minute baseline sampling events (*i.e.* 8 minutes after experiment start), with lactated Ringer's solution as a flush. For the ultrasonic ketamine uncaging experiments, nanoparticles were prepared according to the procedure described previously.[329] The nanoparticles were defrosted shortly before the start of the session, and injected after the first probe (*i.e.* 4 minutes after experiment start). 10 minutes after nanoparticle injection, sonication was started at the sonication site (infralimbic cortex; **Table 4.2**), with sonication parameters provided in **Table 4.1**. The experimental protocol and timelines have been schematically depicted in **Figure 4.3**.

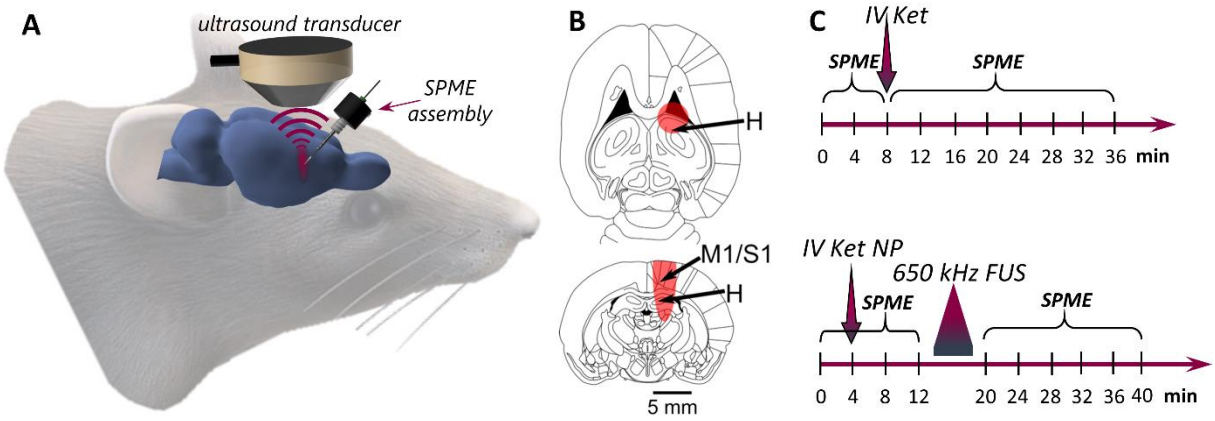

Figure 4.3: Experimental protocol for *in vivo* SPME in rat brain employed in this study. **A)** Schematic of the sampling setup in rat brain with the ultrasound transducer for drug uncaging and the custom made SPME sampler; **B)** Full-width half-maximum of the targeted area of the infralimbic cortex. Applied sonication field (red) estimated to have dimensions or approx. 1.6 mm in diameter and 4-5 mm in length (the drug release zone was estimated to be ~80% of this volume). H- hippocampus; M1- primary motor cortex; S1- primary somatosensory cortex; **C)** Sampling timeline before and after systemic ketamine administration (*IV Ket*, top) and ultrasonic uncaging (FUS) of injected ketamine nanoparticles (*IV Ket NP*, bottom).

LC-MS/MS analysis

The SPME probes were desorbed into 50 µm of methanol/water 90:10 solution containing IS at 20 ng/mL for 1 h with agitation at 1500 rpm. The LC-MS/MS analysis was carried out using an Ultimate 3000RS HPLC system coupled to a TSQ Quantiva triple quadrupole mass spectrometer (Thermo Fisher Scientific, San Jose, California, USA). Data acquisition and processing was performed using Xcalibur 4.0 and Trace Finder 3.3 software (Thermo Fisher Scientific, San Jose, California, USA). The chromatographic separation employed Kinetex® PFP column, 100 x 2.1 mm, 1.7 µm particle size (Phenomenex, Torrance, CA, USA) held at 35°C. The aqueous mobile phase (A) consisted of water with 0.1 % formic acid, while the organic mobile phase (B) consisted of acetonitrile with 0.1% formic acid. The following chromatographic gradient at a flow rate of 400 µL/min was applied (%B): 0-0.5 min 20%; 0.5-3 min linear gradient to 100%; 3-3.65 min held at 100%; 3.65-3.7 min linear gradient to 20%; re-equilibration at 20% until 4.5 min. The injection volume was 10 µL. The MS/MS analysis was

performed in positive ionization mode under selected reaction monitoring (SRM) conditions. The capillary voltage was set at 3.5 kV, with the remaining electrospray source conditions set to the following values: vaporizer temperature 358 °C, ion transfer tube temperature 342 °C, sheath gas pressure 45, auxiliary gas pressure 13, and sweep gas pressure 1 (arbitrary units). The instrumental stability throughout the sequence was monitored by analysis of an instrumental QC sample consisting of all target analytes and their internal standards spiked into a neat desorption solvent at 20 ng/mL.

Quantitation of ketamine and its metabolites

The resulting concentration of ketamine and metabolites was determined using modified external surrogate matrix-matched calibration approach developed in previous work.[211,343] The surrogate matrix consisting of agarose gel (1% agarose in PBS solution, *w/v*) mixed with lamb brain homogenate in the ratio 1:1 (*v/w)*. Prior to combining the agarose gel with the brain homogenate, the latter was spiked with the analytes in the concentration range 25-15000 ng/g and incubated overnight. Extractions were carried out in static mode from 1g of the matrix for 4 min, corresponding to the 4 min extraction time for *in vivo* experiments. The probes were subsequently rinsed with water and desorbed into 50 µL of desorption solvent consisting of methanol/water 90:10 and 20 ng/mL of internal standards. The analytical response in the form of peak area ratios (analyte to IS) was converted to amounts extracted by employing instrumental calibration curve consisting of analytes in neat desorption solvent in the range 0.1-100 ng/mL. The resulting matrix-matched calibration curve was expressed as amounts extracted in the function of concentration in tissue (**Figure 4.4**). A weighted linear regression equation fitted to the analytical response in the function of concentration was applied to quantify the analytes in the QC samples at 3 concentration levels to estimate accuracy and precision. Limits of quantitation (LOQ) were determined as the lowest concentration of analyte producing a signal to noise ratio ≥ 5, with a relative standard deviation (RSD) of 4 replicate measurements below 20%, and accuracy within

20% of the relative error.[143] The method's precision was expressed as percent RSD of 3 replicate measurements at each QC concentration level. Accuracy was calculated as the relative percent error of concentrations of analytes in the QC samples determined experimentally with the use of calibration curves versus theoretical (spiked) concentrations.

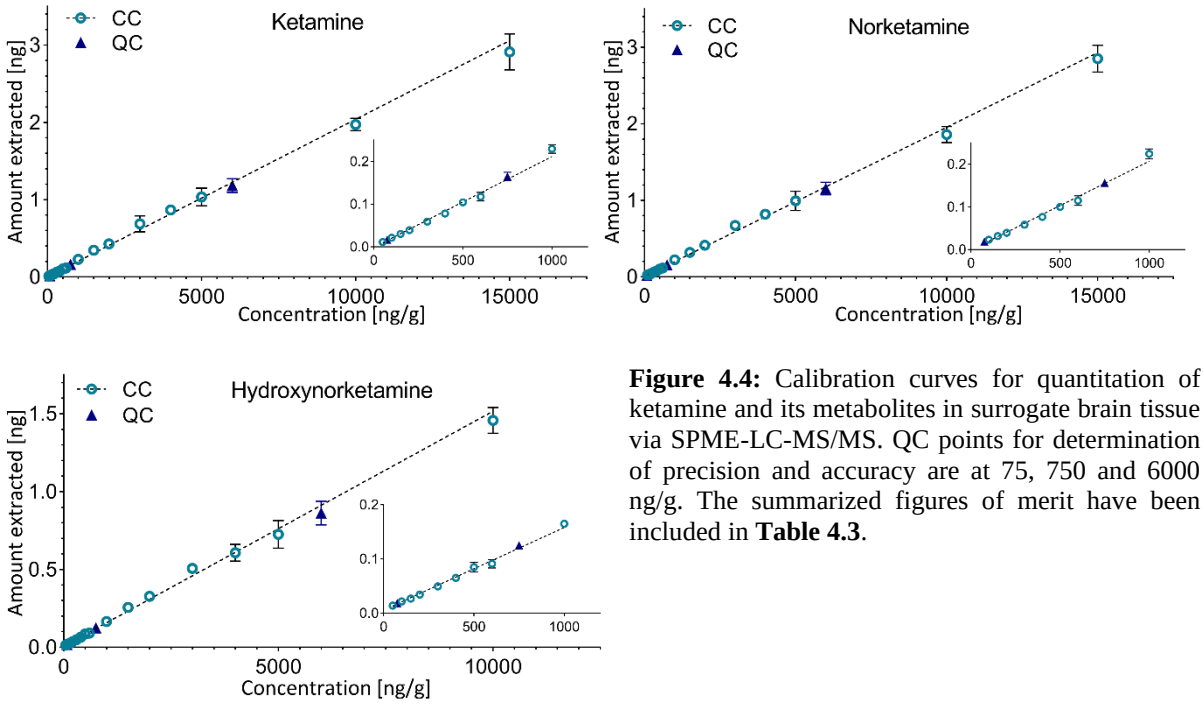

Figure 4.4: Calibration curves for quantitation of ketamine and its metabolites in surrogate brain tissue via SPME-LC-MS/MS. QC points for determination of precision and accuracy are at 75, 750 and 6000 ng/g. The summarized figures of merit have been included in **Table 4.3**.

Table 4.3: Figures of merit for quantitation of ketamine and its metabolites in surrogate brain tissue via SPME-LC-MS/MS.

Compound	Slope	Intercept	R^2	Weight	LOQ [ng/g]	Accuracy: % Error (*n*=4)			Precision: %RSD (*n*=4)		
						75 ng/g	750 ng/g	6000 ng/g	75 ng/g	750 ng/g	6000 ng/g
Ketamine	2.04e-4	1.74e-3	0.991	1/x	25	4	7	3	13	6	8
Norketamine	1.95e-4	4.74e-3	0.990	1/x	75	3	4	2	5	4	7
Hydroxynorketamine	1.51e-4	6.55e-3	0.990	1/x	50	8	5	5	11	5	9

Stability of ketamine and its metabolites under various storage conditions

Due to the storage and transportation involved in the protocol, stability of ketamine and its metabolites was examined over the course of 15 days of storage under various conditions (**Figure 4.5**). Ketamine and metabolites were spiked into brain homogenate at 1 µg/g. A 3 min extraction in static mode was followed by storage in the following conditions: immediate desorption and analysis (baseline samples); desorption and storage in solution in -80°C; placement of the probes in vials that have been purged with nitrogen gas in order to ensure inert oxygen-free atmosphere and storage in -80°C; placement in vials (ambient atmosphere) and storage in room temperature (average of 18°C). Samples stored in all conditions have been analyzed by LC-MS/MS after 1, 4, 8 and 15 days.

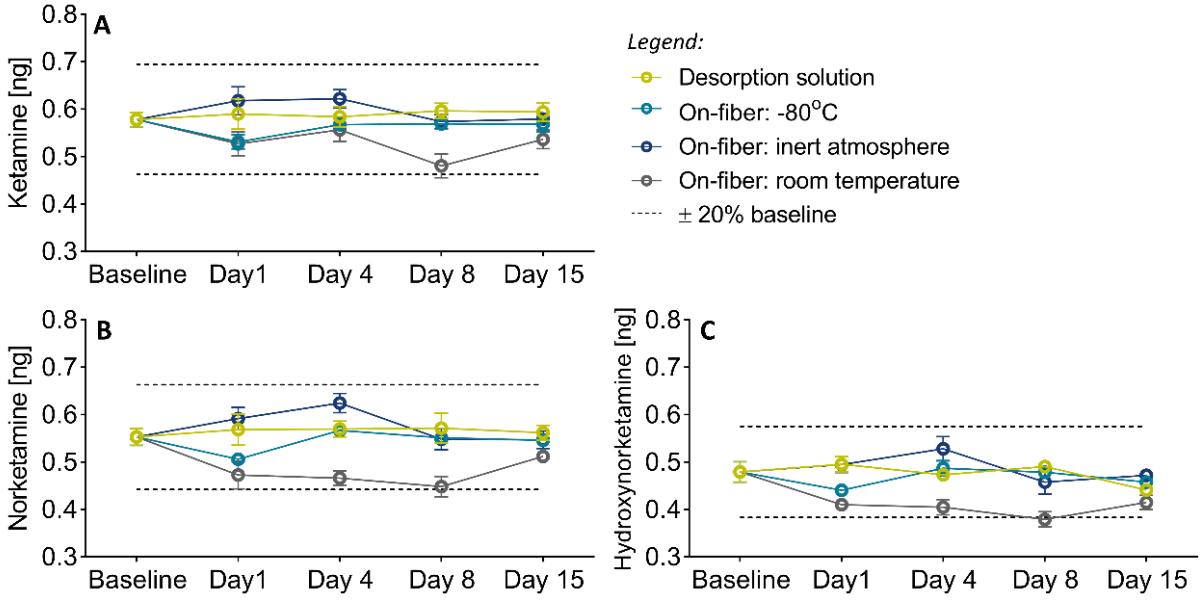

Figure 4.5: Stability of ketamine **(A)** and its metabolites norketamine **(B)** and hydroxynorketamine **(C)** under 4 storage conditions over the period of 15 days. All analytes exhibited good stability under in-solution and on-fiber storage in -80°C freezer. It was concluded that storage on fiber and shipment on dry ice does not pose a risk of significant analytes loss, even in an emergency situation of the samples spending up to 4 days in room temperature.

4.2.3 Results and discussion

The infralimbic region of the medial prefrontal cortex (mPFC) has been implicated in the antidepressant behavior of ketamine.[352,353] Besides cognition and behavioral control, mPFC is suggested to be involved in the pathophysiology of mood and anxiety disorders, including the treatment-resistive major depressive disorder (MDD).[354] In the light of growing evidence for the infralimbic subregion of the mPFC regulating behavioral adaptation through projections to PFC, amygdala, and other regions,[354] and the glutamatergic projections from infralimbic cortex being implicated in the antidepressant response to ketamine,[352] the functional complexity of mPFC circuitry is a viable target for investigations of ketamine's antidepressant mechanism of action.

The functional relations between different brain structures are generally investigated via localized modulation (pharmacological, electrical, optogenetic, etc.) of a target brain area and monitoring of secondary changes in structurally distant but functionally connected brain regions.[355] Specifically, pharmacological microinjections locally administer small volumes of ion channel blockers, agonists or antagonists, etc. into discrete brain regions which then modulate the brain activity with spatiotemporal characteristics dependent on the drug's pharmacokinetics and allowing insight into brain circuitry.[356] Although commonplace in neuroscientific investigations, the microinjection technique is associated with challenges related to accurate and precise positioning of the infusion device (additionally requiring postmortem target validation),[357] as well as the invasiveness of this approach. Moreover, inherently to any local delivery technique, the resulting brain concentration of the administered agent has to be locally measured in order to be empirically adjusted to determine the minimal effective concentration/dose.[358] Thus, beneficial effects of neuromodulation via pharmacological microinjection strategies do not present a straightforward path to clinical translation. In this context, the transcranial neuromodulation using ultrasound-triggered ketamine release from nanoparticles presents itself as a non-invasive alternative, addressing the issue of invasiveness by not requiring drilling into the skull or

cannula implantation and applying focused ultrasound (FUS) with parameters non-disruptive to the BBB.[338] Ketamine itself rapidly and easily crosses the BBB due to its high lipophilicity and low plasma protein binding.[359] It achieves up to five-fold higher levels in highly perfused tissues such as the brain, with a distribution half-life of 24 seconds after intravenous administration. The challenges of determining the effective brain concentration of the pharmaceutical modulator and confirmation of accurate and precise drug release area are examined in this study using SPME as an exploratory tool.

Pharmacokinetics of ketamine associated with systemic drug administration

Even though systemic or intracerebroventricular injections are not suitable for investigations of functional networks, as they do not allow for differentiation between the contribution from specific brain regions to the overall modulatory effect,[357] in this study systemic administration of ketamine was used to measure the resulting parenchymal concentration of the drug and its metabolites in the infralimbic cortex at three typical doses (**Figure 4.6**).

The established SPME protocol allowed determination of ketamine and its metabolites in brain *in vivo*, with good temporal resolution and figures of merit suitable to quantify the target analytes after systemic drug administration including the low dose of 1 mg/kg. A single infusion of ketamine may exhibit therapeutic effects within a few hours lasting up to a week, well beyond the expected lifetime of it and its active metabolites.[360] However, the widespread adoption of ketamine for MDD treatment has been limited by its hallucinogenic, sedative, and addictive properties.[361] Recently, hydroxynorketamine (specifically, (*2R,6R*)-HNKet) has been postulated to exert strong antidepressant properties through activation of α-amino-3-hydroxy-5-methyl-4-isoxazolepropionic acid (AMPA) receptor, without the abuse potential and dissociative effects.[360,361] These facts illustrate the importance of simultaneous *in vivo* monitoring of ketamine's metabolites.

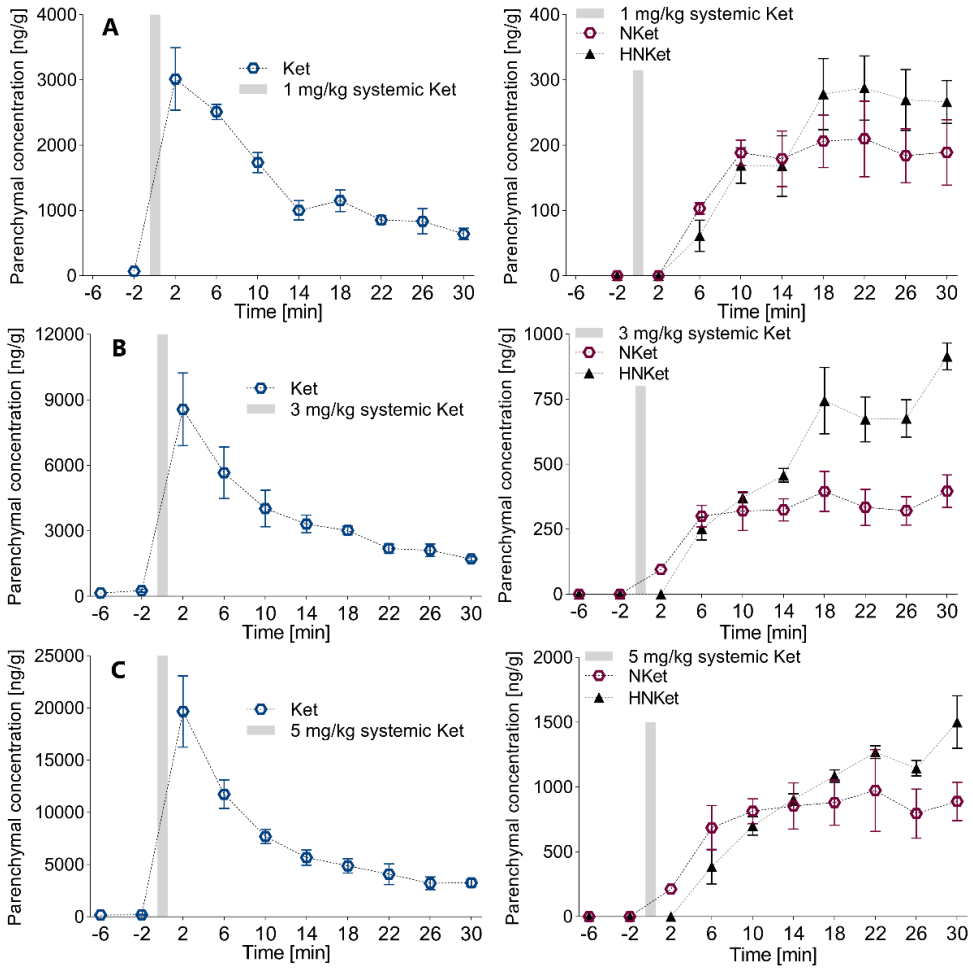

Figure 4.6: *In vivo* pharmacokinetics of ketamine (left) and its metabolites (right) in infralimbic cortex associated with systemic drug delivery after intravenous administration of 1 mg/kg (A), 3 ng/kg (B) and 5 mg/kg (C) ketamine. Each point represents average of measurements in 3 animals (*n*=3), error bars represent SEM.

The immediate next step is the application of this protocol to studying pharmacokinetics of ketamine released locally from drug-loaded nanoparticles. The next subchapter addresses the spatially resolved component of this study by the development of a protocol for *in vivo* profiling of ketamine's distribution in the infralimbic cortex.

4.3 Unidimensional quantitative *in vivo* imaging of locally released drugs in brain via SPME-DESI-MS

4.3.1 Introduction

The remarkable expanse of methodologies based on desorption electrospray ionization (DESI) in recent years is a direct emanation of the technique's unique capabilities and versatility of applications. Specifically, two operation modes representing opposite ends of the spectrum of the analytical goals prevail in the current analytical landscape: high throughput analysis and mass spectrometric imaging (MSI).

The high throughput analysis by DESI-MS found its niche in many disciplines related to drug monitoring and development,[362] forensic science,[363] doping control,[291] and reaction product monitoring.[364] Since in these applications the quantitative information if often of interest, it has been promptly recognized that as a member of the ambient ionization techniques family (AIMS), this approach is equally prone to the adverse effects of eliminating the separation step, often resulting in poor quantitative performance.[362,365] The main contributors to the subpar quantitation include severe matrix effects experienced by the analytes[362,365] as well as high LOQ attained as compared with respective LC-MS approaches due to the small desorption area.[366] While the latter is an intrinsic problem of the throughput versus sensitivity trade-off,[367] and can be partially mitigated by increasing the solvent spray plume in non-spatially resolved analysis, matrix effects can be also relatively easily limited in high throughput analysis via internal standard correction.[368] Recently, matrix effects have been alleviated via implementation of extracting techniques prior to DESI-MS analysis. Examples employing this approach include solid phase microextraction (SPME),[290,293,369] solid phase extraction (SPE),[370,371] liquid-liquid extraction (LLE),[372,373] liquid phase microextraction (LPME),[374] and thin liquid membrane extraction (TLME).[362]

The MSI branch of DESI-MS analysis has also begun to recognize the benefits of implementation of substrates for spatially resolved analysis. Reported approaches focus on the use of porous substrates such as paper, TLC plates or PTFE in order to address the signal instability issues prevalent in analysis of irregularly-shaped objects such as plants,[375,376] or to enhance the signal for certain molecules affected by suppression in direct MSI.[377] However, the predominant use of MSI in scrutinization of heterogeneous tissue samples and spatially resolved character of the investigations substantially complicates the implementation of the same strategies for essential sample clean-up and improvement of quantitative capabilities which have proven to be effective in high-throughput spot analysis.

Thus far, the reported attempts at spatially resolved quantitation via DESI-MS without sophisticated correction and signal processing methods yielded less than reliable results.[378,379] With the challenges of bypassing the strong reliance of AIMS methods utilizing the ESI mechanism on isotopically labelled internal standards analogous to the analytes of interest[380,381] some MSI methods adapt the matching labeled IS strategy to the spatially resolved conditions of complex and multidimensional data using software-heavy methodologies,[382] or inclusion of the IS in the desorption solvent.[383] While this is more suitable for targeted imaging of drugs and endogenous compounds, some untargeted approaches abandoned the labeled standards altogether in favor of utilizing endogenous molecules and regression models to correct for the effects of heterogeneity within biological microenvironments in the spatially resolved tissue analysis.[384]

Small endogenous compounds (e.g. neurotransmitters, amino acids) and drugs can very easily become suppressed in traditional DESI-MS from tissue sections due to the overwhelming abundance of ionizable molecules such as lipids,[385,386] competing for ionization efficiency and affecting the ESI droplet formation. Similar effects are exerted by the inorganic salts and molecules with quaternary ammonium moieties natively present in the tissue.[387] Moreover, the distribution maps obtained via DESI-MS can be additionally affected by the tissue density.[388] In MSI experiments these effects not

only hinder reliable quantitation but also bias the perceived analyte distribution within the tissue by the variable molecular profile of each substructure existing in the sample. Without a doubt, proper quantitative imaging of small molecules in tissue samples calls for a creative approach where some level of sample pre-treatment (so much avoided by the AIMS methodologies) may be necessary and beneficial. The gains associated with analytical performance produced by selectivity enhancement for AIMS methods tend to outweigh the extra steps required to achieve them.[389] The application of SPME in conjunction with the spatially resolved DESI-MS aims at taking the tissue heterogeneity effects out of the equation by selective analyte isolation from the sample.

The high level of customizability and range of capabilities of DESI-MS comes at the cost of an increased number of optimizable parameters, which are often interlinked and may exhibit day-to-day variability,[335] adding to the complexity of method development for DESI-MS. Introduction of a porous extractive substrate to this equation on one side further escalates this complexity and requires the underlying fundamental basis of extraction and desorption effects to be considered in conjunction with the positioning,[390] droplet dynamics,[391,335] and ionization components.[368] On the other hand, the substrate offers selectivity for the molecules of interest and an opportunity for internal standard integration to aid quantitative efforts.[343]

The MSI feature of linking the comprehensive molecular information with spatial distribution within the tissue sample is of paramount importance in neuroscience,[16,392] which endures the challenges of studying the most complex organ there is. However, the timescale of neurochemical and metabolic events oftentimes requires an *in vivo* approach to capture the state of the chemical environment multiple times during dynamic events or to record pharmacokinetic profile after drug administration using the same subject for all timepoints. The conventional MSI from tissue sections does not poses these capabilities.[16] The few examples of *in vivo* applications linking the molecular fingerprint with particular area include rapid evaporative ionization mass spectrometry (REIMS),[393] probe electrospray ionization

(PESI),[394] MassSpec Pen,[332] and DESI-based endoscopic probes,[395,396] however these methodologies are inherently surface-based or intraoperative[397] and would not be able to provide information about the spatial distribution of molecules in brain regions beneath the brain surface or subcortical regions without severe disruption to the tissue. Moreover, these techniques reconstruct the spatial distribution from a collective of discrete spot samples, rather than provide continuous imaging capabilities, and most of them was never adapted beyond the proof-of-principle stage.[397] The utilization of other AIMS techniques for *in vivo* probing without spatially resolved mode was limited to surface analysis of plants and skin.[398]

This work explores stepping back from the prevalent two-dimensional (and attempts to create a three-dimensional) molecular imaging[368] in order to gain *in vivo* capability via spatially resolved unidimensional analysis employing the previously developed SPME-DESI-MS methodology.[343] The use of extractive substrate was leveraged to obtain quantitative information about the distribution of ketamine and its metabolites after systemic and targeted administration in rats.

4.3.2 Experimental

Target analytes

Additionally to ketamine and its metabolites, the development of an *in vivo* protocol for spatially resolved analysis encompassed several more analytes with varying hydrophobicity levels (**Table 4.4**). These compounds have been previously reported and characterized *in vitro* as suitable for encapsulation and ultrasonic release from perfluorocarbon nanoemulsion.[399]

Table 4.4: Properties of drugs and pharmaceuticals targeted in this study.

Compound	Role/properties	logP*	pKa*	Physiol. Charge*	Structure*
Ketamine (Ket)	NMDA receptor antagonist; potent anesthetic effect	3.12	7.5	1	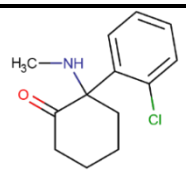
Norketamine (NKet)	Ketamine metabolite	2.22	7.27	1	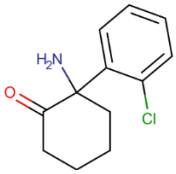
Hydroxy-norketamine (HNKet)	Ketamine metabolite	1.11	7.09	1	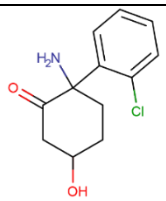
Doxorubicin (Dox)	cytotoxic anthracycline antibiotic; anticancer agent	1.27	8.94	1	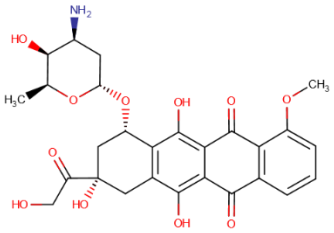
Nicardipine (Nic)	potent calcium channel blockader; antihypertensive properties	3.82	8.18	1	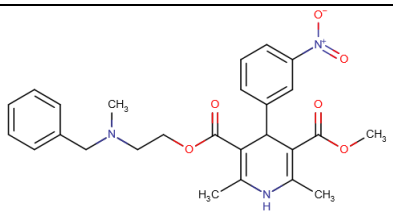
Propofol (Pro)	anesthetic effect	3.79	11.1	0	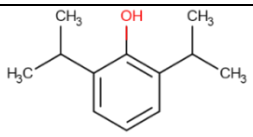

* values and structures from DrugBank (version 5.1.5)[400]; pKa values for ketamine and propofol are experimental, while pKa for the remaining compounds represent the strongest basic values estimated computationally.

LC-MS/MS analysis

Due to varying column chemistry and ionization mode requirements for the target analytes, a total of three LC-MS/MS methods were employed **(Table 4.5** and

Table 4.6) Quality control samples (20 ng/mL) as well as samples used to build the instrumental calibration curves in the range of 0.1-100 ng/mL were prepared in desorption solvent, mixture of methanol and water 90:10 (*v/v*). The concentration of the internal standards (added to the desorption solvent) was kept constant at 20 ng/mL in all samples.

Table 4.5: Details of the LC-MS/MS methods employed for quantitation of targeted compounds in positive electrospray ionization mode.

Tandem Mass Spectrometry	**Thermo Quantiva Triple Stage Quadrupole** (heated electrospray ionization source; **positive ion mode**)				
	Analytes (IS)	Ketamine (ketamine-D4) Norketamine (norketamine-D4) Hydroxynorketamine (norketamine-D4) Doxorubicin (daunorubicin)		Nicardipine (benidipine)	
	Spray voltage [kV]	3.5			
	Sheath gas [Arb]	45			
	Auxiliary gas [Arb]	13			
	Sweep gas [Arb]	1			
	Ion transfer tube temperature [°C]	342			
	Vaporizer temperature [°C]	358			
	Acquisition mode	SRM, dwell time 50 ms			
	Data acquisition and processing software	Xcalibur 4.0, Trace Finder 4.1			
	Monitored transitions	Ket	238 → 125 (Quan) 238 → 220 (Qual)		
		NKet	224 → 207 (Quan) 224 → 179 (Qual)		
		HNKet	240 → 125 (Quan) 240 → 177 (Qual)	Nicardipine	480 → 315 (Quan) 480 → 166 (Qual)
		Doxorubicin	544 → 397 (Quan) 544 → 361 (Quan)	Benidipine	506 → 174
		Ket-D4	242 → 129		
		NKet-D4	228 → 183		
		Daunorubicin	528 → 321		
Ultra High Pressure Liquid Chromatography	**Dionex UltiMate 3000 UHPLC**				
	Column	Phenomenex Kinetex PFP, 1.7 µm, 2.1 x 100 mm		Thermo Scientific Hypersil GOLD C18, 1.9 µm, 2.1 x 50 mm	
	Mobile phase A	H_2O + 0.1% FA			
	Mobile phase B	ACN + 0.1% FA			
	Flow rate [µL/min]	400			
	Column temperature [°C]	35			
	Samples temperature [°C]	5			
	Injection volume [µL]	10			
	Gradient [%B]	0 min-20%; 0.5 min-20%; 3 min-100%; 3.65 min-100%; 3.7 min-20%; 4.5min-20%		0 min-0%; 0.5 min-0%; 3min-100%; 3.65 min-100%; 3.7 min-0%; 4.5min-0%	

Table 4.6: Details of the LC-MS/MS method employed for quantitation of propofol in negative electrospray ionization mode.

Tandem Mass Spectrometry	**Waters Xevo G2-S QTof** (heated electrospray ionization source; **negative ion mode**)	
	Analytes (IS)	Propofol (propofol-D17)
	Spray voltage	-2.5
	Cone voltage	40
	Source offset	80
	Desolvation temperature [°C]	450
	Source block temperature [°C]	120
	Desolvation gas flow [L/h]	800
	Cone gas flow [L/h]	10
	Scan time	300 ms
	Mass range	150-250 m/z
	Mass calibration	0.5 mM sodium formate in the m/z range 80-400 (weekly); real-time correction with LockMass
	LockMass correction	LeuEnk MS/MS (fragment m/z: 236.1035), scan time 300 ms; interval 30 s
	Acquisition mode	Sensitivity; MS/MS (Tof MRM)
	Data acquisition and processing software	MassLynx 4.1
	Monitored transitions	Propofol 177→ 177.1287 (6V) Quan; 177→161.1006 (20V) Qual Propofol-D17 194 → 194.2335 (6V)
Ultra Performance Liquid Chromatography	**Waters Acquity I-class UPLC Plus with Flow Through Needle Sample Manager**	
	Column	Waters Acquity UPLC BEH C18 1.7 um, 2.1 x 50 mm
	Mobile phase A	H_2O
	Mobile phase B	ACN + 0.025% NH_4OH
	Flow rate [µL/min]	0.3
	Column temperature [°C]	30
	Samples temperature [°C]	5
	Injection volume [µL]	5
	Gradient [%B]	0 min-20%; 0.5 min-20%; 3.5 min-100%; 4.5 min-100%; 5 min-20%; 6 min-20%

DESI-MS/MS analysis

Space-resolved analysis was performed using the setup and experimental protocol reported previously,[343] with the addition of a triple quadrupole mass spectrometer as an alternative instrument for the analysis. This modification involved design and building of a DESI interface fitting the front-end of the Thermo TSQ Quantiva mass spectrometer followed by finding optimal positioning of the

spray head relative to the MS inlet and the SPME probe. The triple quadrupole MS was in principle expected to provide the option to analyze all target analytes within one experiment due to the capability of ionization polarity switching[401] (propofol ionizes in negative mode, while the remaining analytes are analyzed in positive ionization mode). However, the observed low ionization efficiency of propofol using the DESI setup for TSQ Quantiva and drastically different conditions required for proper desorption and ionization of this analyte led to the need for a dedicated method development. The DESI source and the MS were operated under the conditions listed in **Table 4.7**.

Table 4.7: Experimental conditions used for SPME-DESI-MS/MS.

		Xevo G2-S QTof	TSQ Quantiva
DESI source	Nebulizing gas pressure	100 psi	87 psi
	Solvent flow rate	3 µL/min	
	Spray solvent	methanol/water (95:5, v/v) + 0.1% FA + 5 ppm LeuEnk	
	Tip-to-surface height	2 mm	
	Distance inlet-sample	2 mm	
	Angle tip-sample	45°	30°
	Angle inlet	10°	0°
	Distance tip-inlet	4.5 mm	
	Fiber scanning speed	50 µm/s	
Waters Xevo G2-S QTof	Spray voltage	3.5 kV	
	Cone voltage	40 V	
	Source offset	80 V	
	Heated capillary temperature	250 ˚C	
	Source block temperature	100 ˚C	
	Acquisition mode	Sensitivity; MS/MS (Tof MRM)	
	Scan time	250 ms	
	Mass range	80-400 m/z	
	LockMass correction	LeuEnk (fragment m/z 120.0813); scan time 300 ms; interval 5 s	
	Mass calibration	0.5 mM sodium formate in MS/MS mode between 80-400 m/z (weekly); real-time correction with LockMass (LeuEnk included in desorption solvent)	
Thermo TSQ Quantiva	Spray voltage	5 mm probes: 3.5 kV (0min- 0kV; 0.2min- 3.5kV; 1.3min- 0kV) 15 mm probes: 3.5 kV (0min- 0kV; 0.2min- 3.5kV; 4min- 0kV)	
	Ion transfer tube temperature [°C]	325	
	Acquisition mode	SRM	
	Dwell time	40 ms	
	Acquisition window	0.3- 1.1 min	

Spatially resolved quantitation of target analytes in brain tissue

The same protocol for surrogate matrix-matched calibration as in the case of LC-MS/MS analysis was employed, with the exception of the analytical response consisting of ratio of the analyte signal intensity to its corresponding IS signal intensity, calculated scan by scan (according to the quantitation workflow described in Chapter 3).[343] Briefly, quantitation was performed by averaging and plotting the ratios of all scans collected from a given calibrator sample against the concentration of the calibrator. For unknown samples the obtained calibration curve equation was applied to each scan acquired across the probe. The resulting concentration was plotted as a function of fiber length. Limits of quantitation were defined in the same way as in the case of LC-MS/MS analysis.

Probe geometry vs. extraction kinetics

The surrogate matrix was spiked with analytes at the following concentration levels: 1 µg/g of ketamine and its metabolites, 1.5 µg/g of propofol and nicardipine, 5 µg/g of doxorubicin. 5 replicate extractions were performed in static mode from 1 g of spiked matrix with extraction times ranging from 1 min to 60 min. 5 types of probes were used, characterized by various geometries and coating thickness: ***flat***- wire with rectangular cross-section and dimensions of 100 x 200 µm coated with thin layer of extracting phase; ***thin core***- round wire with 100 µm diameter and 10 µm coating thickness; ***thin***- 200 µm wire with 10 µm coating thickness; ***mid***- 200 µm wire with 25 µm coating thickness; ***thick***- 200 µm wire with 50 µm coating thickness. SPME probes were rinsed, wiped and desorbed into 60 µL of methanol/water 90:10 containing internal standards at 20 ng/mL. The extracts were analyzed by LC-MS/MS methods summarized in **Table 4.5** and

Table 4.6.

Probe geometry vs. desorption efficiency

Surrogate matrix calibration curves for ketamine and norketamine were prepared in the range 10-2000 ng/g. 4 replicate 4-minute extractions were performed in static mode with three sets of probes (both having the coating length of 5 mm): the *thin*, *mid*, and *thick* variants, described above. All probes were preloaded with IS spiked into 300 µL of water at 500 ng/mL overnight in static mode. Probes were analyzed by DESI-MS according to the workflow, parameters, and LOQs determination described above.

IS incorporation into the extracting phase for *in vivo* measurements by SPME-DESI-MS/MS

The PAN-DMF-HLB suspension was spiked with IS (ketamine-D4, norketamine-D4, daunorubicin, and propofol-D17) dissolved in DMF to yield 50 µg/mL in the extracting phase suspension. It was then used to manufacture probes with 5 mm long and ≈10 µm thick coating. A set of probes with identical dimensions was made with extracting phase not containing IS. This set of probes was pre-loaded with IS by 15 min static extraction from 300 µL of water containing the IS at 1 µg/mL. Desorption of IS into the tissue potentially occurring during extraction was evaluated using both sets of probes and three conditions: 1) immediate desorption into 60 µL of desorption solvent containing 20 ng/mL of respective analytes (for reverse quantitation of the amount of IS preloaded)- baseline; 2) 4 min immersion into blank surrogate matrix in static conditions; 3) 4 mm immersion into blank surrogate matrix placed in ultrasonic bath at the frequency of 35 kHz.

Desorption solvent selection for SPME-DESI-MS/MS

The *mid* variant of probes (25 µm coating thickness) was used, with IS incorporated into the extracting phase suspension. The 4-minute extraction was performed from surrogate matrix spiked with ketamine and its metabolites, and nicardipine at 500 ng/g and 1250 ng/g, respectively. Probes were analyzed by DESI-MS/MS, using 7 solvent combinations detailed in **Figure 4.8**. The criteria of choice of the optimal desorption solvent were the signal intensity ratio (analyte/IS) averaged across each probe and its variability across 4 replicate measurements as well as the variability of the intensity ratios within a single probe, on a scan-to-scan basis (**Figure 4.7**). Any solvent combination resulting in any of the investigated variabilities above 25% RSD was discarded from further consideration.

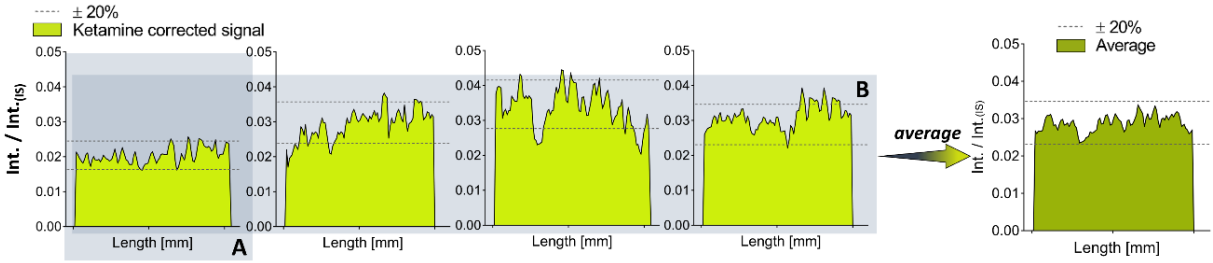

Figure 4.7: Schematic depiction of the signal processing and averaging for spatially resolved analysis of samples without heterogeneous distribution of analytes (test samples or calibrators). The signal reproducibility criteria include **A)** variability of the intensity ratio across each probe and **B)** %RSD of average corrected signal from 4 replicate probes.

Stability of spatial imprint during storage

The surrogate brain matrix was arranged in two sets of layer configurations (each layer was 5 mm thick) spiked with analytes at different concentrations in each layer. For investigation of the band broadening the center layer at 1000 ng/g was surrounded by two blank layers. For investigation of concentration averaging, two neighboring layers were spiked at 500 and 1000 ng/g, respectively. 15 cm coated probe preloaded with IS was inserted through all layers for 4 min exposure time and immediately analyzed by DESI-MS/MS (baseline samples). Several sets of probes extracted at the same time in identical conditions were kept in -80°C freezer and in ambient temperature to be analyzed after 1, 3, 7 and 15 days to investigate possible changes in the imprint during storage.

4.3.3 Results and discussion

The prerequisites and fundamental investigations for an optimal quantitative protocol

DESI solvent optimization

Along with the positioning of the DESI interface components respective to one another, the composition of the desorption spray solvent in one of the most important optimizable parameters during the DESI method development, affecting signal intensity and stability.[402] While the intricate relations between the solvent properties and quality of the obtained molecular information have been extensively

discussed elsewhere,[303,403,402] the presence of extractive substrate in SPME-DESI brings additional requirements to be met by the desorption solvent. For instance, any solvents threatening the integrity of the PAN binder, such as the histologically compatible solvent containing DMF used for DESI imaging of tissue sections[404] will not be suitable (DMF dissolves the binder leading to the probe coating disintegration). Wettability is another important aspect to consider in conjunction with the highly porous structure of the SPME coating. It affects all aspects of DESI process by influencing the desorption kinetics and efficiency related to the penetration into the substrate pores, as well as contributes to the ionization by participating in the charge-transfer phenomena.[405]

The desorption solvent for SPME-DESI has not been previously optimized, as the solvent composition followed the legacy of other SPME-MS methods which determined that mostly methanolic solution with 5% water and 0.1% formic acid provides superior signal stability. Moreover, the employed Oasis HLB extracting phase exhibits excellent wettability even in fully aqueous conditions.[406] In this study, the spray solvent fine-tuning was attempted to boost the method's performance for hydroxynorketamine, characterized by relatively high hydrophilicity (logP 1.1) and therefore high LOQ values attained by SPME-DESI-MS/MS. We set out to examine if there exists an acceptable trade-off between the signal intensity and stability when increasing the aqueous content of the spray solvent, which in principle should benefit the desorption of more hydrophilic analyte. Several binary and tertiary solvent compositions were tested, as showed in **Figure 4.8**. The spray solvent optimization process was of no avail, which would perhaps be expected based on the results of a study decoupling the desorption and ionization components of DESI,[407] concluding that the compromise between the optimal conditions satisfying the desorption and ionization is imminent (as well as surface- and analyte-dependent). In this case, the increased viscosity and aqueous character of tested solvents contributing to the deterioration of ionization stability[408] and to the unfavorable droplet dynamics[409]

clearly outweighed the assumed benefit of increased aqueous content on the desorption of hydrophilic analyte.

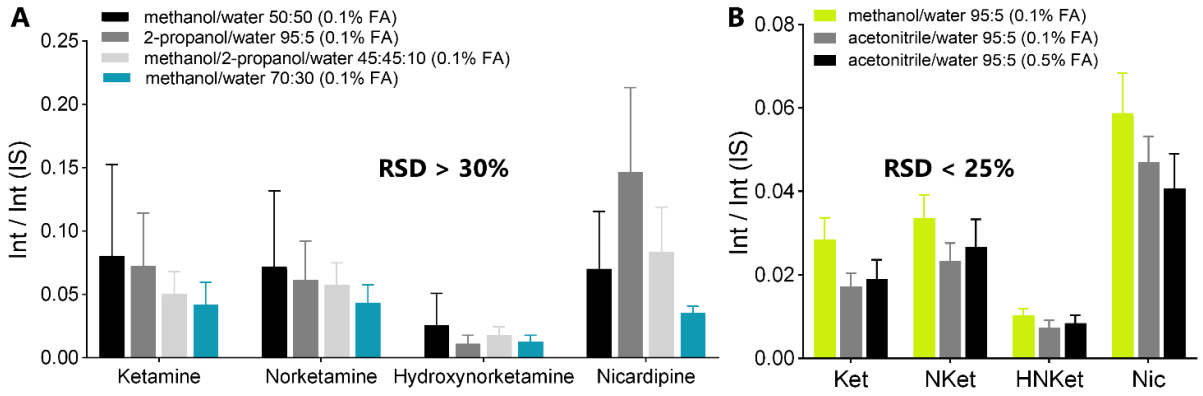

Figure 4.8: Selection of optimal solvent for SPME-DESI-MS/MS. The criteria of choice were the signal intensity ratio (analyte/IS) averaged across each probe and its variability across 4 replicate measurements as well as the variability of the intensity ratios within a single probe, on a scan-to-scan basis. Any solvent combination resulting in any of the investigated variabilities above 25% RSD was discarded from further consideration. The mixture of methanol and water in volumetric ratio 95:5 with 0.1% formic acid was ultimately selected.

Considering that the efforts to improve the signal intensity and quantitative accuracy for relatively hydrophilic analytes by SPME-DESI-MS, including the desorption solvent composition and pre-wetting strategy (discussed in subchapter 3.3), have so far been futile, modifying the extracting phase chemistry remains the last strategy to be explored in future studies.

Extraction kinetics dependence on the probe geometry and coating thickness

The flux of analyte towards the microextraction device is inversely related to the diameter of the probe, resulting in generally quicker arrival to equilibrium of thinner devices. This trend is also shape-dependent, as cylindrical probes tend to be slower than their flat equivalents. However, this relation becomes independent of the probe geometry for any device exceeding 30 µm.[410] In the real world of SPME devices that can be realistically manufactured on minimum 100 µm diameter support, the equilibration time becomes a domain of the coating thickness, while analyte properties and presence of binding matrix add to the complexity of this aspect, the latter being relatively unexplored and

challenging in case of tissue sampling. In the complex case of tissue analysis when mass transfer still remains the limiting factor, it is the binding matrix presence that enables accelerated arrival to equilibrium with small amounts of analyte extracted, rather than the increased rate of extraction for thinner coatings.[58] Extraction time profiles for five types of devices differing by shape, core diameter or coating thickness were evaluated as a first step in selecting the optimal probe for spatially resolved analysis in brain (**Figure 4.9**), from the perspective of the extraction efficiency.

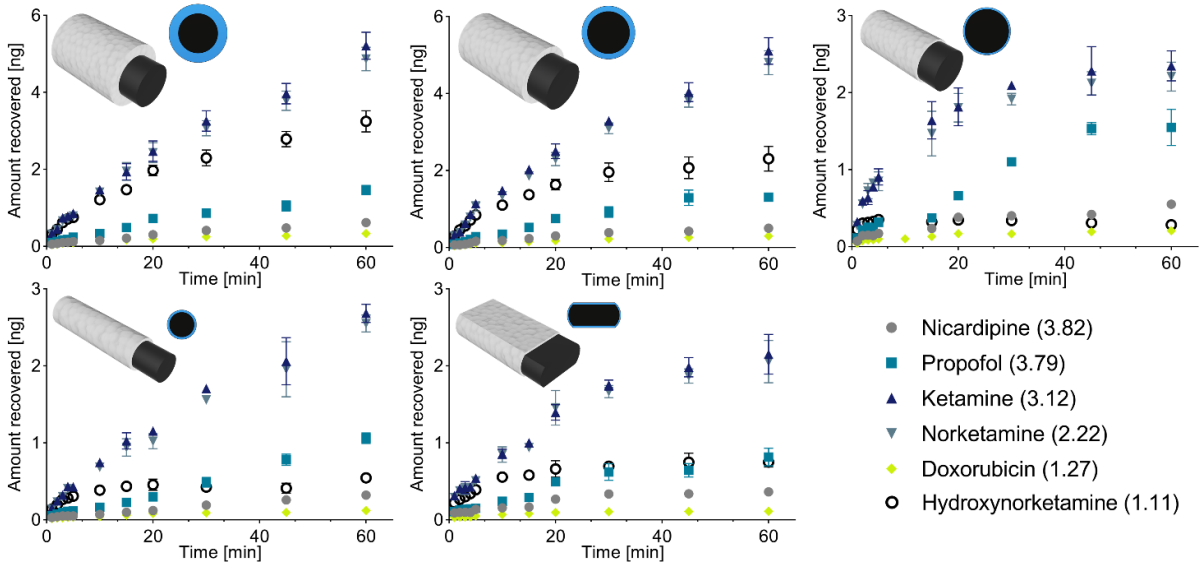

Figure 4.9: Extraction time profiles for 5 tested probe types used as a preliminary criterion for optimal probe choice. The three probes based on 200 µm cylindrical support follow the anticipated trend of faster equilibration with decreasing coating thickness. The two non-standard types based on flat support or 100 µm cylindrical core seem to deviate from the expected trend, requiring longer time to equilibrium despite the thin coating. It is very likely to be attributed to the unexplored mass transfer phenomena occurring in tissue. LogP values for the analytes are given in brackets in the legend.

In this work, all choices were guided predominantly by practicality of a given approach as the very clearly defined goal of measuring the zone of drug release in brain *in vivo* promotes fit-for-purpose solutions rather than competitive figures of merit, which are the domain of proof-of-concept studies. Therefore, the choice of the extraction time for *in vivo* experiments was not guided by the SPME time profiles. The 4 min sampling time was pre-determined as suitable for capturing pharmacokinetics of

ketamine and its metabolites *in vivo* in brain with sufficient temporal resolution as well as being compatible with the protocol for local drug release by ultrasonic uncaging established before.

Plotting of the extraction time profiles for each analyte separately and respective to the probe geometry (**Figure 4.10**) allowed for detailed investigation of how the probe and analyte properties interact in various regimes of the SPME kinetics.

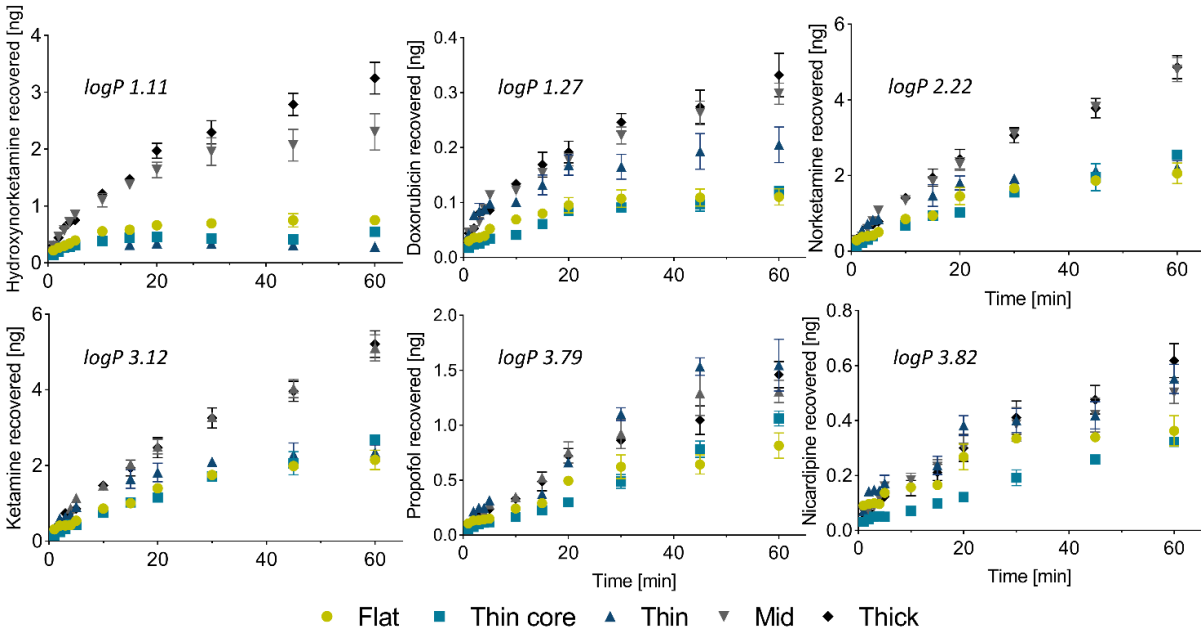

Figure 4.10: Probe geometry and coating thickness versus extraction kinetics shown for each target compound. In the tested conditions the kinetics slows down with increasing hydrophobicity of the compound, indicating that even for very thin coatings equilibrium is not reached within 60 min for any analyte characterized with logP above 2.

Focusing only on the selected 4 min extraction time (**Figure 4.11**) indicates that for all target analytes except the most hydrophilic one (hydroxynorketamine) there was no significant difference between the amounts extracted by 10, 25 or 50 µm thick coating deposited on a standard cylindrical support. The two probe types employing *flat* or *thin core* support were excluded from further investigations due to the fact the thin wire did not provide robust enough support to withstand the conditions of SPME-DESI-MS/MS, involving highly dynamic solvent plume and gas blow.

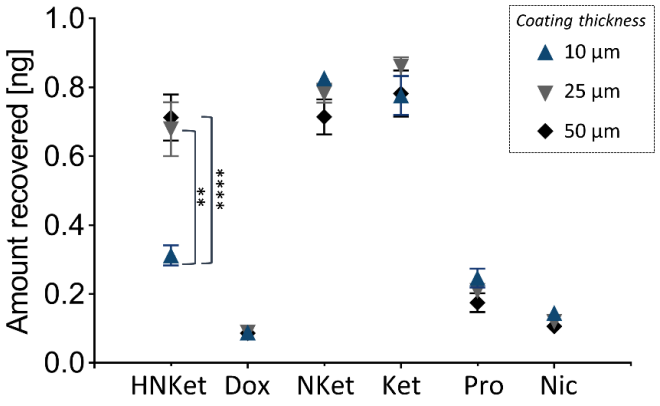

Figure 4.11: Amounts of analytes extracted from surrogate brain matrix within 4 min as a function of coating thickness. Only in case of hydroxynorketamine there was a significant difference between amounts extracted by the thin coating (10 µm) compared to the thicker coatings (**- p<0.001; ****- P<0.0001; two-tailed unpaired t-test).

Based on these results it becomes apparent that the ultimate probe characteristic choice must be guided by the limiting factor of SPME-DESI approach, namely the desorption efficiency.

Desorption efficiency and quantitation capability via SPME-DESI-MS/MS depend on coating thickness

The high level of preconcentration of the analytes associated with the SPME phase remains unmatched by the efficiency of DESI. This is made evident by the fact that multiple DESI runs from the same probe result in carryover signal, which may reach substantial intensity when operating in higher concentration range. Moreover, desorption only occurs from one side of the probe meaning that half (or more, depending on the DESI spot size and probe's circumference) of the analyte pool is unutilized.

We therefore hypothesized that use of the thinnest coatings (10-15 µm) should be beneficial for attainment of quantitative results. This was tested by evaluating quantitative figures of merit for the 3 remaining compared probe geometries. The practical aspect of SPME-DESI analysis instantly excluded the *flat* and *thin core* geometries, as the lack of robustness of the thin support deemed them too feeble to provide stable and reproducible signal without substantially customizing the probe holder, sprayer

nozzle positioning and DESI parameters. Moreover, these geometries would not be suitable for unsheathed insertion into the brain, hence they were discarded from further consideration. Out of the three remaining geometries evaluated by construction of surrogate matrix calibration curves for ketamine and norketamine in the range10-2000 ng/g, only the *thin* variant was suitable for quantitation (**Figure 4.12A**). Analysis of the *mid* thickness probes resulted in poor linearity and high variability across 5 replicate measurements (**Figure 4.12B**), while thicker coating was not suitable for quantitation, additionally attaining unsuitably high limits of detection.

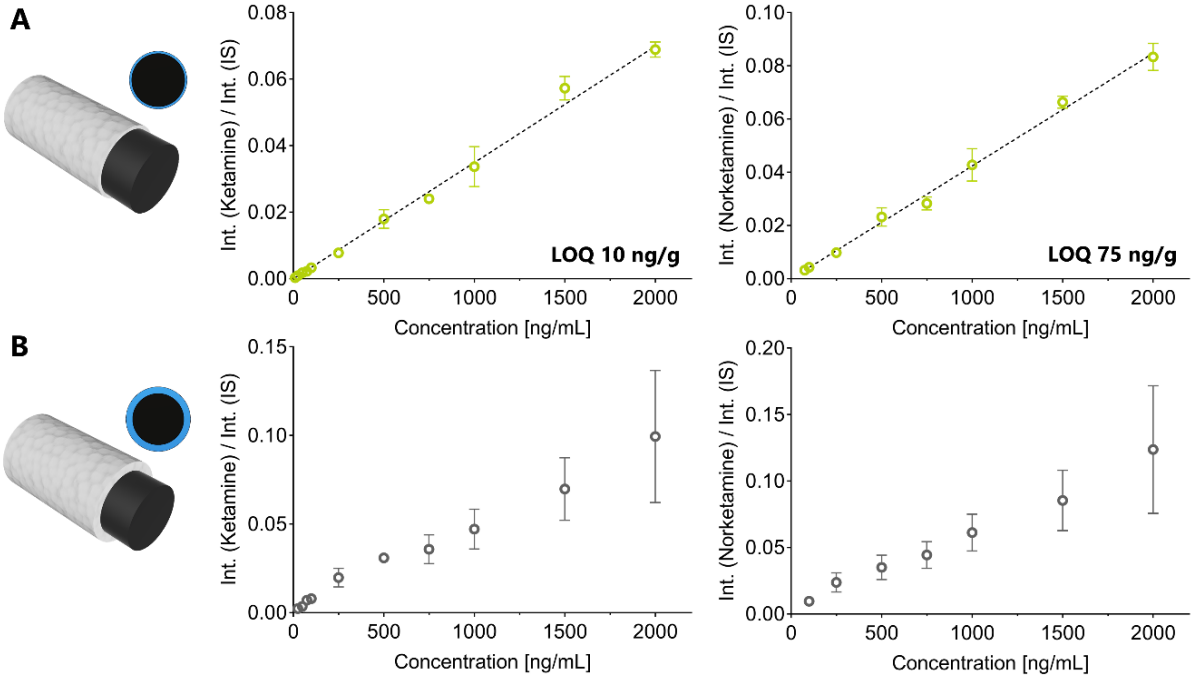

Figure 4.12: Calibration plots for ketamine and norketamine extracted from surrogate brain matrix by *thin* probes (A; coating thickness 10 μm) and *mid* probes (B; coating thickness 25 μm). Quantitation was possible only in case of the thinly coated probes.

These findings reveal the secondary to the improved extraction kinetics implication of thin film SPME (TFME) in its capability to facilitate rapid and efficient desorption. TFME traditionally refers to devices characterized by increased size capable of accommodating larger volume of extracting phase, often leading to depletive extraction and faster extraction kinetics favorable for rapid sampling.[146]

While this geometry is often employed to attain lower LOD and LOQ values due to larger amounts of adsorbed analyte, the desorption process is rarely of concern, as it is generally conducted in bulk mode (desorption of the whole device into the solvent or thermal desorption) and therefore it is invariably exhaustive.[411] However, the by-product of thin extracting phase is also faster desorption kinetics, which only becomes noticeable and important in case of micro-desorption phenomena accompanying the DESI process. A thicker extracting phase causes effects similar to that of peak broadening in chromatography in the instance of insufficiently fast mass transfer (**Figure 4.13**). Even though increased desorption solvent flow rate could potentially contribute to better quantitative capabilities attained with thicker SPME coatings, this would in turn also increase the spot size and decrease the spatial resolution.

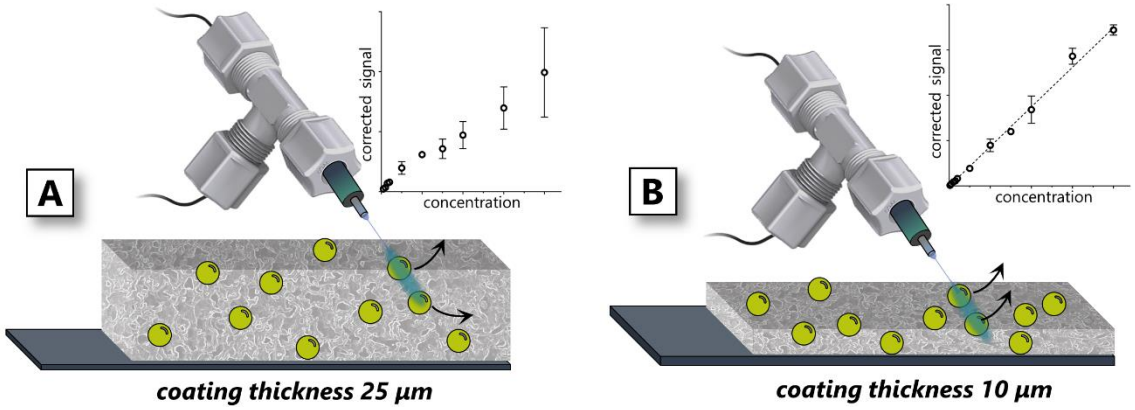

Figure 4.13: Schematic depiction of the effect of extracting phase thickness on desorption efficiency via DESI mechanism. **A)** Relatively thick SPME coating gives the opportunity for the analytes to diffuse into areas less accessible for penetration by DESI solvent or become relocated within the coating upon wetting by the desorption solvent. **B)** Thin coating ensures higher level of accessibility to the analytes by the desorption solvent contributing to attaining linear relationship between the amount of analyte desorbed and its concentration in the sample and better overall quantitative figures of merit.

It is also noteworthy that the extent of quantitative improvement achieved by employing the thinnest possible SPME coating depends on the character of the analyte and its interaction with the extracting phase, as the 25 µm thickness suitable for various analytes in the previous work[343] (Chapter 3) was sub-optimal for ketamines, as demonstrated on **Figure 4.12**. Nevertheless, the 10 µm thickness of the

extracting phase was selected for all subsequent SPME-DESI-MS investigations involving ketamines and other model compounds, due to the dual benefit of improved desorption efficiency and reduction of the overall size of the device intended for *in vivo* sampling.

The microdroplet-based mechanism of DESI is the primary reason for both the difficulties and advantages of employing an extractive substrate in conjunction with this technique. The reliance of this mechanism on formation of secondary droplets upon the electrospray impacting the sample surface determines a set of favorable conditions and substrate properties for maximum efficiency and signal stability achieved in this process.[412] Those properties include minimal conductivity, uniformity, rigidity, and smoothness, while porous and adsorptive character of the substrate is expected to cause elution of the analytes within the substrate at higher desorption solvent flow rates rather than their effective desorption and mobilization towards the MS inlet.[413] The conclusion from this simplified summary is that the SPME properties facilitating high level of analyte preconcentration also constitute a hindrance for desorption via DESI mechanism. However, in practice porous and rough surfaces have been proven to enhance DESI signal by limiting the area of sample spreading upon impact of the spray solvent plume. This led to the appreciation of certain level of porosity in DESI substrate for analysis of small molecules,[414,415] provided that a suitable strategy of correction for resulting signal instabilities and positioning challenges has been established. Nevertheless, the vast majority of these investigations perceive the substrate merely as a sample *carrier*, without exploring the possibilities of integrated analyte isolation properties.

IS incorporated into the extracting phase suspension is suitable for *in vivo* measurements by SPME-DESI-MS/MS

Quantitation by SPME-DESI-MS (and DESI-MS and other imaging methodologies in general) relies very strongly on signal correction by deuterated isotopologues that can alleviate the effects of

sample heterogeneity and local matrix effects,[416,382] as well as coating morphology in case when SPME phase is used as a substrate.[343] In fact, it is impossible to accurately observe concentration heterogeneity in the sample across the SPME probe when considering only the raw, uncorrected signal of the analyte (**Figure 4.14**). We have previously reported IS preloading on the SPME probe and subsequent scan-by-scan correction as a suitable strategy for quantitation via SPME-DESI-MS/MS. However, when the concentration of a neuromodulating drug is measured locally *in vivo* in brain area functionally related to the site at which the effect of this modulation is being simultaneously observed, desorption of the isotopically labeled modulating agent from the pre-loaded probe can potentially contribute to the observed effect. We have therefore investigated an alternative strategy of IS preloading devoid of *in vivo* desorption side-effects based on preloading of the IS at the stage of probe manufacturing rather than preloading by the SPME process.

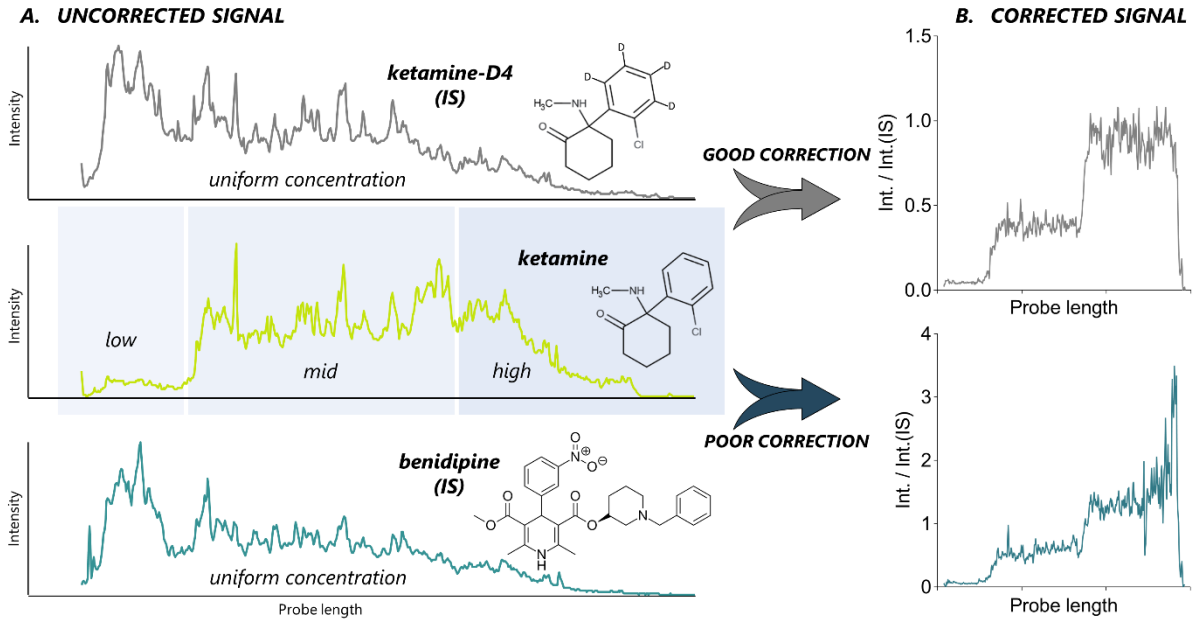

Figure 4.14: Demonstration of the strong reliance of space resolved profiling via SPME-DESI-MS on correction with well-matched internal standard. **A)** Raw signal obtained for ketamine and two internal standards ketamine-D4 and benidipine across 15 mm SPME probe. Three distinct layer-specific concentration levels of ketamine (*low*, *mid*, and *high*) were present in the sample, while the internal standards were homogeneously incorporated into the extracting phase. **B)** Ketamine signal corrected with its corresponding isotopologue ketamine-D4 (top) or structurally unrelated benidipine (bottom). Only the case of well-matched IS results in accurate representation of the laminar gradient of ketamine present in the sample.

Incorporating the IS into the extracting phase suspension resulted in retainment of the preloaded amount after 4 min static extraction as well as 4 min extraction with ultrasound, while probes preloaded with IS from spiked solution (with the exception of benidipine- IS for nicardipine) desorbed significant amounts of their cargo into the tissue in both cases (**Figure 4.15**). Interestingly, upon desorption into solvent IS was exhaustively removed from both variants of preloaded probes without significant carry-over (note, this was tested via whole-probe solvent desorption followed by LC-MS/MS analysis). It is suspected that the stronger association of the IS with the SPME coating is due to different mechanisms of its incorporation into the extracting phase (IS being built into the structure of the coating rather than reversibly adsorbed via the SPME process) indicated by drastically different recoveries of the IS (1% recovered from spiked solution versus 0.001-0.003% built into the probe from particles suspension), however further assessments are yet to investigate this in more depth.

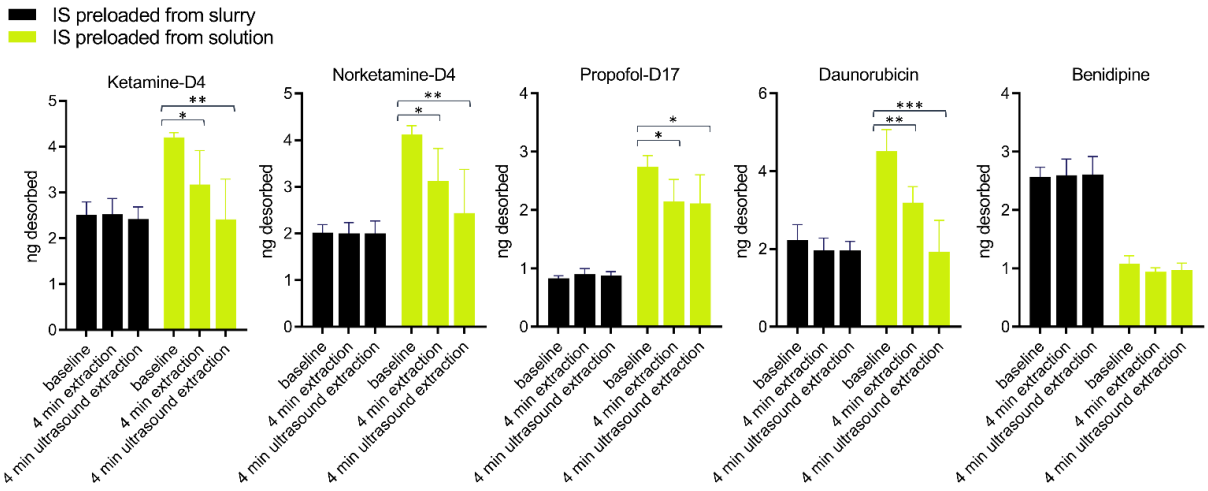

Figure 4.15: Comparison of desorption (or lack of thereof) of the internal standards preloaded onto the SPME probe from spiked solution or spiked particle suspension into the surrogate brain tissue. Two tested sets of conditions included 4 min static extraction and 4 min extraction with ultrasound application. *- $p<0.05$; **- $p<0.01$; ***- $P<0.001$; one-tailed unpaired t-test.

The physicochemical properties of the IS are also expected to be a contributing factor to this mechanism, as benidipine did not follow the trend of other analytes and was strongly associated with

the extracting phase regardless of the preloading strategy (the most distinct differentiating feature of this analyte is the presence of a charged nitro group in its structure).

This approach is nevertheless suitable for implementation *in vivo* as well as compatible with DESI-MS, as despite the lack of desorption into the tissue the IS could be desorbed by the solvent spray with an efficiency ensuring a signal well above the LOQ. This strategy for IS preloading was implemented in the subsequent experiments, including the spatial imprint stability study as well as the *in vivo* trials.

Stability of spatial imprint during storage

Due to the distance between the laboratories collaborating in this study, storage and transportation of the samples were involved between the *in vivo* sampling and instrumental analysis. As discussed above, ketamine and its metabolites in samples destined for LC-MS/MS analysis were stable up to 15 days in cold storage or up to 4 days at room temperature. However, the bulk desorption of the entire extracting phase into the solvent only pertains to the average concentration across the SPME probe. Reliable spatially-resolved analysis requires preserving the original distribution of the chemicals in the sample, which in case of SPME-DESI means retaining the amounts and *positions* of molecules imprinted into the extracting phase at the time of *in vivo* sampling. The hypothesis that there is no significant "shift" of analytes within the coating during short-term storage has its theoretical basis in two-dimensional LC with stop-flow mode, where analytes associated with the stationary phase do not diffuse laterally, thus no band broadening is observed.[417] Even the presence of mobile phase during the stop-flow event does not contribute to the lack of broadening, as only small portion of analyte pool is present in the mobile phase at that time. In the absence of any mobile phase in case of storage of the SPME probes we anticipated the imprint distortions to only become significant in room temperature after many days.

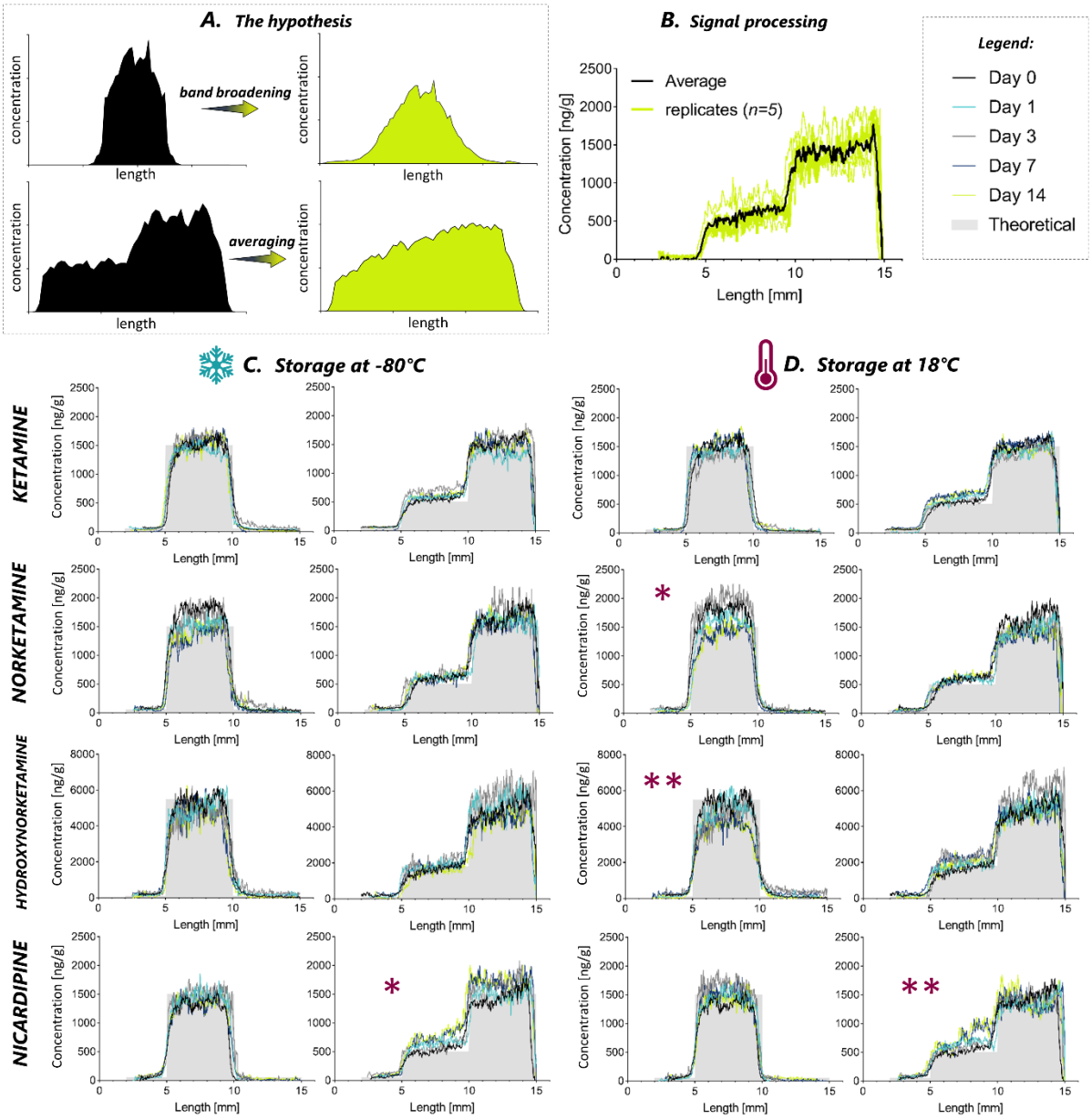

Figure 4.16: Stability of spatial imprint of the SPME probe during storage tested via DESI-MS/MS. **A)** Hypothesized effects potentially leading to imprint distortions during SPME probe storage. **B)** The employed strategy of combining multiple spatial profiles by scan-by-scan averaging of replicate measurements. **C)** Stability of target analytes in low-temperature storage over the course of 14 days. **D)** Stability of target analytes in ambient temperature storage over the course of 14 days. *- examples of visible but rather mild imprint distortions; **- examples of significant imprint distortions.

Two models of potential imprint distortions were investigated: band broadening and concentration averaging (**Figure 4.16A**). Due to the possible day-to-day variability of response of both the DESI and

the MS, the stability was tested in terms of the concentration of analytes determined on a particular day, with the matrix-matched calibration curve prepared on each of those days. Due to the presence of heterogeneous distribution of the analytes in the samples, the averaging of replicate measurements was carried out in scan-by-scan fashion (**Figure 4.16B**).

The two tested configurations were designed to reflect the patterns that could be hypothetically observed after local drug release in brain. The configuration with two distinct levels of concentration followed by a blank area reflects the situation in which a clear border of the drug release is defined on the bottom and there exists a distinctly different uptake of the drug by two neighboring cortical layers. The configuration with only one distinct layer of measurable analyte concentration represents an idealized situation of spatially constricted local drug release with clearly defined borders. In this case the stability test and its outcome are particularly informative – if the determined *in vivo* area of drug release has less defined borders and resembles the peak shape with a clear maximum, this can be attributed solely to the factual shape of the release zone rather than the effect of band broadening occurrence, as all analytes demonstrated high level of stability of this configuration in the cold storage.

Generally, no imprint distortions were observed in either configuration when the probes were stored in a freezer, with the exception of nicardipine showing mild averaging after 7 days of storage. The absence of a visible pattern amongst the cases where both mild and significant distortions were detected suggests that the potential deterioration of the imprinted spatial distribution occurs when certain combination of factors is fulfilled, including the analyte properties, and the direction/shape of the heterogeneous distribution.

In vivo quantitation of ketamine in brain via SPME-DESI-MS/MS followed by confirmation by LC-MS/MS after systemic drug administration

Challenging novel strategies by cross-validation against the existing and proven approaches is a very important way of reality-checking and obtaining insight into the method's limitations. Oftentimes, the proof-of principle oriented applications of AIMS tend to define their own internal criteria for acceptance of quantitative results, as this field lacks stringent and agreed upon regulations, which are in place for hyphenated separation techniques.[368] Therefore, cross-validation with LC-MS methodology should accompany the claimed-to-be quantitative AIMS approaches, whenever possible.[386] In reality, the SPME-DESI and SPME-LC methodologies would never be used competitively for the same purpose, with the former aiming to provide continuous spatially resolved information from a single probe and the latter not having such capabilities. However, the fact that the SPME device can be coupled to both instrumental modes provided the opportunity to cross-check these two approaches via sequential analysis of the same set of probes by DESI-MS/MS first, followed by LC-MS/MS (**Figure 4.17**). This experiment also documents the first trial of spatially resolved *in vivo* analysis by SPME-DESI-MS/MS. Since the sampling was performed after systemic administration of ketamine, the expected outcome was uniform concentration of the drug in the sampled area, suitable for comparing the average concentrations imprinted across the SPME probe.

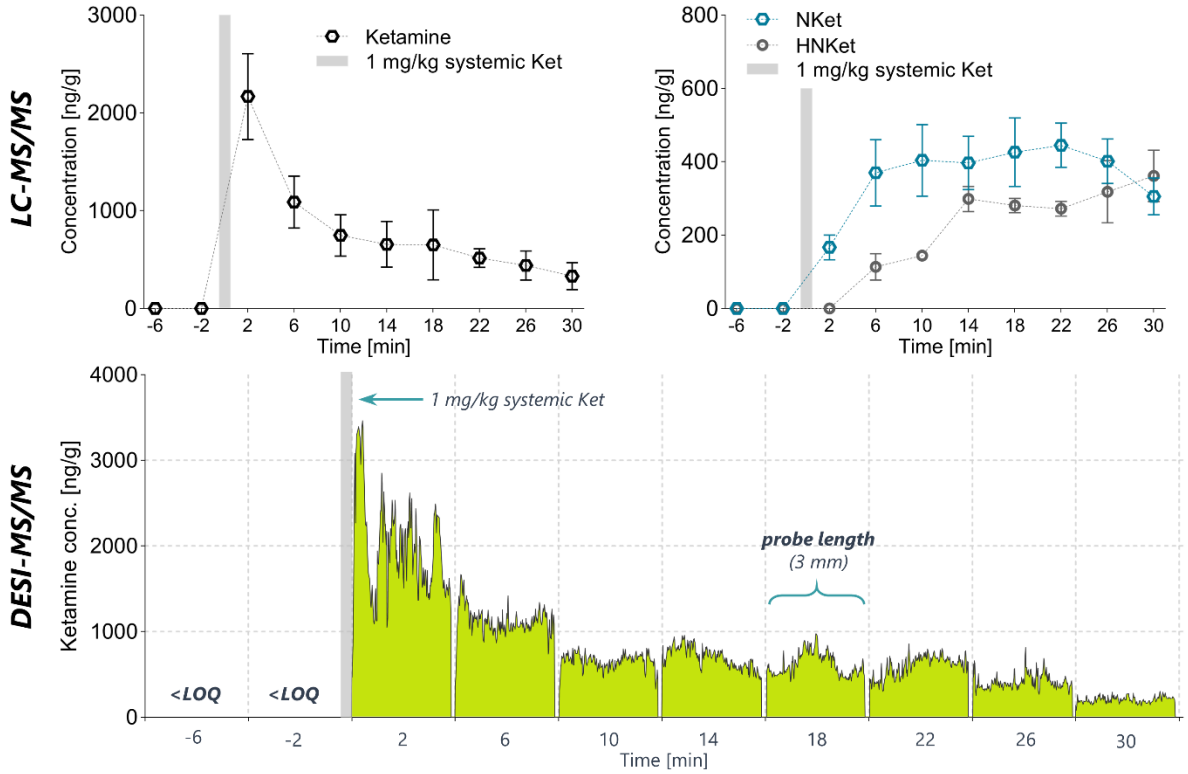

Figure 4.17: Summary of the comparison between performance of the developed *in vivo* SPME-DESI protocol and solvent desorption followed by LC-MS/MS analysis. The pharmacokinetic profiles of ketamine extracted from brain *in vivo* after systemic 1 mg/kg administration represent average of three animals with error bars illustrating standard error of mean (LC-MS/MS) and profiles of spatial distribution averages scan-by-scan (DESI-MS/MS).

Obtained pharmacokinetic profiles of ketamine in brain summarize the performance of the developed protocol very well by illustrating that at the current stage the SPME-DESI-MS/MS approach demonstrates good quantitative performance and the advantage of providing spatially resolved information, while it suffers from difficulties related to sensitivity by not being able to detect metabolites of ketamine at levels resulting from 1 mg/kg dose, which are clearly detectable and quantifiable via LC-MS/MS. Interestingly, norketamine was previously quantified in surrogate brain samples with the LOQ of 75 ng/g, therefore the reason for the lack of detection of this metabolite in the *in vivo* samples by DESI-MS/MS will be a point of future investigation. Nevertheless, an excellent agreement of the DESI-MS/MS and LC-MS/MS data was achieved for ketamine (**Figure 4.18**) at all

time points of the pharmacokinetic profile. These findings give confidence that the protocol for spatially resolved analysis will be capable of providing quantitative information about the heterogeneous distribution of the drug in brain following its local release in the future.

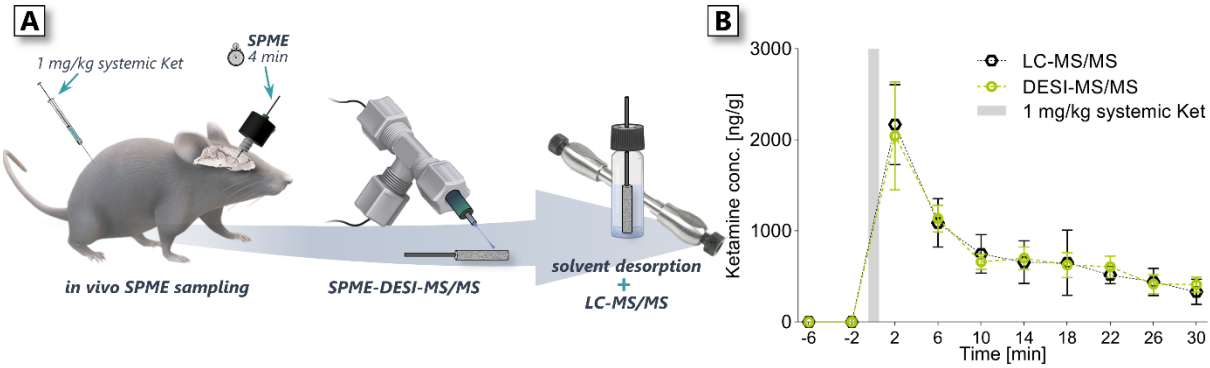

Figure 4.18: *In vivo* SPME brain sampling (*n=3*) followed by spatially resolved DESI-MS/MS analysis followed by solvent desorption and LC-MS/MS analysis using the same probe **(A)**. The negligible analyte desorption via DESI and good quantitative properties of the method were confirmed via the LC-MS/MS analysis **(B)**.

The good quantitative agreement between the two techniques also indicates the lack of matrix effects affecting ketamine and related to elimination of the separation step in DESI-MS/MS. While this illustrates an example of a benefit of a well-matched pairing between the analyte and the IS, future experiments will focus on performing similar comparisons for analytes without an isotopically labeled IS available (hydroxynorketamine and nicardipine) in order to further assess the practicality of the demonstrated approach.

Inherent to the SPME-DESI approach utilizing the probe geometry, unidimensionality is the trade-off for the ability to access non-surface brain structures without collecting the sample. MS-based imaging of additional dimension comes at the price of tissue slicing and loss of *in vivo* analysis capability[392] or alternatively conserving the *in vivo* feature while only having access to the superficial areas of exposed tissue.[418] Employment of SPME probes in this case also afforded elimination of tissue

excision for confirmatory analysis by LC-MS/MS due to the *in vivo* sampling capabilities extended to less superficially located brain areas.

4.4 Summary and immediate future directions

Understanding the mechanism of ketamine's antidepressant efficacy in the medial prefrontal cortex and inferring the roles of other, functionally related brain regions that participate in response to these effects requires localized drug delivery. Ketamine's influence on multiple domains of brain functioning has been extensively studied, however interpretation its cortical effects remains challenging due to the fact that the predominantly employed neuroimaging methods reported surrogate measures of an outcome rather than direct measurements.[349] Establishing a protocol for local delivery and release of ketamine in reproducible way and with full control over dosage is a prerequisite for advancement towards answering the complex questions about brain's response to the neuromodulation by this drug with the eventual clinical translation as a long-term goal.

Ultrasonic uncaging of pharmacological agents in brain presents itself as an innovative way of targeting neurons in select brain regions in pursuit of gaining insights into modulation of neural circuits. Behavioral approaches and electrophysiological recordings are aiding diagnostic tools for assessment of secondary changes in brain areas functionally interlinked with the pharmacologically stimulated target area. Our proposed approach to obtaining quantitative chemical information in a non-disruptive way adds a formerly missing puzzle piece, allowing for characterization of the focal drug release *in vivo*, which constitutes an unprecedented advantage as characterization by *in vitro* assays might not necessarily reliably reflect the release in *in vivo* conditions.[419]

The prospect for monitoring of pharmacokinetics of ketamine associated with local delivery via ultrasound uncaging

Currently, the three outcomes of systemic ketamine administration at different dose levels are being experimentally matched by three sets of ultrasound uncaging parameters, employing the developed measurement protocol and the experimental timeline depicted in **Figure 4.3C**. While the preliminary phase attempted finding the initial set of ultrasound conditions (e.g. sonication burst lengths) *in vitro* in PBS solution, it became apparent that the *in vitro* conditions do not provide appropriate environment to create a representative sink for ketamine and reflect its free concentration in brain, therefore further investigations are being completed and fine-tuned *in vivo*. The final protocol will yield a local drug delivery strategy with control over and knowledge of the parenchymal concentration of ketamine as well as its pharmacokinetic profile in the infralimbic region of the mPFC following ultrasonic uncaging. Further neurochemical monitoring with SPME can subsequently focus on the endogenous molecules on the receiving end of the neural circuits involved in response to ketamine, simultaneously to the drug release in the mPFC.

The prospect for investigating the drugs' release zone in brain by spatially resolved SPME-DESI-MS/MS

In order to demonstrate how the drug release from the ketamine-loaded nanoemulsion is related to the applied sonication site, *in vivo* sampling is being conducted employing the protocol optimized for spatially resolved SPME-DESI-MS/MS analysis described here. A study utilizing positron emission tomography (PET) imaging visualized a pattern of propofol release that coincided exactly with the sonication target area.[329] However, the used method provides only indirect evidence by imaging the uptake of a glucose analog. Our MS-based approach allows for obtaining direct chemical information, including concentration of the drug and borders of the release zone in one dimension per sampling

event. In the indirect approach, where the drug effect and not the drug itself is measured, the extent of the observed effect is influenced by the extent of brain parenchyma perfused by the same blood vessels in which the drug is released. Direct spatially-resolved ketamine measurement by SPME is only dependent on the rate of the drug diffusion in the brain tissue, which is presumably low. Therefore, the borders of ketamine in the SPME imprint are expected to represent the diameter of the release zone, while the quantitative feature of the imprint will indicate the concentration gradient created during the ultrasonic uncaging.

Chapter 5

Investigation of early death-induced changes in rat brain by solid phase microextraction via untargeted high resolution mass spectrometry: *in vivo* versus *post mortem* comparative study

5.1 Preamble

This chapter has already been published as an article entitled *Investigation of early death-induced changes in rat brain by solid phase microextraction via untargeted high resolution mass spectrometry: in vivo versus postmortem comparative study* by Sofia Lendor, Mariola Olkowicz, Ezel Boyaci, Miao Yu, Mustansir Diwan, Clement Hamani, Michael Palmer, Nathaly Reyes-Garcés, Germán Augusto Gómez-Ríos, and Janusz Pawliszyn, *Chemical Neuroscience* **2020**, 11, 1827-1840. The content of the article is herein being reprinted with permission of the American Chemical Society and in compliance with the publisher and the University of Waterloo policies.

5.2 Introduction

The identification of markers of various brain diseases in pursuit of better understanding the pathophysiology of prevalent disorders represents a rapidly expanding field. Associated outcomes are expected to improve treatment and prevention strategies for neurodegenerative diseases such as Alzheimer's Disease (AD) and Amyotrophic Lateral Sclerosis (ALS) , in the long run.[420,421] The main shortcoming of existing approaches for small molecular weight metabolites and lipids is the fact that the brains are analyzed *post mortem* (often, in case of animals and inherently, in case of humans). Therefore, their representativeness for living systems is diminished due to *post mortem* delay,[256] as well as fixation and preservation treatments applied to the tissue so as to prevent further changes.[422]

With increasing *post mortem* interval (PMI), not only do the mechanical properties of the brain change,[423] but so does the pH, DNA, RNA, proteins, and variety and quantity of lipid species. Many of

those changes are suspected to be most prominent within the first hour[424] or minutes[425] of the PMI. In such cases, some changes that are occurring only due to death may be falsely attributed to the disease, if appropriate controls are not employed. To date, it is unclear what level of similarity is shared between metabolic regulation (or rather, dysregulation) mechanisms at the moment of death and after adaptation to chronic psychiatric disorders.[426] Moreover, studies conducted *post* mortem are not capable of monitoring dynamic processes, which may be very important for a better understanding of diseases. The solution to this problem would be studying the sample *in vivo*, which is very difficult or impossible in humans via non-imaging techniques. To date, the best opportunities for harvesting human brain tissue *in vivo* were provided by biopsies performed during neurosurgical procedures.[427] While this material is generally free from PMI influence, provided appropriate preservation methods and rapid processing, it may still be affected by the disease or its treatment, and does not allow for deliberate selection of the target brain area of interest. In animal studies, however, it is possible to acquire a baseline sample *in vivo* and further characterize the *post mortem* changes in either healthy animals (for monitoring only death-induced changes) or diseased ones (for monitoring markers of pathophysiology).

The morphological and chemical tissue changes after death and their importance are a domain of yet another field, forensic science, from which the neuroscience can source useful information from. The clinical and forensic literature oftentimes asks the same questions but from different perspectives (specifically, the alive and the dead). The brain's suitability for the purpose of PMI investigations is determined by the fact that it is protected well enough inside the skull to minimize external influences and preserve its integrity for a certain time after death, but not well enough for the *post mortem* changes to be significantly delayed (as in the case of tissues completely enclosed inside the bones, e.g. bone marrow).[428] At the same time, due to the presence of enzymes, the brain can be one of the first tissues to undergo *post mortem* autolysis.[429] Previous studies focused predominantly on PMI-induced changes in DNA, RNA, and proteins,[422,430] while small soluble metabolites and lipids have only started to attract

growing attention more recently.[244,431–435] With untargeted, MS-based metabolomic and lipidomic approaches becoming more popular in attempts to identify potential candidates for biomarkers of neurodegenerative diseases[245] and PMI,[436] investigation of purely death-induced changes presents itself as a necessary fundamental research minimizing potential future false positive biomarker discoveries.

Sub-optimal sample acquisition and storage leads to more artefacts that will consequently hinder proper interpretation of the obtained results. Approaches with involved and invasive methods of sample collection are especially prone to yielding wrong conclusions, as the observed changes represent a combination of tissue damage effects and PMI influence. Solid phase microextraction (SPME) emerges as non-imaging technique capable of broad, untargeted biochemical analysis both *in vivo* and *post mortem*.[132,135,136,437–439] We have chosen to use this technique in the current work as it operates through the so-called chemical biopsy mode,[440] which ensures that no tissue is removed or collected. Furthermore, since depletion of the free fraction of molecules in the tissue by the biocompatible probe is negligible, the system is spared any drastic physiological re-adjustments to replenish its metabolites, and the binding equilibrium state remains unchanged.[441] These features, in principle, would minimize disturbances to the studied system, making the *in vivo* results a true representation of its physiological state at the time of sampling.

In this study, we aimed to determine changes in brain neurochemistry occurring immediately and shortly (up to 1 h) after death based on untargeted metabolic profiling of the rodent hippocampus as the target brain area. The animals were healthy and not subjected to any treatment, therefore our study can be considered as a baseline, where the observed changes are attributed only to death, with other (unknown) factors contributing in a negligible way. The choice of SPME as sampling method facilitates minimal *post mortem* delay, as there is no need for brain dissection and fixation. The use of *in vivo* sampling in freely moving, awake animals as a starting point (**Figure 5.1**), instead of monitoring only changes between time points occurring *post mortem*, provides a more accurate picture of death-induced

changes in the brain. This can help to remove ambiguity from the identification of disease-specific changes assumed to occur *in vivo*.

5.3 Experimental

Animals

Animal subjects used in this study were adult male Sprague Dawley rats (220-230 g; *n*=5). The animals were housed in a normal 12:12-h dark-light cycle and received food and water *ad libitum*. All experimental procedures involving the use of animals were approved by the Animal Care Committee of the Centre for Addiction and Mental Health (CAMH) in Toronto. Prior to surgical implantation of the guide cannulas needed for SPME fiber sampling, rats were anesthetized with isoflurane. The guide cannulas (MAB 4.15.IC, SciPro, Sanborn, NY, USA) were unilaterally implanted into the right hippocampi (AP -5.0 mm, ML 4.6 mm, and DV -2.5 mm), 4 mm above the target location of the SPME probe (corresponding to the 4 mm coating length of the fiber). SPME sampling and further procedures were performed after one week of post-operative recovery.

Solid Phase Microextraction Protocol

The SPME fibers used in this work (kindly provided by Millipore Sigma, Bellefonte, PA, USA) contained a mixed-mode extraction phase consisted of silica-based octadecyl functionalized with benzenesulfonic acid. The SPME coating had a length of 4 mm and a thickness of 45 µm (total probe diameter ≈ 290 µm). Prior to extraction, SPME fibers were cleaned by rinsing with 1:1:2 ACN/IPA/MeOH, preconditioned overnight in 1:1 MeOH/H_2O, then subsequently submerged in a fresh batch of the same preconditioning solvent for transportation to the sampling site. A previously reported custom brain sampler[442,251] was employed in this work to facilitate rapid and easy insertion and withdrawal of the fiber into and from the brain. The sampler was designed to fit the employed cannula guides in a manner that allowed for precise and accurate positioning of the fiber in the target brain area while also allowing for free movement of the animal during *in vivo* sampling. Fibers were assembled

with the sampler and stored in the preconditioning solvent until extraction. Shortly before their insertion into the brain, the fibers were briefly rinsed with ultrapure water in order to remove any residual organic solvent from the coating. Sampling was conducted according to the timeline presented in **Figure 5.1**. The first sampling event was carried out *in vivo* in awake, freely moving animals. The animals were then anesthetized with isoflurane. After ensuring that respiration had completely ceased, animals were sacrificed through decapitation, whereupon two *post mortem* sampling events were performed. In total, three sequential extractions of 30 min were carried out in brain tissue: an *in vivo* extraction, and two *post mortem* extractions.

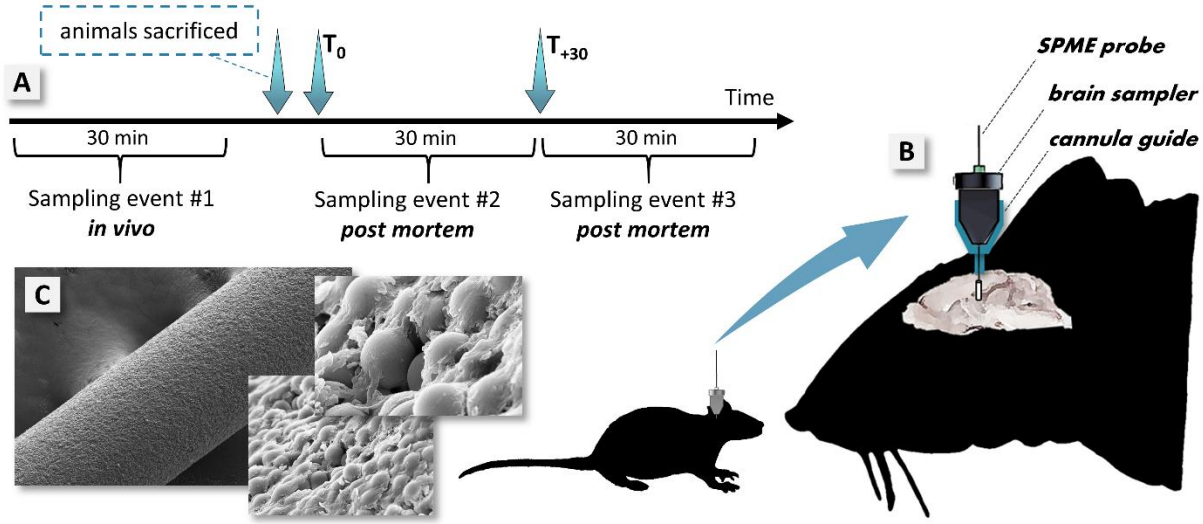

Figure 5.1: Experimental timeline (**A**). The in vivo sampling in awake, freely moving animals was enabled with the use of a specially developed SPME brain sampler (**B**) designed to fit the used microdialysis cannula guide.[251,442] The SPME probe is pre-positioned in the sampler based on the depth of the target brain area. Subsequent deployment of the sampler in the cannula guide is achieved in a matter of seconds. The SPME probe (**C**) provides minimally-invasive sampling and is manufactured from fully biocompatible materials.

Following their withdrawal from brain, fibers were wiped using lint-free tissue, rinsed in ultrapure water, then stored in glass vials. The vials containing the fibers were kept in dry ice during transportation, then subsequently stored at a temperature of -80° until fiber desorption and instrumental analysis. The fibers were desorbed into 50 µL of methanol for 60 min at an agitation rate of 1500 rpm.

The extracts were then diluted with 50 µL of water. The same post-processing was applied to blank fibers (*n*=3), which were not subjected to extraction and served as negative controls. Before separation on hydrophilic interaction liquid chromatography, extracts were evaporated to dryness while kept at 40°C under nitrogen flow, and subsequently reconstituted in 40 µL of an acetonitrile/water 4:1 mixture.

Liquid chromatography and high-resolution mass spectrometry (HPLC-HRMS) analysis

Extracts were analyzed by liquid chromatography-mass spectrometry. In this work, a high resolution mass spectrometer with an Orbitrap mass analyzer was used for instrumental analysis. Since SPME provides broad coverage of extracted compounds (the extracting phase possesses both hydrophobic and hydrophilic sites), two chromatographic methods were employed with the aim to increase the amount of information attained from the studied system. Reversed phase chromatography (RPLC) with a pentafluorophenyl column was used for profiling of metabolites and lipids, while hydrophilic interaction liquid chromatography (HILIC) was employed to retain small polar molecules. Details regarding both methods and acquisition parameters are listed in **Table 5.1**. Data acquisition was carried out using Xcalibur software (versions 2.0.7 and 3.0.63 for RP-LC and HILIC runs, respectively) and Thermo Exactive Tune (version 1.1). Mass accuracy of the MS instrument was calibrated using the Pierce™ LTQ Velos ESI Ion Calibration Solutions for positive and negative ionization modes (Thermo Scientific, San Jose, USA). Real-time calibration was performed throughout all runs with the use of the lockmass function. Monitoring of instrument performance was carried out by injecting a standard quality control (QC) sample (mixture of standards at 100 ng/mL), as well as a pooled QC sample (prepared by mixing 10 µm of each extract, including blank fiber extracts; separate samples for RP-LC and HILIC separations) after every 5 samples. The peak areas of the standards included in the instrumental QC samples did not exceed 20% of the relative standard deviation (RSD) throughout each sequence.

Table 5.1: MS acquisition parameters and LC method details for analysis of metabolites and lipids in rat brain SPME extracts.

High Performance Liquid Chromatography		
	Reversed-phase	HILIC
Instrument	Thermo Accela 1250	Thermo Vanquish Flex
Column	Supelco Discovery HS F5, 3 µm, 100 x 2.1 mm, 20 x 2.1 mm guard column	Merck SeQuant ZIC-HILIC, 3.5 µm, 100 x 2.1 mm with 20 x 2.1 mm guard column
Mobile phase A	H_2O + 0.1% FA (+ 1mM AA)	
Mobile phase B	ACN + 0.1% FA (+ 1mM AA)	
Flow rate [µL/min]	300	350
Column temperature [°C]	25	40
Samples temperature [°C]	5	
Injection volume [µL]	10	
Desorption solvent	methanol/water 1:1	acetonitrile/water 4:1
Gradient [%B]	0 min-0%; 3 min-0%; 25 min-90%; 34 min-90%; 35 min-0%; 40 min-0%	0 min-90%; 2 min-90%; 22 min-50%; 27 min-50%; 27.5 min-90%; 35 min-90%
Thermo Exactive Mass Spectrometer (heated electrospray ionization source)		
Spray voltage [kV]	4.0 (-2.9)	3.5 (-3.2)
Sheath gas	55	60
Auxiliary gas	30	20
Sweep gas	5	2
Capillary temperature [°C]	300 (300)	275 (250)
Vaporizer temperature [°C]	300	300
Mass range [m/z]	100-1000	75-1000
Acquisition mode	Full Scan	
Max. inject time [ms]	100	
AGC target	Balanced: 1e6	
Resolution	High: 50,000 @ 2Hz	
Lock Mass	m/z 391.2843 (positive); m/z 255.2329 (negative)	

Negative ionization mode parameters in brackets; FA- formic acid; AA- acetic acid

The identities of some of the significantly changing and biologically relevant compounds were confirmed based on MS/MS analysis of pooled QC samples in parallel reaction monitoring mode (PRM) on a quadrupole-orbitrap Q-Exactive mass spectrometer (Thermo Fisher Scientific, Waltham, MA, USA). The acquisition parameters and method details are listed in **Table 5.2.**

Table 5.2: MS/MS acquisition parameters for confirmation of identities of significant metabolites and lipids found in rat brain extracts.

Thermo Q-Exactive Mass Spectrometer (heated electrospray ionization source)	
Spray voltage [kV]	3.5 (-2.8)
Sheath gas	35
Auxiliary gas	5
Sweep gas	0
Capillary temperature [°C]	300 (300)
Vaporizer temperature [°C]	300
S-Lens RF level [V]	60
Acquisition mode	Parallel Reaction Monitoring
Max. inject time [ms]	100 (50)
AGC target	1e6
Resolution	35,000
Normalized Collision Energy [V]	20 and 40
Lock Mass	m/z 391.28429 (positive); m/z 255.23295 (negative)

Negative ionization mode parameters in brackets

Data processing, statistical analysis, and compound identification

Raw data files were converted into the mzXML format required for further data processing with the use of the MSconvert toolkit (ProteoWizard 3.0).[229] The IPO package[230] was then applied to pooled QC samples in order to optimize the number of settings, including peak picking and retention time correction. Subsequent peak extraction, filling, grouping, alignment, and filling were performed with the use of the XCMS package.[231] The above operations (except for raw data conversion) were integrated in an in-house developed R-script.[232,130] The m/z versus intensity list then underwent filtering so as to discard artefacts present in blank samples as well as peaks with significant variance. According to the criteria of acceptance, peaks exhibiting a relative standard deviation of intensity across all pooled QC samples exceeding 30%, as well as a signal-to-noise value of less than 5 (relative to blank desorption solvent samples as well as blank SPME fiber samples) were discarded.

Identified differences across the three studied sampling timepoints (*in vivo- IV*, *post mortem* at T_0- *PM*T0, and *post mortem* at T_{+30}- *PM*T30) were investigated based on univariate and multivariate data analyses carried out employing MetaboAnalyst.[233] Data pre-treatment involved logarithm transformation and auto scaling in order to transform the analytical response into a form that is

comparable between different features as well as to transform the distribution of data into one resembling normal distribution, suitable for t-testing. The first step of multivariate analysis encompassed generating a principal component analysis (PCA) score plot of all groups, including pooled QC samples, so as to evaluate and confirm the stability of the instrument performance based on pooled QC samples clustering.

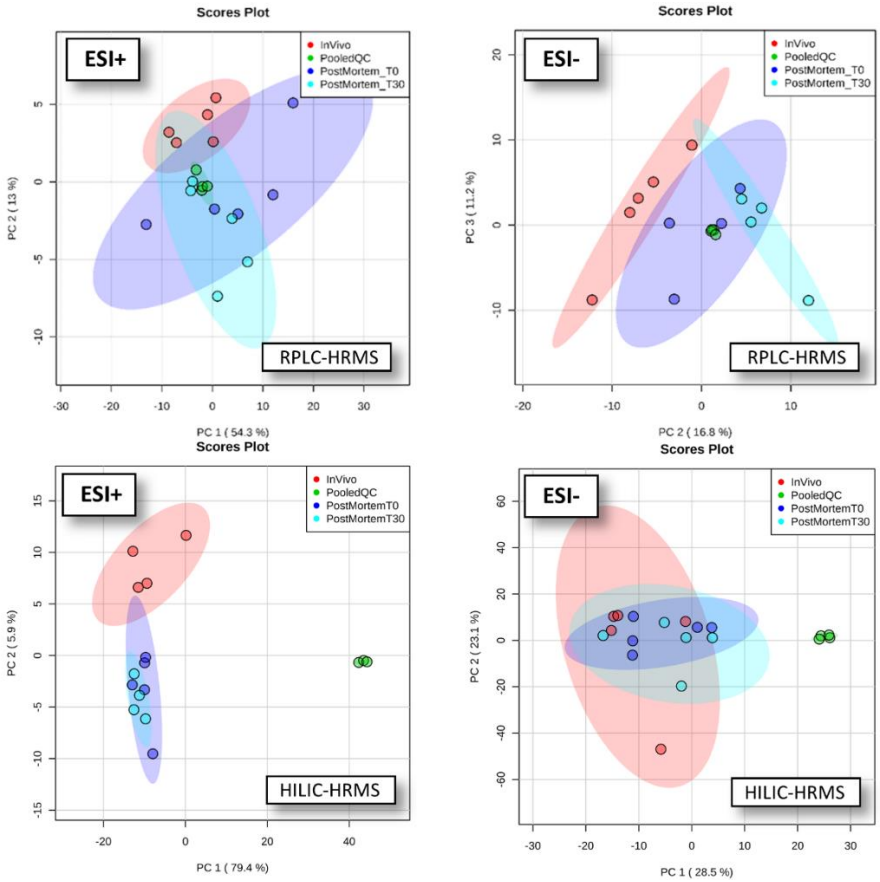

Figure 5.2: Principal component analysis (PCA) scores plots for analyses via RPLC-HRMS (top) and HILIC-HRMS (bottom) in positive and negative ionization modes (left and right, respectively). The plots display two components and the group of pooled QC samples is included to prove stability and reliability of the instrumental analysis.

Subsequent operations on data, including unbiased PCA and supervised partial least square discriminant analysis (PLSDA), were carried out using only the three compared sampling timepoints. Compounds whose levels differed in a statistically significant fashion between sampling timepoints

were then chosen based on their Variable Importance in Projection (VIP) scores, with significance defined as a VIP score >1. The PLSDA model underwent a cross validation procedure for every set of compared groups in order to ensure that any observed clustering was not a result of overfitting. Next, the Leave-one-out Cross Validation method (LOOCV) was applied to assess the quality of the model based on the predictive ability and goodness-of-fit values, Q^2 and R^2, respectively,[443] with the criteria of acceptance being an R^2 value not exceeding the Q^2 value by more than 0.2.[444] For the 3-group comparisons, a permutation test was additionally performed, using 2000 permutations, and an acceptance criterion for the empirical *p*-value below 0.05.

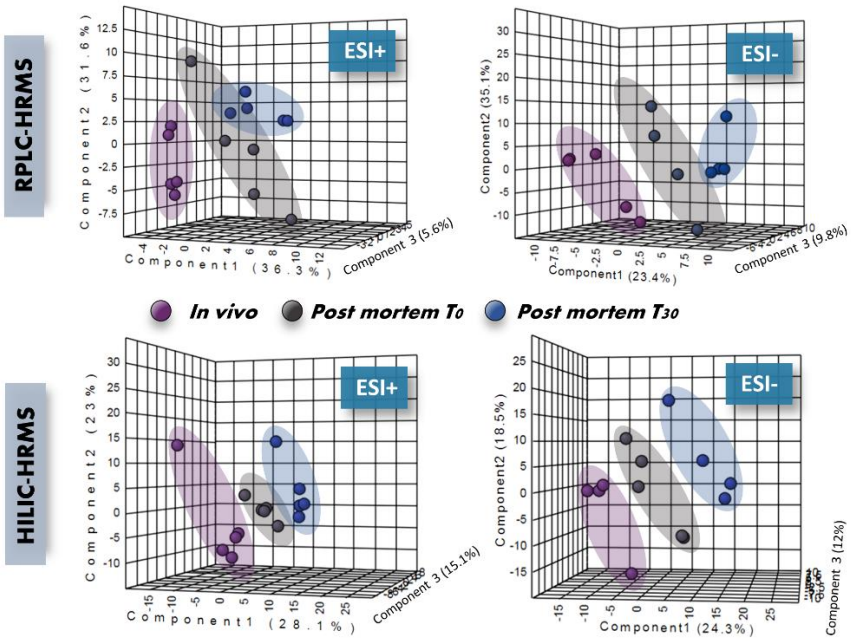

Figure 5.3: PLSDA models for all acquired HPLC methods and MS ionization modes. The extent of separation between studied sampling timepoints becomes increasingly apparent as the PMI increases. The Leave-one-out cross validation was optimized at 2 components with R2=0.79, Q2=0.55 and R2=0.91, Q2=0.71 for RPLC-HRMS analysis in positive and negative ionization mode, respectively. For HILIC-HRMS analysis the models were optimized at two components with R2=0.97, Q2=0.76 and three components with R2=0.98, Q2=0.71 in positive and negative ionization mode, respectively. Two-group PLSDA plots for each combination between two studied time points were included in Figure S3 of the Supporting Information.

Statistically important compounds (as identified by univariate analysis, specifically the t-test) that demonstrated a variation in abundance between any two sampling timepoints underwent fold change

analysis (FC) in order to quantify the extent of the variation. A change of 30% or higher was considered as statistically significant in this study. Due to lack of unified criteria for untargeted metabolomic workflows in terms of the fold change threshold this value is somewhat arbitrary across the studies. Here, the motivation behind the 30% threshold was that the change considered as significant should be larger than what is assumed to be an acceptable experimental error (up to 20%). At the same time, setting the threshold too high (e.g. 1.5-fold or 2-fold change) was avoided, as the changes in metabolite abundance observed immediately after death and only within the first hour *post mortem* were expected to be subtle in case of some metabolites. Therefore, the 30% threshold represents a balance between avoiding picking up noise if set too low and neglecting some subtle changes if set too high. Box plots for each significant compound were prepared using GraphPad Prism software (version 8.0.1), with the median of intensity as response, and range describing variability. The significance threshold for the *p*-value and the false discovery rate (*q*-value) were set to 0.05. Metabolites exhibiting significant changes between the *in vivo* and *post mortem* samples were taken into account even if their *q*-values were above the threshold, especially in cases when there was strong evidence that these compounds were associated with certain identified pathways affected by the animal's death.

Annotation of compounds found to present variations between any of the studied sampling timepoints at statistically significant levels was performed with the use of the xMSannotator Integrative Scoring Algorithm.[445] This tool facilitates annotation utilizing a multistage clustering algorithm which takes into account mass defect, isotope and adduct formation patterns, retention time and intensity profiles, as well as signal for metabolically related species. Reference databases included METLIN,[234] the Human Metabolome Database,[446] LIPID MAPS,[235] and KEGG.[447] The resulting annotations with multiple matches filtered off were assigned confidence levels by the algorithm. In the instance of multiple matches at medium or high confidence level, the annotations were further verified using criteria pertaining to MS and brain biochemistry expertise, as well as previous reports of particular

compounds or classes of compounds in the context of brain tissue analysis. Whenever possible, metabolites were identified based on analysis of authentic standards or MS/MS fragmentation spectra, which were compared with those available in databases using Metlin MS/MS Spectrum Match Search, MS-FINDER,[448] and mzCloud.[449]

The MetPA (Metabolomics Pathway Analysis) functionality of the MetaboAnalyst was used to summarize and visualize the most significantly affected metabolic pathways.[450] HMDB identifiers of all significantly changed compounds (in all ionization modes and all chromatographic methods) were used as input. The pathway analysis algorithms used for this analysis included a hypergeometric test for over-representation analysis and a relative-betweenness centrality test for pathway topology analysis.

5.4 Results and discussion

Understanding the complexity of the human brain is arguably the greatest challenge of modern science; however, such a feat remains extremely taxing to achieve, given that human brain tissue obtained from autopsies is practically the only source of brain tissue that can be used to study its intricate organization (at any discussed level: molecular, biochemical, or anatomical). In addition to the scarcity of samples, investigative challenges are compounded by the condition of said samples, since *post mortem* time delay exerts a negative impact on reliable measurements at all levels of the biological organization of the brain. In this work, we used a biocompatible probe for a microscale metabolomic/lipidomic investigation of the nervous system as a means to provide insight into *post mortem* hypoxic and decomposition reactions. Special emphasis has been placed on metabolic alterations occurring in hippocampus tissue over time in the very early period of time following death.

Table 5.3: List of metabolites showing statistically significant differences among *in vivo* and *post mortem* samplings in the hippocampus at different time points.

Compound	Rt (min)	LC method	m/z	Adduct	Mass error [ppm]	Level †	IV vs. PM T_0		PM T_0 vs. T_{30}		IV vs. PM T_{30}		Pathway/Function
							FC	*p*-value	FC	*p*-value	FC	*p*-value	
15-deoxy-delta-12,14-Prostaglandin J2	15.2	RPLC	315.1968	$[M-H]^-$	1	3	↓ 2.45	0.090	↓ 1.72	0.023	↓ 4.23	0.038	Arachidonic acid metabolism/anti-inflammatory prostaglandin
	0.84	HILIC	317.2115	[M+H-H2O]+	0		↓ 1.68	0.073	↓ 2.10	0.085	↓ 3.54	0.019	
	0.81	HILIC	315.1966	$[M-H]^-$	0		↓ 2.18	0.031	↓ 1.35	0.17	↓ 2.93	0.021	
Prostaglandin	15.3	RPLC	335.2218	$[M+H]^+$	0	1	↓ 3.03	0.043	↓ 1.54	0.11	↓ 4.67	0.021	Arachidonic acid metabolism
Prostaglandin (cyclopentenone prostaglandin or cyclopentenone isoprostane)	0.8	HILIC	333.2071	$[M-H]^-$	0	1	↓ 2.61	0.0071	↓ 1.16	0.51	↓ 3.03	0.0089	Arachidonic acid metabolism
	0.8	HILIC	351.2175	$[M-H2O-H]^-$	0		↓ 3.39	0.011	↓ 1.42	0.27	↓ 4.81	0.013	
Prostaglandin	0.8	HILIC	353.2333	[M-H]-	0	1	↓ 1.71	0.033	↓ 1.08	0.79	↓ 1.85	0.0032	Arachidonic acid metabolism
FA 17:4	18.3	RPLC	263.2006	$[M+H-H2O]^+$	1	1	↓ 1.78	0.095	↓ 1.44	0.46	↓ 2.56	0.013	Arachidonic acid metabolism
GlcCer(d40:1)/GalCer(d40:1)	26.1	RPLC	784.6661	$[M+H]^+$	0	1	↑ 1.18	0.83	↑ 1.48	0.39	↑ 1.77	0.035	Cell signal transduction
GlcCer(d42:1)/GalCer(d42:1)	26.8	RPLC	812.6974	$[M+H]^+$	0	1	↑ 1.35	0.28	↑ 1.40	0.045	↑ 1.86	0.035	Cell signal transduction
5alpha-Androst-16-en-3-one or 5alpha-Androst-3-en-17-one	15.2	RPLC	271.2069	$[M-H]^-$	1	1	↓ 2.54	0.089	↓ 1.76	0.031	↓ 4.47	0.039	Cell signal transduction
Adenosine monophosphate	1.3	RPLC	348.0704	$[M+H]^+$	0	1	↓ 2.15	0.022	↓ 1.86	0.052	↓ 4.00	0.0032	Energy metabolism
Creatine	2.3	RPLC	132.0769	$[M+H]^+$	1	5	↑ 3.55	0.036	↑ 1.41	0.25	↑ 5.02	0.0087	Energy metabolism
	2.17	RPLC	130.0613	[M-H]-	6		↑ 3.47	0.076	↑ 1.48	0.33	↑ 5.14	0.0015	
Phytanic Acid	2.7	HILIC	330.3363	$[M+NH4]^+$	1	1	↑ 1.17	0.74	↓ 3.15	0.050	↓ 2.70	0.11	Energy-related function
/roglutamic acid or glutamine or glutamate	1.4	RPLC	130.0500	$[M+H]^+$	1	4	↑ 1.97	0.022	↑ 1.22	0.29	↑ 2.40	0.0002	Glutathione metabolism
S-formylglutathione	1.1	RPLC	176.1031	$[M+H+Na]^{2+}$	5	1	↑ 1.88	0.15	↑ 1.26	0.49	↑ 2.37	0.024	Glutathione metabolism
PE(O-36:6)/PE(P-36:5)	28.2	RPLC	722.5095	$[M+H]^+$	3	1	↑ 1.39	0.22	↑ 1.35	0.17	↑ 1.88	0.050	Glycerophospholipid metabolism
PE(O-38:6)/ PE(P-38:5)	28.2	RPLC	750.5419	$[M+H]^+$	1	1	↑ 1.48	0.22	↑ 1.25	0.72	↑ 1.85	0.051	Glycerophospholipid metabolism
PS(P-29:0)	6.2	HILIC	678.4701	$[M+H]^+$	0	1	↑ 1.59	0.050	↓ 1.06	0.75	↑ 1.50	0.076	Glycerophospholipid metabolism
L-lactic acid	1.8	RPLC	135.0029	$[M+Na]^+$	0	1	↑ 2.41	0.026	↓ 1.76	0.40	↑ 1.37	0.17	Glycolysis/Energy metabolism
Beta-D-Fructose 1,6-bisphosphate	0.9	HILIC	360.9726	$[M+Na-2H]^-$	5	1	↓ 7.36	0.019	↑ 2.42	0.20	↓ 3.03	0.10	Glycolysis/Energy metabolism
L-Tryptophan	12.7	RPLC	205.0973	$[M+H]^+$	1	5	↑ 1.24	0.60	↑ 1.14	0.81	↑ 1.49	0.051	Serotonin precursor
L-Glutamine	1.4	RPLC	147.0765	$[M+H]^+$	1	5	↑ 2.01	0.084	↑ 1.28	0.33	↑ 2.58	0.0003	Glutamate precursor
	1.35	RPLC	145.0612	$[M-H]^-$	4		↑ 2.35	0.12	↑ 1.25	0.55	↑ 2.94	0.0013	
L-Glutamic acid	1.5	RPLC	148.0605	$[M+H]^+$	0	5	↑ 2.16	0.040	↑ 1.67	0.021	↑ 3.62	<0.0001	Neurotransmission
N-stearoyl GABA	20.5	RPLC	370.3316	$[M+H]^+$	0	4	↓ 1.35	0.28	↑ 1.50	0.052	↑ 1.11	0.18	Neurotransmission
N-Acetyl-L-aspartate	2.0	RPLC	176.0556	$[M+H]^+$	1	4	↑ 1.37	0.023	↑ 1.63	0.027	↑ 2.23	0.0027	Neurotransmission
Tyramine	9.7	RPLC	120.0810	$[M+H-H_2O]^+$	2	4	↓ 1.19	0.75	↓ 1.42	0.29	↓ 1.69	0.041	Neurotransmission
GABA	1.4	RPLC	102.0552	$[M-H]^-$	8	5	↑ 2.33	0.068	↑ 2.22	0.0065	↑ 5.19	<0.0001	Neurotransmission
5-Deoxyadenosine	2.2	RPLC	288.0516	$[M+K-2H]^-$	4	1	↑ 3.52	0.068	↑ 1.40	0.37	↑ 4.93	0.0003	Purine degradation/salvage
5-Phosphoribosylamine	2.17	RPLC	228.0301	$[M-H]^-$	9	1	↑ 3.83	0.071	↑ 1.38	0.41	↑ 5.30	0.0004	Purine synthesis
Xanthine	1.6	RPLC	151.0254	[M-H]-	5	2	↑ 5.45	0.055	↑ 1.54	0.41	↑ 8.42	0.014	Purine degradation
	2.14	HILIC	151.0254	$[M-H]^-$	4		↑ 8.76	0.078	↑ 1.96	0.28	↑ 17.14	0.050	
2'-Deoxyinosine 5'-phosphate (dIMP)	2.1	HILIC	331.0453	$[M-H]^-$	1	1	↓ 1.31	0.20	↓ 1.33	0.18	↓ 1.74	0.041	Purine degradation/salvage
5,6-dihydrouridine	1.4	RPLC	227.0650	$[M-H2O-H]^-$	7	1	↑ 2.10	0.14	↑ 1.30	0.45	↑ 2.73	0.0012	Purine metabolism/tRNA synthesis

Table 5.3: Continued.

Compound	Rt (min)	LC method	m/z	Adduct	Mass error [ppm]	Level †	IV vs. PM T_0		PM T_0 vs. T_{30}		IV vs. PM T_{30}		Pathway/Function
							FC	*p*-value	FC	*p*-value	FC	*p*-value	
3-Deoxyvitamin D3	25.4	RPLC	369.3516	$[M+H]^+$	0	4	↑ 1.37	0.084	↑ 1.03	0.90	↑ 1.45	0.050	Vitamin D metabolism
1,25-dihydroxy-22-oxavitamin D3	25.8	RPLC	419.3156	$[M+H]^+$	0	1	↑ 1.16	0.65	↑ 1.27	0.010	↑ 1.47	0.22	Vitamin D metabolism
1,11,25-trihydroxyvitamin D3	26.2	RPLC	433.3313	$[M+H]^+$	0	1	↑ 1.12	0.73	↑ 1.61	0.011	↑ 1.79	0.068	Vitamin D metabolism
N-Formyl-L-glutamate	1.4	RPLC	176.0555	$[M+H]^+$	1	1	↓ 1.75	0.0069	↑ 1.78	0.025	↑ 1.02	0.90	Histidine metabolism
Dihydroxy-3-methylvalerate	0.9	HILIC	129.0548	$[M-H2O-H]^-$	2	1	↓ 3.77	0.0033	↑ 1.07	0.62	↓ 3.51	0.010	BCAA metabolism
L-Leucine/Isoleucine	7.7	RPLC	132.1020	$[M+H]^+$	1	5	↑ 1.02	0.95	↑ 1.40	0.36	↑ 1.43	0.055	BCAA metabolism
L-Phenylalanine	9.7	RPLC	166.0864	$[M+H]^+$	1	5	↓ 1.28	0.33	↓ 1.31	0.23	↓ 1.73	0.050	AAA metabolism
L-Tyrosine	7.6	RPLC	182.0813	$[M+H]^+$	1	5	↓ 1.11	0.78	↓ 1.55	0.045	↓ 1.68	0.047	AAA metabolism
LacCer(d30:0)	28.2	RPLC	790.5646	$[M+H-H2O]^+$	2	1	↑ 1.36	0.31	↑ 1.33	0.47	↑ 1.81	0.040	Regulation of permeability of blood-brain barrier
PA(O-38:6)/ PA(P-38:5)	28.2	RPLC	707.4996	$[M+H]^+$	2	1	↑ 1.36	0.42	↑ 1.30	0.64	↑ 1.77	0.044	Mediators in brain functions
PA(45:8)/ PA(O-45:9)	28.2	RPLC	815.5606	$[M+H]^+$	1	1	↑ 1.28	0.69	↑ 1.67	0.25	↑ 2.12	0.050	Mediators in brain functions
MGDG(36:5)	28.2	RPLC	777.5521	$[M+H]^+$	1	1	↑ 1.73	0.12	↑ 1.31	0.26	↑ 2.26	0.043	Myelin component
Betaine	1.9	RPLC	156.0422	$[M+K]^+$	0	4	↑ 1.36	0.56	↑ 1.12	0.91	↑1.50	0.049	Osmolytic activity
4,5-dehydrodocosahexaenoic acid	1.1	HILIC	344.2616	$[M+H-H2O]^+$	1	1	↑ 2.18	0.24	↑ 4.29	0.058	↑ 9.33	0.053	Docosahexaenoic acid metabolism
Acetyl-L-carnitine	9.4	RPLC	204.1232	$[M+H]^+$	1	4	↑ 1.56	0.30	↑ 1.21	0.53	↑ 1.89	0.0087	Acetyl-CoA transport
Deoxyribose 1-phosphate/Deoxyribose 5-monophosphate	2.1	HILIC	427.0448	$[2M-H]^-$	8	1	↓ 1.65	0.023	↓ 1.22	0.43	↓ 2.01	0.022	Pyrimidine metabolism/pentose phosphate pathway
L-Citrulline	1.5	RPLC	176.1031	$[M+H]^+$	1	5	↓ 1.36	0.24	↓ 1.17	0.54	↓ 1.44	0.051	Urea cycle/NO generation

AAA – aromatic amino acids; BCAA – branched-chain amino acids; PA- phosphatidic acid; PE- phosphatidylethanolamine; PS- phosphatidylserine; GlcCer- glucosylceramide; GalCer- galactosylceramide; LacCer- lactosylceramide; MGDG- monogalactosyldiacylglycerol; FA- fatty acid

† Levels of identification: 1- annotation using xMSannotator Integrative Scoring Algorithm (details on this tool can be found in the *Data processing, statistical analysis, and compound identification* section); 2- found in 2 ionization modes, 2 employed chromatography types or combination of those; 3- found in 3 methods (e.g. two ionization polarities in RPLC and 1 polarity in HILIC); 4- MS/MS spectrum match with database or Rt match with standard; 5- combination of multiple confirmation methods.

FC- fold change; *p*-values represent false discovery rate adjusted values

The rate and extent of early post mortem metabolic alterations in the rat hippocampus

A total of 221 and 163 features were found after RPLC-HRMS analysis in positive and negative ionization mode, respectively, whereas 190 and 528 peaks were obtained after HILIC-HRMS analysis. All data was submitted to the statistical data treatment workflow (described in detail in the Data processing, statistical analysis, and compound identification section), whereupon a narrowed list compounds (**Table 5.3**) exhibiting statistically significant changes between the three compared groups were tentatively identified by database search or comparisons with standards, whenever possible. The applied PLSDA model revealed grouping of the samples according to the progressing PMI. The majority of the identified species were more abundant in *post mortem* samples than *in vivo* samples. Interestingly, changes between *in vivo* and the first *post mortem* period were more pronounced than those occurring between the first and the second post mortem period. Compounds with significantly changed levels were categorized according to their participation in related metabolic pathways. The most affected processes, having multiple compounds affected by death, were found to be energy metabolism, signal transduction and neurotransmission, inflammatory response, oxidation-reduction balance, purine metabolism, vitamin D metabolism, as well as lipid metabolism and transport. Several other processes were altered in a less significant way, with only one representative compound undergoing death-induced changes.

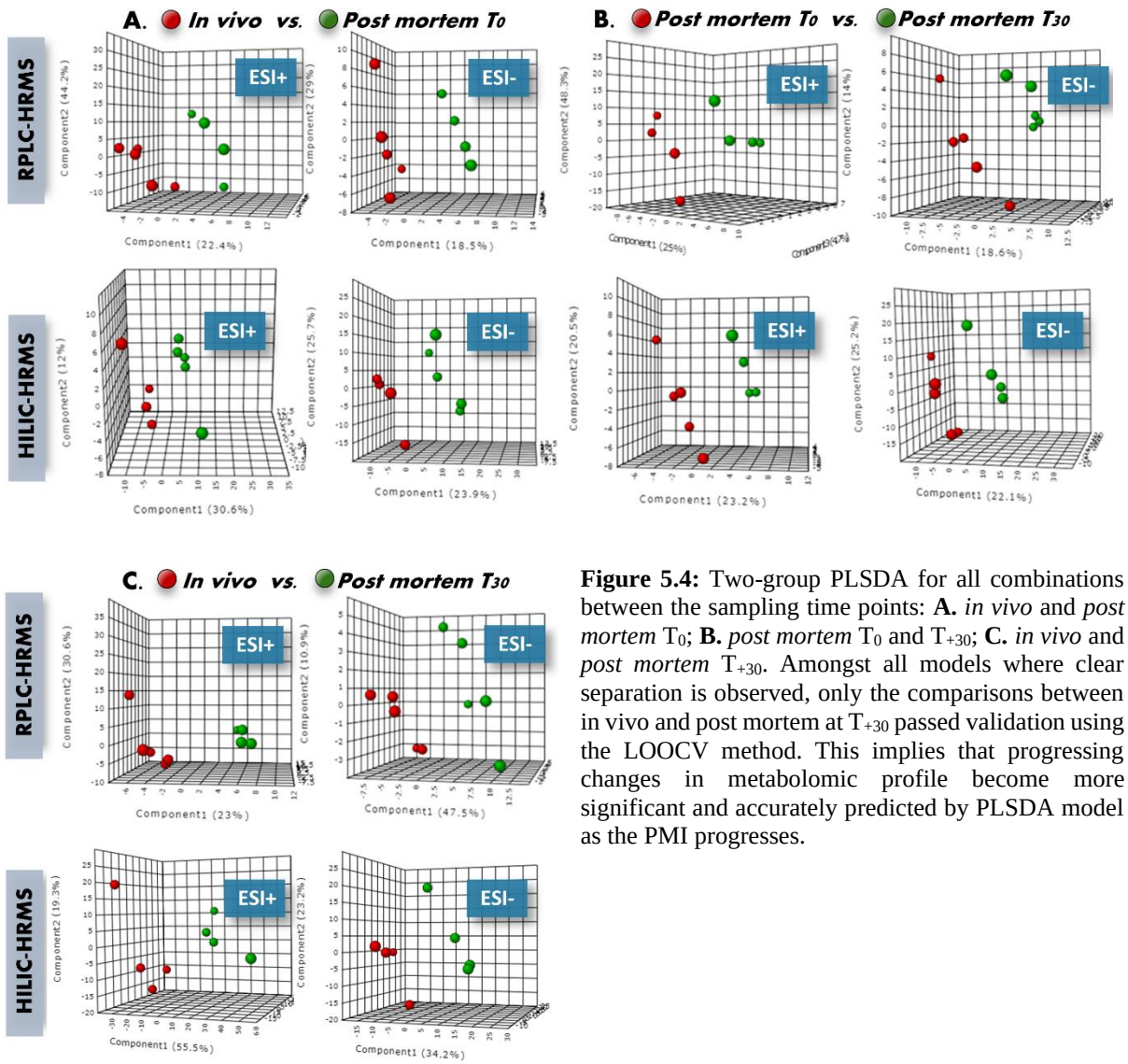

Figure 5.4: Two-group PLSDA for all combinations between the sampling time points: **A.** *in vivo* and *post mortem* T_0; **B.** *post mortem* T_0 and T_{+30}; **C.** *in vivo* and *post mortem* T_{+30}. Amongst all models where clear separation is observed, only the comparisons between in vivo and post mortem at T_{+30} passed validation using the LOOCV method. This implies that progressing changes in metabolomic profile become more significant and accurately predicted by PLSDA model as the PMI progresses.

Energy metabolism-related processes, purine metabolism, and neurotransmitters generation are the most affected pathways following death

Energy depletion is considered the major factor leading to the activation of dopaminergic neuronal death, mostly through two characteristic pathways: alteration of glucose oxidation and decrease of respiration due to inhibition of Complex I.[451,452] It is well recognized that oxidative glycolysis is the main energy resource of brain cells, responsible for glucose transformation into acetyl-CoA that is

further converted into NADH through the TCA cycle, which in turn is used during ATP generation.[453] Indeed, we have noted a pronounced decrease in AMP levels along with alterations in several metabolites of glycolysis (i.e. β-D-Fructose 1,6-bisphosphate, pyruvate). Moreover, the significantly elevated creatine levels observed in this work as a function of death suggest that the balance between the phosphorylated and dephosphorylated forms of this compound was altered, indicating that the storage of energy in the form of phosphocreatine was clearly compromised (**Figure 5.5-a,b**).

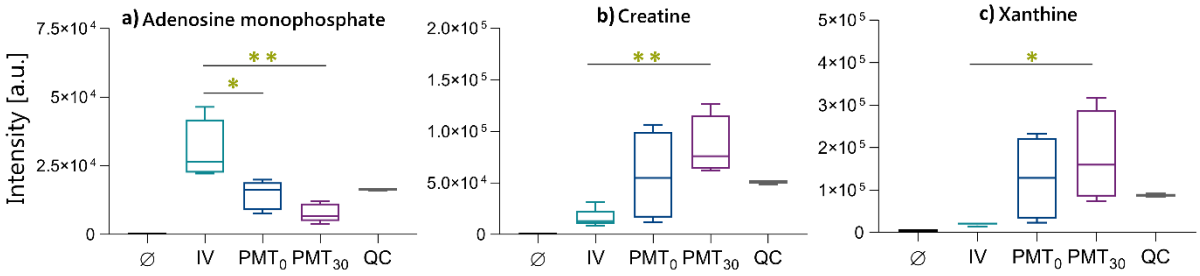

Figure 5.5: Abundance variability across the sampling timepoints for the key metabolites related to energy metabolism pathways (shown as absolute intensities). ⦸ - SPME fiber blank; IV – in vivo sampling; PM_{T0} –post mortem sampling at 0 min of PMI; PM_{T30} –post mortem sampling at 30 min of PMI; QC – pooled quality control samples; * - $p<0.05$; ** - $p<0.005$

The observed increase of adenine nucleotide catabolites, with 6 altered metabolites (within the purine metabolism pathway) of its 45 total compounds (in the pathway enrichment analysis, **Figure 5.6**), represents another noteworthy trend in this work. It is commonly accepted that substantial accumulation of adenine nucleotide catabolites in a given organ with a high energy demand (such as heart and brain) can be interpreted as a very sensitive indicator of ischemic conditions.[454] To support this conclusion, the observed increase in xanthine levels was as much as 8-fold within one hour of PMI, indicating excessive ATP degradation under hypoxic conditions (**Figure 5.5-c**). Our results seem to be in line with a study by Kaminsky et al.[455], in which significant increases in hypoxanthine and xanthine in rat brain were observed 11 min after injection of a lethal dose of ammonium acetate (imitating conditions observed under dramatic decrease in ATP level, adenine nucleotide pool size, and adenylate

energy charge) with no significant change in the abundance of uric acid (the end product of the purine catabolic pathway).

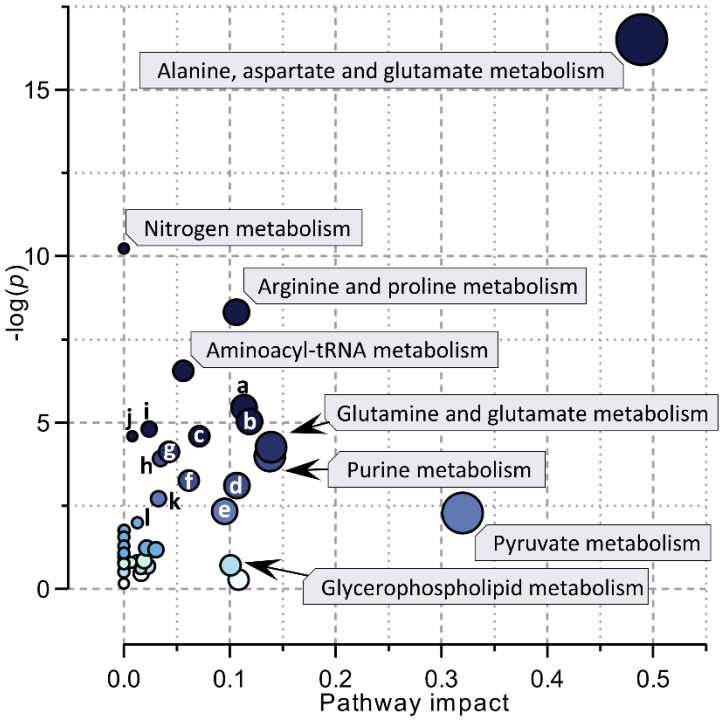

Figure 5.6: The most important metabolic pathways influenced in the hippocampus. A total of 42 metabolic pathways were disturbed in the brain following death, 23 of which were affected by more than 1 metabolite change. (a) butanoate metabolism; (b) phenylalanine metabolism; (c) valine, leucine and isoleucine biosynthesis; (d) citrate cycle (TCA cycle); (e) glycolysis or gluconeogenesis; (f) tyrosine metabolism; (g) pentose phosphate pathway; (h) arachidonic acid metabolism; (i) glycine, serine and threonine metabolism); (j) phenylalanine, tyrosine and tryptophan biosynthesis (k) sphingolipid metabolism; (l) glutathione metabolism, and vitamin D3 metabolism (not included in graph). The affected pathways are plotted according to p-values from the pathway enrichment analysis and pathway impact scores from the pathway topology analysis. Circle size and color gradient indicate the significance of the pathway ranked by p-value (increasing p-value with darker color) and pathway impact score (increasing impact score with larger circle).

In addition to the changes indicated above, we also identified glutamate metabolism as one of the most affected pathways. Glutamate, GABA, and glutamine, together with succinic acid and GMP, are involved in an interconnected common metabolic pathway that has been proven to become dysregulated in numerous neurological disorders, such as multiple sclerosis (MS), Parkinson's disease, stroke, ALS, and AD.[456–459]

We observed a steady and significant increase in glutamate levels following death (**Figure 5.7-a),** an observation that is consistent with several previous studies showing that this major excitatory neurotransmitter is excessively released under hypoxic conditions.[460] In the presence of regulatory mechanisms, taurine fulfills a neuroprotective role by interacting with glutamate receptors to prevent further metabolic damage induced by hypoxia.[461] Taurine was indeed detected in our samples (m/z 124.0068; $[M-H]^-$; Δ4 ppm); however, its abundance was not significantly changed as a function of PMI, which may indicate a lack of an effective compensatory mechanism to counteract excessive stimulation of glutamatergic receptors.

Branched-chain amino acids (BCAAs), namely leucine and isoleucine, play a critical role in the "buffering" mechanism of brain glutamate whenever levels of this excitatory neurotransmitter become elevated (with a reversible BCAA transamination balance shifted towards production of BCAA rather than production of glutamate);[462,463] however the detected 40% increase in their levels (probably due to excessive protein degradation occurring after death) was not sufficient to counteract the pronounced glutamate increase. This is additionally supported by significantly decreasing abundance of 2,3-dihydroxy-3-methylvalerate (**Figure 5.8-a**), which is an intermediate in leucine and isoleucine biosynthesis. Glutamate is a prominent example of a compound that has been found to exhibit discrepancies in comparisons between autopsied brains of patients with neurological disorders and healthy controls, with its levels showing either a decreasing trend or no change in healthy brains compared to the pathophysiologically changed brain. These discrepancies have been attributed to the use of different strategies to correct for the PM interval or, in some cases, to the lack of such corrections.[464–466] In the current work, glutamate was found to exhibit increasing abundance as a result of death, with the same increasing trend being also reported as implicated in the pathophysiology of mental and neurodegenerative disorders, cerebral ischemia, head and spinal cord injury, as well as prolonged seizure activity.[467] Such disorders have been associated with excessive release of glutamate

into the extracellular space, which in turn leads to neurotoxicity. The findings of the current investigation certainly highlight the importance of carrying out a systematic examination of the influence of PMI on metabolites of diagnostic importance.

Glutamate may also serve as a precursor for the synthesis of GABA taking place inside GABAergic neurons in a one-step enzymatic reaction catalyzed by glutamate decarboxylase (GAD).[468] The complex interactions between the GAD, its cofactor pyridoxal phosphate, and ATP (additionally dependent on the presence of glutamate) suggest that ATP promotes inactive state of the enzyme via an allosteric mechanism.[469,470] It was postulated that GAD activity can be altered by post mortem ATP changes, as these are much greater than fluctuations observed under in vivo physiological conditions.[471] It is thus not surprising that continuous secretion of GABA could be observed under conditions of significant ATP depletion[244,472] (**Figure 5.7-c**) evidenced by 4-fold decrease in adenosine monophosphate pool. Our finding is consistent with several previous studies demonstrating that limited amounts of oxygen (as in the case of anaerobic conditions after death) induce a considerable increase in the content of GABA present in brain.[244,473,474] However, the possibility that GABA is released in response to excessive glutamatergic stimulation due to its inhibitory mode of action cannot be discarded either.

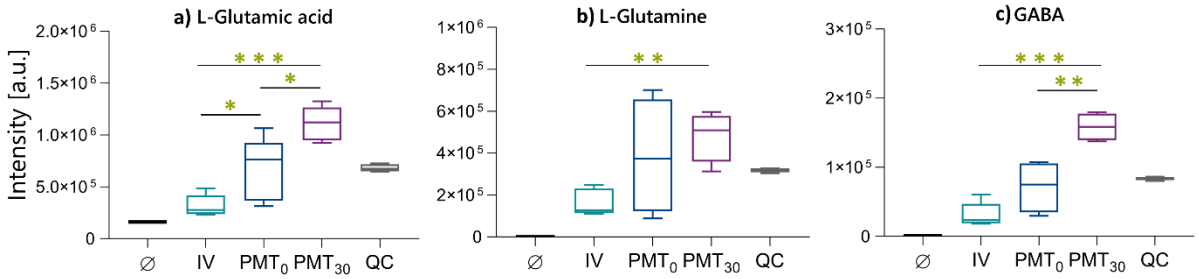

Figure 5.7: Abundance variability across the sampling timepoints for the key metabolites related to neurotransmission (shown as absolute intensities). ⦸ - SPME fiber blank; IV – in vivo sampling; PM_{T0} –post mortem sampling at 0 min of PMI; PM_{T30} –post mortem sampling at 30 min of PMI; QC – pooled quality control samples; * - $p<0.05$; ** - $p<0.005$; *** $p<0.0001$.

In addition to increased levels of glutamate, GABA, and glutamine (**Figure 5.7-b**), we found that one derivative of aspartic acid, namely N-Acetyl-L-aspartate (NAA), was also present at elevated levels after death (**Figure 5.8-b**). It is well recognized that NAA, synthesized primarily in neurons, is the second most concentrated molecule in the brain after glutamate, functioning as an important neurotransmitter.[475,476] NAA has also been suggested to be an important marker of neuronal viability in many cerebral pathologies, as a decline in its concentration has been associated with neuronal or axonal dysfunction, or death.[477] Nevertheless, an excessive increase in NAA concentration (as detected in the current study) might have also a detrimental effect on neuronal cells, as it induces extensive oxidative damage to proteins, nucleic acids, and lipids, mostly due to an increase in nitric oxide production as a response to the elevated concentration of NAA.[478] It is worth noting that this metabolite has also been found to be a marker of cancer cells formation of diagnostic importance.[479,315] Being able to detect this metabolite and its changes in brain tissue in a minimally-invasive way (also adaptable to a properly quantitative analysis) opens up the path for SPME-based protocols to find broader use in brain studies.

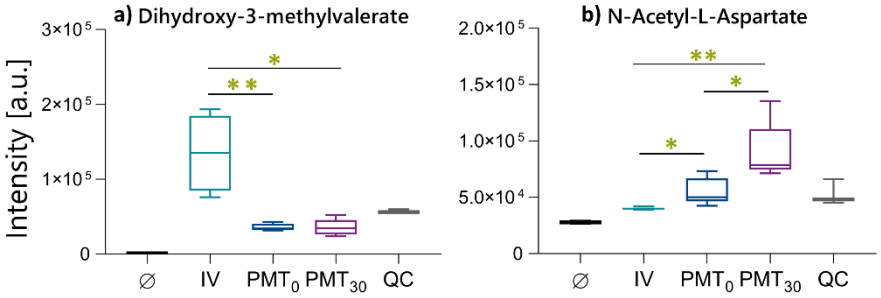

Figure 5.8: Abundance variability across the sampling timepoints for the key metabolites related to amino acids and neurotransmitter metabolism (shown as absolute intensities). ⦸ - SPME fiber blank; IV – in vivo sampling; PM_{T0} –post mortem sampling at 0 min of PMI; PM_{T30} –post mortem sampling at 30 min of PMI; QC – pooled quality control samples; * - $p<0.05$; ** - $p<0.005$

Oxidative stress and a pronounced inflammatory response constitute distinctive features of metabolic changes occurring after death

It is generally accepted that the hippocampus is highly vulnerable to oxidative damage due to its high metabolic demand and high oxygen consumption.[468] Furthermore, it possesses a relatively low content of antioxidants; thus, cellular defense-related mechanisms against excessive generation of reactive oxygen species (ROS) are amongst the most critical mechanisms for normal brain development/function.[480] Moreover, the broad distribution of processes regulating oxidative stress and mediating glutamatergic neurotransmission in the brain may explain (at least in part) the wide range of disorders in which both have been implicated.[481] Our results seem to support this idea, as alteration in metabolites related to glutathione (GSH) was one of the most prominent changes detected after death. Although we did not detect changes in cysteine, required for GSH synthesis, or direct changes in GSH abundance, we noted a clear increasing trend following death for amino acids associated with GSH hydrolysis (glycine or pyroglutamic acid), as well as GSH synthesis intermediate S-formylglutathione. As re-synthesis of GSH is driven by the availability of ATP, the lack of ATP related to the *post mortem* hypoxia state clearly compromised the glutathione system. This is in line with several previous studies, which have shown that brain GSH metabolism is influenced by the PMI, and that GSH content drops rapidly after death.[244,482] These findings should be taken into account during analysis of metabolic alterations occurring in age-related neurodegenerative diseases (i.e. Alzheimer's Disease and Parkinson's Disease), as numerous previous studies have confirmed that altered GSH metabolism is a distinctive feature of these disorders.[482,483]

Furthermore, we found that brain cells showed a pro-inflammatory phenotype with progressing PMI, and more markedly at 1h of PMI, as reflected by a significant decrease in abundance of several compounds belonging to the prostaglandins class, including 15-deoxy-delta-12,14-Prostaglandin J2 with proved anti-inflammatory activity (**Figure 5.9-a,b**).[484] These findings might be of high importance

for limiting the false attribution of PMI changes to a disease, as previous studies have indicated that inflammation and oxidative stress play an integral/critical role in the pathophysiology of many chronic brain diseases by making the blood-brain barrier (BBB) more permeable.[485]

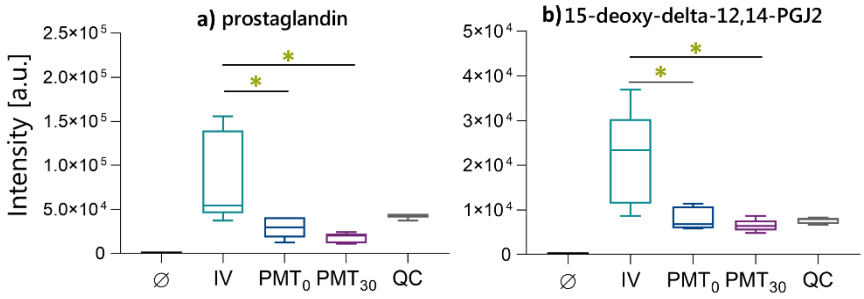

Figure 5.9: Abundance variability across the sampling timepoints for compounds belonging to the prostaglandin class (shown as absolute intensities). ⦸ - SPME fiber blank; IV – in vivo sampling; PM_{T0} –post mortem sampling at 0 min of PMI; PM_{T30} –post mortem sampling at 30 min of PMI; QC – pooled quality control samples; * - $p<0.05$

Region-specific changes in multiple bioactive lipids in early period following death were revealed

It is well known that the brain, in comparison to other organs, has a high content of lipids (40–75% of its dry weight), some two-thirds of which are phospholipids.[486] However, recent studies have also shown that sphingolipids (SLs) such as sphingomyelin, ceramides, cerebrosides, glucosylceramides, and gangliosides, which make up approximately 20% of the hippocampus, also play important roles in brain activity, especially in neuronal function through regulation of neuronal growth rates, differentiation, and cell death.[487] Among them, gangliosides, which are found in relatively high levels in brain, have gained special interest as important signaling molecules in neuronal tissue.[488] Indeed, our study seems to support the hypothesis that SLs play a critical role in brain homeostasis, as gangliosides were among the compounds displaying significant dysregulation after death.

Phospholipids such as phosphatidylethanolamine (PE) and phosphatidylcholine (PC) are major constituents of brain membranes.[486] Previous experimental studies have shown a reduction in total PE/PC mass that reflects brain degeneration *post mortem*.[489] However, the current research revealed an

opposite trend (**Figure 5.10-a**), a factor which may be attributed to discrepancies among the sampling approaches used in this and previous works (exhaustive extraction vs. non-depletive microextraction), as well as to the fact that only extensive breakdown of these compounds (exceeding 10% of their total population) would allow for observations of significant changes in their abundance between the studied groups. Moreover, we can also assume that phospholipase A2 did not change its activity at any *post mortem* interval under evaluation, since no significant differences in any of Lyso-PC compounds were observed over time.[244]

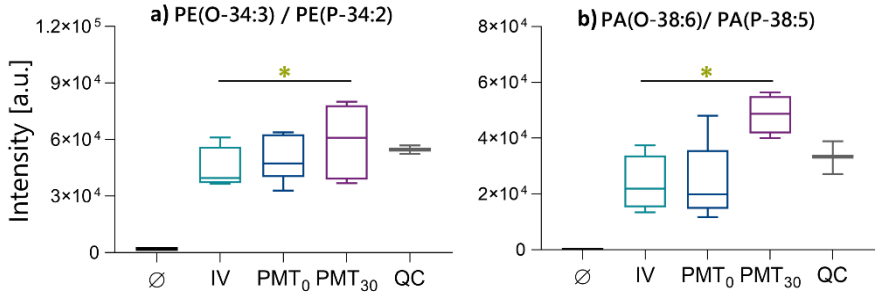

Figure 5.10: Abundance variability across the sampling timepoints for selected phospholipids (shown as absolute intensities). ⦸ - SPME fiber blank; IV – in vivo sampling; PM_{T0} –post mortem sampling at 0 min of PMI; PM_{T30} –post mortem sampling at 30 min of PMI; QC – pooled quality control samples; * - $p<0.05$

Neutral glycerides (glycerolipids), which consist of mono- (MAG), di-(DAG), and triacylglycerols (TAG), represent a low-abundance fraction of brain lipids, but their levels can become elevated under pathological conditions (including those after death). Interestingly, we have observed an increased level of only one lipid belonging to DAG class. Given that TAGs are present in low concentrations in brain tissue (accounting for <0.2% of the total lipid pool), it can be assumed that the detected, statistically significantly changing monogalactosyldiacylglycerol example comes from glycerophospholipid hydrolysis, suggesting an increase in phospholipase C activity, however with insufficient evidence. Another explanation could be the increased solubility and availability for extraction of MGDG species as a result of hydrolysis of other cell membrane constituents. Previous studies have shown preserved activity of phospholipase A2 and significant increase of activity of isoform C following death,[244,490]

however we did not detect representative number of glycerophospholipids with increasing abundances. This is most likely due to the fact that only immediate changes were monitored in this study, or that the employed LC-MS methodology was sub-optimal for detection of these species.

Despite several detected representatives of the phosphatidic acid (PA) group of lipids (**Figure 5.10-b**), their roles in brain in the context of *post mortem* changes are difficult to infer, due to the multitude of functions these lipids have,[491] including a signaling role. However, the consistent trend of increase of their abundance with the progressing PMI indicates that it may be a result of the hydrolysis of lipids belonging to the PC, PE and PI classes. Future study should focus on employing a dedicated LC-MS protocol for lipidomics in order to obtain less speculative conclusions about the changes in lipids throughout the progressing PMI.

Inter-individual variability of response to death and the role of sampling technique choice

The magnitude of the inter-individual variability (n=5) was evaluated by calculating distributions of RSDs for each of the detected features (**Figure 5.11-A1**) as well as for all compounds found to undergo statistically significant abundance changes after death (**Figure 5.11-A2**) for each sampling time point. Statistical analysis eliminated all features with RSDs over 100% and decreased the number of features with RSDs between 50 and 100%, while the ratio of features with RSDs of less than 20% and between 20 and 50% remained unchanged. As well, the ratios of numbers of features in each of the compared groups in these two RSD ranges were conserved before and after statistical analysis. This represents a long way of saying that the inter-individual variability obscures the findings by eliminating potentially meaningful metabolites which are characterized by high RSD. Comparisons of signal intensities of significant changing compounds (according to progressing PMI) across the three sampling events for the five sampled (theoretically) identical laboratory animals reveal significant intra-group variations in metabolic responses to the occurrence of death, both with respect to the magnitude of said responses, as well as their response time. The two major inhibitory and excitatory neurotransmitters undergo the

same increase in terms of trends between animals, levels, and magnitude of change (**Figure 5.11-B1**). Rat #1 exhibits a delayed reaction to death (no change in the first PMI period and very pronounced change in metabolite levels in the second period of PMI) with respect to these compounds, as well as xanthine and 5'-deoxyadenosine (both pairs are metabolically related). However, the same animal was also the first to abruptly respond to death with a threefold decrease in adenosine monophosphate levels (**Figure 5.11-B2**), a factor which discards the possibility of categorizing the subjects as slower or faster death-responders. Similarly, rat #3 presented a delayed increase of L-glutamine, but a fast decrease of adenosine monophosphate and 5-phosphoribosylamine in the first PMI period.

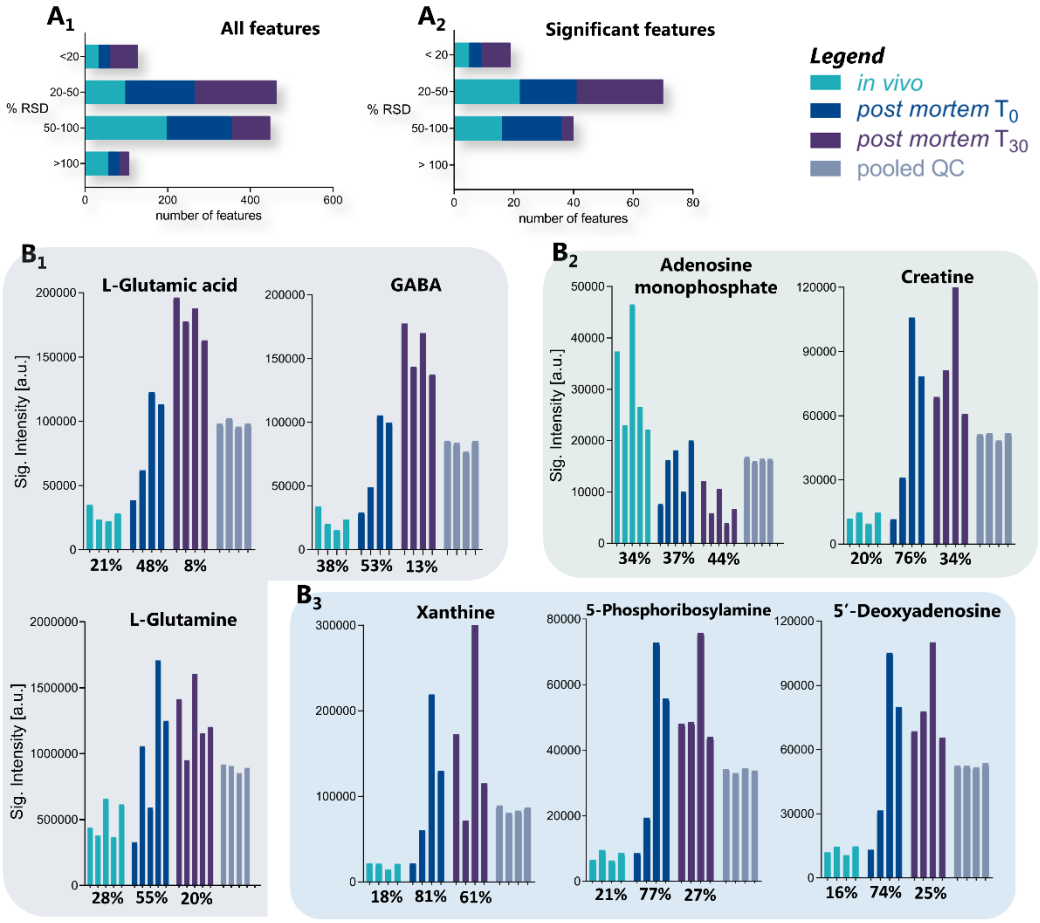

Figure 5.11: Inter-animal variability. B1- metabolites related to neurotransmission; B2- metabolites related to energy metabolism; B3- metabolites related to purine metabolism. Percentage values under the graphs represent the relative standard deviations (RSDs) of signal intensities within a given group.

Several compounds exhibited a similar trend, producing initial in vivo RSDs within the intermediate level, followed by very high variability in first PMI period, and low RSDs at the last time point (compounds involved in neurotransmission as well as purine metabolism, **Figure 5.11-B1** and **B3**, respectively). This is indicative of initially regulated processes that suddenly become unbalanced due to the occurrence of death, revealing the extent of inter-animal variability in response to dysregulation. In the last studied PMI period, these effects arrive at a plateau, demonstrating that all subjects arrived at a similar metabolic state. It could be hypothesized that continued sampling at longer PMIs would yield even lower inter-individual variability. However, this described trend is not consistent between different metabolites, even those belonging to related pathways (e.g. purine metabolism group, **Figure 5.11-B3**).

It has been generally postulated and proven experimentally that contributions to observed metabolite variability increase in the following order: instrumental analysis, sample preparation, and biological contribution.[492,493] Within the biological contribution, the inter-individual variability usually exceeds the intra-individual variability; however, a reverse or insignificant relation may also be observed depending on the employed techniques, subjects used, and focus of study, etc.[494,495] Precautions such as using animals from the same strain to ensure very close genetic similarity, standardizing the housing, dietary, and experimentalconditions, as well as closely synchronizing the time of sacrifice immediately following respiratory arrest all help to decrease but do not eliminate the inherent inter-individual variability. The suggested natural inter-individual diversity in brain networks underlying multiple brain processes,[496] would in turn leave a molecular trace which would vary accordingly.[497] The existence of inherent inconsistencies among metabolic profiles of a study group can be at least partially compensated by proper choice of sampling strategy. Techniques with multi-compound extraction and in vivo capabilities that additionally provide broad (or relatively broad) analyte coverage such as SPME and

microdialysis (MD) allow for repeated sampling of a single subject,[438,492,498] decreasing the required number of animals and consequently also inter-animal variability. To achieve this through MD, the recovery of each probe would ideally have to be determined for each animal, which is not always feasible due to technical and time constraints.[499] Therefore, the choice of SPME as the most suitable in vivo sampling technique for this study is facilitated by the simplicity of use of each animal as its own control. At the same time, the persistent inter-individual variability demonstrated in this study necessitates use of a larger study population (definitely beyond 5 animals, which represent a rather statistically underpowered population) to ensure arrival at reliable and correct biological conclusions. Additional dependence of this variability on the metabolites under consideration implies that perhaps individual metabolite abundances are subjected to different changes in comparison to groups of correlated metabolites under altered physiological conditions,[500] including the occurrence of death. Identification of these correlations and comparisons between studied sampling timepoints in terms of significant correlations rather than significant compounds could provide improved and more conclusive discrimination, despite high inter-animal variability at the single-metabolite level.

Sampling strategy affects the recovered metabolic profile

When setting out to measure purely endogenous phenomena one must also consider how the sampling method itself affects the metabolic profile of neural tissue. The claimed non-disruptive nature of SPME remains true due to the negligible extraction characteristics and as compared to non-in vivo techniques. However, when zooming in only on the in vivo methods requiring probe insertion (including chemical sensors, recording microelectrodes, MD, and SPME) the tissue damage is unavoidable, therefore the invasiveness constitutes a limitation shared amongst them. The indirect evidence for non-disruptive character of SPME has been its capability of monitoring changes in elusive metabolites such as adenosine monophosphate or glutathione.[492] However, no direct evidence for the adverse effects of SPME probe insertion or lack of thereof are available in literature in the aspect of

affecting the recovered metabolite profile. By similarity, these would be analogous to the effects of the MD sampling, for which studies offer more explanation. Any probe larger than 60 μm in diameter is in turn larger than the approximate spacing between blood vessels in brain tissue, meaning that probe insertion undeniably leads to local blood-brain-barrier disruption.[501] This changes the availability of some metabolites present in blood, deeming them extractable by the probe. The evoked inflammatory response would logically affect the metabolic profile obtained via SPME to a greater extent than MD, due to SPME's proven capability of extracting hydrophobic inflammation mediators.[251] The immobilization of anti-inflammatory agents such as dexamethasone has been proposed for SPME[251] and MD[502] probes to mitigate the adverse outcomes, however introducing pharmaceuticals may be counterproductive to monitoring unchanged endogenous environments. Another consequence of brain tissue penetration injury is response of glial cells, ultimately leading to formation of scar tissue, whose influence on analyte diffusion towards the probe is yet unexplored,[502] however it is expected to play less of a role in case of short-term probe insertion. Even though the SPME probe is not inserted into brain for long enough to cause scar tissue formation (here the SPME's lack of continuous sampling capabilities can be considered an advantage), microglia still respond to the injury within minutes,[502] potentially affecting the observed metabolic profile. Conversely, the fact that in vivo SPME only allows discrete sampling events introduces the necessity of multiple probe insertions.[136] The listed effects have been reported to cause underestimation of absolute concentrations of extracellular neurochemicals by MD, while remaining suitable for relative measurements.[503] The consequences of probe implantation influencing the metabolic status of neurochemical environment has also deemed the invasive in vivo techniques a domain of scientific explorations rather than common clinical practice.[504]

Nevertheless, in vivo sampling with probes remains less disruptive to the metabolic profile than tissue excision followed by sample preparation. Even small delay between tissue excision and fixation can significantly alter the recovered metabolic profile due to the hypoxic conditions and rapid

enzymatic degradation.[505] Moreover, even in the realm of in vivo techniques, procedures such as anesthesia have been shown to affect recovered metabolite profile significantly, pointing out the advantage of employing probes that allow free movement of the animals during sampling.[492,503] The described adverse effects also do not diminish the undoubtable biocompatibility of the SPME device, as they concern only the damage upon tissue penetration, which is unavoidable. Ultimately, the sampling technique choice for broad metabolic profiling represents a *lesser of two evils* scenario and a trade-off between the adverse effects of more invasive techniques and the gains in chemical information enabled by monitoring multitude of analytes in awake subjects.

Since sampling of extracellular fluid with probes inevitably leads to rupturing of some cells upon probe insertion, the extracted metabolic profile represents mostly extracellular environment with contribution of the intracellular contents from the ruptured cells. After death and with progressing PMI larger population of cells undergoes disintegration even without external intervention due to the *post mortem* autolysis and apoptosis triggered by ATP depletion under hypoxic conditions.[506] However, despite the fact that parts of hippocampus are particularly susceptible to cell autolysis under hypoxia, these effects only gain significance after several hours of PMI.[506,507] Therefore, in this study the pronounced effect of post mortem cell autolysis, involving increase of the intracellular contribution to the sampled metabolic profile, would not be captured due to the very short period of PMI taken into consideration. Future studies entailing sampling throughout extended period of PMI followed by metabolic profiling could contribute new findings into the metabolic aspect of *post mortem* cell autolysis and its correlation with the PMI.

5.5 Conclusions

We demonstrated that changes in levels of low molecular mass metabolites and lipids significantly alter brain neurochemistry as soon as within the first 30 min of PMI. Amongst the affected pathways,

some are especially alarming as their members, direction, and magnitude of changes are consistent with disease-specific changes reported in literature and assumed to occur *in vivo*. Capturing these changes was enabled by the choice of SPME as sampling technique. The experimental model of sampling the same brain area in the same animal subjects repeatedly and both *in vivo* as well as *post mortem* is quite unique and relatively underutilized in neuroscience, where reliance on *post mortem* samples remains (somewhat understandably in case of human samples) strong. We envision this model approach as a necessary pre-requisite in future studies aiming at disease biomarkers identification in *post mortem* tissue samples. The preliminary experiments should focus on identifying metabolites and pathways undergoing significant alterations solely in response to death and sample treatment (should any be employed). The findings should then be applied as a filtering criteria to the data acquired in subsequent studies focusing on disease-specific changes, adding in this way to the relevance of investigations of pathophysiologically changed tissue, as changes observed only due to death will be discarded as artefacts.

The analysis of samples affected by progressing *post mortem* changes combined with the target sample being as complex as the brain tissue adds another level of complexity to interpretation of data from any experimental workflow. Even with proven reduction of inter-animal variability of measurements by SPME, we experienced severe diversity in our study in response to death amongst animals in identical conditions in terms of fast/delayed change in metabolites levels. This prompted a postulate to rethink the approach to untargeted metabolomics data analysis and interpretation, suggesting that correlated metabolite changes are perhaps more informative than alterations at single metabolite levels.

5.5.1 Constructive self-criticism and future directions

Throughout data processing and interpretation of the results we have identified several shortcomings of the employed approach which contributed to obtaining findings of limited usefulness for the

neuroscience community. At the same time, the general consensus exists that the concern for delays in processing brain tissue samples leading to metabolic artefacts is well-founded and largely unresolved. Based on this study we believe that employment of SPME for studies like such can be beneficial as a basic research aiding removal of ambiguity from the metabolic alterations arising from death-induced changes in neurochemical environment.

We therefore propose an improved experimental protocol to be explored in the future, taking into account elimination of the identified shortcomings. The insufficient number of animal subjects (*n=5*) will be at least doubled to attain more powerful statistical representation and further decrease the effect of inter-individual variability in response to death. The improved experimental protocol will be conducted according to the timeline depicted in **Figure 5.12**. The modifications include increasing the number of *in vivo* sampling events to 3 consecutive extractions for each animal, in order to establish a stronger baseline. The sampling duration will be decreased to 15 min aiming at improvement of temporal resolution and decreasing the data variability in an instance where significant metabolite alterations occur within the previously longer (30 min) sampling period with different magnitude in different subjects. This is expected to aid obtaining data points corresponding to more discrete metabolic states and decrease the contribution from the time-weighted average character of SPME sampling.

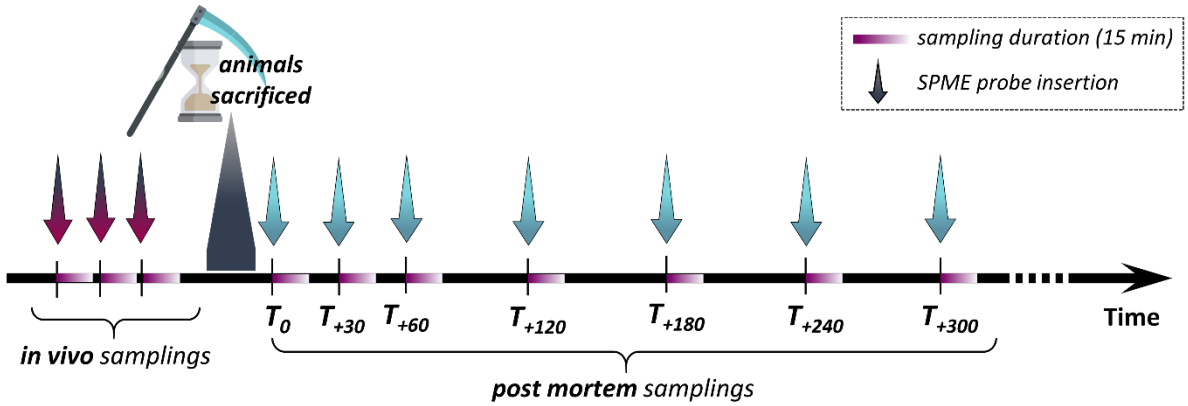

Figure 5.12: Proposed experimental timeline for improved protocol of a follow-up study.

Furthermore, additionally to focusing on the changes occurring within the first hour of PMI, the sampling will continue up to 5-10 h of PMI, with the time intervals between SPME events increasing to one collection per hour. Lastly, new design involves bilateral probe insertion into the brain, with probe dedicated for metabolomic investigation (mixed-mode extracting phase) in one hemisphere and probe dedicated for lipidomic analysis (C18 extracting phase) simultaneously inserted into the other hemisphere.

The post-sampling protocol modifications involve inclusion of antioxidant into the desorption solution in order to protect metabolites with compromised stability against degradation. To better capture short-lived and labile metabolites, the desorption and LC-MS analysis will occur immediately after probe collection. Finally, as emphasized in subchapter 2.4 the metabolites unaffected by death and the progressing PMI are of equal importance as the altered metabolites for inferring the involvement of certain pathways in the response to death. Properly taking both groups into consideration relies upon conclusive feature identification employing annotation algorithms, MS/MS fragmentation patterns matching and comparison with authentic standards whenever possible. Since constant progress in building MS/MS fragmentation databases is being made, we expect the improved protocol to be met with more reliably identified metabolites.

These protocol enhancements are expected to truly take advantage of the unique properties of *in vivo* SPME sampling by capturing the changes in short-lived compounds and decreasing the inter-individual variability brought by using each animal as its own control (for this purpose, paired statistical analysis will be explored at the data processing stage). The advantage gained on the *post mortem* side by significant extension of the investigated PMI window is expected to benefit the field of forensic science, as well as give the ability corroborate the findings with literature pertaining to the markers of progressing PMI.

Chapter 6
Conclusions and Future Explorations

Conclusions

Chemical analysis of such immensely complex matrix as brain tissue, additionally carried out *in vivo* constitutes a real challenge and an ultimate test for an analytical technique's adaptability to real-life scenarios. It was demonstrated how some strategies deemed suitable for certain purpose and thoroughly validated in simulated laboratory conditions undergo a harsh reality check during *in vivo* sampling in real exploratory applications. For example, detection and quantitative analysis of small hydrophilic molecules present at notoriously low physiological levels in brain, such as epinephrine and norepinephrine, currently remains a limitation of SPME. Additionally, the diffusion-based extraction mechanism inherently imposes temporal resolution that may be orders of magnitude lower than required for observation of transient dynamic neurotransmission events. At the same time, creativity of analytical solutions for brain tissue analysis is often rewarded, as a comprehensive set of guidelines for the *in vivo* analysis of solid tissues does not exist.

Fulfillment of the need for interdisciplinary approach as well as coexistence and cooperation of multiple tools in pursuit of innovation in brain studies has been demonstrated by the electrophysiology guided multi-site measurement of several neurotransmitters across the fronto-striatal network in nonhuman primates employing *in vivo* SPME and analysis by LC-MS/MS. The spatially resolved analysis utilizing the SPME-DESI-MS coupling added one more operation mode to the portfolio of SPME and an additional dimension of information obtained from *in vivo* sampling. This analysis mode has also highlighted some fundamental aspects of the extracting phase properties in conjunction with microdesorption mechanism, as well as the influence of diffusion-based mechanism of SPME on the method's performance in terms of spatial resolution and sensitivity. A culmination of the quantitative and spatially resolved capabilities of *in vivo* SPME was illustrated in application to characterization of

systemic and local release of ketamine in brain via a multi-purpose platform involving SPME-LC-MS/MS and SPME-DESI-MS/MS. Finally, the broad analyte coverage provided by SPME was explored in the context of untargeted metabolomic profiling of the response to the death in rat hippocampus as well as metabolomic profiling of macaque brain in three locations at a baseline of stable behavioral conditions.

Throughout this thesis a high emphasis was placed on method development with the real life conditions of *in vivo* sampling in mind. All instances of *in vivo* experiments also represented on site sampling, as the animal facilities and the analytical chemistry core facility were located within significant distances from one another (different cities or countries). This required increased attention to the technical aspect of the SPME sampling events, illustrated by development of custom probe assemblies and ways of accessing brain with the probes convenient for scientists not necessarily accustomed to SPME. Moreover, in case of targeted studies, experimental evaluation of the stability of analytes under various storage conditions over the period of several weeks has become an indispensable part of method development, resulting in recommendations for the time and type of storage eliminating or limiting potential analytes loss.

The work presented in this thesis fulfills the research objectives by demonstrating that solid phase microextraction-based strategies are capable of keeping up with the requirements of current-day neuroscientific investigations. This is further supported by the evident interest in this technology amongst the neuroscientific community for quantitative monitoring of endogenous molecules and drug pharmacokinetics, as well as distribution of molecules within brain tissue. This work epitomizes an interdisciplinary approach to brain studies with the end result of the developed strategies being taken outside of the analytical chemistry lab.

Future explorations

Future efforts will inevitably focus on increasing SPME device affinity towards small hydrophilic molecules, including polar compounds such as neurotransmitters. Although a high level of specialization and customization can aid achieving these goals, such as has been illustrated by the example of synthesis of a dedicated extracting phase for isolation of neurotransmitters, this solution can, in hindsight, delay or hinder broad availability of the technology. Therefore, further expansion of SPME into neuroscience investigations will strongly rely on the efforts to make the tool available for others by commercialization or streamlining the process of probes manufacturing. On the other hand, the same example of probe customization also illustrates that the *one size fits all* solution is an unrealistic concept in brain studies, therefore some extent of tool personalization and modification cannot be avoided.

While the binder used to prepare SPME coatings has been often neglected in optimization processes and treated as a constant, it nevertheless constitutes a biocompatible membrane and an integral part of the extracting phase. This realization opens up a whole realm of opportunities to focus on the binder as the source of modifications and improvements. One example, discussed in Chapter 2, is the modification of pH of the binder by immobilization of certain moieties which would in turn improve affinity and reproducibility for isolation of polar molecules.

The frequently observed and discussed properties of SPME extracting phases providing superior extracting efficiency and sensitivity for lipophilic compounds should be leveraged in future studies, as *in vivo* lipid analysis in brain is an unexplored area of undisputed importance. Lipids have been associated with brain injury and diseases, and the current state of the research could benefit from robust and quantitative methods for their analysis *in vivo*. However, to establish SPME in this field, more basic targeted and untargeted studies are required, to characterize the classes of lipids available for SPME, existence of the quantitative relationship between repeated *in vivo* SPME and the levels of lipids in

brain tissue, as well as an assessment of the lipid measurement accuracy and its sufficiency to capture regulatory variation of lipids in brain.

Coupling of SPME with direct-to-MS approaches is often perceived as one of the ways of maximizing analytical sensitivity by matching the level of analyte preconcentration on the SPME device with low dilution compared to LC-MS approaches. However, approaches compatible with minimally-invasive brain sampling using probes, such as nano-ESI and microfluidic open interface (MOI), rely on conducting the desorption and MS analysis in real time, effectively giving only one attempt at the instrumental analysis, without the option of re-running the samples. For this reason, these approaches were not explored here, since every sample collected *in vivo* is unique and multiple types of analyses were often intended for a single sample (*e.g.* targeted analysis and untargeted metabolomic profiling). However, while the sensitivity gain by direct-to-MS coupling remains somewhat speculative due to the lack of systematic cross-validation against LC-MS, these techniques unquestionably provide higher speed and throughput of analysis. Therefore, implementation of SPME-nanoESI-MS or SPME-MOI-MS for the analysis of *in vivo* brain samples could benefit applications such as targeted monitoring of pharmacokinetics of xenobiotics for therapeutic drug monitoring, drug discovery, and drug development studies.

One of the most significant leaps towards widespread use of SPME in brain studies will be achieved by its validation for *in vivo* analysis of peptides, predicted to happen in the near future. The largest subclass of neuromodulators with tremendous importance for regulation of proper brain function has been so far unexplored by SPME. However, this state is about to change, as development of protocols and extracting phases suitable for peptide analysis are currently underway.

Molecular imaging by mass spectrometry has been widely adapted to brain studies as the linkage of molecular information with its spatial distribution within the sample perfectly complements the

structural and functional heterogeneity of brain. The advantage of being able to image whole brain tissue sections with virtually no pre-treatment and cleanup needed, combined with the staggering advancements in mass spectrometry, signal processing and bioinformatic platforms have ultimately led to the current undeniable success of DESI imaging, perhaps suggesting that derivative techniques relying on the use of substrate may be obsolete. However, the use of substrates such as SPME sorbents immobilized on an appropriate DESI-amenable support could in principle enhance the chemical information obtained by DESI imaging, bringing in versatility of the substrate chemistries that could answer different scientific questions. Therefore, future studies should explore a side-by-side comparison of tissue section versus SPME imprint imaging in two dimensions.

While the contribution of SPME to 2D imaging is yet to be evaluated, giving up one dimension in exchange for the spatially-resolved analysis *in vivo*, without the need of animals sacrifice and tissue slicing is undoubtedly one of the outcomes of this work with serious prospects of being adapted in neuroscience. There is a high demand for minimally-invasive *in vivo* measurements of distribution of neurochemicals across cortical layers and visualization of the effective area of drug release and metabolite formation, following local drug administration. The success of the SPME-DESI-MS platform for these purposes will depend on gaining further insight into the principles governing the extraction-desorption-ionization interactions, as well as lowering the technical barrier to entry of this practically challenging approach.

Even though the strategy of broad extraction by SPME followed by untargeted detection by MS and *post hoc* decision about what molecules are important may be foreign to hypothesis-oriented biological sciences, MS-based metabolomics is undoubtedly capable of revealing the properties of a biological system in a comprehensive way. SPME presents itself as a technique currently providing the broadest analyte coverage with *in vivo* capabilities. Even though MS-based and presumably also SPME-based metabolomics are now integral part of the brain studies landscape, metabolites inherently reflect the

phenotype and therefore a functional status of the system. This constitutes a confounding factor for indisputable and reproducible inference of roles of small metabolites in etiology of brain disorders, or their involvement in brain circuitry. Therefore, future metabolomic investigations should always be validated by methods capable of confirming the causality of the observed metabolic changes (lesions, gene inactivation, *etc.*), rather than rely purely on observed correlations.

Lastly, the ultimate goal is to transfer SPME from within the analytical chemistry lab to the hands of specialists from other fields, including the field of neuroscience. With the demonstrated simplicity, versatility and broad applicability of this tool, the outlined objective does not only seem realistic, but is also in motion at the moment these words are being written. The final evaluation of SPME in brain studies will be in the hands of the users.

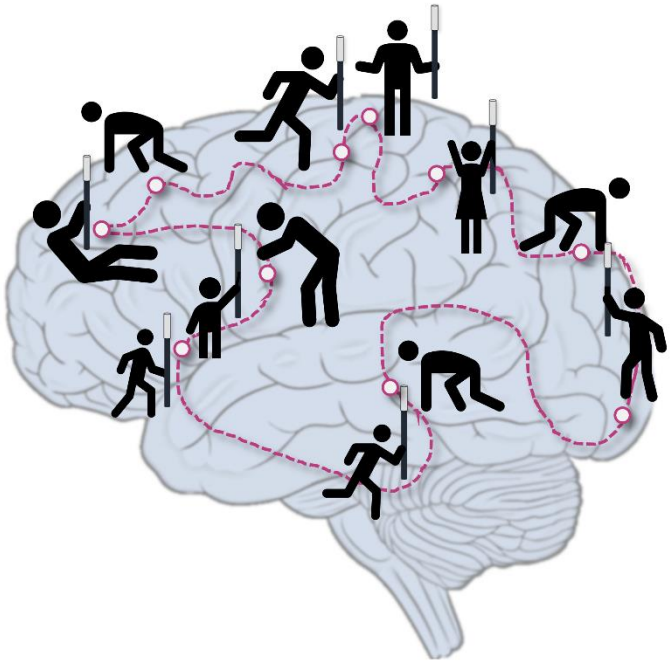

Letters of copyright permission

Chapter 2

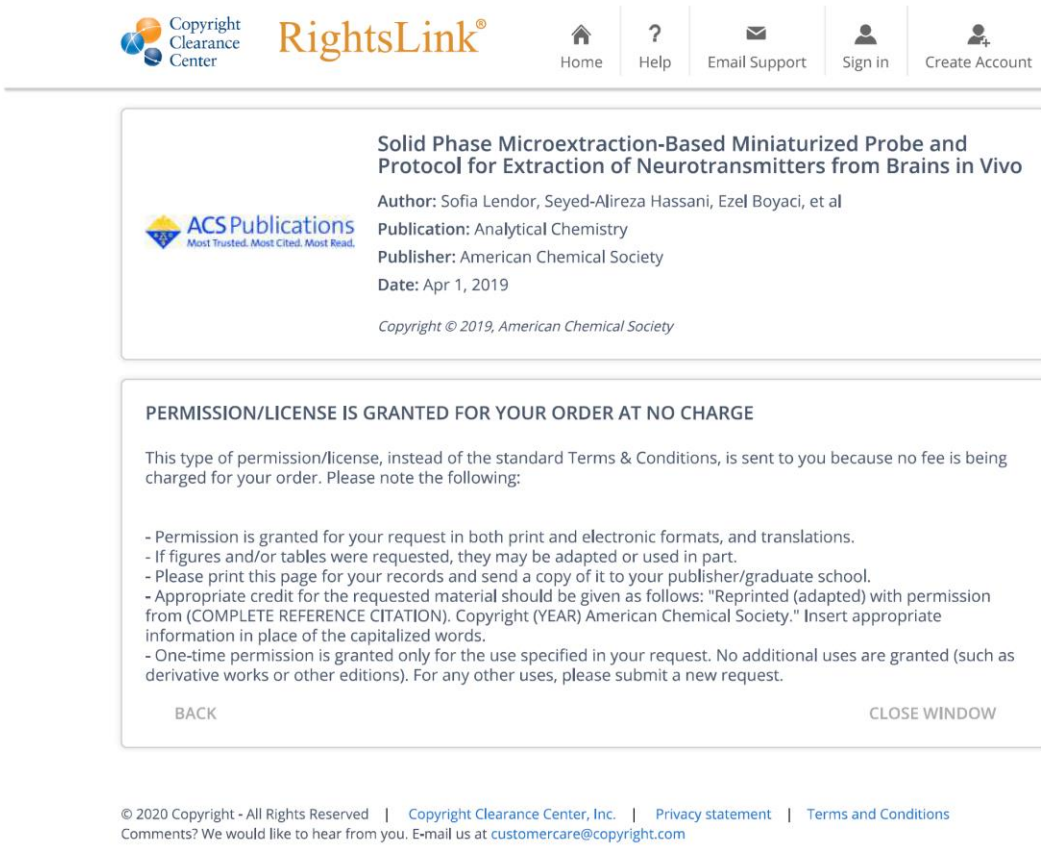

Copyright Clearance Center RightsLink®

Home | Help | Email Support | Sign in | Create Account

ACS Publications
Most Trusted. Most Cited. Most Read.

Solid Phase Microextraction-Based Miniaturized Probe and Protocol for Extraction of Neurotransmitters from Brains in Vivo

Author: Sofia Lendor, Seyed-Alireza Hassani, Ezel Boyaci, et al

Publication: Analytical Chemistry

Publisher: American Chemical Society

Date: Apr 1, 2019

Copyright © 2019, American Chemical Society

PERMISSION/LICENSE IS GRANTED FOR YOUR ORDER AT NO CHARGE

This type of permission/license, instead of the standard Terms & Conditions, is sent to you because no fee is being charged for your order. Please note the following:

- Permission is granted for your request in both print and electronic formats, and translations.
- If figures and/or tables were requested, they may be adapted or used in part.
- Please print this page for your records and send a copy of it to your publisher/graduate school.
- Appropriate credit for the requested material should be given as follows: "Reprinted (adapted) with permission from (COMPLETE REFERENCE CITATION). Copyright (YEAR) American Chemical Society." Insert appropriate information in place of the capitalized words.
- One-time permission is granted only for the use specified in your request. No additional uses are granted (such as derivative works or other editions). For any other uses, please submit a new request.

BACK CLOSE WINDOW

Copyright and Permissions

Reuse by Authors of Their Work Published by APS | Reuse by Non-authors of APS Published Content

Reuse in APS Publications of non-APS Published Content

Reuse by Authors of Their Work Published by APS

The APS Journals are copyrighted for the protection of authors and the Society. The Mandatory Submission Form serves as the Society's official copyright transfer form. Author's rights to reuse their APS-published work are described below:

Republication in New Works	Authors may republish parts of their final-published work (e.g., figures, tables), without charge and without requesting permission, provided that full citation of the source is given in the new work.
Meeting Presentations and Conferences	Authors may use their work (in whole or in part) for presentations (e.g., at meetings and conferences). These presentations may be reproduced on any type of media in materials arising from the meeting or conference such as the proceedings of a meeting or conference. A copyright fee will apply if there is a charge to the user or if the materials arising are directly or indirectly commercially supported[1]. Full citation is required.
Theses and Dissertations	Authors may reproduce whole published articles in dissertations and post to thesis repositories without charge and without requesting permission. Full citation is required.
Open Courseware	Authors may post articles, chapters or parts thereof to a public access courseware website. Permission must be requested from the APS[1]. A copyright fee will apply to a book chapter and during the first 12 months of a journal article's publication. Full citation is required.
Websites	Authors may not post a PDF of the accepted or final version of their published work to any website including social and research networking platforms; instead, links may be posted to the APS or publisher partner website where the work is published[1] (see exception to authors' own institution's repository, as note below).
Institutional Repositories (non-theses)	Authors may deposit their accepted, peer-reviewed journal manuscripts into an institutional repository providing: ◦ the APS retains copyright to the article[1] ◦ a 12-month embargo period from the date of final publication of the article is observed by the institutional repository and the author ◦ a link to the article published on the APS or publisher-partner website is prominently displayed alongside the article in the institutional repository ◦ the article is not used for commercial purposes ◦ self-archived articles posted to repositories are without warranty of any kind
	[1]Unless it is published under the APS Open Access (*AuthorChoice*) option, which allows for immediate public access under a Creative Commons license (CC BY 4.0) (See also the APS Policy on Depositing Articles in PMC.)

Rights and permissions

About this article

Cite this article

Hassani, S., Oemisch, M., Balcarras, M. *et al.* A computational psychiatry approach identifies how alpha-2A noradrenergic agonist Guanfacine affects feature-based reinforcement learning in the macaque. *Sci Rep* **7,** 40606 (2017). https://doi.org/10.1038/srep40606

Chapter 3

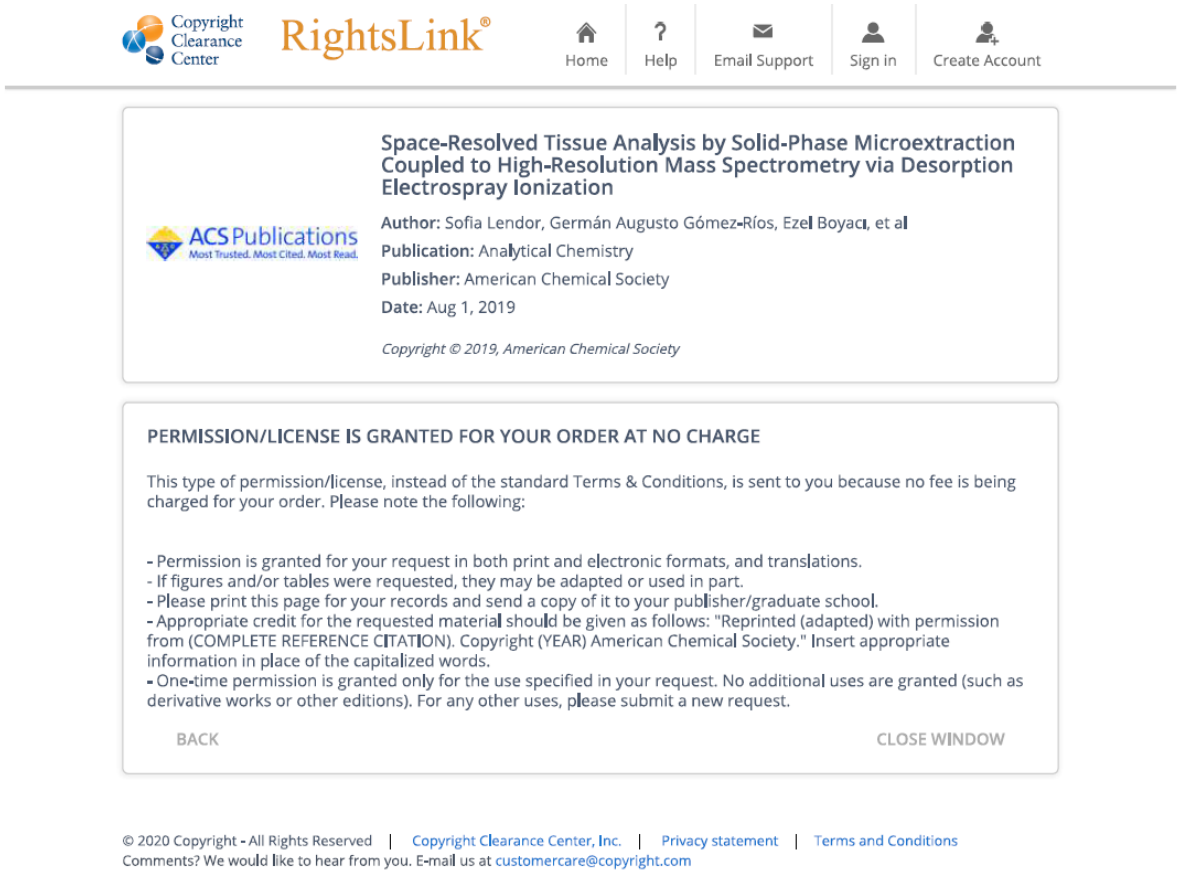
Copyright Clearance Center
RightsLink®
Home
Help
Email Support
Sign in
Create Account
Space-Resolved Tissue Analysis by Solid-Phase Microextraction Coupled to High-Resolution Mass Spectrometry via Desorption Electrospray Ionization
ACS Publications
Most Trusted. Most Cited. Most Read.
Author: Sofia Lendor, Germán Augusto Gómez-Ríos, Ezel Boyacı, et al
Publication: Analytical Chemistry
Publisher: American Chemical Society
Date: Aug 1, 2019
Copyright © 2019, American Chemical Society
PERMISSION/LICENSE IS GRANTED FOR YOUR ORDER AT NO CHARGE
This type of permission/license, instead of the standard Terms & Conditions, is sent to you because no fee is being charged for your order. Please note the following:
- Permission is granted for your request in both print and electronic formats, and translations.
- If figures and/or tables were requested, they may be adapted or used in part.
- Please print this page for your records and send a copy of it to your publisher/graduate school.
- Appropriate credit for the requested material should be given as follows: "Reprinted (adapted) with permission from (COMPLETE REFERENCE CITATION). Copyright (YEAR) American Chemical Society." Insert appropriate information in place of the capitalized words.
- One-time permission is granted only for the use specified in your request. No additional uses are granted (such as derivative works or other editions). For any other uses, please submit a new request.
BACK
CLOSE WINDOW
© 2020 Copyright - All Rights Reserved | Copyright Clearance Center, Inc. | Privacy statement | Terms and Conditions
Comments? We would like to hear from you. E-mail us at customercare@copyright.com

Chapter 5

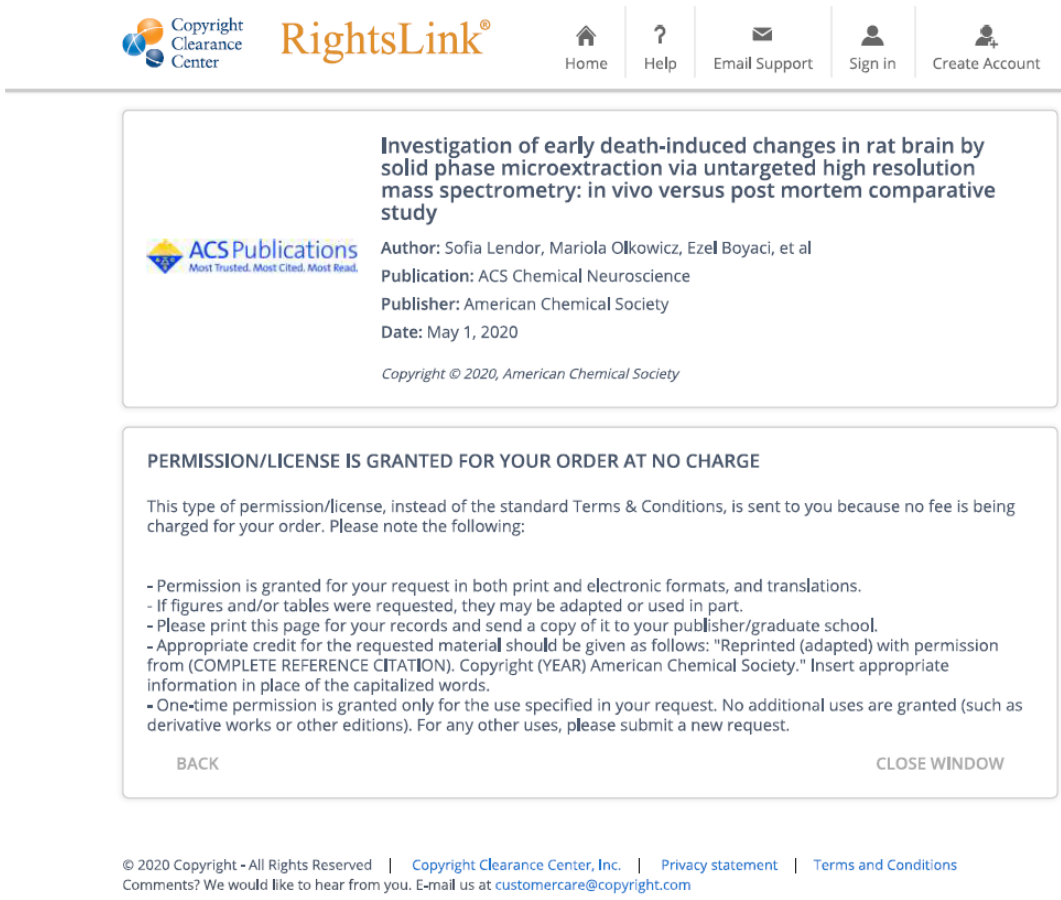

Copyright Clearance Center RightsLink®

Home | Help | Email Support | Sign in | Create Account

Investigation of early death-induced changes in rat brain by solid phase microextraction via untargeted high resolution mass spectrometry: in vivo versus post mortem comparative study

ACS Publications
Most Trusted. Most Cited. Most Read.

Author: Sofia Lendor, Mariola Olkowicz, Ezel Boyaci, et al
Publication: ACS Chemical Neuroscience
Publisher: American Chemical Society
Date: May 1, 2020

Copyright © 2020, American Chemical Society

PERMISSION/LICENSE IS GRANTED FOR YOUR ORDER AT NO CHARGE

This type of permission/license, instead of the standard Terms & Conditions, is sent to you because no fee is being charged for your order. Please note the following:

- Permission is granted for your request in both print and electronic formats, and translations.
- If figures and/or tables were requested, they may be adapted or used in part.
- Please print this page for your records and send a copy of it to your publisher/graduate school.
- Appropriate credit for the requested material should be given as follows: "Reprinted (adapted) with permission from (COMPLETE REFERENCE CITATION). Copyright (YEAR) American Chemical Society." Insert appropriate information in place of the capitalized words.
- One-time permission is granted only for the use specified in your request. No additional uses are granted (such as derivative works or other editions). For any other uses, please submit a new request.

BACK CLOSE WINDOW

© 2020 Copyright - All Rights Reserved | Copyright Clearance Center, Inc. | Privacy statement | Terms and Conditions
Comments? We would like to hear from you. E-mail us at customercare@copyright.com

References

(1) Dick, P. K. Do Androids Dream of Electric Sheep? Doubleday, 1968.

(2) Herculano-Houzel, S. *Front. Hum. Neurosci.* **2009**, *3* (November), 1–11.

(3) Drachman, D. A. *Neurology* **2005**, *64* (12), 2004–2005.

(4) Kaku, M.; Lane, A. 1st Ed.; The Future of the Mind (The Scientific Quest to Understand, Enhance, and Empower the Mind); Doubleday: United States, 2014.

(5) Licata, G. *J. Comput. Sci. Syst. Biol.* **2015**, *8* (3), 124–126.

(6) Fox, K. C. R.; Andrews-Hanna, J. R.; Christoff, K. *Neuroscience* **2016**, *335*, 134–150.

(7) Marblestone, A. H.; Wayne, G.; Kording, K. P. *Front. Comput. Neurosci.* **2016**, *10* (SEP), 1–41.

(8) Sirignano, J.; Spiliopoulos, K. *SIAM J. Appl. Math.* **2020**, *80* (2), 725–752.

(9) Buffalo, E. A.; Movshon, J. A.; Wurtz, R. H. *PNAS* **2019**, *116* (52), 26167–26172.

(10) Fornito, A.; Zalesky, A.; Breakspear, M. *Nat. Publ. Gr.* **2015**, *16* (3), 159–172.

(11) Uhlhaas, P. J.; Singer, W. *Neuron* **2006**, *52* (1), 155–168.

(12) Eccles, J. C. *Perspect. Biol. Med.* **1968**, *12* (1), 61–68.

(13) Jorgenson, L. A.; Newsome, W.; Anderson, D. J.; Bargmann, C. I.; Brown, E. N.; Deisseroth, K.; Donoghue, J. P.; Hudson, K. L.; Ling, G. S. F.; Macleish, P. R.; et al. *Philos. Trans. R. Soc. B Biol. Sci.* **2015**, *370* (1668), 20140164.

(14) Bonner, A. M. *Neurodiagn. J.* **2015**, *55* (1), 46–53.

(15) Devor, A.; Bandettini, P. A.; Boas, D. A.; Bower, J. M.; Buxton, R. B.; Cohen, L. B.; Dale, A. M.; Einevoll, G. T.; Fox, P. T.; Franceschini, M. A.; et al. *Neuron* **2013**, *80* (2), 270–274.

(16) Ganesana, M.; Lee, S. T.; Wang, Y.; Venton, B. J. *Anal. Chem.* **2017**, *89* (1), 314–341.

(17) Wu, F.; Yu, P.; Mao, L. *ACS Omega* **2018**, *3* (10), 13267–13274.

(18) Zilberter, Y.; Zilberter, T.; Bregestovski, P. *Trends Pharmacol. Sci.* **2010**, *31* (9), 394–401.

(19) Opitz, A.; Falchier, A.; Linn, G. S.; Milham, M. P.; Schroeder, C. E. *PNAS* **2017**, *114* (20), 5243–5246.

(20) Kennedy, R. T. *Curr. Opin. Chem. Biol.* **2013**, *17* (5), 860–867.

(21) Darvesh, A. S.; Carroll, R. T.; Geldenhuys, W. J.; Gudelsky, G. A.; Klein, J.; Meshul, C. K.; Van Der Schyf, C. J. *Expert Opin. Drug Discov.* **2011**, *6* (2), 109–127.

(22) Loryan, I.; Fridén, M.; Hammarlund-Udenaes, M. *Fluids Barriers CNS* **2013**, *10* (1), 1–9.

(23) Palmer, M.; Chan, A.; Dieckmann, T.; Honek, J. Biochemical Pharmacology, John Wiley & Sons, Inc.: Hoboken, New Jersey, 2012.

(24) Anderzhanova, E.; Wotjak, C. T. *Cell Tissue Res* **2013**, 27–39.

(25) Haber, S. N.; Knutson, B. *Neuropsychopharmacology* **2010**, *35* (1), 4–26.

(26) Sykova, E.; Nicholson, C. *Physiol. Rev* **2008**, *88*, 1277–1340.

(27) Lossi, L.; Merighi, A. *Front. Vet. Sci.* **2018**, *5* (July), 1–14.

(28) Carter, M.; Shieh, J. 2nd Ed.; Guide to Research Techniques in Neuroscience; Academic Press, 2015.

(29) Vaidya, A. R.; Pujara, M. S.; Petrides, M.; Murray, E. A.; Fellows, L. K. *Trends Cogn. Sci.* **2019**, *23* (8), 653–671.

(30) Wood, P. L. *Neuropsychopharmacology* **2014**, *39* (1), 24–33.

(31) Römpp, A.; Spengler, B. *Histochem. Cell Biol.* **2013**, *139* (6), 759–783.

(32) Hanrieder, J.; Phan, N. T. N.; Kurczy, M. E.; Ewing, A. G. *ACS Chem. Neurosci.* **2013**, *4* (5), 666–679.

(33) Amstalden van Hove, E. R.; Smith, D. F.; Heeren, R. M. A. *J. Chromatogr. A* **2010**, *1217* (25), 3946–3954.

(34) Wu, C.; Dill, A. L.; Eberlin, L. S.; Cooks, R. G.; Ifa, D. R. *Mass Spectrom. Rev.* **2013**, *32*, 218–243.

(35) Poole, C.; Mester, Z.; Miró, M.; Pedersen-Bjergaard, S.; Pawliszyn, J. *Pure Appl. Chem.* **2016**, *88* (5), 517–558.

(36) Pawliszyn, J. Handbook of Solid Phase Microextraction, Elsevier: Amsterdam, 2012.

(37) Gionfriddo, E. *Phys. Sci. Rev.* **2020**, DOI: https://doi.org/10.1515/psr-2020-0006.

(38) Emmons, R. V.; Tajali, R.; Gionfriddo, E. *Separations* **2019**, *6* (3), 1–22.

(39) Gómez-Ríos, G. A.; Mirabelli, M. F. *TrAC - Trends Anal. Chem.* **2019**, *112*, 201–211.

(40) Souza-Silva, É. A.; Reyes-Garcés, N.; Gómez-Ríos, G. A.; Boyaci, E.; Bojko, B.; Pawliszyn, J. *TrAC - Trends Anal. Chem.* **2015**, *71*, 249–264.

(41) Reyes-Garcés, N.; Gionfriddo, E. *TrAC - Trends Anal. Chem.* **2019**, *113*, 172–181.

(42) Grandy, J.; Lashgari, M.; Singh, V.; Pawliszyn, J. *LCGC North Am.* **2019**, *37* (9), 690–697.

(43) Roszkowska, A.; Yu, M.; Pawliszyn, J. In *A New Paradigm for Environmental Chemistry and Toxicology*; Springer, Singapore, 2020; p 1.

(44) Piri-Moghadam, H.; Ahmadi, F.; Pawliszyn, J. *TrAC - Trends Anal. Chem.* **2016**, *85*, 133–143.

(45) Xu, C. H.; Chen, G. S.; Xiong, Z. H.; Fan, Y. X.; Wang, X. C.; Liu, Y. *TrAC - Trends Anal. Chem.* **2016**, *80*, 12–29.

(46) Kataoka, H.; L.Lord, H.; Pawliszyn, J. *J. Chromatogr. A* **2000**, *880*, 35–62.

(47) He, Y.; Concheiro-Guisan, M. *Biomed. Chromatogr.* **2019**, *33* (1), 1–12.

(48) Pedersen-Bjergaard, S. *TrAC - Trends Anal. Chem.* **2019**, *118* (July), 770.

(49) Lashgari, M.; Singh, V.; Pawliszyn, J. *TrAC - Trends Anal. Chem.* **2019**, *119*, 115618.

(50) Reyes-Garcés, N.; Bojko, B.; Pawliszyn, J. *J. Chromatogr. A* **2014**, *1374*, 40–49.

(51) Rickert, D. A.; Gómez-Ríos, G. A.; Nazdrajić, E.; Tascon, M.; Kulasingam, V.; Pawliszyn, J. B. *Anal. Bioanal. Chem.* **2020**, *doi: 10.10*.

(52) Piri-Moghadam, H.; Alam, M. N.; Pawliszyn, J. *Anal. Chim. Acta* **2017**, *984*, 42–65.

(53) Gómez-Ríos, G. A.; Garcés, N. R.; Tascon, M. In *Handbook of Smart Materials in Analytical Chemistry*; John Wiley & Sons Ltd., 2019.

(54) Godage, N. H.; Gionfriddo, E. *TrAC - Trends Anal. Chem.* **2019**, *111*, 220–228.

(55) Reyes-Garcés, N.; Boyac, E.; Bojko, B.; Singh, V.; Grandy, J.; Pawliszyn, J. *Anal. Chem.* **2018**, *90*, 302–360.

(56) Ouyang, G.; Pawliszyn, J. *J. Chromatogr. A* **2007**, *1168* (1–2), 226–235.

(57) Ai, J. *Anal. Chem.* **1997**, *69* (6), 1230–1236.

(58) Alam, M. N.; Ricardez-Sandoval, L.; Pawliszyn, J. *Anal. Chem.* **2015**, *87* (19), 9846–9854.

(59) Alam, M. N.; Nazdrajić, N.; Singh, V.; Tascon, M.; Pawliszyn, J. *Anal. Chem.* **2018**, *90* (19), 11548–11555.

(60) Roszkowska, A.; Tascon, M.; Bojko, B.; Goryński, K.; dos Santos, P. R.; Cypel, M.; Pawliszyn, J. *Talanta* **2018**, *183* (November 2017), 304–310.

(61) Zhang, X.; Es-haghi, A.; Musteata, F. M.; Ouyang, G.; Pawliszyn, J. *Anal. Chem.* **2007**, *79* (12), 4507–4513.

(62) Alam, M. N.; Pawliszyn, J. *Anal. Chem.* **2018**, *90* (4), 2430–2433.

(63) Vuckovic, D.; Risticevic, S.; Pawliszyn, J. *Angew. Chemie - Int. Ed.* **2011**, *50* (25), 5618–5628.

(64) Vuckovic, D.; Pawliszyn, J. *Anal. Chem* **2011**, *83*, 1944–1954.

(65) Kalvass, J. C.; Maurer, T. S. *Biopharm. Drug Dispos.* **2002**, *23* (8), 327–338.

(66) Gustafsson, S.; Sehlin, D.; Lampa, E.; Hammarlund-Udenaes, M.; Loryan, I. *Sci. Rep.* **2019**, *9* (1), 1–15.

(67) Belli, S.; Assmus, F.; Wagner, B.; Honer, M.; Fischer, H.; Schuler, F.; Alvarez-Sánchez, R. *Mol. Pharm.* **2015**, *12* (12), 4529–4541.

(68) Chen, H.; Yuan, L.; Song, W.; Wu, Z.; Li, D. *Prog. Polym. Sci.* **2008**, *33* (11), 1059–1087.

(69) Ouyang, G.; Vuckovic, D.; Pawliszyn, J. *Chem. Rev.* **2011**, *111* (4), 2784–2814.

(70) Kou, X.; Chen, G.; Huang, S.; Ye, Y.; Ouyang, G.; Gan, J.; Zhu, F. *J. Agric. Food Chem.* **2019**, *67* (8), 2120–2126.

(71) Harding, J. L.; Reynolds, M. M. *Trends Biotechnol.* **2014**, *32* (3), 140–146.

(72) Nie, F. Q.; Xu, Z. K.; Huang, X. J.; Ye, P.; Wu, J. *Langmuir* **2003**, *19* (23), 9889–9895.

(73) Reyes-Garcés, N.; Gionfriddo, E.; Gómez-Ríos, G. A.; Alam, M. N.; Boyacl, E.; Bojko, B.; Singh, V.; Grandy, J.; Pawliszyn, J. *Anal. Chem.* **2018**, *90* (1), 302–360.

(74) Musteata, M. L.; Musteata, F. M.; Pawliszyn, J. *Anal. Chem.* **2007**, *79* (18), 6903–6911.

(75) Tanaka, M.; Sato, K.; Kitakami, E.; Kobayashi, S.; Hoshiba, T.; Fukushima, K. *Polym. J.* **2015**, *47* (2), 114–121.

(76) Zhang, X.; Oakes, K. D.; Luong, D.; Wen, J. Z.; Metcalfe, C. D.; Pawliszyn, J.; Servos, M. R. *Anal. Chem.* **2010**, *82* (22), 9492–9499.

(77) Pawliszyn, J. *J. Chromatogr. Sci.* **2000**, *38* (July), 270–278.

(78) Kenessov, B.; Koziel, J. A.; Baimatova, N.; Demyanenko, O. P.; Derbissalin, M. *Molecules* **2018**, *23* (11), 1–14.

(79) Yeung, J. C. Y.; Vuckovic, D.; Pawliszyn, J. *Anal. Chim. Acta* **2010**, *665* (2), 160–166.

(80) Alam, M. N.; Pawliszyn, J. *Anal. Chem.* **2016**, *88* (17), 8632–8639.

(81) Zhang, X.; Es-haghi, A.; Cai, J.; Pawliszyn, J. *J. Chromatogr. A* **2009**, *1216* (45), 7664–7669.

(82) Vuckovic, D.; de Lannoy, I.; Gien, B.; Yang, Y.; Musteata, F. M.; Shirey, R.; Sidisky, L.; Pawliszyn, J. *J. Chromatogr. A* **2011**, *1218* (21), 3367–3375.

(83) Bai, Z.; Pilote, A.; Sarker, P. K.; Vandenberg, G.; Pawliszyn, J. *Anal. Chem.* **2013**, *85* (4), 2328–2332.

(84) Cudjoe E. (2014). In vivo Solid Phase Microextraction for Brain Tissue Analysis. UWaterloo Thesis http://hdl.handle.net/10012/8302.

(85) Ouyang, G.; Cai, J.; Zhang, X.; Li, H.; Pawliszyn, J. *J. Sep. Sci.* **2008**, *31* (6–7), 1167–1172.

(86) Gu, H.; Varner, E. L.; Groskreutz, S. R.; Michael, A. C.; Weber, S. G. *Anal. Chem.* **2015**, *87* (12), 6088–6094.

(87) Wang, M.; Roman, G. T.; Schultz, K.; Jennings, C.; Kenned Y, R. T. *Anal. Chem.* **2008**, *80* (14), 5607–5615.

(88) Ngo, K. T.; Varner, E. L.; Michael, A. C.; Weber, S. G. *ACS Chem. Neurosci.* **2017**, *8* (2), 329–338.

(89) Lee, W. H.; Ngernsutivorakul, T.; Mabrouk, O. S.; Wong, J. M. T.; Dugan, C. E.; Pappas, S. S.; Yoon, H. J.; Kennedy, R. T. *Anal. Chem.* **2016**, *88* (2), 1230–1237.

(90) Ngernsutivorakul, T.; Steyer, D. J.; Valenta, A. C.; Kennedy, R. T. *Anal. Chem.* **2018**, *90* (18), 10943–10950.

(91) Hershey, N. D.; Kennedy, R. T. *ACS Chem. Neurosci.* **2013**, *4* (5), 729–736.

(92) Fillenz, M. *Neurosci. Biobehav. Rev.* **2005**, *29*, 949–962.

(93) Lei, Y.; Han, H.; Yuan, F.; Javeed, A.; Zhao, Y. *Prog. Neurobiol.* **2017**, *157*, 230–246.

(94) Bargmann, C. I. *BioEssays* **2012**, *34* (6), 458–465.

(95) Marder, E. *Neuron* **2012**, *76* (1), 1–11.

(96) Millan, M. J.; Agid, Y.; Brüne, M.; Bullmore, E. T.; Carter, C. S.; Clayton, N. S.; Connor, R.; Davis, S.; Deakin, B.; Derubeis, R. J. *Nat. Rev. Drug Discov.* **2012**, *11*, 141–168.

(97) Halliday, G.; Leverenz, J.; Schneider, J.; Adler, C. *Mov. Disord.* **2014**, *29* (5), 634–650.

(98) Harris, K. D.; Weiss, M.; Zahavi, A. *F1000Res* **2015**, *179*, 1–10.

(99) Yerkes, R. M.; Dodson, J. D. *J. Comp. Neurol. Psychol.* **1908**, *18*, 459–482.

(100) Vizi, E. S. *Pharmacol. Rev.* **2000**, *52* (1), 63–89.

(101) Syková, E. *Neuroscience* **2004**, *129* (4), 861–876.

(102) Angelovski, G.; Tóth, É. *Chem. Soc. Rev.* **2017**, *46* (2), 324–336.

(103) Badgaiyan, R. D. *Prog Brain Res.* **2014**, *211*, 165–182.

(104) Rupert, A. E.; Ou, Y.; Sandberg, M.; Weber, S. G. *ACS Chem. Neurosci.* **2013**, *4* (5), 849–857.

(105) Kottegoda, S.; Shaik, I.; Shippy, S. A. *J. Neurosci. Methods* **2002**, *121* (1), 93–101.

(106) Ngernsutivorakul, T.; Steyer, D. J.; Valenta, A. C.; Kennedy, R. T. *Anal. Chem.* **2018**, *90* (18), 10943–10950.

(107) König, M.; Thinnes, A.; Klein, J. *J. Neurosci. Methods* **2018**, *300*, 206–215.

(108) Buck, K.; Voehringer, P.; Ferger, B. *J. Neurosci. Methods* **2009**, *182* (1), 78–84.

(109) Perry, M.; Li, Q.; Kennedy, R. T. *Anal. Chim. Acta* **2009**, *653* (1), 1–22.

(110) Watson, C. J.; Venton, B. J.; Kennedy, R. T. *Anal. Chem.* **2006**, *78* (5), 1391–1399.

(111) Zestos, A. G.; Kennedy, R. T. *AAPS J.* **2017**, *19* (5), 1284–1293.

(112) Watson, C. J.; Venton, B. J.; Kennedy, R. T. *Anal. Chem.* **2006**, *78* (5), 1391–1399.

(113) Song, P.; Mabrouk, O. S.; Hershey, N. D.; Kennedy, R. T. *Anal. Chem.* **2012**, *84* (1), 412–419.

(114) Wong, J. M. T.; Malec, P. A.; Mabrouk, O. S.; Ro, J.; Dus, M.; Kennedy, R. T. *J. Chromatogr. A* **2016**, *1446*, 78–90.

(115) Zhang, L. H.; Cai, H. L.; Jiang, P.; Li, H. De; Cao, L. J.; Dang, R. L.; Zhu, W. Y.; Deng, Y. *Anal. Methods* **2015**, *7* (9), 3929–3938.

(116) Kennedy, R. T.; Thompson, J. E.; Vickroy, T. W. *J. Neurosci. Methods* **2002**, *114*, 39–49.

(117) Bowser, M. T.; Kennedy, R. T. *Electrophoresis* **2001**, *22* (17), 3668–3676.

(118) Gu, H.; Varner, E. L.; Groskreutz, S. R.; Michael, A. C.; Weber, S. G. *Anal. Chem.* **2015**, *87* (12), 6088–6094.

(119) Robinson, D. L.; Venton, B. J.; Heien, M. L. A. V; Wightman, R. M. *Clin. Chem.* **2003**, *1773*, 1763–1773.

(120) Dale, N.; Hatz, S.; Tian, F.; Llaudet, E. *Trends Biotechnol.* **2005**, *23* (8), 420–428.

(121) Disney, A. A.; Mckinney, C.; Grissom, L.; Lu, X.; Reynolds, J. H. *J. Neurosci. Methods* **2015**, *255*, 29–37.

(122) Chatard, C.; Meiller, A.; Marinesco, S. *Electroanalysis* **2018**, *30* (6), 977–998.

(123) Baker, K. L.; Bolger, F. B.; Lowry, J. P. *Analyst* **2015**, *140* (11), 3738–3745.

(124) Baker, K. L.; Bolger, F. B.; Doran, M. M.; Lowry, J. P. *Electroanalysis* **2019**, *31*, 129–136.

(125) Wu, F.; Cheng, H.; Wei, H.; Xiong, T.; Yu, P.; Mao, L. *Anal. Chem.* **2018**, *90* (21), 13021–13029.

(126) Zhou, L.; Hou, H.; Wei, H.; Yao, L.; Sun, L.; Yu, P.; Su, B.; Mao, L. *Anal. Chem.* **2019**, acs.analchem.8b05658.

(127) Ding, S.; Liu, Y.; Ma, C.; Zhang, J.; Zhu, A.; Shi, G. *Electroanalysis*. 2018, pp 1041–1046.

(128) Zaitsu, K.; Hayashi, Y.; Murata, T.; Yokota, K.; Ohara, T.; Kusano, M.; Tsuchihashi, H.; Ishikawa, T.; Ishii, A.; Ogata, K.; et al. *Anal. Chem.* **2018**, *90* (7), 4695–4701.

(129) Birjandi, A. P.; Mirnaghi, F. S.; Bojko, B.; Wa¸sowicz, M.; Pawliszyn, J. *Anal. Chem.* **2014**, *86* (24), 12022–12029.

(130) Roszkowska, A.; Yu, M.; Bessonneau, V.; Bragg, L.; Servos, M.; Pawliszyn, J. *Sci. Rep.* **2018**, *8* (1), 1–10.

(131) Boyaci, E.; Bojko, B.; Reyes-Garcés, N.; Poole, J. J.; Gómez-Ríos, G. A.; Teixeira, A.; Nicol, B.; Pawliszyn, J. *Sci. Rep.* **2018**, *8* (1), 1–10.

(132) Vuckovic, D.; De Lannoy, I.; Gien, B.; Shirey, R. E.; Sidisky, L. M.; Dutta, S.; Pawliszyn, J. *Angew. Chemie - Int. Ed.* **2011**, *50* (23), 5344–5348.

(133) Bojko, B.; Gorynski, K.; Gomez-Rios, G. A.; Knaak, J. M.; MacHuca, T.; Cudjoe, E.; Spetzler, V. N.; Hsin, M.; Cypel, M.; Selzner, M.; et al. *Lab. Investig.* **2014**, *94* (5), 586–594.

(134) Poole, J. J.; Grandy, J. J.; Yu, M.; Boyaci, E.; Gómez-Ríos, G. A.; Reyes-Garcés, N.; Bojko, B.; Heide, H. Vander; Pawliszyn, J. *Anal. Chem.* **2017**, *89* (15), 8021–8026.

(135) Deng, J.; Li, W.; Yang, Q.; Liu, Y.; Fang, L.; Guo, Y.; Guo, P.; Lin, L.; Yang, Y.; Luan, T. *Anal. Chem.* **2018**, *90* (11), 6936–6944.

(136) Cudjoe, E.; Bojko, B.; Delannoy, I.; Saldivia, V.; Pawliszyn, J. *Angew. Chemie - Int. Ed.* **2013**, *52* (46), 12124–12126.

(137) Renaud, J. B.; Sabourin, L.; Topp, E.; Sumarah, M. W. *Anal. Chem.* **2017**, *89* (5), 2747–2754.

(138) Manier, M. L.; Spraggins, J. M.; Reyzer, M. L.; Norris, J. L.; Caprioli, R. M. *J. Mass Spectrom.* **2014**, *49* (8), 665–673.

(139) Li, W.; Zhang, J.; Tse, F. L. S. *Biomed. Chromatogr.* **2011**, *25* (1), 258–277.

(140) Purwaha, P.; Silva, L. P.; Hawke, D. H.; Weinstein, J. N.; Lorenzi, P. L. *Anal. Chem.* **2014**, *86* (12), 5633–5637.

(141) Shah, A. J.; Crespi, F.; Heidbreder, C. *J. Chromatogr. B* **2002**, *781* (1–2), 151–163.

(142) Cudjoe, E.; Pawliszyn, J. *J. Chromatogr. A* **2014**, *1341*, 1–7.

(143) Guidance for Industry Bioanalytical Method Validation. Tel, 2001; Vol. 20857.

(144) Matuszewski, B. K.; Constanzer, M. L.; Chavez-Eng, C. M. *Anal. Chem.* **2003**, *75*, 3019–3030.

(145) Gómez-ríos, G. A.; Tascon, M.; Reyes-garcés, N.; Boyacı, E.; Poole, J.; Pawliszyn, J. *Sci. Rep.* **2017**, *7* (November), 1–7.

(146) Piri-Moghadam, H.; Alam, M. N.; Pawliszyn, J. *Anal. Chim. Acta* **2017**, *984*, 42–65.

(147) Fernández, E.; Vårdal, L.; Vidal, L.; Canals, A.; Gjelstad, A.; Pedersen-Bjergaard, S. *Anal. Bioanal. Chem.* **2017**, *409* (17), 4215–4223.

(148) Restan, M. S.; Jensen, H.; Shen, X.; Huang, C.; Martinsen, Ø. G.; Kubáň, P.; Gjelstad, A.; Pedersen-Bjergaard, S. *Anal. Chim. Acta* **2017**, *984*, 116–123.

(149) Gjelstad, A.; Rasmussen, K. E.; Parmer, M. P.; Pedersen-Bjergaard, S. *Bioanalysis* **2013**, *5* (11), 1377–1385.

(150) Zhang; Rauch; Lee; Xiao; Rainer; Logothetis. *Rapid Commun. Mass Spectrom.* **2008**, *22*, 2161–2175.

(151) Bicker, J.; Fortuna, A.; Alves, G.; Falcão, A. *Anal. Chim. Acta* **2013**, *768* (1), 12–34.

(152) de Jong, W. H. A.; de Vries, E. G. E.; Wolffenbuttel, B. H. R.; Kema, I. P. *J. Chromatogr. B*

Anal. Technol. Biomed. Life Sci. **2010**, *878* (19), 1506–1512.

(153) Konieczna, L.; Roszkowska, A.; Niedźwiecki, M.; Baczek, T. *J. Chromatogr. A* **2016**, *1431*, 111–121.

(154) Askar, K. A.; Kudi, A. C.; Moody, A. J. *Enzyme Res.* **2010**, *2010*, 10–12.

(155) Li, H.; Li, C.; Yan, Z. ying; Yang, J.; Chen, H. *J. Neurosci. Methods* **2010**, *189* (2), 162–168.

(156) Li, W.; Cohen, L. H. **2003**, *75* (21), 5854–5859.

(157) Schintu, N.; Shariatgorji, M.; Nilsson, A.; Goodwin, R. J. A.; Ka, P.; Zhang, X.; Crossman, A. R.; Bezard, E.; Svenningsson, P.; Andren, P. E. **2014**, 697–707.

(158) Ahmadkhaniha, R.; Shafiee, A.; Rastkari, N.; Kobarfard, F. *Anal. Chim. Acta* **2009**, *631* (1), 80–86.

(159) Lerma, J.; Herranz, A. S.; Herreras, O.; Abraira, V.; del Rio, R. M. *Brain Res.* **1986**, *384* (1), 145–155.

(160) Giarman, N. J.; Pepeu, G. *Br. J. Pharmacol. Chemother.* **1964**, *23* (1), 123–130.

(161) Christiansen, P.; Toft, P.; Larsson, H. B. W.; Stubgaard, M.; Henriksen, O. *Magn. Reson. Imaging* **1993**, *11* (6), 799–806.

(162) Bonilla, E.; Diez-Ewald, M. *J. Neurochem.* **1974**, *22* (2), 297–299.

(163) Ramakrishnan, R.; Namasivayam, A. *Neurosci. Lett.* **1995**, *186* (2–3), 200–202.

(164) Roth, K. a; Mefford, I. M.; Barchas, J. D. *Brain Res.* **1982**, *239*, 417–424.

(165) Schwartz, J. C.; Lampart, C.; Rose, C. *J. Neurochem.* **1972**, *19* (3), 5–9.

(166) Moussawi, K.; Riegel, A.; Nair, S.; Kalivas, P. W. *Front. Syst. Neurosci.* **2011**, *5* (November), 1–9.

(167) Meldrum, B. S. *J. Nutr.* **2000**, *130* (4S Suppl), 1007S-15S.

(168) Oliver von Bohlen und Halbach; Dermietzel, R. 2nd Ed.; Neurotransmitters and Neuromodulators. Handbook of Receptors and Biological Effects, WILEY-VCH Verlag GmbH & Co.: Weinheim, 2006.

(169) Thiele, A.; Bellgrove, M. A. *Neuron* **2018**, *97* (4), 769–785.

(170) Avery, M. C.; Krichmar, J. L. *Front. Neural Circuits* **2017**, *11* (December), 1–18.

(171) Millan, M. J.; Agid, Y.; Brüne, M.; Bullmore, E. T.; Carter, C. S.; Clayton, N. S.; Connor, R.; Davis, S.; Deakin, B.; Derubeis, R. J.; et al. *Nat. Rev. Drug Discov.* **2012**, *11* (2), 141–168.

(172) Gobert, A.; Rivet, J. M.; Audinot, V.; Newman-Tancredi, A.; Cistarelli, L.; Millan, M. J. *Neuroscience* **1998**, *84* (2), 413–429.

(173) Moehle, M. S.; Pancani, T.; Byun, N.; Yohn, S. E.; Wilson, G. H.; Dickerson, J. W.; Remke, D. H.; Xiang, Z.; Niswender, C. M.; Wess, J.; et al. *Neuron* **2017**, *96* (6), 1358-1372.e4.

(174) Arnsten, A. F. T.; Paspalas, C. D.; Gamo, N. J.; Yang, Y.; Wang, M. *Trends Cogn. Sci.* **2010**, *14* (8), 365–375.

(175) Hassan, S. F.; Zumut, S.; Burke, P. G.; McMullan, S.; Cornish, J. L.; Goodchild, A. K. *Neuroscience* **2015**, *295*, 209–220.

(176) Santana, N.; Mengod, G.; Artigas, F. *Int. J. Neuropsychopharmacol.* **2013**, *16* (5), 1139–1151.

(177) Ghersi, C.; Bonfanti, A.; Manzari, B.; Feligioni, M.; Raiteri, M.; Pittaluga, A. *Neurochem. Int.* **2003**, *42* (4), 283–292.

(178) Grilli, M.; Zappettini, S.; Zanardi, A.; Lagomarsino, F.; Pittaluga, A.; Zoli, M.; Marchi, M. *J. Neurochem.* **2009**, *110* (5), 1598–1606.

(179) Luccini, E.; Musante, V.; Neri, E.; Brambilla Bas, M.; Severi, P.; Raiteri, M.; Pittaluga, A. *Br. J. Pharmacol.* **2007**, *151* (7), 1087–1094.

(180) Pittaluga, A. *Front. Pharmacol.* **2016**, *7* (AUG), 1–15.

(181) Pittaluga, A.; Feligioni, M.; Longordo, F.; Luccini, E.; Raiteri, M. *Neuropharmacology* **2006**, *50* (3), 286–296.

(182) Wang, J. K. T.; Andrews, H.; Thukral, V. *J. Neurochem.* **1992**, *58* (1), 204–211.

(183) Bohnen, N. I.; Albin, R. L.; Müller, M. L. T. .; Petrou, M.; Kotagal, V.; Koeppe, R. A.; Scott, P. J. H.; Frey, K. A. *JAMA Neurol.* **2015**, *74*, 194–200.

(184) Halliday, G. M.; Leverenz, J. B.; Schneider, J. S.; Adler, C. H. *Mov. Disord.* **2014**, *29* (5), 634–650.

(185) Remy, P.; Doder, M.; Lees, A.; Turjanski, N.; Brooks, D. *Brain* **2005**, *128* (6), 1314–1322.

(186) Cudjoe, E.; Bojko, B.; Delannoy, I.; Saldivia, V.; Pawliszyn, J. *Angew. Chemie - Int. Ed.* **2013**, *52* (46), 12124–12126.

(187) Cudjoe, E.; Pawliszyn, J. *J. Chromatogr. A* **2014**, *1341*, 1–7.

(188) Oemisch, M.; Westendorff, S.; Everling, S.; Womelsdorf, T. *J. Neurosci.* **2015**, *35* (38), 13076–13089.

(189) Paxinos, G.; Huang, X.; Toga, A. 2nd Ed.; The Rhesus Monkey Brain in Stereotaxic Coordinates, Academic Press: San Diego, 2000.

(190) Hassani, S. A.; Oemisch, M.; Balcarras, M.; Westendorff, S.; Ardid, S.; Van Der Meer, M. A.; Tiesinga, P.; Womelsdorf, T. *Sci. Rep.* **2017**, *7* (April 2016), 1–19.

(191) Parikh, V.; Kozak, R.; Martinez, V.; Sarter, M. *Neuron* **2007**, *56* (1), 141–154.

(192) D'Ascenzo, M.; Fellin, T.; Terunuma, M.; Revilla-Sanchez, R.; Meaney, D. F.; Auberson, Y. P.; Moss, S. J.; Haydon, P. G. *Proc. Natl. Acad. Sci. U. S. A.* **2007**, *104* (6), 1995–2000.

(193) Moghaddam, B. *J. Neurochem.* **1993**, *60* (5), 1650–1657.

(194) Santello, M.; Cali, C.; Bezzi, P. Kreutz, M., Sala, C., Eds.; Gliotransmission and the tripartite synapse. In: Synaptic Plasticity. Advances in Experimental Medicine and Biology, Springer: Vienna, 2012.

(195) Schwartz, J.; Javitsch, J. 5th Ed.; Kandel E, Schwartz J, Jessell T, Siegelbaum S, H. A., Ed.; Neurotransmitters. In: Principles of Neural Science, McGraw-Hill: New York, 2013.

(196) Vizi, E. S. *Pharmacol. Rev.* **2000**, *52* (1), 63–89.

(197) Goldman-Rakic, P. S.; Lidow, M. S.; Gallager, D. W. *J. Neurosci.* **1990**, *10* (7), 2125–2138.

(198) Vijayraghavan, S.; Wang, M.; Birnbaum, S. G.; Williams, G. V.; Arnsten, A. F. T. *Nat.*

Neurosci. **2007**, *10* (3), 376–384.

(199) Watanabe, M.; Kodama, T.; Hikosaka, K. *J. Neurophysiol.* **1997**, *78* (5), 2795–2798.

(200) Holloway, Z. R.; Freels, T. G.; Comstock, J. F.; Nolen, H. G.; Sable, H. J.; Lester, D. B. *Synapse* **2019**, *73* (2), 1–15.

(201) Kreitzer, A. C. *Annu. Rev. Neurosci.* **2009**, *32* (1), 127–147.

(202) Zapata, A.; Chefer, V. I.; Shippenberg, T. S.; Denoroy, L. *Curr. Protoc. Neurosci.* **2009**, No. SUPPL. 48, 1–37.

(203) Granger, A. J.; Mulder, N.; Saunders, A.; Sabatini, B. L. *Neuropharmacology* **2016**, *100*, 40–46.

(204) Howe, W. M.; Gritton, H. J.; Lusk, N. A.; Roberts, E. A.; Hetrick, V. L.; Berke, J. D.; Sarter, M. *J. Neurosci.* **2017**, *37* (12), 3215–3230.

(205) McGinley, M. J.; Vinck, M.; Reimer, J.; Batista-Brito, R.; Zagha, E.; Cadwell, C. R.; Tolias, A. S.; Cardin, J. A.; McCormick, D. A. *Neuron* **2015**, *87* (6), 1143–1161.

(206) Reimer, J.; Froudarakis, E.; Cadwell, C. R.; Yatsenko, D.; Denfield, G. H.; Tolias, A. S. *Neuron* **2014**, *84* (2), 355–362.

(207) Reimer, J.; McGinley, M. J.; Liu, Y.; Rodenkirch, C.; Wang, Q.; McCormick, D. A.; Tolias, A. S. *Nat. Commun.* **2016**, *7* (May), 1–7.

(208) Kodama, T.; Hikosaka, K.; Honda, Y.; Kojima, T.; Tsutsui, K. ichiro; Watanabe, M. *Behav. Brain Res.* **2015**, *294*, 194–197.

(209) Kodama, T.; Hikosaka, K.; Watanabe, M. *Exp. Brain Res.* **2002**, *145* (2), 133–141.

(210) Kodama, T.; Kojima, T.; Honda, Y.; Hosokawa, T.; Tsutsui, K. I.; Watanabe, M. *J. Neurosci.* **2017**, *37* (9), 2387–2394.

(211) Lendor, S.; Hassani, S. A.; Boyaci, E.; Singh, V.; Womelsdorf, T.; Pawliszyn, J. *Anal. Chem.* **2019**, *91* (7), 4896–4905.

(212) Deng, J.; Yang, Y.; Wang, X.; Luan, T. *TrAC - Trends Anal. Chem.* **2014**, *55*, 55–67.

(213) Li, J.; Von Pföstl, V.; Zaldivar, D.; Zhang, X.; Logothetis, N.; Rauch, A. *Anal. Bioanal. Chem.* **2012**, *402* (8), 2545–2554.

(214) Zhang, X.; Rauch, A.; Lee, H.; Xiao, H.; Rainer, G.; Logothetis, N. K. *Rapid Commun. Mass Spectrom.* **2007**, *21*, 3621–3628.

(215) Tamiji, J.; Crawford, D. A. *NeuroSignals* **2011**, *18* (2), 98–112.

(216) Yehuda, S.; Rabinovitz, S.; Mostofsky, D. I. *J. Neurosci. Res.* **1999**, *56* (6), 565–570.

(217) Kao, C.-Y.; Anderzhanova, E.; Asara, J. M.; Wotjak, C. T.; Turck, C. W. *Mol. Neuropsychiatry* **2015**, *1* (1), 60–67.

(218) Lapiz, M. D. S.; Morilak, D. A. *Neuroscience* **2006**, *137* (3), 1039–1049.

(219) Wang, M.; Ramos, B. P.; Paspalas, C. D.; Shu, Y.; Simen, A.; Duque, A.; Vijayraghavan, S.; Brennan, A.; Dudley, A.; Nou, E.; et al. *Cell* **2007**, *129* (2), 397–410.

(220) Cudjoe, E.; Bojko, B.; de Lannoy, I.; Saldivia, V.; Pawliszyn, J. *Angew. Chemie Int. Ed.* **2013**,

52 (46), 12124–12126.

(221) Dunn, W. B.; Erban, A.; Weber, R. J. M.; Creek, D. J.; Brown, M.; Breitling, R.; Hankemeier, T.; Goodacre, R.; Neumann, S.; Kopka, J.; et al. *Metabolomics* **2013**, *9* (SUPPL.1), 44–66.

(222) Kruve, A. *Anal. Chem.* **2020**, DOI: 10.1021/acs.analchem.9b03481.

(223) González-Riano, C.; Dudzik, D.; Garcia, A.; Gil-De-La-Fuente, A.; Gradillas, A.; Godzien, J.; López-Gonzálvez, Á.; Rey-Stolle, F.; Rojo, D.; Ruperez, F. J.; et al. *Anal. Chem.* **2020**, *92* (1), 203–226.

(224) Hu, Y.; Cai, B.; Huan, T. *Anal. Chem.* **2019**, DOI: 10.1021/acs.analchem.9b02980.

(225) Kuhl, C.; Tautenhahn, R.; Böttcher, C.; Larson, T. R.; Neumann, S. *Anal. Chem.* **2012**, *84* (1), 283–289.

(226) Yu, M.; Olkowicz, M.; Pawliszyn, J. *Anal. Chim. Acta* **2019**, *1050*, 16–24.

(227) Keller, B. O.; Sui, J.; Young, A. B.; Whittal, R. M. *Anal. Chim. Acta* **2008**, *627* (1), 71–81.

(228) Mahieu, N. G.; Patti, G. J. *Anal. Chem.* **2017**, *89* (19), 10397–10406.

(229) Chambers, M. C.; MacLean, B.; Burke, R.; Amodei, D.; Ruderman, D. L.; Neumann, S.; Gatto, L.; Fischer, B.; Pratt, B.; Egertson, J.; et al. *Nat. Biotechnol.* **2012**, *30* (10), 918–920.

(230) Libiseller, G.; Dvorzak, M.; Kleb, U.; Gander, E.; Eisenberg, T.; Madeo, F.; Neumann, S.; Trausinger, G.; Sinner, F.; Pieber, T.; et al. *BMC Bioinformatics* **2015**, *16* (118), 1–10.

(231) Smith, C. A.; Want, E. J.; O'Maille, G.; Abagyan, R.; Siuzdak, G. *Anal. Chem.* **2006**, *78* (3), 779–787.

(232) R Core Team; Foundation for Statistical Computing, Vienna (2014) R: A language and environment for statistical computing, http:// www. R. org. (accessed 2019/04/14). .

(233) Chong, J.; Soufan, O.; Li, C.; Caraus, I.; Li, S.; Bourque, G.; Wishart, D. S.; Xia, J. *Nucleic Acids Res.* **2018**, *46* (W1), W486–W494.

(234) Smith, C. A.; O'Maille, G.; Want, E. J.; Qin, C.; Trauger, S. A.; Brandon, T. R.; Custodio, D. E.; Abagyan, R.; Siuzdak, G. *Ther. Drug Monit.* **2005**, *27* (6), 747–751.

(235) Fahy, E.; Subramaniam, S.; Murphy, R. C.; Nishijima, M.; Raetz, C. R. H.; Shimizu, T.; Spener, F.; van Meer, G.; Wakelam, M. J. O.; Dennis, E. A. *J. Lipid Res.* **2009**, *50* (Supplement), S9–S14.

(236) Höglund, E.; Øverli, Ø.; Winberg, S. *Front. Endocrinol. (Lausanne).* **2019**, *10* (APR).

(237) Moroni, F. *Eur. J. Pharmacol.* **1999**, *375* (1–3), 87–100.

(238) Yabut, J. M.; Crane, J. D.; Green, A. E.; Keating, D. J.; Khan, W. I.; Steinberg, G. R. *Endocr. Rev.* **2019**, *40* (4), 1092–1107.

(239) Meiser, J.; Weindl, D.; Hiller, K. *Cell Commun. Signal.* **2013**, *11* (1), 1–18.

(240) Golan, D. E. Principles of Pharmacology: The Pathophysiologic Basis of Drug Therapy, Lippincott Williams & Wilkins, 2008.

(241) Ripps, H.; Shen, W. *Mol. Vis.* **2012**, *18* (August), 2673–2686.

(242) Wu, J. Y.; Prentice, H. *J. Biomed. Sci.* **2010**, *17* (SUPPL. 1), 2–7.

(243) Hashimoto-Kitsukawa, S.; Okuyama, S.; Aihara, H. *Pharmacol. Biochem. Behav.* **1988**, *31* (2), 417–423.

(244) Gonzalez-Riano, C.; Tapia-González, S.; García, A.; Muñoz, A.; DeFelipe, J.; Barbas, C. *Brain Struct. Funct.* **2017**, *222* (6), 2831–2853.

(245) Gonzalez-Riano, C.; Garcia, A.; Barbas, C. *J. Pharm. Biomed. Anal.* **2016**, *130*, 141–168.

(246) Roth, F. C.; Draguhn, A. *Neural Plast.* **2012**, *2012*, 1–12.

(247) Hertz, L. *Front. Endocrinol. (Lausanne).* **2013**, *4* (MAY), 1–16.

(248) Tracey, T. J.; Steyn, F. J.; Wolvetang, E. J.; Ngo, S. T. *Front. Mol. Neurosci.* **2018**, *11* (January), 1–25.

(249) Martínez-Gardeazabal, J.; González de San Román, E.; Moreno-Rodríguez, M.; Llorente-Ovejero, A.; Manuel, I.; Rodríguez-Puertas, R. *Biochim. Biophys. Acta - Biomembr.* **2017**, *1859* (9), 1548–1557.

(250) Aslam, M.; Feleder, C.; Newsom, R. J.; Campeau, S.; Musteata, F. M. *Bioanalysis* **2019**, *11*, 1523–1534.

(251) Napylov, A.; Reyes-Garces, N.; Gomez-Rios, G.; Olkowicz, M.; Lendor, S.; Monnin, C.; Bojko, B.; Hamani, C.; Pawliszyn, J.; Vuckovic, D. *Angew. Chemie - Int. Ed.* **2020**, *59* (6), 2392–2398.

(252) Ricciotti, E.; A, G.; Fitzgerald. *Arter. Thromb Vasc Biol.* **2011**, *31* (5), 986–1000.

(253) Liu, X.; Davis, C. M.; Alkayed, N. J. *Antioxid. Redox Signal.* **2017**, *00*, 1–21.

(254) Borroni, M. V.; Vallés, A. S.; Barrantes, F. J. *Biochim. Biophys. Acta - Biomembr.* **2016**, *1858* (11), 2662–2670.

(255) Bozek, K.; Wei, Y.; Yan, Z.; Liu, X.; Xiong, J.; Sugimoto, M.; Tomita, M.; Pääbo, S.; Pieszek, R.; Sherwood, C. C.; et al. *PLoS Biol.* **2014**, *12* (5), e1001871.

(256) Xing, F.; Giavalisco, P.; Liu, X.; Catchpole, G.; Fu, N.; Ning, Z.-B.; Guo, S.; Yan, Z.; Somel, M.; Paabo, S.; et al. *PNAS* **2011**, *108* (15), 6181–6186.

(257) Van Eeckhaut, A.; Maes, K.; Aourz, N.; Smolders, I.; Michotte, Y. *Bioanalysis* **2011**, *3* (11), 1271–1285.

(258) Wang, Y.; Schneider, B. B.; Covey, T. R.; Pawliszyn, J. *Anal. Chem.* **2005**, *77* (24), 8095–8101.

(259) Feider, C. L.; Krieger, A.; DeHoog, R. J.; Eberlin, L. S. *Anal. Chem.* **2019**, *91*, 4266–4290.

(260) Badu-Tawiah, A. K.; Eberlin, L. S.; Ouyang, Z.; Cooks, R. G. *Annu. Rev. Phys. Chem.* **2013**, *64* (1), 481–505.

(261) Monge, M. E.; Harris, G. A.; Dwivedi, P.; Fernández, F. M. *Chem. Rev.* **2013**, *113* (4), 2269–2308.

(262) Venter, A. R.; Douglass, K. A.; Shelley, J. T.; Hasman, G.; Honarvar, E. *Anal. Chem.* **2014**, *86* (1), 233–249.

(263) Tillner, J.; Mckenzie, J. S.; Jones, E. A.; Speller, A. V. M.; Walsh, J. L.; Veselkov, K. A.; Bunch, J.; Takats, Z.; Gilmore, I. S. *Anal. Chem.* **2016**, *88*, 4808–4816.

(264) Chumbley, C. W.; Reyzer, M. L.; Allen, J. L.; Marriner, G. A.; Via, L. E.; Barry, C. E.; Caprioli, R. M. *Anal. Chem.* **2016**, *88*, 2392–2398.

(265) Stolee, J. A.; Shrestha, B.; Mengistu, G.; Vertes, A. *Angew. Chem. Int. Ed. Engl.* **2012**, *51* (41), 10386–10389.

(266) Roach, P. J.; Laskin, J.; Laskin, A.; Cooks, R. G.; Suzuki, S.; O'Connor, G.; Cooks, R. G.; Wang, M. D.; Hay, M. E.; Fernandez, F. M.; et al. *Analyst* **2010**, *135* (9), 2233.

(267) Kertesz, V.; Van Berkel, G. J. *J. Mass Spectrom.* **2010**, *45* (3), 252–260.

(268) Shrestha, B.; Walsh, C. M.; Boyce, G. R.; Nemes, P. In *Advances in MALDI and Laser-Induced Soft Ionization Mass Spectrometry*; Springer International Publishing: Cham, 2016; pp 149–167.

(269) Nguyen, S. N.; Sontag, R. L.; Carson, J. P.; Corley, R. A.; Ansong, C.; Laskin, J. *J Am Soc Mass Spectrom* **2018**, *29* (2), 316–322.

(270) Watrous, J.; Roach, P.; Alexandrov, T.; Heath, B. S.; Yang, J. Y.; Kersten, R. D.; van der Voort, M.; Pogliano, K.; Gross, H.; Raaijmakers, J. M.; et al. *Proc. Natl. Acad. Sci.* **2012**, *109* (26), E1743–E1752.

(271) Jarmusch, A. K.; Pirro, V.; Baird, Z.; Hattab, E. M.; Cohen-gadol, A. A.; Cooks, R. G. *PNAS* **2016**, *113* (6), 1486–1491.

(272) Inglese, P.; McKenzie, J. S.; Mroz, A.; Kinross, J.; Veselkov, K.; Holmes, E.; Takats, Z.; Nicholson, J. K.; Glen, R. C. *Chem. Sci.* **2017**, *8* (5), 3500–3511.

(273) Eberlin, L. S.; Ifa, D. R.; Wu, C.; Graham Cooks, R. *Angew. Chemie - Int. Ed.* **2010**, *49* (5), 873–876.

(274) Cooks, R. G.; Ouyang, Z.; Chen, C.-H.; Lin, Z.; Eberlin, L. S. 2019, p United States Patent no. US10213143.

(275) Venter, A.; Robert Graham Cooks. 2010, p United States Patent no. US7847244.

(276) Klein, D. R.; Feider, C. L.; Garza, K. Y.; Lin, J. Q.; Eberlin, L. S.; Brodbelt, J. S. *Anal. Chem.* **2018**, *90* (17), 10100–10104.

(277) Liu, C.; Qi, K.; Yao, L.; Xiong, Y.; Zhang, X.; Zang, J.; Tian, C.; Xu, M.; Yang, J.; Lin, Z.; et al. *Anal. Chem.* **2019**, acs.analchem.9b00520.

(278) Garza, K. Y.; Feider, C. L.; Klein, D. R.; Rosenberg, J. A.; Brodbelt, J. S.; Eberlin, L. S. *Anal. Chem.* **2018**, *90* (13), 7785–7789.

(279) Nguyen, S. N.; Sontag, R. L.; Carson, J. P.; Corley, R. A.; Ansong, C.; Laskin, J. **2018**, 316–322.

(280) Wleklinski, M.; Loren, B. P.; Ferreira, C. R.; Jaman, Z.; Avramova, L.; Sobreira, T. J. P.; Thompson, D. H.; Cooks, R. G. *Chem. Sci.* **2018**, *9*, 1647–1653.

(281) Wiseman, J. M.; Evans, C. A.; Bowen, C. L.; Kennedy, J. H. *Analyst* **2010**, *135* (4), 720–725.

(282) Pruski, P.; MacIntyre, D. A.; Lewis, H. V.; Inglese, P.; Correia, G. D. S.; Hansel, T. T.; Bennett, P. R.; Holmes, E.; Takats, Z.; St John, E. R.; et al. *Anal. Chem.* **2016**, *85* (3), 2–9.

(283) Hemalatha, R. G.; Ganayee, M. A.; Pradeep, T. *Anal. Chem.* **2016**, *88*, 5710–5717.

(284) Bianchi, F.; Agazzi, S.; Riboni, N.; Erdal, N.; Hakkarainen, M.; Ilag, L. L.; Anzillotti, L.; Andreoli, R.; Marezza, F.; Moroni, F.; et al. *Talanta* **2019**, *202*, 136–144.

(285) Gómez-Ríos, G. A.; Mirabelli, M. F. *TrAC - Trends Anal. Chem.* **2019**, *112*, 201–211.

(286) Vasiljevic, T.; Singh, V.; Pawliszyn, J. *Talanta* **2019**, *199* (January), 689–697.

(287) Zhang, X.; Oakes, K. D.; Hoque, E.; Luong, D.; Taheri-nia, S.; Lee, C.; Smith, B. M.; Metcalfe, C. D.; Solla, S. De; Servos, M. R. *Anal. Chem.* **2012**, *84*, 6956–6962.

(288) Zhang, X.; Oakes, K. D.; Cui, S.; Bragg, L.; Servos, M. R.; Pawliszyn, J. *Environ. Sci. Technol.* **2010**, *44* (9), 3417–3422.

(289) Nemes, P.; Barton, A. A.; Li, Y.; Vertes, A. **2008**, *80* (12), 4575–4582.

(290) Kennedy, J. H.; Aurand, C.; Shirey, R.; Laughlin, B. C.; Wiseman, J. M. *Anal. Chem.* **2010**, *82* (17), 7502–7508.

(291) Huang, G.; Chen, H.; Zhang, X.; Cooks, R. G.; Ouyang, Z. *Anal. Chem.* **2007**, *79* (21), 8327–8332.

(292) D'Agostino, P. A.; Chenier, C. L.; Hancock, J. R.; Lepage, C. R. J. *Rapid Commun. Mass Spectrom.* **2007**, 543–549.

(293) Strittmatter, N.; During, R.-A.; Takats, Z. *Analyst* **2012**, 4037–4044.

(294) Takats, Z.; Jones, E.; Langridge, J. I.; Morris, M. R.; Karanecsi, T.; Pringle, S. D.; Balog, J.; Simon, D.; Godorhazy, L.; Szalay, D.; et al. 2018.

(295) Li, W.; Chen, X.; Wang, Z.; Wong, Y. L. E.; Wu, R.; Hung, Y. L. W.; Chan, T. W. D. *Eur. J. Mass Spectrom.* **2018**, *24* (1), 66–73.

(296) Airan, R. *Science (80-.).* **2017**, *357* (6350), 465–465.

(297) Brinker, C. J.; Frye, G. C.; Hurd, A. J.; Ashley, C. S. *Thin Solid Films* **1991**, *201* (1), 97–108.

(298) Covey, T. R.; Thomson, B. A.; Bradley, B. S. *Mass Spectrom. Rev.* **2008**, *28*, 870–897.

(299) Zhang, X.; Cai, J.; Oakes, K. D.; Servos, M. R. *Anal. Chem.* **2009**, *81* (17), 7349–7356.

(300) Gómez-Ríos, G. A.; Reyes-Garcés, N.; Bojko, B.; Pawliszyn, J. *Anal. Chem.* **2016**, *88* (2), 1259–1265.

(301) Campbell, D. I.; Ferreira, C. R.; Eberlin, L. S.; Cooks, R. G. *Anal. Bioanal. Chem.* **2012**, *404* (2), 389–398.

(302) Tillner, J.; Wu, V.; Jones, E. A.; Pringle, S. D.; Karancsi, T.; Dannhorn, A.; Veselkov, K.; McKenzie, J. S.; Takats, Z. *J. Am. Soc. Mass Spectrom.* **2017**, *28* (10), 2090–2098.

(303) Green, F. M.; Salter, T. L.; Gilmore, I. S.; Stokes, P.; O'Connor, G. *Analyst* **2010**, *135* (4), 731–737.

(304) Zhang, X.; Cai, J.; Oakes, K. D.; Breton, F.; Servos, M. R.; Pawliszyn, J. *Anal. Chem.* **2009**, *81* (17), 7349–7356.

(305) Ifa, D. R.; Wiseman, J. M.; Song, Q.; Cooks, R. G. *Int. J. Mass Spectrom.* **2007**, *259* (1–3), 8–15.

(306) Kertesz, V.; Gary J. Van Berkel. *Rapid Commun. Mass Spectrom.* **2008**, *22*, 2639–2644.

(307) Nicholson, C. *Reports Prog. Phys.* **2001**, *64*, 815–884.

(308) Souza-Silva, É. A.; Gionfriddo, E.; Alam, M. N.; Pawliszyn, J. *Anal. Chem.* **2017**, *89* (5), 2978–

2985.

(309) Semenov, S. N.; Koziel, J. A.; Pawliszyn, J. *J. Chromatogr. A* **2000**, *873* (1), 39–51.

(310) Huq, M.; Tascon, M.; Nazdrajic, E.; Roszkowska, A.; Pawliszyn, J. *Anal. Chem.* **2019**, *91*, 7719–7728.

(311) U.S. Department of Health and Human Services Food and Drug Administration; (CVM), C. for D. E. and R. (CDER) C. for V. M. 2001.

(312) Li, A.; Paine, M. R. L.; Zambrzycki, S.; Stryffeler, R. B.; Wu, J.; Bouza, M.; Huckaby, J.; Chang, C. Y.; Kumar, M.; Mukhija, P.; et al. *Anal. Chem.* **2018**, *90* (6), 3981–3986.

(313) Haber, G. P.; White, M. A.; Autorino, R.; Escobar, P. F.; Kroh, M. D.; Chalikonda, S.; Khanna, R.; Forest, S.; Yang, B.; Altunrende, F.; et al. *Urology* **2010**, *76* (6), 1279–1282.

(314) Santagata, S.; Eberlin, L. S.; Norton, I.; Calligaris, D.; Ide, J. L.; Feldman, D. R.; Liu, X.; Wiley, J. S.; Vestal, M. L.; Ramkissoon, S. H.; et al. *Proc. Natl. Acad. Sci.* **2014**, *111* (30), 11121–11126.

(315) Yannell, K. E.; Smith, K.; Alfaro, C. M.; Jarmusch, A. K.; Pirro, V.; Cooks, R. G. *Clin. Chem.* **2017**, *63* (11), 1766–1770.

(316) Protsyuk, I.; Melnik, A. V.; Nothias, L. F.; Rappez, L.; Phapale, P.; Aksenov, A. A.; Bouslimani, A.; Ryazanov, S.; Dorrestein, P. C.; Alexandrov, T. *Nat. Protoc.* **2018**, *13* (1), 134–154.

(317) Norrholm, S. D.; Ouimet, C. C. *Brain Res.* **2000**, *883*, 205–215.

(318) Alboni, S.; Dijk, R. M. Van; Poggini, S.; Milior, G.; Perrotta, M.; Drenth, T.; Brunello, N.; Wolfer, D. P.; Limatola, C.; Amrein, I.; et al. *Mol. Psychiatry* **2015**, No. November, 1–10.

(319) Marwari, S.; Dawe, G. S. *J. Psychopharmacol.* **2018**, *32* (4), 441–457.

(320) Ludka, F. K.; Dal-cim, T.; Binder, L. B.; Constantino, L. C.; Massari, C.; Tasca, C. I. *Mol. Neurobiol.* **2017**, *54*, 3149–3161.

(321) Hajj, E.; David, P. *Brain. Behav. Immun.* **2016**, *58*, 261–271.

(322) Paxinos, G.; Watson, C. 6th Ed.; The rat brain in stereotaxic coordinates, Academic Press, 2007.

(323) Hassani, S.-A.; Lendor, S.; Boyaci, E.; Pawliszyn, J.; Womelsdorf, T. *J. Neurophysiol.* **2019**, *122* (4), 1649–1660.

(324) Lankeoff, I.; Stevens, S. L.; P., S.-P. M.; Laskin, J. *Analyst* **2014**, *139* (14), 3483–3646.

(325) Kerian, K. S.; Jarmusch, A. K.; Cooks, R. G. *Analyst* **2014**, *139* (11), 2714–2720.

(326) Graaf, R. A. De; Pan, J. W.; Telang, F.; Lee, J.; Brown, P.; Novotny, E. J.; Hetherington, H. P.; Rothman, D. L. *J. Cereb. Blood Flow Metab.* **2001**, *21*, 483–492.

(327) Fowler, J. S.; Volkow, N. D.; Logan, J.; Alexoff, D.; Telang, F.; Wang, G.; Wong, C.; Ma, Y.; Kriplani, A.; Pradhan, K.; et al. *Neuroimage* **2008**, *43* (4), 756–763.

(328) Kalasinsky, K. S.; Bosy, T. Z.; Schmunk, G. A.; Reiber, G.; Anthony, R. M.; Furukawa, Y.; Guttman, M.; Kish, S. J. *Forensic sci* **2001**, *116*, 163–169.

(329) Wang, J. B.; Aryal, M.; Zhong, Q.; Vyas, D. B.; Airan, R. D. *Neuron* **2018**, *100* (3), 728-738.e7.

(330) Balog, J.; Kumar, S.; Alexander, J.; Golf, O.; Huang, J.; Wiggins, T.; Abbassi-Ghadi, N.;

Enyedi, A.; Kacska, S.; Kinross, J.; et al. *Angew. Chemie - Int. Ed.* **2015**, *54* (38), 11059–11062.

(331) Fatou, B.; Saudemont, P.; Leblanc, E.; Vinatier, D.; Mesdag, V.; Wisztorski, M.; Focsa, C.; Salzet, M.; Ziskind, M.; Fournier, I. *Sci. Rep.* **2016**, *6* (April), 1–14.

(332) Zhang, J.; Katta, N.; Suliburk, J.; Rector, J.; Garza, K. Y.; Sans, M.; Zahedivash, A.; Ludolph, B.; Bensussan, A.; Giese, N.; et al. *Sci. Transl. Med.* **2017**, *9* (406), eaan3968.

(333) Maser, T. L.; Honarvar, E.; Venter, A. R. *J. Am. Soc. Mass Spectrom.* **2020**.

(334) Kiontke, A.; Oliveira-Birkmeier, A.; Opitz, A.; Birkemeyer, C. *PLoS One* **2016**, *11* (12), 1–16.

(335) Green, F. M.; Stokes, P.; Hopley, C.; Seah, M. P.; Gilmore, I. S.; O'Connor, G. *Anal. Chem.* **2009**, *81* (6), 2286–2293.

(336) Mura, S.; Nicolas, J.; Couvreur, P. *Nat. Mater.* **2013**, *12* (11), 991–1003.

(337) Upton, R. N. *Clin. Exp. Pharmacol. Physiol.* **2007**, *34* (8), 695–701.

(338) Airan, R. D.; Meyer, R. A.; Ellens, N. P. K.; Rhodes, K. R.; Farahani, K.; Pomper, M. G.; Kadam, S. D.; Green, J. J. *Nano Lett.* **2017**, *17* (2), 652–659.

(339) Groothuis, D. R. *Neuro. Oncol.* **2000**, *2* (1), 45–59.

(340) Pawliszyn, J.; Vuckovic, D.; Bojko, B.; Napylov, A.; Reyes Garces, N.; Gomez-Rios, G.; Olkowicz, M.; Lendor, S.; Monnin, C.; Hamani, C. *Angew. Chemie Int. Ed.* **2019**, *DOI: 10.10*.

(341) Reyes-Garcés, N.; Diwan, M.; Boyacı, E.; Gómez-Ríos, G. A.; Bojko, B.; Nobrega, J. N.; Bambico, F. R.; Hamani, C.; Pawliszyn, J. *Anal. Chem.* **2019**, *91* (15), 9875–9884.

(342) Matys, J.; Gieroba, B.; Jóźwiak, K. *J. Pharm. Biomed. Anal.* **2020**, *180*.

(343) Lendor, S.; Gómez-Ríos, G. A.; Boyacı, E.; Vander Heide, H.; Pawliszyn, J. *Anal. Chem.* **2019**, *91* (15), 10141–10148.

(344) Carreno, F. R.; Lodge, D. J.; Frazer, A. *Behav. Brain Res.* **2020**, *383* (October 2019), 112532.

(345) Mathew, S. J. *Psychiatr. Ann.* **2020**, *50* (2), 44–45.

(346) Sleigh, J.; Harvey, M.; Voss, L.; Denny, B. *Trends Anaesth. Crit. Care* **2014**, *4* (2–3), 76–81.

(347) Niesters, M.; Martini, C.; Dahan, A. *Br. J. Clin. Pharmacol.* **2014**, *77* (2), 357–367.

(348) Hashimoto, K. *Psychiatry Clin. Neurosci.* **2019**, *73* (10), 613–627.

(349) Schwertner, A.; Zortea, M.; Torres, F. V.; Ramalho, L.; Alves, C. F. da S.; Lannig, G.; Torres, I. L. S.; Fregni, F.; Gauer, G.; Caumo, W. *Front. Neurosci.* **2019**, *13* (SEP), 1–13.

(350) Hocking, G.; Cousins, M. J. *Anesth. Analg.* **2003**, *97* (6), 1730–1739.

(351) Blonk, M. I.; Koder, B. G.; Bemt, P. M. L. A. va. den; Huygen, F. J. P. M. *Eur. J. Pain* **2010**, *14* (5), 466–472.

(352) Fuchikami, M.; Thomas, A.; Liu, R.; Wohleb, E. S.; Land, B. B.; DiLeone, R. J.; Aghajanian, G. K.; Duman, R. S. *Proc. Natl. Acad. Sci. U. S. A.* **2015**, *112* (26), 8106–8111.

(353) Shirayama, Y.; Hashimoto, K. *Eur. Arch. Psychiatry Clin. Neurosci.* **2017**, *267* (2), 177–182.

(354) Wood, M.; Adil, O.; Wallace, T.; Fourman, S.; Wilson, S. P.; Herman, J. P.; Myers, B. *Brain Struct. an* **2019**, *224* (1), 73–97.

(355) Davidson, S.; Truong, H.; Nakagawa, Y.; Giesler, G. J. *Brain Res.* **2010**, *1307*, 43–52.

(356) Poland, R. S.; Bull, C.; Syed, W. A.; Bowers, M. S. *J. Vis. Exp.* **2015**, *2015* (103), 1–9.

(357) Lohman, R. J.; Liu, L.; Morris, M.; O'Brien, T. J. *J. Neurosci. Methods* **2005**, *146* (2), 191–197.

(358) Yi, J.; Khobrekar, N. V.; Dantas, T. J.; Zhou, J.; Vallee, R. B. *Methods Cell Biol.* **2016**, *131*, 453–465.

(359) World Health Organization Thirty-seventh Meeting. *Geneva, 16-20 Novemb.* **2015**.

(360) Tyler, M. W.; Yourish, H. B.; Ionescu, D. F.; Haggarty, S. J. *ACS Chem. Neurosci.* **2017**, *8* (6), 1122–1134.

(361) Torrice, M. *C&EN Glob. Enterp.* **2020**, *98* (3), 18–22.

(362) Rosting, C.; Pedersen-Bjergaard, S.; Hansen, S. H.; Janfelt, C. *Analyst* **2013**, *138* (20), 5965–5972.

(363) Wójtowicz, A.; Wietecha-Posłuszny, R. *Appl. Phys. A* **2019**, *125* (5), 312.

(364) Ingram, A. J.; Boeser, C. L.; Zare, R. N. *Chem. Sci.* **2016**, *7* (1), 39–55.

(365) Laskin, J.; Lanekoff, I. *Anal. Chem.* **2016**, *88* (1), 52–73.

(366) Wiseman, J. M.; Evans, C. A.; Bowen, C. L.; Kennedy, J. H. *Analyst* **2010**, *135* (4), 720–725.

(367) Barbula, G. K.; Robbins, M. D.; Yoon, O. K.; Zuleta, I.; Zare, R. N. *Anal. Chem.* **2009**, *81* (21), 9035–9040.

(368) Chen, H.; Gamez, G.; Zenobi, R. *J. Am. Soc. Mass Spectrom.* **2009**, *20* (11), 1947–1963.

(369) Huang, G.; Chen, H.; Zhang, X.; Cooks, R. G.; Ouyang, Z. *Anal. Chem.* **2007**, *79* (21), 8327–8332.

(370) Dénes, J.; Katona, M.; Hosszú, Á.; Czuczy, N.; Takáts, Z. *Anal. Chem.* **2009**, *81* (4), 1669–1675.

(371) Bianchi, F.; Gregori, A.; Braun, G.; Crescenzi, C.; Careri, M. *Anal. Bioanal. Chem.* **2015**, *407* (3), 931–938.

(372) Kauppila, T. J.; Talaty, N.; Kuuranne, T.; Kotiaho, T.; Kostiainen, R.; Cooks, R. G. *Analyst* **2007**, *132* (9), 868–875.

(373) Mulligan, C. C.; MacMillan, D. K.; Noll, R. J.; Cooks, R. G. *Rapid Commun. Mass Spectrom.* **2007**, *21*, 3729–3736.

(374) Thunig, J.; Flø, L.; Pedersen-Bjergaard, S.; Hansen, S. H.; Janfelt, C. *Rapid Commun. Mass Spectrom.* **2012**, *26* (2), 133–140.

(375) Ifa, D. R.; Srimany, A.; Eberlin, L. S.; Naik, H. R.; Bhat, V.; Cooks, R. G.; Pradeep, T. *Anal. Methods* **2011**, *3* (8), 1910–1912.

(376) Thunig, J.; Hansen, S. H.; Janfelt, C. *Anal. Chem.* **2011**, *83* (9), 3256–3259.

(377) Müller, T.; Oradu, S.; Ifa, D. R.; Cooks, R. G.; Kräutler, B. *Anal. Chem.* **2011**, *83* (14), 5754–5761.

(378) Muramoto, S.; Forbes, T. P.; Van Asten, A. C.; Gillen, G. *Anal. Chem.* **2015**, *87* (10), 5444–5450.

(379) Van Biesen, G.; Wiseman, J. M.; Li, J.; Bottaro, C. S. *Analyst* **2010**, *135* (9), 2237–2240.

(380) Kasperkiewicz, A.; Gómez-Ríos, G. A.; Hein, D.; Pawliszyn, J. *Anal. Chem.* **2019**, *91* (20), 13039–13046.

(381) Beach, D. G.; Gabryelski, W. *Anal. Chem.* **2013**, *85* (4), 2127–2134.

(382) Källback, P.; Nilsson, A.; Shariatgorji, M.; Andrén, P. E. *Anal. Chem.* **2016**, *88* (8), 4346–4353.

(383) Bergman, H. M.; Lundin, E.; Andersson, M.; Lanekoff, I. *Analyst* **2016**, *141* (12), 3686–3695.

(384) Song, X.; He, J.; Pang, X.; Zhang, J.; Sun, C.; Huang, L.; Li, C.; Zang, Q.; Li, X.; Luo, Z.; et al. *Anal. Chem.* **2019**.

(385) Fernandes, A. M. A. P.; Vendramini, P. H.; Galaverna, R.; Schwab, N. V.; Alberici, L. C.; Augusti, R.; Castilho, R. F.; Eberlin, M. N. *J. Am. Soc. Mass Spectrom.* **2016**, *27* (12), 1944–1951.

(386) Vismeh, R.; Waldon, D. J.; Teffera, Y.; Zhao, Z. *Anal. Chem.* **2012**, *84* (12), 5439–5445.

(387) Song, X.; Luo, Z.; Li, X.; Li, T.; Wang, Z.; Sun, C.; Huang, L.; Xie, P.; Liu, X.; He, J.; et al. *Anal. Chem.* **2017**, *89* (12), 6318–6323.

(388) Bilkey, J.; Tata, A.; McKee, T. D.; Porcari, A. M.; Bluemke, E.; Woolman, M.; Ventura, M.; Eberlin, M. N.; Zarrine-Afsar, A. *Anal. Chem.* **2016**, *88* (24), 12099–12107.

(389) Chipuk, J. E.; Gelb, M. H.; Brodbelt, J. S. *Anal. Chem.* **2010**, *82* (1), 16–18.

(390) Yarger, T. J.; Yuill, E. M.; Baker, L. A. *J. Am. Soc. Mass Spectrom.* **2018**, *29* (3), 558–565.

(391) Pasilis, S. P.; Kertesz, V.; Van Berkel, G. J. *Anal. Chem.* **2007**, *79* (15), 5956–5962.

(392) Barre, F. P. Y.; Heeren, R. M. A.; Potocnik, N. O. *Curr. Pharm. Des.* **2017**, *23* (5), 1–11.

(393) Schäfer, K. C.; Dénes, J.; Albrecht, K.; Szaniszló, T.; Balogh, J.; Skoumal, R.; Katona, M.; Tóth, M.; Balogh, L.; Takáts, Z. *Angew. Chemie - Int. Ed.* **2009**, *48* (44), 8240–8242.

(394) Yoshimura, K.; Chen, L. C.; Yu, Z.; Hiraoka, K.; Takeda, S. *Anal. Biochem.* **2011**, *417* (2), 195–201.

(395) Chen, C. H.; Lin, Z.; Garimella, S.; Zheng, L.; Shi, R.; Cooks, R. G.; Ouyang, Z. *Anal. Chem.* **2013**, *85* (24), 11843–11850.

(396) Chen, L. C.; Naito, T.; Tsutsui, S.; Yamada, Y.; Ninomiya, S.; Yoshimura, K.; Takeda, S.; Hiraoka, K. *Analyst* **2017**, *142* (15), 2735–2740.

(397) Brown, H. M.; Pirro, V.; Graham Cooks, R. *Clin. Chem.* **2018**, *64* (4), 628–630.

(398) So, P. K.; Hu, B.; Yao, Z. P. *Mol. Biosyst.* **2013**, *9* (5), 915–929.

(399) Zhong, Q.; Yoon, B. C.; Aryal, M.; Wang, J. B.; Ilovitsh, T.; Baikoghli, M. A.; Hosseini-Nassab, N.; Karthik, A.; Cheng, R. H.; Ferrara, K. W.; et al. *Biomaterials* **2019**, *206* (March), 73–86.

(400) Wishart, D. S.; Feunang, Y. D.; Guo, A. C.; Lo, E. J.; Marcu, A.; Grant, J. R.; Sajed, T.; Johnson, D.; Li, C.; Sayeeda, Z.; et al. *Nucleic Acids Res.* **2018**, *46*, D1074–D1082.

(401) Lamont, L.; Eijkel, G. B.; Jones, E. A.; Flinders, B.; Ellis, S. R.; Porta Siegel, T.; Heeren, R. M. A.; Vreeken, R. J. *Anal. Chem.* **2018**, *90* (22), 13229–13235.

(402) Manicke, N. E.; Wiseman, J. M.; Ifa, D. R.; Cooks, R. G. *J. Am. Soc. Mass Spectrom.* **2008**, *19*,

531–543.

(403) Badu-Tawiah, A.; Bland, C.; Campbell, D. I.; Cooks, R. G. *J. Am. Soc. Mass Spectrom.* **2010**, *21* (4), 572–579.

(404) Eberlin, L. S.; Ferreira, C. R.; Dill, A. L.; Ifa, D. R.; Cheng, L.; Cooks, R. G. *ChemBioChem* **2011**, *12* (14), 2129–2132.

(405) Volný, M.; Venter, A.; Smith, S. A.; Pazzi, M.; Cooks, R. G. *Analyst* **2008**, *133* (4), 525–531.

(406) Reyes-Garcés, N. 2017.

(407) Douglass, K. A.; Jain, S.; Brandt, W. R.; Venter, A. R. *J. Am. Soc. Mass Spectrom.* **2012**, *23* (11), 1896–1902.

(408) Cech, N. B.; Enke, C. G. *Mass Spectrom. Rev.* **2001**, *20* (6), 362–387.

(409) Costa, A. B.; Graham Cooks, R. *Chem. Phys. Lett.* **2008**, *464* (1–3), 1–8.

(410) Alam, M. N.; Nazdrajić, E.; Singh, V.; Tascon, M.; Pawliszyn, J. *Anal. Chem.* **2018**, *90* (19), 11548–11555.

(411) Reyes-Garcés, N.; Gionfriddo, E.; Gómez-Ríos, G. A.; Alam, M. N.; Boyac, E.; Bojko, B.; Singh, V.; Grandy, J.; Pawliszyn, J. *Anal. Chem.* **2018**, *90*, 302−360.

(412) Watrous, J.; Hendricks, N.; Meehan, M.; Dorrestein, P. C. *Anal. Chem.* **2010**, *82* (5), 1598–1600.

(413) Van Berkel, G. J.; Ford, M. J.; Deibel, M. A. *Anal. Chem.* **2005**, *77* (5), 1207–1215.

(414) Chipuk, J. E.; Brodbelt, J. S. *J. Am. Soc. Mass Spectrom.* **2009**, *20* (4), 584–592.

(415) Schwab, N. V.; Ore, M. O.; Eberlin, M. N.; Morin, S.; Ifa, D. R. *Anal. Chem.* **2014**, *86* (23), 11722–11726.

(416) Shariatgorji, M.; Strittmatter, N.; Nilsson, A.; Källback, P.; Alvarsson, A.; Zhang, X.; Vallianatou, T.; Svenningsson, P.; Goodwin, R. J. A.; Andren, P. E. *Neuroimage* **2016**, *136*, 129–138.

(417) Bedani, F.; Kok, W. T.; Janssen, H. G. *J. Chromatogr. A* **2006**, *1133* (1–2), 126–134.

(418) Chen, C. H.; Lin, Z.; Garimella, S.; Zheng, L.; Shi, R.; Cooks, R. G.; Ouyang, Z. *Anal. Chem.* **2013**, *85* (24), 11843–11850.

(419) Whittlesey, K. J.; Shea, L. D. *Exp. Neurol.* **2004**, *190* (1), 1–16.

(420) Tan, V. X.; Guillemin, G. J. *Front. Neurosci.* **2019**, *13* (September), 1–11.

(421) Varma, V. R.; Oommen, A. M.; Varma, S.; Casanova, R.; An, Y.; Andrews, R. M.; O'Brien, R.; Pletnikova, O.; Troncoso, J. C.; Toledo, J.; et al. *PLoS Med.* **2018**, *15* (1), 1–31.

(422) Ferrer, I.; Martinez, A.; Boluda, S.; Parchi, P.; Barrachina, M. *Cell Tissue Bank.* **2008**, *9* (3), 181–194.

(423) Vappou, J.; Breton, E.; Choquet, P.; Willinger, R.; Constantinesco, A. *J. Biomech.* **2008**, *41* (14), 2954–2959.

(424) Stan, A. D.; Ghose, S.; Gao, X. M.; Roberts, R. C.; Lewis-Amezcua, K.; Hatanpaa, K. J.; Tamminga, C. A. *Brain Res.* **2006**, *1123* (1), 1–11.

(425) Schweitzer, M. H. *Annu. Rev. Earth Planet. Sci.* **2011**, *39* (1), 187–216.

(426) Li, J. Z.; Vawter, M. P.; Walsh, D. M.; Tomita, H.; Evans, S. J.; Choudary, P. V.; Lopez, J. F.; Avelar, A.; Shokoohi, V.; Chung, T.; et al. *Hum. Mol. Genet.* **2004**, *13* (6), 609–616.

(427) Alonso-Nanclares, L.; Gonzalez-Soriano, J.; Rodriguez, J. R.; DeFelipe, J. *Proc. Natl. Acad. Sci.* **2008**, *105* (38), 14615–14619.

(428) Cartiser, N.; Bévalot, F.; Fanton, L.; Gaillard, Y.; Guitton, J. *Int. J. Legal Med.* **2011**, *125* (2), 181–198.

(429) Schotsmans, E. M.; Márquez-Grant, N.; Forbes, S. Taphonomy of Human Remains: Forensic Analysis of the Dead and the Depositional Environment, John Wiley & Sons Ltd, 2017.

(430) Hunsucker, S. W.; Solomon, B.; Gawryluk, J.; Geiger, J. D.; Vacano, G. N.; Duncan, M. W.; Patterson, D. *J. Neurochem.* **2008**, *105* (3), 725–737.

(431) Kaszynski, R. H.; Nishiumi, S.; Azuma, T.; Yoshida, M.; Kondo, T.; Takahashi, M.; Asano, M.; Ueno, Y. *Anal. Bioanal. Chem.* **2016**, *408* (12), 3103–3112.

(432) Hirakawa, K.; Koike, K.; Uekusa, K.; Nihira, M.; Yuta, K.; Ohno, Y. *Leg. Med.* **2009**, *11* (SUPPL. 1), S282–S285.

(433) Wood, P. L. *J. Postgenomics Drug Biomark. Dev.* **2012**, *03* (03), 3–5.

(434) Kang, Y. R.; Park, Y. S.; Park, Y. C.; Yoon, S. M.; JongAhn, H.; Kim, G.; Kwon, S. W. *J. Pharm. Investig.* **2012**, *42* (1), 41–46.

(435) Donaldson, A. E.; Lamont, I. L. *Metabolomics* **2014**, *11* (1), 237–245.

(436) Castillo-Peinado, L. S.; Luque de Castro, M. D. *Anal. Chim. Acta* **2016**, *925*, 1–15.

(437) Chen, L.; Qiu, J.; Tang, Y.; Xu, J.; Huang, S.; Liu, Y.; Ouyang, G. *Talanta* **2017**, *171* (May), 179–184.

(438) Lendor, S.; Hassani, S. A.; Boyaci, E.; Singh, V.; Womelsdorf, T.; Pawliszyn, J. *Anal. Chem.* **2019**, *91* (7), 4896–4905.

(439) Roszkowska, A.; Yu, M.; Bessonneau, V.; Ings, J.; McMaster, M.; Smith, R.; Bragg, L.; Servos, M.; Pawliszyn, J. *Environ. Pollut.* **2019**, *249*, 109–115.

(440) Poole, J. J.; Grandy, J. J.; Yu, M.; Boyaci, E.; Bojko, B.; Heide, H. Vander; Pawliszyn, J. *Anal. Chem.* **2017**, *89* (15), 8012–8026.

(441) Artola-Garicano, E.; Vaes, W. H. J.; Hermens, J. L. M. *Toxicol. Appl. Pharmacol.* **2000**, *166* (2), 138–144.

(442) Reyes-garcés, N.; Diwan, M.; Boyaci, E.; Gomez-rios, G. A. *Anal. Chem.* **2019**, *91* (15), 9875–9884.

(443) Szymańska, E.; Saccenti, E.; Smilde, A. K.; Westerhuis, J. A. *Metabolomics* **2012**, *8*, 3–16.

(444) Wiklund, S.; Johansson, E.; Sjöström, L.; Mellerowicz, E. J.; Edlund, U.; Shockcor, J. P.; Gottfries, J.; Moritz, T.; Trygg, J. *Anal. Chem.* **2008**, *80* (1), 115–122.

(445) Uppal, K.; Walker, D. I.; Jones, D. P. *Anal. Chem.* **2017**, *89* (2), 1063–1067.

(446) Wishart, D. S.; Tzur, D.; Knox, C.; Eisner, R.; Guo, A. C.; Young, N.; Cheng, D.; Jewell, K.; Arndt, D.; Sawhney, S.; et al. *Nucleic Acids Res.* **2007**, *35* (SUPPL. 1), 521–526.

(447) Kanehisa, M.; Furumichi, M.; Tanabe, M.; Sato, Y.; Morishima, K. *Nucleic Acids Res.* **2017**, *45* (D1), D353–D361.

(448) Lai, Z.; Tsugawa, H.; Wohlgemuth, G.; Mehta, S.; Mueller, M.; Zheng, Y.; Ogiwara, A.; Meissen, J.; Showalter, M.; Takeuchi, K.; et al. *Nat. Methods* **2018**, *15* (1), 53–56.

(449) MZCloud: Advanced Mass Spectral Database, https://www. mzcloud.org/ (accessed 2019/04/14).

(450) Xia, J.; Wishart, D. S.; Valencia, A. *Bioinformatics* **2011**, *27* (13), 2342–2344.

(451) Blandini, F.; Braunewell, K. H.; Manahan-Vaughan, D.; Orzi, F.; Sarti, P. *Cell Death Differ.* **2004**, *11* (4), 479–484.

(452) Michel, P. P.; Hirsch, E. C.; Hunot, S. *Neuron* **2016**, *90* (4), 675–691.

(453) Vaishnavi, S. N.; Vlassenko, A. G.; Rundle, M. M.; Snyder, A. Z.; Mintun, M. A.; Raichle, M. E. *Proc. Natl. Acad. Sci. U. S. A.* **2010**, *107* (41), 17757–17762.

(454) Hagberg, H.; Andersson, P.; Lacarewicz, J.; Jacobson, I.; Butcher, S.; Sandberg, M. *J. Neurochem.* **1987**, *49* (1), 227–231.

(455) Kaminsky, Y.; Kosenko, Y. *Brain Res.* **2009**, *1294*, 193–201.

(456) Ramamoorthi, K.; Lin, Y. *Trends Mol. Med.* **2011**, *17* (8), 452–462.

(457) Lewerenz, J.; Maher, P. *Front. Neurosci.* **2015**, *9* (DEC), 1–20.

(458) Perutz, M. F. *Trends Biochem. Sci.* **1999**, *24* (2), 58–63.

(459) Tretter, L.; Patocs, A.; Chinopoulos, C. *Biochim. Biophys. Acta - Bioenerg.* **2016**, *1857* (8), 1086–1101.

(460) Choi, D. W. (Stanford U.; Rothman, S. M. (Washington U. *Annu. Rev. Neurosci.* **1990**, *13*, 171–182.

(461) Oja, S. S.; Saransaari, P. *Prog. Neurobiol.* **2000**, *62* (4), 407–425.

(462) Murín, R.; Hamprecht, B. *Micronutr. Brain Heal.* **2009**, *42* (6), 403–415.

(463) Cole, J. T.; Mitala, C. M.; Kundu, S.; Verma, A.; Elkind, J. A.; Nissim, I.; Cohen, A. S. *Proc. Natl. Acad. Sci. U. S. A.* **2010**, *107* (1), 366–371.

(464) Purcell, E. A.; Jeon, O. H.; Blue, N.; Jeon, D. *Neurology* **2001**, *57* (9), 1–18.

(465) Hashimoto, K.; Sawa, A.; Iyo, M. *Biol. Psychiatry* **2007**, *62* (11), 1310–1316.

(466) Magi, S.; Piccirillo, S.; Amoroso, S. *Cell. Mol. Life Sci.* **2019**, *76* (8), 1473–1488.

(467) Maragakis, N. J.; Rothstein, J. D. *Nat. Clin. Pract. Neurol.* **2006**, *2* (12), 679–689.

(468) Bélanger, M.; Allaman, I.; Magistretti, P. J. *Cell Metab.* **2011**, *14* (6), 724–738.

(469) Meeley, M. P.; Martin, D. L. *Cell. Mol. Neurobiol.* **1983**, *3* (1), 39–54.

(470) Wu, S. J.; Martin, D. L. *J. Neurochem.* **1984**, *42* (6), 1607–1612.

(471) Meeley, M. P.; Martin, D. L. *Cell. Mol. Neurobiol.* **1983**, *3* (1), 55–68.

(472) David M. Karam. 1st Editio.; Trafford Publishing, 2012.

(473) Wood, J. D.; Wood, W. J.; Ducker, A. J. *J. Neurochem.* **1968**, *15*, 603–608.

(474) Yatsenko, L. N.; Storchak, L. G.; Parkhomenko, N. T.; Himmelreich, N. H. *Neurophysiology* **2008**, *40* (4), 243–251.

(475) Yan, H. D.; Ishihara, K.; Serikawa, T.; Sasa, M. *Epilepsia* **2003**, *44* (9), 1153–1159.

(476) Baslow, M. H. *J. Neurochem.* **2000**, *75* (2), 453–459.

(477) Tyson, R. L.; Sutherland, G. R. *Neurosci. Lett.* **1998**, *251* (3), 181–184.

(478) Surendran, S.; Bhatnagar, M. *Int. J. Neurosci.* **2011**, *121* (6), 305–309.

(479) Asaka, R.; Le, A. *Mol. Cell. Oncol.* **2019**, *6* (5), 1–3.

(480) Chen, R.; Lai, U. H.; Zhu, L.; Singh, A.; Ahmed, M.; Forsyth, N. R. *Front. Cell Dev. Biol.* **2018**, *6* (OCT), 1–12.

(481) Magura, I. S.; Rozhmanova, O. M. *Biopolym. Cell* **1997**, *13* (6), 513–515.

(482) Gawryluk, J. W.; Wang, J. F.; Andreazza, A. C.; Shao, L.; Young, L. T. *Int. J. Neuropsychopharmacol.* **2011**, *14* (1), 123–130.

(483) Sedlak, T. W.; Paul, B. D.; Parker, G. M.; Hester, L. D.; Snowman, A. M.; Taniguchi, Y.; Kamiya, A.; Snyder, S. H.; Sawa, A. *Proc. Natl. Acad. Sci. U. S. A.* **2019**, *116* (7), 2701–2706.

(484) Li, J.; Guo, C.; Wu, J. *PPAR Res.* **2019**, *2019*, 1–10.

(485) Freeman, L. R.; Keller, J. N. *Biochim. Biophys. Acta - Mol. Basis Dis.* **2012**, *1822* (5), 822–829.

(486) Müller, C. P.; Reichel, M.; Mühle, C.; Rhein, C.; Gulbins, E.; Kornhuber, J. *Biochim. Biophys. Acta - Mol. Cell Biol. Lipids* **2015**, *1851* (8), 1052–1065.

(487) Hussain, G.; Wang, J.; Rasul, A.; Anwar, H.; Imran, A.; Qasim, M.; Zafar, S.; Kamran, S. K. S.; Razzaq, A.; Aziz, N.; et al. *Lipids Health Dis.* **2019**, *18* (1), 1–12.

(488) Posse de Chaves, E.; Sipione, S. *FEBS Lett.* **2010**, *584* (9), 1748–1759.

(489) Yao, J. K.; Leonard, S.; Reddy, R. D. *Schizophr. Res.* **2000**, *42* (1), 7–17.

(490) Cocco, L.; Follo, M. Y.; Manzoli, L.; Suh, P. G. *J. Lipid Res.* **2015**, *56* (10), 1853–1860.

(491) Tanguy, E.; Wang, Q.; Moine, H.; Vitale, N.; Salvador, G. A. **2019**, *13* (January), 1–8.

(492) Vuckovic, D. *Anal. Bioanal. Chem.* **2012**, *403* (6), 1523–1548.

(493) Martin, J. C.; Maillot, M.; Mazerolles, G.; Verdu, A.; Lyan, B.; Migné, C.; Defoort, C.; Canlet, C.; Junot, C.; Guillou, C.; et al. *Metabolomics* **2015**, *11* (4), 807–821.

(494) Colyer, A.; Gilham, M. S.; Kamlage, B.; Rein, D.; Allaway, D. *Br. J. Nutr.* **2011**, *106* (S1), S146–S149.

(495) Martic-Kehl, M. I.; Ametamey, S. M.; Alf, M. F.; Schubiger, P. A.; Honer, M. *EJNMMI Res.* **2012**, *2* (1), 1–10.

(496) Bastin, C.; Yakushev, I.; Bahri, M. A.; Fellgiebel, A.; Eustache, F.; Landeau, B.; Scheurich, A.; Feyers, D.; Collette, F.; Chételat, G.; et al. *Neuroimage* **2012**, *63* (2), 713–722.

(497) Vasilopoulou, C. G.; Margarity, M.; Klapa, M. I. *Front. Physiol.* **2016**, *7* (MAY), 1–8.

(498) Goryński, K.; Goryńska, P.; Górska, A.; Harężlak, T.; Jaroch, A.; Jaroch, K.; Lendor, S.;

Skobowiat, C.; Bojko, B. *J. Pharm. Biomed. Anal.* **2016**, *130*, 55–67.

(499) Westerhout, J.; Ploeger, B.; Smeets, J.; Danhof, M.; de Lange, E. C. M. *AAPS J.* **2012**, *14* (3), 543–553.

(500) Whitfield Åslund, M.; Celejewski, M.; Lankadurai, B. P.; Simpson, A. J.; Simpson, M. J. *Chemosphere* **2011**, *83* (8), 1096–1101.

(501) Soto, R. J.; Hall, J. R.; Brown, M. D.; Taylor, J. B.; Schoenfisch, M. H. *Anal. Chem.* **2017**, *89* (1), 276–299.

(502) Nesbitt, K. M.; Jaquins-Gerstl, A.; Skoda, E. M.; Wipf, P.; Michael, A. C. *Anal. Chem.* **2013**, *85* (17), 8173–8179.

(503) McNay, E. C.; Sherwin, R. S. *J. Neurosci. Methods* **2004**, *132* (1), 35–43.

(504) Meixensberger, J.; Kunze, E.; Barcsay, E.; Vaeth, A.; Roosen, K. *Neurol. Res.* **2001**, *23* (8), 801–806.

(505) Ivanisevic, J.; Epstein, A. A.; Kurczy, M. E.; Benton, P. H.; Uritboonthai, W.; Fox, H. S.; Boska, M. D.; Gendelman, H. E.; Siuzdak, G. *Chem. Biol.* **2014**, *21* (11), 1575–1584.

(506) Sheleg, S. V; Lobello, J. R.; Hixon, H.; Coons, S. W.; Lowry, D.; Nedzved, M. K. *Int. J. Clin. Exp. Pathol.* **2008**, *1* (3), 291–299.

(507) Hostiuc, S.; Rusu, M. C.; Mănoiu, V. S.; Vrapciu, A. D.; Negoi, I.; Popescu, M. V. *Rom. J. Morphol. Embryol.* **2017**, *58* (2), 377–384.